2012-10-26

Syngas Impurity Effects on Cell Growth, Enzymatic Activities and Ethanol Production via Fermentation

Deshun Xu
Brigham Young University - Provo

Syngas Impurity Effects on Cell Growth, Enzymatic Activities and Ethanol Production via Fermentation

Deshun Xu

A dissertation submitted to the faculty of
Brigham Young University
in partial fulfillment of the requirement for the degree of

Doctor of Philosophy

Randy S. Lewis, Chair
Larry L. Baxter
William R. McCleary
Ken A. Solen
William C. Hecker

Department of Chemical Engineering

Brigham Young University

October 2012

ABSTRACT

Syngas Impurity Effects on Cell Growth, Enzymatic Activities and Ethanol Production via Fermentation

Deshun Xu
Department of Chemical Engineering, BYU
Doctor of Philosophy

A syngas compositional database with focus on trace impurities was established. For this work, ammonia (NH_3) and benzene (C_6H_6) effects on cell growth, enzymatic activities of hydrogenase and alcohol dehydrogenase (ADH), and product formation were studied.

NH_3, after entering media, will be converted rapidly to NH_4^+, which will raise the total osmolarity of the media. NH_3, as a common nutrient for the cell growth, is not the real culprit for cell growth inhibition. In essence, it is the high osmolarity resulting from the accumulation of NH_4^+ in the media which disrupts the normal regulation of the cells. It was concluded that at NH_4^+ concentration above 250 mM, the cell growth was substantially inhibited. However, P11 cells used in this study can likely adapt to an elevated osmolarity (up to 500 mM) although the mechanism is unknown. It was also found that higher osmolarity will eventually lead to higher ethanol per cell density. In conclusion, NH_3 needs to be cleaned out of syngas feeding system.

The realistic C_6H_6 concentration in the media coming from a gasifier was simulated in bioreactors and was measured by a GC/MS. The most realistic C_6H_6 concentration in the media was around 0.41 mM (upper limit 0.83 mM). However, five elevated concentrations of 0.64, 1.18, 1.72, 2.33, and 3.44 mM were doped into the media. It was found that at 3.44 mM cell growth and ethanol production were significantly affected. However, there was only negligible adverse effect on cell growth and ethanol production at 0.41 mM, which is the expected concentration in bioreactors exposed to syngas. Therefore, it is unnecessary to remove C_6H_6 from the gas feeding stream.

A kinetic model for hydrogenase activity that included inhibition effects of NH_4^+ and C_6H_6 was developed. Experimental results showed that NH_4^+ is a non-competitive inhibitor for hydrogenase activity with K_{NH4+} of (649 ± 35) mM and K_{H2} of (0.19 ± 0.1) mM. This K_{H2} value is consistent with those reported in literature. C_6H_6 is also a non-competitive inhibitor but a more potent one compared to NH_4^+ (K_{C6H6}=11.4 ± 1.32 mM). A K_{H2} value of (0.196 ± 0.022) mM is also comparable with literature and also with the NH_4^+ study. At a realistic C_6H_6 concentration of 0.41 mM expected in bioreactors exposed to syngas, hydrogenase activity is expected to be reduced by less than 5%. Forward ADH activity was not adversely affected up to 200 mM [NH_4^+].

From the current work, NH_3 should be targeted for removal but it is not necessary to remove C_6H_6 when designing an efficient gas cleanup system.

Keywords: syngas impurity, hydrogenase activity, ethanol formation, inhibition, fermentation

ACKNOWLEDGEMENTS

First and foremost, I am very grateful for completing my PhD project at Brigham Young University (BYU) which provides an enlightening and safe environment for us. Needlessly to say, I am indebted to Dr. Randy S. Lewis who has guided me patiently over the years. Equally thankful, I appreciated the help from my committee members: Dr. Larry L. Baxter, Dr. William R. McCleary, Dr. Ken A. Solen, and Dr.William C. Hecker. They all helped me during different stages via their research specialty. Lastly, I do appreciate the funding from SunGrant and full support from my family members and numerous others at BYU.

TABLE OF CONTENTS

LIST OF TABLES

LIST OF FIGURES

1. Introduction

1.1 Ethanol as a substitute for gasoline

Ethanol, which may come from cellulosic sources in the future, is promoted by its advocates as a "green" substitute for gasoline. Bio-ethanol will help reduce the reliance on fossil fuels, especially foreign oil. This transition is a priority of the Obama administration [1]. Fuels such as bio-ethanol derived from biomass offer one such alternative to conventional energy sources that can dramatically impact national economic growth, national energy security, and environmental goals [2]. When ethanol made from biomass is burned, it returns to CO_2 which can then be reincorporated back into biomass, thus making this cycle mostly renewable. Currently, most energy produced in the US is from coal, natural gas, and crude oil as shown in Figure 1-1. This trend will run into the next decade or two. Among all the energy consumed, renewable energy accounts for around 8% for the year 2009 in the U.S. Furthermore, biofuels including bio-ethanol account for 20% among all the renewable energy categories as shown in Figure 1-2 [3]. Ethanol, as a possible alternative liquid fuel for automobiles, can be mixed with gasoline such that it can be fed into current petrol engines without modification. E85, a blend of 85% ethanol and 15% gasoline, can be used in flexible fuel vehicles (FFVs).

FFVs operating on E85 experience a 20-30% drop in miles per gallon due to ethanol's lower energy content. However, E85 reduces emissions of particulates and smog-forming nitrogen oxides (NOx) [4].

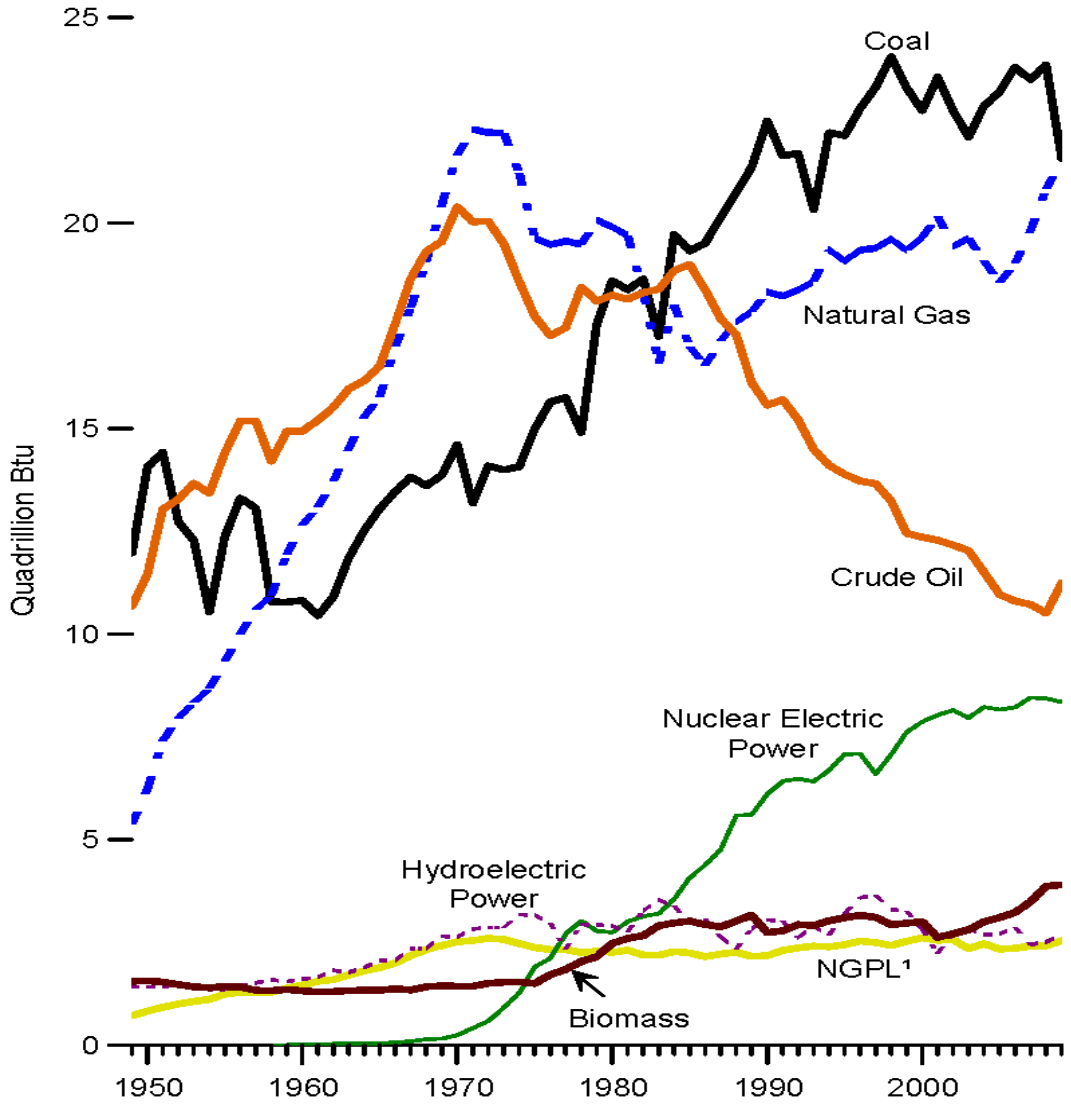

Figure 1-1. Primary Energy Production by Major Source (NGPL[1]: Natural gas plant liquids) (U.S. Energy Information Administration/Annual Energy Review 2009)

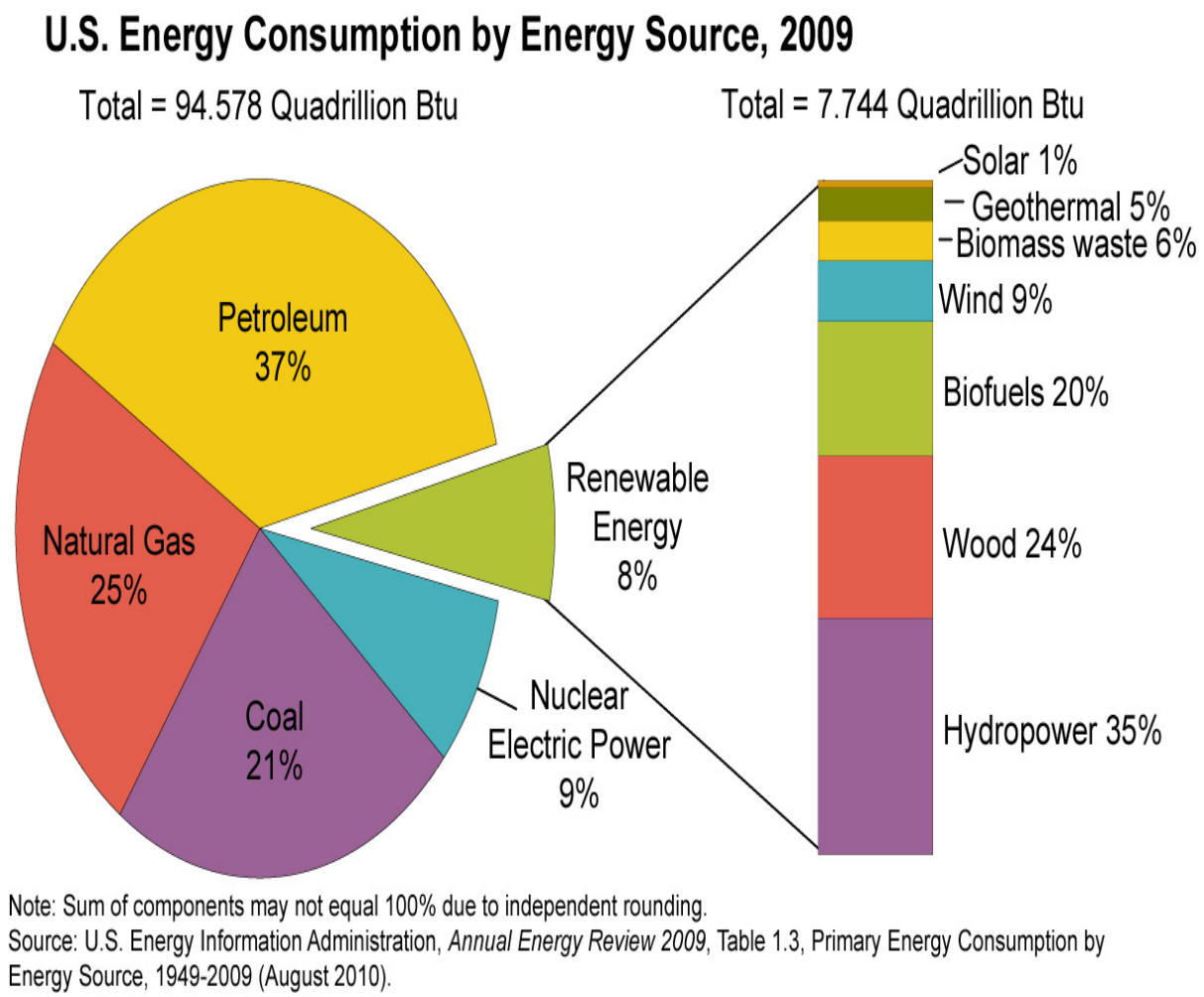

Figure 1-2. US energy consumption by energy source, 2009. (U.S. Energy Information Administration, Annual Energy Review 2009)

Owing to fossil fuels' unsustainable nature and negative environmental impact, the world is increasing its commitment to renewable energy. In the meantime, various efficient and cost-effective new technologies are being developed to convert all kinds of feed stocks to motor fuel grade ethanol (MFGE). To sum up, bio-ethanol and other biofuels can play a vital role in the future energy supply.

1.2 Pros and cons of fuel ethanol

The debate over the advantages and disadvantages of ethanol fuel has been raging for years. Bio-ethanol produced from biomass will reduce the dependency on imported fuels in the long run. With more commercial plants in production, it will decrease the US trade deficit and create more job opportunities. Cars designed to run on E85 blend will emit fewer toxic emissions such as lead and benzene. By going through carbon dioxide recycle, greenhouse gases and ozone created by transportation will be lowered. Currently, most ethanol is produced from sugar cane, corn, etc. This organic origin owing to its renewable nature is regarded as an advantage. However, this can also potentially compete with food production. Other drawbacks concerning ethanol as a fuel or fuel additive include [5]:

- The energy used to transport biomass and additional energy input may be larger than the energy content of ethanol, resulting in neutral or negative energy return.
- The soil used to cultivate corn, if over-cultivated, may be depleted most of its mineral or organic nutrients.
- Ethanol can easily absorb water and can be corrosive to the engine block.
- The energy content of ethanol is lower compared with gasoline. Thus, drivers need more volume of ethanol to drive the same distance.

1.3 Overviews of current bio-ethanol production technologies

In 2008, the United States consumed 1.5 EJ of biofuels, an increase of more than 40% from the previous year [6]. The rising demand of biofuels provides an opportunity for the

improvement of biofuel production technologies. Most ethanol production in the US occurs by fermentation of sugars (primarily obtained from corn) and costs are estimated at around 446 US$ m^{-3} in 2007 before subtracting the government subsidy. These production costs are heavily influenced by corn prices and the industry depends on a 135 US$ m^{-3} subsidy [7, 8]. Processes utilizing sugar and starch based crops typically involve the following steps [9]:

- Pre-treatment of the biomass by the dry milling (grinding) or wet milling (chemical treatment) process
- Enzymatic treatment of the biomass to convert starch into fermentable glucose sugars
- Yeast fermentations of biomass sugars into ethanol and carbon dioxide
- Fuel ethanol is obtained through a combination of distillation and molecular sieve dehydration.

The use of corn to produce ethanol has had a damaging impact on food markets, especially in poorer countries since corn-ethanol intensified competition for land and water. Therefore, there has been a recent interest in finding alternative sources of biomass for ethanol production. Lignocelluloses including prairie grasses, wood chips, paper wastes etc. are considered economically viable feed stocks owing to their abundance and much cheaper prices. Since marginal land can be utilized to cultivate these grasses, it will not interfere with food security [10].

Lignocellulose is typically comprised of 35-50% cellulose, 20-35% hemi-cellulose and 15-25% lignin [11]. Cellulose and hemi-cellulose are long-chain polymers of five and six carbon sugars. These polymers must go through de-polymerization processes such as dilute/concentrated acid hydrolysis or enzymatic hydrolysis to release their monomers [12]. As for the lignin, the

third constituent of lignocellulose, its complex structure cannot be broken down by these methods and the efficiency of carbon conversion will be reduced.

The dilute acid hydrolysis consists of two steps: (a) Dilute acid and steam convert the cellulose and hemi-cellulose to sugars; (b) The sugars are neutralized and fermented to produce ethanol. This process does not require acid recovery but relatively low conversion efficiencies are expected (50-60%) [13]. In addition, another drawback of this process is the degradation of sugars to form furfural and other undesirable by-products [11]. In contrast, for the concentrated hydrolysis process, the feedstock is dried to avoid dilution of the acid. Running this process at a moderate temperature prevents the degradation of sugars, resulting in higher yields. However, the large quantities of acid consumed and costly recovery process render this hydrolysis process unattractive [11].

As for the enzymatic hydrolysis, the feedstock is pretreated to allow the enzymes to penetrate the material and convert the cellulose to fermentable sugars which are then converted to ethanol by yeast fermentation. Since enzymes are highly specific, this process avoids the formation of unwanted by-products. Moreover, enzymatic reactions take place at relatively mild conditions and can achieve high product yields. As with other processes, the cons of this process is slower reaction rate coupled with costly enzymes [14].

Since most of biomass sources like straw and wood contain a large portion of material which cannot be easily converted by microorganisms to ethanol [15], an alternative to the above-mentioned process, gasification of biomass, is currently being explored as another alternative. Gasification is a thermal process that converts most of the lignocellulosic material into synthesis gas (syngas) [16]. Syngas is normally called producer gas when it is specifically generated from

a gasifier. Syngas, a mixture of primarily CO, H_2 and CO_2, is a major building block of fuels and chemicals. Anaerobic microorganisms can utilize these gaseous compounds as their carbon and energy sources to produce ethanol and other biofuels. By adopting this innovative process which involves the gasification of biomass to syngas, followed by fermentation of syngas to ethanol by a microbial catalyst, more carbon in the biomass can be converted to end products— such as ethanol. Another advantage of using syngas instead of dissolved sugar as a feedstock is that the use of gaseous substrates can shorten the hydraulic retention time, which can minimize substrate inhibition and enhance production formation [17]. This process can be simply illustrated as shown in Figure 1-3.

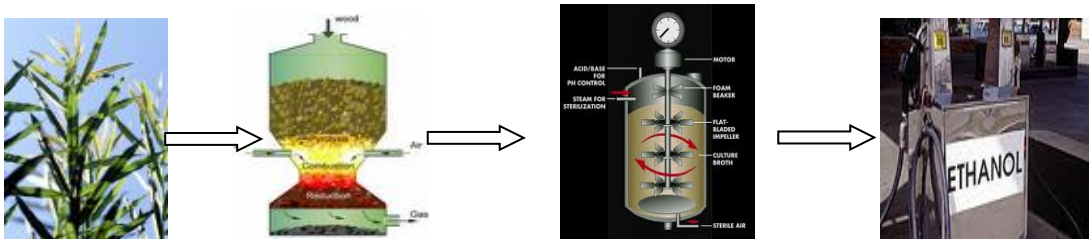

Biomass/coal Gasifier Bioreactor Product

Figure 1-3. Ethanol fermentation process via gasification

Currently, there are still other processes under development to produce ethanol, such as catalytic processes (or Fischer–*Tropsch* Synthesis). This above-mentioned biological process, although slower, has several advantages over metal catalytic processes, such as a higher specificity of the biocatalyst, higher yields, lower energy costs and generally greater resistance to poisoning and independence of a fixed H_2/CO ratio [17].

Cellulosic ethanol production costs have fallen from $5 a gallon in 2001 to $2.65 a gallon in 2011. However, to truly compete with crude oil imports, the Department of Energy estimates that cellulosic ethanol production must reach a targeted cost of $1.07 per gallon [18]. In the past, the metal catalytic process used precious metals as components of catalyst which rendered it cost uncompetitive. Recently, Synthenol Energy Corporation tried to use a non-precious-metal catalytic processor to produce ethanol at $1.58/gallon with natural gas as feedstock. This new catalyst will significantly drive down the ethanol production cost [19]. As for the syngas fermentation, Coskata is leading the way and has made significant technical progresses such as versatile feedstocks, streamlined bioreactor design, and vapor permeation process to separate ethanol from fermentation broth. Coskata's microorganisms can extract almost the entire energy value available in the incoming syngas stream, producing approximately 100 gallons of ethanol per dry ton of biomass input material [20]. These technological advances in Coskata's process have significantly increased its cost-competitiveness. Since each method has its own pros and cons, it is obvious that there is no single ethanol producing method that will prevail to the exclusion of others to meet the mandated ethanol requirements of 35 billions of gallons in 2022.

Recently, algal fuel has emerged as a promising alternative besides the biofuels obtained from the above-mentioned technologies. Algae's potential for biofuel production lies in its high energy content, fast growth rate and its ability to grow in water of varying quality. The oil content in algae can reach as high as 70% with oil levels of 20~50% on the average [21]. However, there are many obstacles to overcome to make algal fuel commercially feasible. Currently, algae cultivation simply for biofuel (such as biodiesel) production is not profitable by itself. The industry must produce other high-value co-products such as nutraceuticals, fertilizers and the biomass waste as a cellulosic ethanol feedstock [22]. Algae can be grown both in an open

or closed system known as bioreactor. Bioreactors have been tested as the most effective way to grow high-quality algae at the fastest pace. As for the open ponds, they are cheaper but susceptible to contamination. The US National Renewable Energy Lab (NREL) concluded that only the open system has the potential to meet large-scale production economically [23]. In the US, a few companies such as Sapphire Energy, Solazyme, and Orgin Oil are trying to make algal biofuel production economically competitive in a few years [22]. With so many challenges and technical problems to resolve, the European Algae Biomass Association estimated that it would take another 10 to 15 years to turn the research in the laboratory into large-scale industrial production [24].

1.4 Metabolic pathway of syngas fermentation

Anaerobic microorganisms such as *Clostridium ljungdahlii* [25], *Butyribacterium methylotrophicum* [26], *Clostridium autoethanogenum* [27], and *Clostridium carboxidivorans* [28] can utilize syngas as both their carbon and energy sources to produce biofuels. Syngas-fermenting bacteria use the acetyl-CoA pathway to produce ethanol, acetic acid, butanol and butyrate from syngas. The electrons required for the conversion is supplied either by H_2 or CO, via the hydrogenase or carbon monoxide dehydrogenase enzymes (CODH) respectively [29]. In addition, bi-functional CODH is responsible for the reduction of CO_2 to CO which serves as a carbonyl group to form acetyl-CoA. Another branch to form acetyl-CoA is a methyl group which can be obtained through a series of reductive reactions starting with CO_2. Acetyl-CoA synthase/CODH catalyzes the formation of acetyl-CoA from coenzyme A, a bound methyl group, and a bound CO group. Acetyl-CoA can be further reduced to acetate

and ethanol. It can also be reduced to butyrate and butanol via acetoacetyl-CoA which is formed from two acetyl-CoA molecules [17]. Acetyl-CoA also serves as precursor for cell macromolecules as well as an adenosine triphosphate (ATP) source as shown in Figure 1-4.

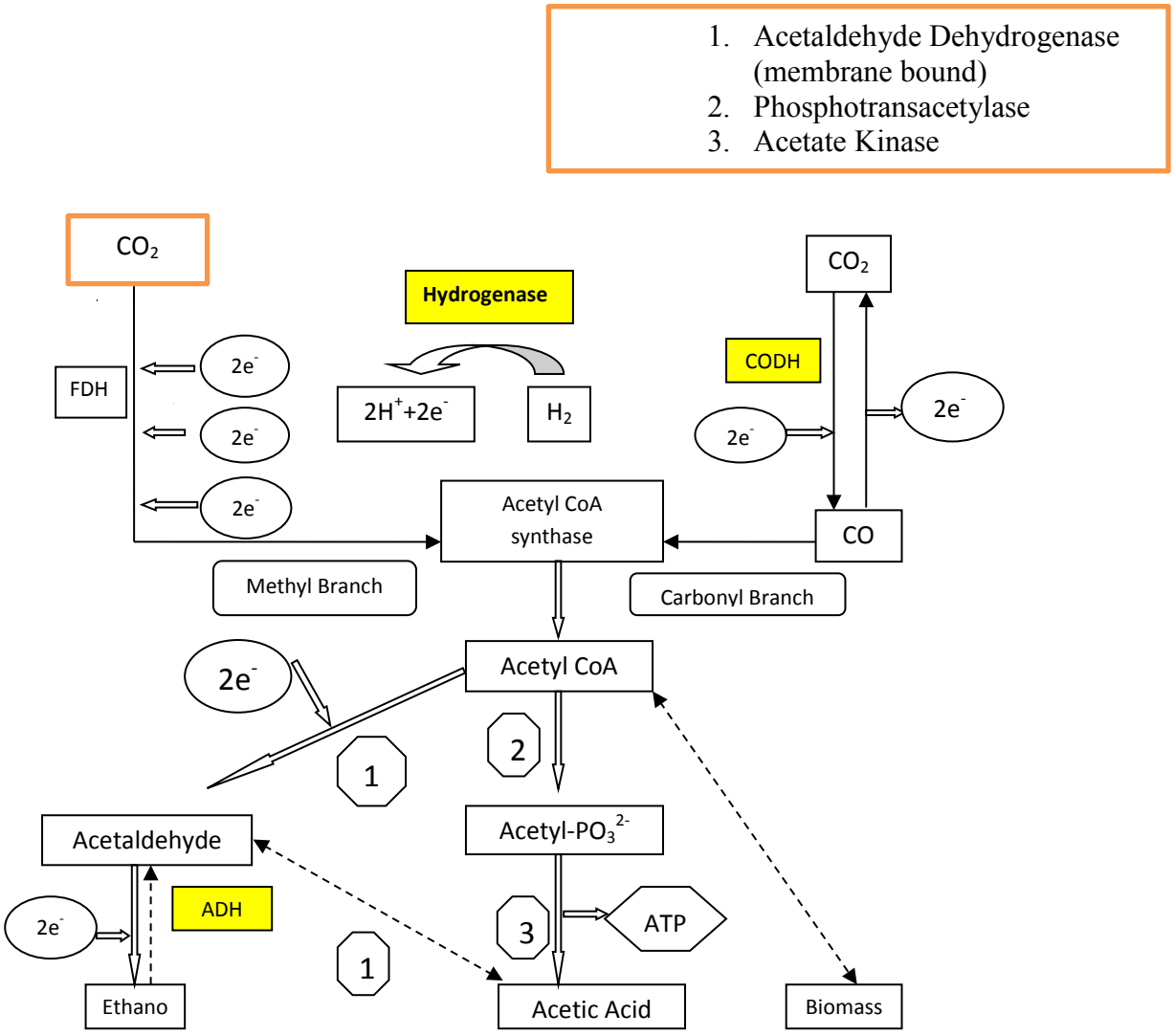

Figure 1-4. The enzymatic pathway to the formation of ethanol, acetic acid and cell mass, modified from [16]

1.5 Stoichiometry of ethanol and acetate production

The overall biochemical reactions that take place in the above-mentioned acetyl-CoA pathway appear below [30] .

$$6CO + 3H_2O \rightarrow C_2H_5OH + 4CO_2 \qquad \Delta H = -217.9 \text{ kJ/mol} \qquad (1)$$

$$2CO_2 + 6H_2 \rightarrow C_2H_5OH + 3H_2O \qquad \Delta H = -97.3 \text{ kJ/mol} \qquad (2)$$

$$4CO + 2H_2O \rightarrow CH3COOH + 2CO_2 \qquad \Delta H = -154.9 \text{ kJ/mol} \qquad (3)$$

$$2CO_2 + 4H_2 \rightarrow CH3COOH + 2H_2O \qquad \Delta H = -75.3 \text{ kJ/mol} \qquad (4)$$

As is evident, only one-third of the carbon from CO is converted into ethanol according to Equation (1). However, when Equations (1) and (2) are combined together, theoretically 2/3 of carbon from CO can be transferred into ethanol. Similarly, by coupling Equations (3) and (4), it shows that all the carbon from CO can be theoretically converted into acetic acid. In practice, the overall carbon conversion efficiency depends on multiple factors such as the raw syngas compositions (raw syngas, referred to as syngas in the remaining text), enzyme activities etc. For example, hydrogenase can utilize H_2 to provide the electrons (or reducing equivalents) needed for the production of ethanol. If the hydrogenase activity is inhibited, the decrease in reducing equivalents could potentially be offset by the utilization of CO via CODH at the expense of using CO for the product formation [31].

1.6 Challenges of ethanol production from syngas

For ethanol production via syngas fermentation, several issues must be addressed to assess the commercial feasibility of the process. These issues include carbon utilization efficiency, cell growth, ethanol production, product distribution, gas mass-transfer rates, effects of syngas impurities, energy output vs. input, and product recovery. The quality of syngas is being widely regarded as the number two challenge besides the gas-liquid mass-transfer limitation [30].

Biomass-generated syngas contains additional constituents such as ethylene, tar, sulfur and nitrogen compounds, which can affect the efficiency of the fermentation process by inhibiting the microbial catalysts. This project will identify and investigate the effects of two potential syngas impurities (benzene and ammonia) on the cell growth, enzyme activity (which plays a key role in the ethanol production) and ethanol production.

2. Literature Review

2.1 Current research progress on syngas fermentation

The conversion of biomass-generated syngas to biofuels using microorganisms has attracted more attention recently as a promising alternative for biofuel production mainly due to its use of non-edible, inexpensive feed-stocks. The major advantages of using this technology include: (a) utilization of whole biomass and elimination of the costly pre-treatment steps such as steam explosion, acid, alkaline or enzymatic hydrolysis to obtain fermentable sugars; (b) high selectivity of microbial catalysts; (c) independent of a fixed H_2/CO ratio required in Fischer-Tropsch synthesis; (d) bioreactors run at lower temperature and pressure; (e) no poisoning of noble metal catalysts. Since syngas fermentation for ethanol production based on the acetyl-CoA metabolic pathway is a microbial-mediated process, it can be affected by the following parameters such as types of biocatalyst, mass-transfer efficiency (reactor configuration), operating conditions (temperature, pH, redox potential etc.), gas partial pressure, gas compositions, and growth media [30, 32]. Typically, lower product yield from biocatalysts and poor mass-transfer efficiency of gaseous substrates (such as H_2, CO and CO_2) limit the commercialization of this process.

Since *Clostridium ljungdahlii* was discovered in 1987 to demonstrate the ability to ferment syngas into ethanol, tremendous progress has been made in the areas of process microbiology and process engineering such as the discovery of dozens of new biocatalysts and at least half a dozen of new bioreactor designs to improve mass transfer. In the following sections, new developments in each area will be elaborated.

2.2 Microbiology of syngas fermentation

As lignin in the biomass cannot readily be converted into biofuels by fermentation, gasification of these biomass feedstocks to produce syngas becomes feasible with the discovery of micro-organisms which can convert syngas into biofuels. Currently, there are two kinds of bacteria under investigation: mesophilic versus thermophilic microorganisms. Mesophilic microorganisms are the predominant bacteria which can produce short-chain fatty acids and ethanol from syngas. In addition, H_2 can be produced by carboxydotrophic hydrogenogenic bacteria [17]. Since thermophilic bacteria can grow at a higher temperature, less cooling of syngas from a gasifier is needed before feeding into a bioreactor. Furthermore, reactions run at elevated temperature can increase the conversion rate and benefit the separation of end products by distillation. As obvious, the disadvantage of running a bioreactor at a high temperature is the reduction of the solubility of syngas leading to even poorer mass-transfer efficiency. Generally speaking, even though it is advantageous to use thermophilic bacteria, currently few successful attempts have been made to produce organic compounds by consuming syngas. The discovery of new isolates which are capable of producing ethanol from syngas is demanding. Metabolic engineering is also a hot spot to increase the yield of targeted products and broaden the spectrum of end products.

2.3 Effects of mass transfer

It reaches consensus in literature that mass-transfer efficiency severely limits the conversion rate for syngas fermentation since nearly all the substrates are only sparingly soluble. However, there are a few steps to enhance the K_La (mass-transfer coefficient): (a) increase the bioreactor headspace pressure to increase the solubility of the substrates; (b) break large bubbles to micro-ones to increase the ratio of gas-liquid inter-facial area to volume; (c) increase gas or liquid flow rates; (d) seek innovative bio-reactor designs. Reactor configuration is closely related to the gas-liquid mass-transfer efficiency. Low cost and maintenance, high mass-transfer rates and easily scalable for commercial production are among some of the key concerns for bioreactor design.

Continuous stirred tank reactors (CSTR) are the most commonly used bioreactors, owing to its higher K_La at higher impeller speeds[26]. At higher impeller speeds, more micro-bubbles can be created, thus increasing the gas-liquid inter-facial area to volume ratio. Moreover, it will take longer for micro-bubbles to reach the headspace. More retention time and consequently higher K_La can be obtained. To cut down energy consumption, micro-dispersion systems could be designed with surfactant added into liquid as a stabilizer to increase the K_La. As reported by Klasson, among three bioreactors under his study, it was found that bio-trickling filter offered higher efficiency than both CSTR and bubble column reactors. It was proposed that approaching plug flow under his experimental conditions was the key for this high efficiency [33]. Besides the above mentioned three types of bioreactors, monolithic biofilm reactor, micro-bubble dispersion stirred-tank reactor and membrane-based systems have also been examined for syngas fermentation. For the monolithic biofilm reactor, the microbes grow on the media as a biofilm through which gaseous substrates can pass. It can be operated at atmospheric pressure, rendering

it economically viable. As for the micro-bubble dispersion stirred-tank reactor, basically it is a normal CSTR reactor equipped with a micro-bubble sparger. Bredwell mentioned that decreasing the bubble size will increase the internal pressure, leading to higher driving force. It was also proposed that the flux (the steady-state liquid phase concentration gradient at the surface of the bubble) increases as the diameter of the bubble decreases [26].

Of particular interest are membrane bioreactors. Composite hollow fiber membranes (HFM) can effectively facilitate the mass-transfer in aqueous media. In the HFM, syngas is diffused through the walls of the membranes reaching the biocatalysts grown as a film on the outer wall of the membranes, where the conversion takes place. One major drawback of this system is the media may owing to the variation in pressure enter the pores, leading to pore-wetting. However, membrane supported bioreactors (MSB) overcome this disadvantage by having a micro-porous layer to support a biofilm at the outer surface, while inserting a liquid impermeable layer (a silicone coating) in the gas contacting side (lumen) [34]. Overall, membrane bioreactors offer significant advantages in achieving higher yields and reaction rates. Moreover, these membrane reactors can be operated at elevated pressure with high pressure tolerable bacteria to significantly increase the mass-transfer rates, thereby having the potential to reduce the volume of the reactor.

2.4 Effects of redox potential

In addition to choosing the most suitable reducing agents for syngas fermentation, there has been on-going research studying the effects of redox potential levels on the cell growth and production distribution for more than a decade. Kim reported a strong relationship between redox

potential of broth and the cellular metabolism using *Clostridium acetobutylicum* in both batch and continuous cultivations. At a redox potential of -250 mV (SHE), the specific productivity of butyric acid and butanol reached their optimal levels. According to Kwong, cultural redox potential (CRP) would not only affect cell growth but also initiate the transition from acetogenesis to solventogenesis [35]. Girbal and his co-workers reported that artificial electron carriers such as neutral red could alter the electron flow by the formation of NADH thus leading to the increased production of alcohol. It was reported in Girbal's work that adding 1 mM neutral red into an acetogenic culture redirected the electron flow towards NADH production which could be responsible for the induction of the solventogenesis. Threefold increases in ethanol production with the addition of 1 mM neutral red to the cultures of C. acetobutylicum were recorded [36]. Lee's research group proposed that the relative ratio of NAD^+ to NADH was correlated to the redox state of a cell [37]. It is possible that the fluctuation of the redox levels in a bioreactor could affect the NAD^+ to NADH ratio and further impact on the cell growth and product formation.

Frankman observed that P11can only grow at around -200 mV (SHE) and the conversion from acetogenesis to solventogenesis was initiated with further drop of 50 mV in the redox level[38]. Most recently, Peng conducted a series of experiments to try to find the optimal redox level for the cell growth and ethanol production using P11. It was concluded that a more negative redox was conducive for the cell growth and conversion of acetic acid to ethanol [39].

2.5 Effects of temperature and pH

The temperature effect on syngas fermentation can be seen in two aspects. First, it can affect the cell growth and substrate utilization. Secondly, it can affect the solubility of gaseous

substrates in media. For mesophilic microorganisms, the bacteria can grow well within the temperature range from 37~40 °C. For thermophilics, it can grow within the temperature range from 55~80 °C. The reduction in gas solubility at a higher temperature can be partially offset by increased mass-transfer due to low viscosity [30].

The value of pH plays an important role in maintaining optimal activity of biocatalysts. The optimal pH for syngas fermentation microbes varies from 5.5~7.5 depending on the species being used. For example, pH between 5.8~6.0 is considered as the optimal pH for the growth of *C. ljungdahlii.* There is a strong relationship between pH and product distribution owing to the fact that pH can influence the regulation of the metabolism. A general trend of shifting the product spectrum from acidogenic to solventogenic phase had been observed with lower pH [34]. Since a lower pH will decrease the electron and carbon flow towards cell mass and increase ethanol production, currently running bioreactors at two stages with two different pH values has been under investigation. It has been tested in Peng's experiment that it is feasible to run a bioreactor at pH of 5.8 for the cell growth phase and switch to pH value of 4.5 for the ethanol production using biocatalyst P11 at a fixed redox level. The concentration of ethanol for this pH switch approach is about 9% or 58% higher than running bioreactors at pH value of 5.8 or 4.0 alone [39].

2.6 Effects of media compositions

Growth media typically comprises of minerals, trace metals, and vitamins, which are all vital for cell growth and product formation [40]. However, the selection of media recipe will depend on the biocatalyst being used and the end products being targeted. For instance,

American Type Culture Collection (ATCC) medium 1754 is suitable for the growth of *C. ljungdahlli* [30]. In the recent study, Saxena reported that ethanol yield can be increased up to 400% using *C. ragsdalei* just by optimizing the concentrations of trace metals in the media. This increased ethanol production was further substantiated by the increased enzymatic activities in the acetyl-CoA pathway and the higher cell growth rate. This pinpoints the importance of media optimization, warranting the improvement of the recipes for minerals and vitamins in the future. The optimum trace metal concentrations of Cu^{2+}, Ni^{2+}, Zn^{2+}, SeO_4^-, WO_4^- for ethanol production were 0, 8.5, 35, 7, 5 μM, respectively[40].

In 2011, Maddipati and his co-workers reported that expensive yeast extract (YE) can be replaced with much cheaper corn steep liquor (CSL) using *Clostridium* strain P11 for the syngas fermentation to produce ethanol. It was found that by adding 20 g L^{-1} CSL into 250 mL media, 32% more ethanol can be produced after 360 hours compared with adding 1 g L^{-1} YE. Surprisingly, substituting YE with CSL can also enhance butanol production by sevenfold. This highlights that YE can be replaced with lower cost nutrients such as CSL to drive down the overall cost for the media and improve the ethanol production simultaneously [41].

2.7 Effects of substrate pressure

The partial pressure of syngas constituents such as H_2, CO and CO_2 can vary significantly depending on feedstocks, gasification media (steam, oxygen, air), and gasification design. By observing the ethanol formation reactions mentioned in Chapter 1 Section 1.5, only one third of the carbon from CO can be converted into ethanol and 50% of carbon in CO can be converted into acetic acid in the absence of H_2. This can be explained that CO is being used both as a

carbon source and a source for reducing equivalents. As shown in Figure 1-4 in Chapter 1, reducing equivalents can be obtained either from hydrogenase or CODH. In the worst scenario, when hydrogenase is inhibited or H_2 is not present, reducing equivalents can only come from the oxidation of CO to CO_2 via CODH at the expense of reducing carbon conversion efficiency. Hurst and Lewis reported the effects of CO partial pressure (P_{CO}) on the cell growth and production distribution by varying the P_{CO} from 0.35~2.0 atm and keeping it constant in the headspace during the entire reactor run with the exclusion of H_2. Since H_2 was absence in this experiment, the reducing equivalents had to come from the source of CO. *Clostridium carboxidivorans P7* was used as the biocatalyst in this experiment. Key findings included: (a) with the increasing P_{CO} (from 0.35 to 2.0 atm) the maximum cell concentration also increased up to 440%; (b) ethanol conversion was switched from non-growth related to grow-related mechanism with the increasing P_{CO}; (c) acetic acid appeared to be produced in the latter growth phase for $P_{CO} \geq 1.35$ atm; (d) the production of acetic acid normalized by the cell mass decreased for $P_{CO} \geq 1.05$ atm compared with that for $P_{CO} \leq 0.70$ atm. It was proposed that P_{CO} and the P_{CO} to P_{CO_2} ratio can potentially affect the electron and ATP production, impacting on the metabolic pathway.

2.8 Gasification and effects of syngas impurities

Gasification is a process that converts organic or fossil-based carbonaceous materials into carbon monoxide, hydrogen and carbon dioxide. This is achieved by reacting the material at high temperatures (>700 °C) with a controlled amount of oxygen and/or steam. The resulting gas mixture is called syngas or producer gas and is itself a fuel. In a gasifier, the carbonaceous

material undergoes several different processes such as dehydration, pyrolysis, combustion, and gasification as detailed below.

- The dehydration process occurs at around 100 °C. Typically the resulting steam is mixed into the gas flow.
- The pyrolysis (or devolatilization) process occurs at around 200~300 °C. Volatiles are released and char is produced, resulting in up to 70% weight loss for coal.
- The combustion process occurs as the volatile products and some of the char reacts with oxygen to primarily form carbon dioxide and small amounts of carbon monoxide, which provides heat for the subsequent gasification reactions.
- The gasification process occurs as the char reacts with carbon and steam to produce carbon monoxide and hydrogen. This is what is meant for gasification in this work.
- In addition, the reversible gas phase water gas shift reaction reaches equilibrium very fast at the temperature in a gasifier. This balances the concentrations of carbon monoxide, steam, carbon dioxide and hydrogen.

Syngas may be produced from several sources including coal, oil shale, tar sands, heavy residues, biomass or natural gas using different technologies [15]. Currently, only a fraction of syngas is produced by solid fuel. However, since there is a large coal reserve in the United States and coal is compatible with biomass, syngas production from coal or co-firing biomass with coal by gasification will become an important technology in the future. Because of the diversities of

the feedstocks and other operating conditions, the compositions of syngas can vary to a great extent.

For this gasification-fermentation process, most research is still at the laboratory scale and uses "clean" syngas (clean "bottle-mixed" gases bought from suppliers) instead of syngas to conduct the fermentation process to produce ethanol. For the rapid commercialization of this new process, the syngas must be used. However, there is a great difference in the compositions between the "clean" syngas and syngas. The "clean" syngas is only made of CO, CO_2, and H_2. For the syngas, there are other gas components such as methane (CH_4), acetylene (C_2H_2), ethylene (C_2H_4), ethane (C_2H_6), benzene (C_6H_6), hydrogen sulfide (H_2S), sulfur dioxide (SO_2), ammonia (NH_3), nitrogen (N_2), carbonyl sulfide (COS), oxygen (O_2), water (H_2O), and mono-nitrogen oxides (NO_x) as well as tars and ashes. Some of these minor gases may interfere with the fermentation process [28, 29, 42-44].

Previously, the effects of syngas generated from gasifying switchgrass on the cell concentration and acid/ethanol distribution were investigated in comparison with "clean" bottled gases of similar compositions for CO, CO_2, and H_2. Biocatalyst *clostridium carboxidivorans (P7)* was used in this study. The following key findings were listed in literature: (a) the cell stopped growing after switching to syngas; (b) the cell could recover from its dormancy after switching back to clean syngas; (c) acetic acid was growth-related, while ethanol was non-growth related; (d) the cell stopped consuming H_2 [42]. In addition, biomass-generated syngas affected the acetic acid/ethanol product distribution. Tars were considered as the culprit for the cell dormancy and product redistribution. After a prolonged exposure, the biocatalyst can adapt to the tars. However, the addition of a 0.025 μm filter in the gas clean-up system can minimize this effect to negligible levels [28].

Further studies conducted by the same group showed that NO could inhibit the specific activity of the hydrogenase enzyme. It was shown that NO above 40 ppm was a non-competitive inhibitor of hydrogenase. Syngas containing NO could also increase the ethanol production and affect the cell growth compared to the "clean" bottled syngas. When the concentration of NO was above 150 ppm, the cells stopped growing. However, when the concentration of NO was less than 40 ppm, the cells were barely affected [29]. Do et al. reported that there are both inhibitory and stimulatory compounds in syngas, specifically mentioning tars and H_2S [45].

Despite the few studies demonstrating effects of biomass-generated syngas on fermentation systems, a comprehensive analysis of syngas impurities and their potential effects on microbial fermentation systems has yet to be undertaken. For microbes, the metabolic function can be impacted by even trace amounts of impurities. Understanding the potential impact of syngas impurities on the fermentation processes will be vital in developing syngas cleaning strategies and assessing the opportunity for variable feedstocks which can affect the profitability and commercial feasibility of syngas fermentation processes.

2.9 Research objectives

Objective I: Establish a database of syngas compositions

- Establish a database of syngas compositions from different types of gasifier using different biomass (and coal) feedstocks and operating at a variety of conditions. Since coal is supplementary to biomass, co-firing (biomass and coal) and coal alone are also included in this database.

- Obtain gas composition data of gasifiers from different institutions in the U.S. to augment the database.
- Make rational judgment on impurities to initially select potential impurities that may interfere with the fermentation process.

Objective II: Assess the effects of syngas ammonia on cell growth, enzymatic activities, and ethanol/acetic acid distribution.

The effects of ammonia impurity on the ethanol/acetic acid production and the cell growth will be tested. In some studies, ammonia gas will be added to clean "bottle-mixed" syngas (containing CO, CO_2, and H_2) to conduct a comparative study with clean gas alone. There are numerous enzymes in the microbial catalyst. These enzymes need to function at their maximal capacities so as to produce more ethanol. Specific activity is a good measurement of their functionality. The activities of two key enzymes (ADH and hydrogenase) will be assessed and compared. A kinetic model for the hydrogenase activity in the presence of ammonia impurity will be established by running experiments at varied concentrations of ammonium ion (NH_4^+).

Objective III: Assess the effects of benzene on cell growth, enzymatic activities, and product distribution.

The effects of benzene will be investigated by doping vaporized benzene into a "clean" syngas feeding stream. The most common benzene concentration identified from the syngas compositional database will be used to calculate the realistic benzene concentration in the media. This calculation will be confirmed with a GC/MS measurement. Experiments run at realistic and higher benzene concentrations will be conducted to study the effects of benzene on the cell

growth, end product distribution. In addition, hydrogenase and ADH specific activities will also be assessed.

2.10 Conclusions

From the literature review outlined in Section 2.8, it is necessary to investigate the effects of other potential impurities (such as NH_3, benzene, H_2S, SO_2) generated from gasifying biomass, coal, and coal/biomass on cell growth and ethanol production. Chapter 3 discusses several gasifiers and establishes a syngas compositional database. In Chapter 4, the accumulation of NH_3 in the media and the effects of NH_4^+ on the P11 cell growth and ethanol /acetic acid production are quantitatively defined. In Chapter 5, the inhibitory effects of NH_4^+ on hydrogenase /ADH activity are assessed and an inhibition model for hydrogenase is developed. In Chapter 6, vaporized benzene is doped into "clean" syngas feeding stream to simulate the compositions of the syngas from a gasifier. The effects of benzene on the cell growth and ethanol production are assessed accordingly. In Chapter 7, the effects of benzene on hydrogenase and ADH activities are studied and a model for benzene inhibition of hydrogenase is developed. Future research regarding the effects of trace impurities on syngas fermentation is mapped out in the final chapter.

3. Syngas compositional database and identification of potential impurities

3.1 Introduction

Biomass gasification to generate syngas used in anaerobic fermentation processes is one of several emerging technologies for the production of biofuels from biomass. The gasification-fermentation process can utilize a wide variety of lignocellulosic biomass such as prairie grasses, wood chips, and paper wastes, in addition to non-lignocellulosic biomass such as solid municipal wastes. For this syngas process, lignocellulosic feedstock is first gasified to produce syngas, primarily consisting of carbon monoxide (CO), carbon dioxide (CO_2), water (H_2O), and hydrogen (H_2), along with other hydrocarbons and residual species. Syngas has less than half the energy density of natural gas on a dry basis. It can be used in microbial fermentation and as a fuel source or an intermediate for the production of other chemicals such as methanol and NH_3. Syngas is also used as an intermediate in the production of synthetic petroleum for use as a fuel or lubricant.

Recently, research on co-gasification of woody biomass and coal has been conducted to improve the syngas quality. Although the primary components of syngas used in the fermentation process are CO, H_2, and CO_2, several impurities present in syngas may interfere

with the fermentation process. The composition of impurities and the associated impact on microbial processes can be a result of multitude aspects including gasifier design and performance, gas cleanup methods, and availability of impurities in solution. The impact of impurities may include but not be limited to cell toxicity, enzyme inhibition, varied redox potential, osmolarity, and pH.

3.2 Research objectives

This chapter reports work on the establishment of a database mainly for the impurities generated during the gasification process. This database was developed by extensive literature review and was augmented by other data collected from U.S. institutions. From the established database, a few key impurities, including their upper-limit concentrations, were identified for further study. Finally, the potential accumulation of syngas impurities in the fermentation media based on their solubility and their associated potential effects on the microbial fermentation process (e.g. cell toxicity, enzymatic inhibition and end product distribution) are outlined.

3.3 Feed stocks for gasification

Varied sources such as coal, natural gas, asphalt, visbreaker, petcoke, bitumen, oil shale, tar sands, heavy residues, liquid organic residues, refinery gas, vegetable biomass, animal biomass, black liquor or municipal waste can be fed into a gasifier to produce syngas [15] [46] . Currently, 55% of syngas produced commercially worldwide is still from coal [47]. Since there is a large coal reserve in the United States and coal is compatible with biomass, syngas production from coal or co-firing (biomass with coal) via gasification will likely become an important technology in the future.

Biomass differs from coal in many important ways including organic composition, inorganic composition, energy content and physical properties. Compared with coal, generally speaking, biomass typically is larger in size, has less carbon and more oxygen, more silica and potassium and less aluminum and iron, lower heating value, higher moisture content, and lower density. Woody biomass, a re-generable biofuel, contains virtually no sulfur and is being considered as a CO_2 neutral fuel [48]. As a feed, coal has many desirable properties such as high bulk density, high heating value and low moisture content.

Woody and low moisture content herbaceous plant species are the most efficient biomass sources for thermal conversion to liquid fuels [49]. As compared to coal, biomass gasification will incur a higher cost. On the other hand, a high percentage of sulfur and ash in the coal will generate more sulfur compounds than woody biomass gasification [45] [6]. Some researchers have experimented with co-feeding coal and biomass. Various reports show that co-feeding may provide advantages in gasification, including reduced CO_2, SO_x, and possibly NO_x emissions, and fuel flexibility [7, 8].

Co-firing not only can reduce fuel costs, minimize waste and reduce soil and water pollution but also can reduce the difficulties that occur in plant operation due to the formation of tar [50]. However, biomass can contain considerable alkali and alkaline earth elements and chlorine which promotes a different array of vapor and fine particulate deposition when mixed with sulfur compounds contained in coal [48]. Gasification by coal alone may have an organic fraction too low to support an auto-thermal gasification process. With the high volatile matter content in biomass, a synergic effect can be forged which makes co-gasification an attractive and economic option for the use of poor coals [51].

3.4 Gasifier design and performance

Moving-bed, fluidized-bed, and entrained-flow gasifiers are the most widely used gasifiers in research and industry [46, 52]. Moving-bed gasifiers, the simplest and most traditional of all gasifiers, typically operate in the co-current, counter-current, or cross-current mode. The disadvantage of moving-bed gasifiers is that they can produce a non-uniform temperature distribution [53]. However, co-current moving-bed gasifiers have the lowest tars of any of the working gasifier systems [54]. In fluidized-bed gasifiers, small particles of feed will become fluidized while sand, ash, or char can be utilized to enhance the heat transfer in the gasifier. Advantages of this gasifier include a more uniform temperature and the possibility of a higher feed rate. Finally, entrained-flow gasifiers typically operate in the co-current mode which provides a good carbon conversion rate. To ensure a good conversion rate and mass-transfer efficiency for all gasifiers, the reactor should be run at elevated temperatures and the feedstock particles should be reduced in size [46, 52].

From a recent study involved with co-feeding gasification, the conversion to gas increases with the biomass versus coal ratio while the conversion to char and tar decreases. With increasing biomass versus coal ratio, the H_2 composition decreases and the CO_2 composition increases; the CO and hydrocarbon compositions are independent of the biomass versus coal ratio [45]. From this study, it can be seen that the variability in types of gasifiers, feed (biomass and/or coal), and operating conditions can lead to a wide variation in the quality of syngas that can be used for further processing.

As is evident, even for the same feedstock under different operating conditions and different types of gasification technology, the gas compositions can vary to a great extent.

Therefore it is impossible to generate a database to cover all these variables. However, it is still feasible to survey the data and identify typical and upper limits in the main gas compositions and impurities.

3.5 Syngas impurities

There is a great difference in the composition between "clean" syngas used by research groups and industrially-produced syngas. Clean syngas is only composed of carbon monoxide (CO), carbon dioxide (CO_2), and hydrogen (H_2). Following gasification, the "raw" syngas will contain solids (mostly ash), condensable volatiles, and gases. The major gaseous species are CO, CO_2, H_2, H_2O, and CH_4 [46]. Other identified constituents include methane (CH_4), acetylene (C_2H_2), ethylene (C_2H_4), ethane (C_2H_6), benzene (C_6H_6), hydrogen sulfide (H_2S), sulfur dioxide (SO_2), ammonia (NH_3), nitrogen (N_2), hydrogen cyanide (HCN), carbonyl sulfide (COS), oxygen (O_2), water (H_2O), chlorine compounds, mono-nitrogen oxides (NO_x), tars, and ash. Most of the non-molecular nitrogen comes from fuel nitrogen. The fuel nitrogen is decomposed to NH_3 or HCN and, if conditions permit, it is oxidized to NO_x [46]. Chlorine compounds include metal chlorides and ammonium chloride.

To obtain the syngas compositions under varied operating conditions and different feedstocks, an extensive literature review of syngas composition was conducted. A syngas compositional database was developed for this work that included the upper limit concentrations to facilitate the choice of potential impurities affecting syngas fermentation. The database is shown as Tables A-1 to A-13 in the Appendix. To augment the database, several gasification facilities in the U.S. were contacted to obtain their gas compositions from their gasifiers.

Currently, twelve institutions conducting gasification studies have provided their data or technical reports. The names of these institutions are listed in Table 3-1.

Table 3-1. Gasification institutions contacted in the US

Name	Organization
Kevin Whitty (Associate Professor)	Institute for Clean and Secure Energy (ICSE) Department of Chemical Engineering The University of Utah 50 S. Central Campus Dr., Rm 3290 Salt Lake City, UT 84112 Tel. +1801-585-9388
Mr. Robert Ingraham (Analytical Scientist)	OSU (Oklahoma state university) Stillwater , OK 74078
John E. McDaniel (Senior Engineering Fellow)	Tampa Electric Company; Polk Power Station PO Box 111 Tampa, FL 33601 www.tecoenergy.com
Daniel J. Maloney (Director)	Energy System Dynamics Division National Energy Technology Laboratory 3610 Collins Ferry Road P.O. Box 880 Morgantown, WV 26507 Tel. 304-285-4629 Daniel.maloney@netl.doe.gov
Dr. Fernando Preto	The Canadian Renewable Energy Network (CanREN) 580 Booth Street, 13th Floor, Ottawa (K1A OE4) Ontario, Canada http://www.canren.gc.ca/
Gary J. Stiegel (Gasification Technology Manager)	National Energy Technology Laboratory 626 Cochrans Mill Road P.O. Box 10940, Pittsburgh, PA 15236 Tel: 412-386-4499 Gary.stiegel@netl.doe.gov
Dr. Robert C. Brown (Director)	Center for Sustainable Environmental Technologies 1140 Biorenewables Research Laboratory Iowa State University Ames, IA 50011 Tel: 515-294-7934 rcbrown@iastate.edu
Mr. Phil Amick (Commercialization Director-Gasification)	ConocoPhillips E-Gas™ Technology for Coal Gasification Phil.amick@conocophillips.com
David Denton (Sr. Director, Business Development)	RTI International 3040 East Cornwallis Road Post Office Box 12194 Research Triangle Park, NC 27709-2194, Tel: 919-541-6000
David W. Wakefield (President)	Econo-Power International Corporation 1502 Augusta, Suite 425, Houston, TX 77057 Email: dwakefield@epic-power.com. Tel: 713-979-5191
Vann Bush (Managing Director)	Gas Technology Institute 1700 South Mount Prospect Road, Des Plaines, IL 60018. Tel: 847-768-0500 www.gastechnology.org
Ripudaman Malhotra (Associate Director of the Chemical Science and Technology Laboratory)	SRI International 333 Ravenswood Avenue, Menlo Park, CA 94025-3493 Tel: 650-859-2000

Some gas compositions have been incorporated into the above-mentioned database. For example, in the Wabash River Coal Gasification Repowering Project [55], the compositions of hydrogen (32.21vol %), carbon dioxide (17.13 vol %), carbon monoxide (46.03 vol %), methane (1.99 vol %), hydrogen sulfide (83.36 ppmV), carbonyl sulfide (162.13 ppmV), nitrogen (1.9 vol %), argon (0.6 vol %) were reported and incorporated into this database.

From the established database, measured concentrations for various species in existing gasifiers have been identified. Table 3-2 shows the highest reported impurity concentrations.

Table 3-2. Highest reported measured concentrations of syngas impurities following gasification of biomass, coal, and biomass/coal (co-feeding)

Impurity	**Concentration**		
	Biomass (mol %)	**Coal (mol %)**	**Co-feeding (mol %)**
CH_4	15 [56] and [50]	7.4 [51]	7.5 [51]
C_2H_2	0.69 [57]	0.13 [57]	–
C_2H_4	5.3 [58]	0.1 [59]	0.8 [50]
C_2H_6	0.8 [42]	1.7 [51]	2.3 [51]
C_6H_6	0.6 [60]	–	–
$C_{10}H_8$	0.3 [60]	0.02 [61]	–
Tar	0.61 [60]	–	–
NH_3 & HCN	0.28 [60]	0.4 [61]	–
H_2S & COS	1.0E-4 [60]	1.0 [61]	–
SO_2	0.055 [62]	–	–
NO_X	0.123 [62]	–	–

3.6 Gas cleanup

Syngas impurities may or may not need to be removed depending upon the effect of the impurity on the biological process and the environment. Selection of commercial technologies suitable for syngas cleanup is mainly based on affordability and the ability to meet the end user specifications. Conventionally, cyclones are utilized for particulate removal. In general, tar removal technologies can be branched into primary (treatments inside the gasifier) and secondary (hot gas cleaning after the gasifier) methods. Secondary methods are widely adopted which can either be chemical or physical treatment including downstream tar cracking and use of cyclone, filters, rotating particle separator, electrostatic filter and scrubber. On the other hand, primary methods mainly focus on choosing the proper operating parameters and the use of proper bed additives during gasification [63].

Currently, tar cracking methods (including cracking within the gasifier) can effectively convert the heavy and light hydrocarbons to negligible levels. Water quench scrubbers can be employed for removal of ammonia and trace impurities. Accordingly, amine treatment can be utilized for sulfur and CO_2 treatment after cooling down the syngas. Zinc oxide beds can also be added for additional sulfur removal down to the low levels meeting the requirement for fuel synthesis [43]. For fermentation processes using CO_2 as one of the substrates, a different sulfur treatment method should be considered. Alternatively, H_2S can be removed from gasification processes by using regenerable mixed oxide sorbents such as Zinc titanates [64].

Hot catalytic gas conditioning downstream of the gasifier demonstrates more advantages than physical strategies (scrubber + filter). Catalytic strategies provide the possibility to transform the impurities (especially tars and ammonia) into useful gas compounds. By adding

cobalt and nickel promoters to Zn–Ti sorbents, both NH_3 decomposition and H_2S absorption will occur simultaneously. Most literature has centered on converting tars into useful gases on basic (calcined dolomites) and alumina-supported nickel catalysts at temperatures between 973 and 1173 K. The coupling of a guard made from calcined dolomites with a nickel catalytic unit can effectively reduce the tar levels to a few ppms [64].

3.7 Availability of impurities in solution

In order for an impurity to have an effect on a fermentation process, the impurity must be available to directly or indirectly interact with the microbe in solution. The availability of syngas impurities in a bioreactor after the cleanup process is influenced by the mass-transfer rate of the impurity. This is a critical issue in syngas fermentations as often substrates such as CO and H_2 are mass-transfer limited because of their low solubility in liquid [17] [26]. As previously shown in the syngas compositional database, the most prevalent compounds in syngas besides the major constituents (CO, CO_2, H_2) include carbonaceous species (CH_4, C_2^+ compounds, tars), nitrogenous species (NH_3, HCN, NO_x), and sulfurous species (H_2S, COS, SO_x).

The rate of mass-transfer of an impurity to solution is dependent on the thermodynamic driving force related to gas composition and solubility, the mass-transfer coefficient (k_L) affected by fluid dynamics, and the mass-transfer surface area (*a*) [26]. For similar reactor designs with similar mass-transfer area, the driving force and k_L are the key components that are highly impacted by the impurity. According to boundary layer theory under identical hydrodynamic conditions, k_L for different species can be related to the aqueous diffusivity (D) of species i and j

according to Equation (3-1) [65]:

$$\frac{(k_L)_i}{(k_L)_j} = \left(\frac{D_i}{D_j}\right)^{1/2} \quad (3\text{-}1)$$

Table 3-3. Predicted (using the Wilke-Chang correlation[a] [66]) or literature diffusivities (D_A) of syngas components and Henry's law (H) constants [67]

Compound	**Literature $D_A \times 10^9$(m^2 s^{-1}) 298 K**	**Predicted $D_A \times 10^9$(m^2 s^{-1}) 298 K**	**H (mol m^{-3} Pa^{-1}) 298 K, 101325 Pa**
CO_2	1.96 [68]	2.04	3.36E-04
CO		2.16	9.38E-06
H_2	4.80 [69]	3.42	7.70E-06
CH_4		2.21	1.38E-05
C_2H_6 (ethane)		1.58	1.78E-05
C_2H_4 (ethylene)		1.74	4.64E-05
C_6H_6 (benzene)	1.09 [69]	1.09	2.07E-03
$C_{10}H_8$ (naphthalene)		0.84	2.07E-02
H_2S	1.61 [68]	2.08	8.59E-04
COS		1.59	2.17E-04
SO_2	1.70 [68]	1.73	1.38E-02
NO		2.53	1.38E-05
NO_2	1.23	1.81	6.91E-05
NH_3	1.64	2.40	5.53E-01
HCN		2.03	1.18E-01

[a] Wilke-Chang equation: $D_{AB} = 5.88 \times 10^{-17}(m^2 s^{-1} K^{-1})[\Phi_B M_B/(kg\ mol^{-1})]^{0.5}\ T/[\mu/(Pa\text{-}s)][V_o/(m^3\ mol^{-1})]^{0.6}$ where D_{AB} is the diffusivity of solute at infinite dilution in $m^2\ s^{-1}$,μ is the solution viscosity in Pa-s, T is the absolute temperature in K, Φ_B is the association parameter (2.6 for water), M_B is the solvent molecular weight in kg mol^{-1},and V_o is the molar volume of solute at normal boiling point in $m^3\ mol^{-1}$.

Table 3-3 shows the predicted diffusion coefficients for syngas species according to the Wilke-Chang equation [66]. Additionally, reported diffusion coefficients from measurement are also shown for comparison.

As noticed from Table 3-3, the slowest diffusion coefficients are associated with the tar compounds. Diffusivities do not vary drastically, although among the syngas impurities, the diffusivity for NO is nearly three times the lowest diffusivity which is associated with naphthalene. According to Equation (3-1), k_L for NO would be about 70% greater than k_L for naphthalene. Thus, k_L differences appear to be small between impurities such that k_L differences may not play a major role in the potentially differing accumulation of impurities within the fermentation media.

In contrast, the driving force for mass transfer, which is related to the product of the species composition in the gas and the species solubility in solution, can have large variations among impurities. Thus, impurities with high gas composition and low solubility can potentially have similar driving forces as impurities with low gas composition and high solubility. Table 3-3 shows the Henry's Law constants (related to solubility) for syngas species. It is interesting to note that solubilities vary over several orders of magnitude and that the two least soluble compounds are CO and H_2 which are both required for cell growth and solvent production. However, CO and H_2 are also available at much greater partial pressures. By far the most soluble compound is ammonia (NH_3) which is also readily available in gasifiers. This makes NH_3 an important candidate for assessing its impact on syngas fermentation. Also, of interest are the tar compounds benzene and naphthalene which are quite soluble and present in appreciable concentrations, depending on the type of gasifier. Finally, although it is not the most soluble

compound, H_2S is approximately twice as soluble as CO_2 and is much more likely to be present than other sulfur containing gases.

3.8 Potential effects of microbial exposure to syngas impurities

Once an impurity transfers from the syngas into the bioreactor media, the impurity may directly affect the organism (e.g. cell toxicity, enzyme inhibition, product redistribution, etc.) or indirectly affect the fermentation process by changing process conditions (e.g. pH, osmolarity, redox potential, etc.). Many of the species found in syngas are known enzyme inhibitors. This effect can be particularly important because certain compounds may affect the specific activity of enzymes causing a disruption in the normal regulation of the organism's metabolism.

Since the concentration of a species in the producer gas does not fully indicate the potential for inhibiting or enhancing the ethanol process, a literature search has been conducted to find out all the potential impurities listed in Table 3-4 which have been shown to act as inhibitors of enzymes in biological processes. Specific interest was placed on finding enzymes that catalyze the reactions leading to the production of ethanol. Based on the Brenda Enzyme Database [71], several potential impurities have been identified as shown in Table 3-4. Table 3-4 reports known inhibitors for enzymes in the Wood-Ljungdahl pathway and other common enzymes in acetogens. In addition to the Brenda Enzyme Database, some papers [29, 44] also mentioned that H_2S, COS, NO, and NO_2 are potential impurities for biological process.

One difficulty regarding reported impurity effects, as noted for some impurities in Table 3-4, is that some reports are semi-quantitative at best and may not provide detailed information

(concentrations, kinetic parameters, etc.) that can aid in better understanding the potential impacts of syngas impurities on the fermentation process. It is therefore necessary to address more quantitative effects of syngas impurities on syngas fermentation. The focus of the remaining chapters is on the effects of NH_3 and benzene on the syngas fermentation process.

Table 3-4. Effects of potential impurities on common enzymes

Inhibitors	**Name of enzymes**	**Amount**	**References**
NH_3	Alcohol dehydrogenase (ADH), Amidase	NH_3 Inhibition at very high concentration for ADH.	[72], [73] and [74]
NO	Hydrogenase, Alcohol dehydrogenase (ADH)	For hydrogenase, at 150 ppm level, 100% inhibition, at 40 ppm level, negligible effect.	[28] and [29]
NO_2	Formate dehydrogenase (FDH), Nitrate reductase	1 mM, 5% inhibition for FDH; 1 mM, 20% inhibition of nitrate reductase activity	[75] and [76]
H_2S	Thiosulfate sulfurtransferase, l-ascorbate oxidase	At concentrations above 30 mM for thiosulfate sulfurtransferase; 1 mM, 97% inhibition for l-ascorbate oxidase.	[77] and [78]
COS	Carbon monoxide dehydrogenase (CODH)	Rapid-equilibrium inhibitor largely competitive versus CO, uncompetitive versus methyl viologen.	[79]
SO_2	Ascorbic acid oxidase (AAO)		[80]

3.9 Conclusion

Since the syngas composition from various biomass and coal blends will generate different gas compositions, an understanding of the positive or adverse effects of impurities from syngas on biofuel production will provide critical information regarding the need for efficient gas cleaning processes for commercialization. Although mass-transfer coefficients may not differ significantly among impurities, the impurity solubilities in liquid vary significantly. Thus, impurities with similar syngas compositions can result in significantly different amounts accumulated in fermentation media, which can have a great impact on the metabolic process.

As mentioned in Chapter 2 (literature review), several studies have shown significant effects of impurities, such as tars and nitric oxide, on cell growth and product distribution. Based on the work presented in this chapter, the first impurity of choice to study is NH_3 since NH_3 is a major species of coal and biomass gasification (Table 3-2) and it has been identified as an inhibitor of ADH at very high concentration (Table 3-4). It also has a very high solubility. After a close look at the syngas database, benzene is targeted as the second impurity to study since benzene can reach around 0.6 mol% of total syngas compositions and there is scant information about its potential effects on the biological processes.

4. Effects of ammonium ion on cell growth and ethanol production

4.1 Introduction

Since the biomass syngas composition generated from various biomass and coal blends will vary greatly in gas compositions, an understanding of the positive or adverse effects of impurities from biomass syngas on ethanol production will provide critical data regarding the need for efficient gas cleaning processes for commercialization. From the established database of biomass syngas compositions (Chapter 3), it was shown that ammonia can reach 0.28 mol% for biomass gasification and 0.4 mol% for coal gasification respectively [60, 61]. Since ammonia is very soluble in water at low pH, the ammonia ion (NH_4^+) concentration can increase with time if the biomass syngas goes untreated. This accumulation can potentially impact the fermentation process. In this regard, it is imperative to obtain quantitative assessment of the effects of NH_4^+ on cell growth and end product distribution, such as ethanol, in this research.

4.2 Research objectives

- Find the ammonia accumulation rates under varied gas feeding flow rates and experimental conditions

- From batch studies, find the threshold NH_4^+ concentration which can significantly affect cell growth and ethanol production
- Determine whether the threshold concentration in batch studies is similar for continuous bioreactor studies with pH control
- Investigate the root cause for cell growth inhibition: NH_4^+ versus osmolarity

4.3 Materials and methods

4.3.1 Microorganism and cell growth media preparation

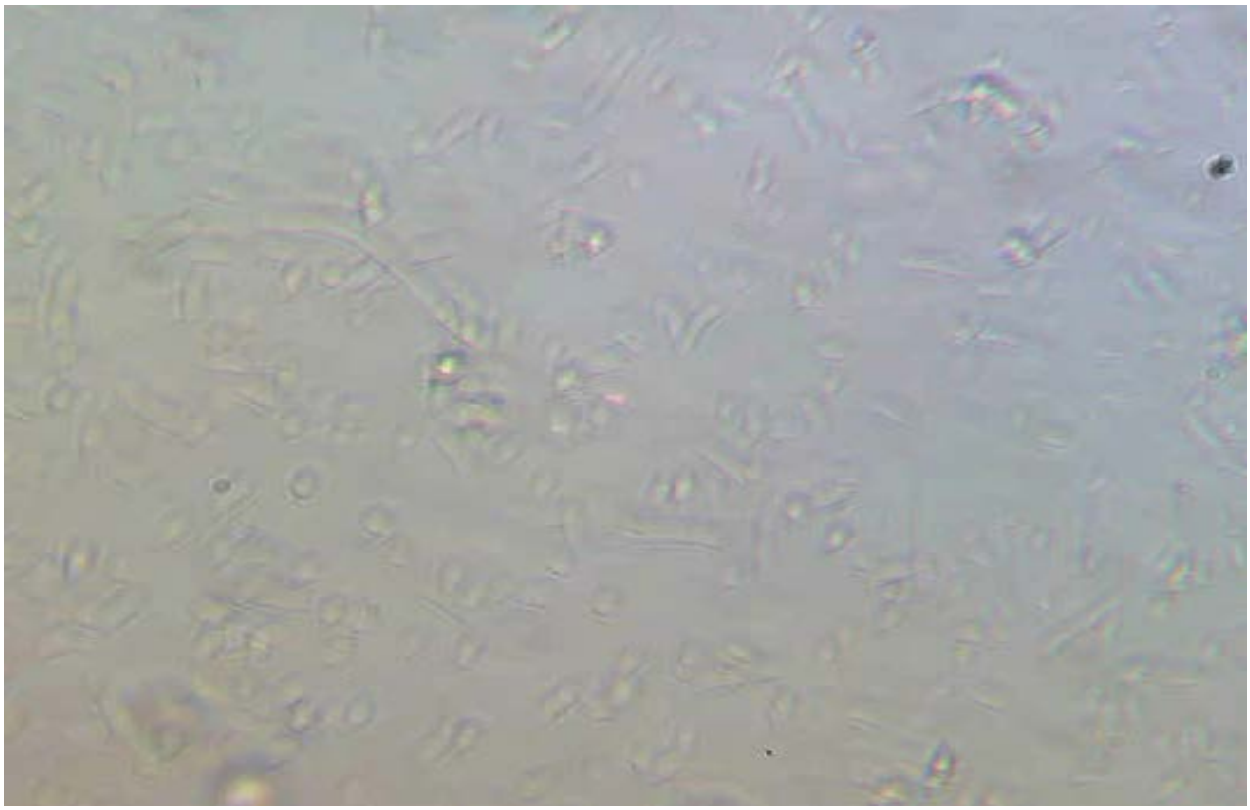

Figure 4-1. P11 bacteria were magnified via a microscope with 0.32 OD in media

Clostridium ragsdalei (Clostridium strain P11; ATCC PTA-7826), denoted as P11shown in Figure 4-1, was kindly donated by Dr. Ralph Tanner and can utilize syngas to produce ethanol and butanol [81]. The anaerobic bacteria were cultivated in a media containing per liter the following: 25 mL mineral stock solution, 10 mL metal stock solution, 10 mL vitamin stock solution, 10 mL calcium solution, 0.5 g yeast extract, 10 g 2-morpholinoethanesulfonic acid (MES), 10 drops Resazurin solution (redox indicator), 10 mL cysteine-sulfide solution (composed of 40 g L^{-1} L-cysteine and 40 g L^{-1} sodium sulfide nonahydrate) and balance DI water. The mineral stock solution contained (per liter) 20 g magnesium sulfate heptahydrate, 10 g potassium chloride, and 10 g potassium phosphate monobasic. The trace metals stock solution contained (per liter) 2 g nitrilotriacetic acid (adjusted to pH 6.0 using potassium hydroxide), 1 g manganese (II) sulfate monohydrate, 0.2 g cobalt (II) chloride hexahydrate, 0.2 g nickel (II) chloride hexahydrate, 0.1 g anhydrous sodium selenate, 0.8 g ammonium iron (II) sulfate hexahydrate, 1 g 99% zinc sulfate heptahydrate, 0.02 g sodium molybdate dihydrate, and 0.2 g sodium tungstate dihydrate. The vitamin stock solution contained (per liter) 0.005 g p-(4)-aminobenzoic acid, 0.002 g d-biotin, 0.005 g d-pantothenic acid hemicalcium salt, 0.002 g folic acid, 0.01 g sodium 2-mercaptoethanesulfonate (MESNA), 0.005 g nicotinic acid, 0.01 g pyridoxine hydrochloride, 0.005 g riboflavin, 0.005 g thiamine hydrochloride, 0.005 g thioctic acid, and 0.005 g vitamin B-12. The calcium solution was made by adding 10 g calcium chloride dihydrate into 1L of DI water. After mixing, the media pH was adjusted to 6.0 using a 5 M potassium hydroxide solution. Cysteine-sulfide solution (1% volume of media) was added into media to scavenge the residual oxygen after purging out most oxygen from media using N_2. The media was autoclaved at 121°C for 15 minutes. $Na_2S \cdot 9H_2O$ was purchased from EMD Chemicals (Gibbstown, New Jersey). Potassium hydroxide was purchased from Fisher

Chemicals (Fair Lawn, New Jersey). The rest of the chemicals listed above were purchased from Sigma-Aldrich (St. Louis, Missouri). The pH of the media was measured using an Oakton portable pH meter (Cole Parmer, Vernon Hills, Illinois) with an Accumet extra-long calomel combo pH electrode (Fisher Scientific, Pittsburgh, Pennsylvania).

P11 was passaged in 50 mL media (the same media noted above) three times using strict anoxic techniques in the presence of 40% CO, 30% H_2, and 30% CO_2 at 37 ºC. The headspace was purged with the gas mixture at 1.38 x 10^5 Pa (20 psig) gauge pressure and the gases were replaced on a daily basis. After each passage, the bottle containing inoculated media was placed in an incubator (New Brunswick Scientific) at 37 °C and 100 rpm. The third passage was labeled as the active cell source for each study.

4.3.2 Accumulation of NH_4^+ in media

A 4.06 mol% NH_3 gas (balance N_2) was used to assess NH_4^+ accumulation in the media as well as the efficiency at which NH_3 is converted to NH_4^+ when media is exposed to a purging gas containing NH_3. Initially, the 4.06 mol% NH_3 gas flowing at 3 sccm (standard cubic centimeter per minute) was mixed with syngas containing 40% CO, 30% H_2 and 30% CO_2 and flowing at 30 sccm. The final mixed gas contained 0.37 mol% NH_3. From published literature, it was found that the highest ammonia concentrations from a gasifier are 0.28 mol% for biomass feedstock [16] and 0.4 mol% for coal [17]. Thus, the simulated mixed gas was similar to gasifier concentrations. The mixed gas was bubbled into a 3-L bioreactor (containing 700 mL media) that was controlled at pH 6 and 37 °C and stirred at 150 rpm. After mixing, the media pH was adjusted to 6.0 using a 5 M potassium hydroxide solution. The media was autoclaved at 121°C for 15 minutes. After purging the oxygen from the media using N_2, a cysteine-sulfide solution (1% volume of media) was added into the media to scavenge the residual oxygen. Since NH_3

forms NH_4^+ upon entering the media, the NH_4^+ concentration was measured in the media as a function of time using an NH_4^+ electrode (Cole-Parmer, Model 27502-03) to obtain the accumulation rate.

The efficiency (η) at which NH_3 is converted to NH_4^+ was also assessed. The efficiency is defined as the NH_4^+ molar accumulation rate measured by the electrode divided by the NH_3 molar flow rate of entering gas (i.e. total gas flow rate multiplied by the concentration). Since the efficiency is a function of the gas flow rate, the efficiency using 4.06 mol% NH_3 gas without syngas dilution was also studied at gas flow rates of 10, 20, 30, 40, and 50 sccm. This higher gas concentration, which is 10x the typical gasifier concentration, provided additional data to assess efficiency. Actual flow rates, used in the calculation of efficiency, were obtained by converting the sccm flow rate to upstream flow conditions using standard conditions of 1atm and 294 K.

4.3.3 Batch and continuous cell growth studies

In this work, NH_4OH was used as the doping agent to study the effects of NH_4^+ on cell growth. NH_4OH was chosen as the NH_4^+ source instead of NH_4Cl to avoid any inhibitory effects from Cl^- [82]. NH_4OH (0, 0.08, 0.2, 0.4, 0.6, 0.8, 1.0, 1.2, 1.4, 1.6, 1.8, or 2 mL) was added into a flask containing 60 mL media to obtain final concentrations of 0, 20, 50, 100, 150, 200, 250, 300, 350, 400, 450, or 500 mM NH_4^+ in the media. Four separate studies were conducted to assess repeatability. The initial pH for all the media doped with NH_4^+ was adjusted to 6 using KOH or H_3PO_4 as needed. For the same concern, H_3PO_4 was chosen as the acid source instead of HCl to avoid potential inhibition effects from Cl^-. Afterwards, all the media bottles went through purging, injecting the cysteine-sulfide solution, and autoclaving as detailed in the previous Section (4.3.1). 6 mL of the active cell source cultivated in Section 4.3.1was injected into each

bottle (11 % of the final total volume). After purging the headspace with syngas mixture as detailed in Section 4.3.1, all the bottles were placed in an incubator to stimulate growth. Liquid samples were taken each day to measure their optical densities (OD).The pH profile for one of the runs was also monitored on a daily basis.

For the continuous bioreactor runs, there were two parallel bioreactors as shown in Figure 4-2. One was denoted as Bioreactor A (doped with NH_3 in the gas inlet) and one was denoted as Bioreactor B (control).

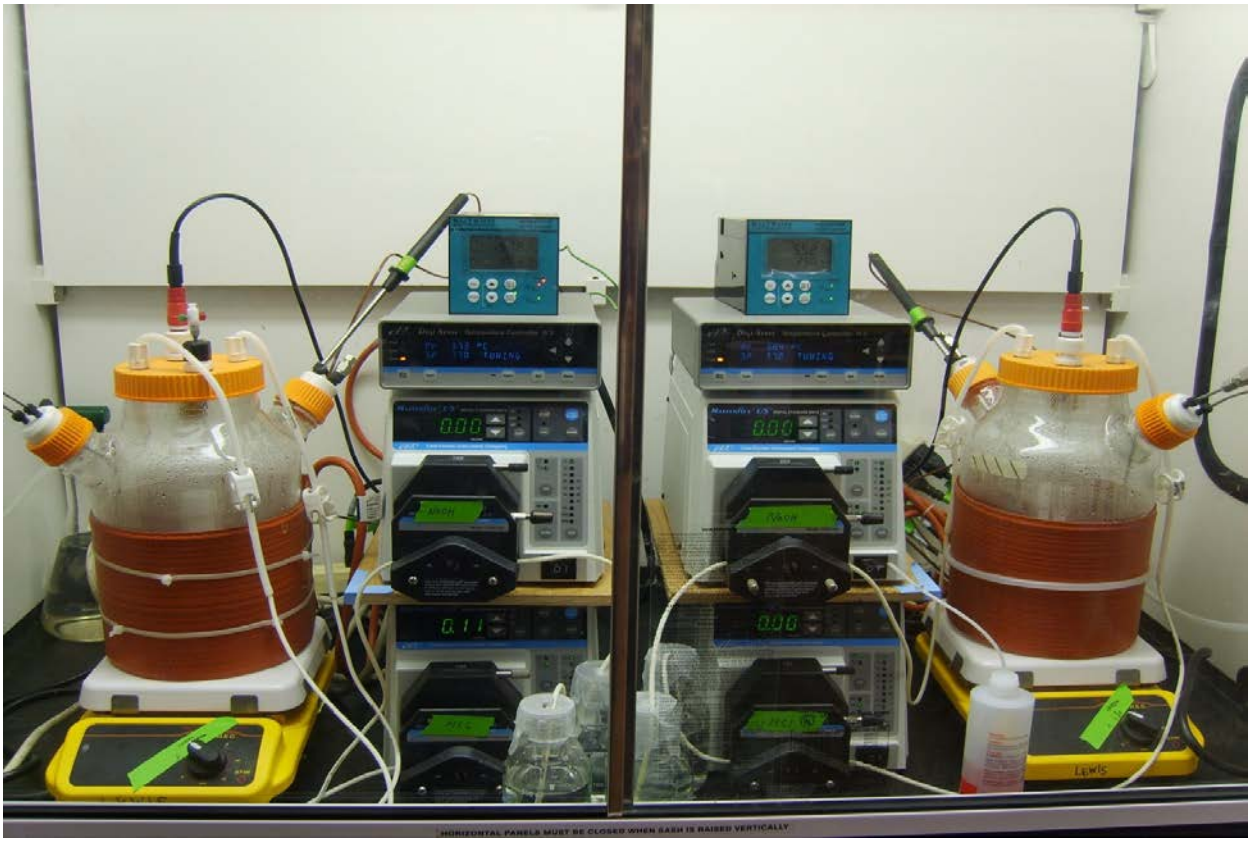

Figure 4-2. The lab-made Bioreactor A (doped with NH_3) and Bioreactor B (control) for continuous gas feeding runs with pH and temperature control

Both Bioreactors A and B were filled with 700 mL media under controlled pH of 5.5 and temperature of 37 °C. Initially, Bioreactor A was purged with an ammonia gas mixture (4.06% NH_3 with balance N_2) at 50 sccm and Bioreactor B was purged with pure N_2 at 50 sccm. The stirring bar was set at 175 rpm calibrated with an optical laser tachometer (Cole-Parmer, No. 08199-22). The concentration of NH_4^+ in the media was monitored with an ammonium ion electrode (Cole-Parmer, Model 27502-03) until a desired NH_4^+ concentration was obtained in Bioreactor A. For this study, five different concentrations of NH_4^+ (59, 110, 158, 204, and 227 mM) were targeted where each concentration was only studied one time. Under these experimental conditions, it took 8.5, 16, 23, 30, and 33 hours to reach [NH_4^+] of 59, 110, 158, 204, and 227 mM, respectively. After Bioreactor A reached the desired NH_4^+ concentration, both Bioreactor A and B were switched to syngas flowing at 33 sccm. After purging with syngas for 3 hours, 1% cysteine sulfide was injected into both bioreactors. Afterwards, a 10% (V %) cell inoculum was injected into both bioreactors. The OD for both bioreactors was measured immediately at the starting point. Liquid samples were taken at least on a daily basis to obtain the values for OD and hydrogenase activity. Hydrogenase activity is the focus of Chapter 5.

4.3.4 Effects of other ions on cell growth

From initial batch runs, it was found that the cell growth was substantially inhibited at 250 mM NH_4OH. Therefore, other NH_4^+-containing species were studied in the batch system to see if they had the same effect as NH_4OH. For this end, four additional chemicals besides NH_4OH were chosen as doping agents to assess their effects on cell growth. In separate bottles, 0.802 g of NH_4Cl, 1.981 g of $(NH_4)_2HPO_4$, 1.725 g of $NH_4H_2PO_4$, 1.982 g of $(NH_4)_2SO_4$, and 0.526 g of NH_4OH were added into a bottle (250 mL) containing 60 mL media and the pH was adjusted to 6. The resultant concentration for each chemical was 250 mM. One bottle without

any doped chemicals served as control. After that, all the bottles went through the same procedure as detailed in Sections 4.3.1 and 4.3.3 for inoculating cells. The OD was monitored on a daily basis for each bottle. However, the pH was not recorded for this particular run.

In addition to assessing other chemicals containing NH_4^+, potential osmolarity effects were also assessed for cell growth. Specifically, K_3PO_4 was added into media to match different levels of total osmolarity that were similar in the NH_4OH studies noted in Section 4.3.3. Thus, 0, 0.4, 0.8, 1.0, 1.4 mL of NH_4OH was added individually into 60 mL media resulting in 0, 100, 200, 250, 350 mM NH_4^+ respectively. KOH or H_3PO_4 was used to adjust media pH to 6. Taking all the ions in media and added KOH or H_3PO_4 into account, the resultant osmolarity was 41, 189, 340, 423, 567 mM for each NH_4OH bottle mentioned above. For comparison, 0, 0.35, 0.72, 0.91, 1.24 gram of K_3PO_4 was added into 60 mL media resulting in 0, 27, 56, 72, 98 mM K_3PO_4, respectively. Counting all the ions in media, the final resultant osmolarity was 41, 186, 338, 418, 564 mM for each bottle doped with K_3PO_4.

Afterward, all the bottles containing media doped with either NH_4OH or K_3PO_4 went through the same cell growth preparation protocol as mentioned in Section 4.3.1. All the bottles were inoculated with 6 mL (10% volume) of the active cell source. The remaining experimental procedure followed the one outlined in Section 4.3.3. Liquid samples were taken daily to measure the OD. The pH time profiles for both NH_4OH and K_3PO_4 were recorded.

4.3.5 Product distribution study

To find out whether NH_4^+ or osmolarity has an effect on ethanol and acetic acid distribution, $NH_4H_2PO_4$ or KH_2PO_4 was doped into 60 mL media to assess product formation in the presence of these species. For the $NH_4H_2PO_4$ study, 0.69 or 1.38 grams was added into

60 mL media resulting in 100 or 200 mM of $NH_4H_2PO_4$, respectively. The pH of the media was adjusted to 6 using KOH. Taking into account the osmolarity contributed from KOH (16 or 25 mM) and the media components (38 mM calculated from media components noted in Section 4.3.1), the corresponding total osmolarity was 276 and 500 mM respectively, Similarly, for KH_2PO_4, 0.816 or 1.632 grams was added into 60 mL media resulting in 100 or 200 mM of KH_2PO_4, respectively. The corresponding total osmolarity was 271 and 484 mM respectively, taking into account the osmolarity coming from KOH (15 or 28 mM) and media components (38 mM). Standard media without any doping agents was used as the control. The preparation and experimental procedures were the same as described in Sections 4.3.1 and 4.3.3. Liquid samples were taken for analysis of the OD and product concentrations. All the chemicals (NH_4OH, K_3PO_4, $NH_4H_2PO_4$, and KH_2PO4) were ordered from Sigma-Aldrich. In addition, total osmolarity in media was measured by a VAPRO® vapor pressure osmometer (Model: 5520) to check the consistency with the calculated total osmolarity in media.

4.3.6 Liquid analysis

For all studies, liquid samples were collected by 3mL cuvettes to measure the optical density (OD) using a Shimadzu UV-1700 spectrophotometer (TCC-240A, Shimadzu Scientific Instruments, Columbia, Maryland) at 660 nm wavelength. The OD is proportional to dry cell concentration (~0.43 dry cell g/L per OD unit) as obtained from a calibration chart valid for the OD ranging from 0 to 0.4 [32]. For OD above 0.4 units, the liquid sample was diluted into that range. For the product distribution study, part of the liquid sample was transferred into a 1 mL vial and centrifuged at 14000 rpm for 10 minutes. The cell-free supernatant was stored in a fridge and later analyzed for ethanol and acetic acid concentrations using a Shimadzu 2014 Gas Chromatograph (Shimadzu Scientific Instruments, Columbia, Maryland) with a flame ionization

detector and a Restek Porapak QS 80/100 Shimadzu 14A column (Bellefont, Pennsylvania). Nitrogen, utilized as the carrier gas, hydrogen, and air were maintained at flow rates of 35, 50, and 400 mL/min respectively. The operating temperatures of 220, 200, and 250 °C were respectively maintained for the injection port, oven, and detector.

4.4 Results and discussions

4.4.1 Accumulation of NH_4^+ in media

To imitate the NH_3 syngas composition from a commercial gasifier, 0.37 mol% NH_3 in a gas feed stream was initially studied. Figure 4-3 shows the measured NH_4^+ concentration in media over time at a total gas flow rate of 33 sccm. The NH_4^+ concentration increased at a linear rate of 0.31 mM/h several hours after initiating the flow. After 330 hours, the NH_4^+ concentration was approaching 140 mM.

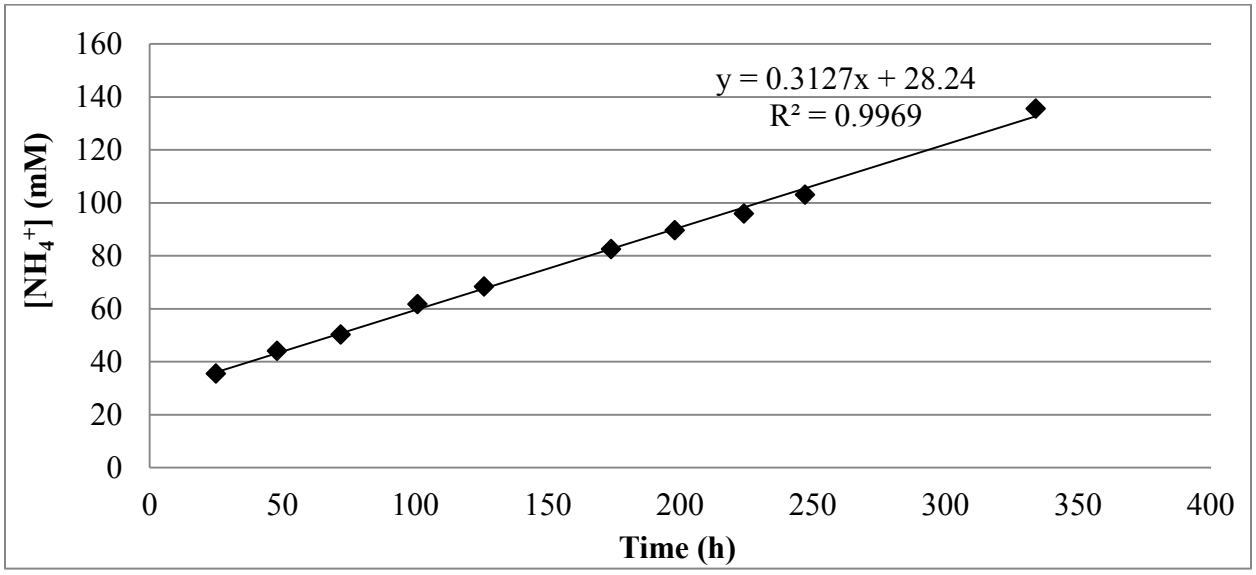

Figure 4-3. NH_4^+ accumulation time course with 0.37 mol% NH_3 in a gas feed stream

As shown in Table 4-1, studies using varying total gas flow rates with a 4.06 mol% NH_3 gas showed that the fraction of NH_3 entering a 3-L bioreactor (containing 700 ml media) that was converted to NH_4^+ (denoted as efficiency η) ranged from 70-96%, depending upon the gas flow rate.

Table 4-1. NH_3-to-NH_4^+ conversion ratio under different inlet gas flow rates for the fixed NH_3 concentration

Inlet gas flow rate (sccm), 4.06 % NH_3 with balance N_2	10	20	30	40	50
Inlet flow rate of NH_3 (mM/h)	1.01	2.02	3.03	4.04	5.05
Measured NH_4^+ accumulation rate in media (mM/h)	0.98 / 0.91	1.87 / 1.84	2.52	3.05	3.56
Residence time of bubble (τ_g^*), seconds	0.155	0.078	0.052	0.039	0.031
Efficiency (η %) of NH_3 accumulation rate to inlet flow rate	96.3 / 90.2	92.7 / 91.2	83.2	75.4	70.5

Measured ammonia absorption efficiency values as shown in Table 4-1 are plotted versus the bubble residence time (τ_g^*) in Figure 4.4. Here, τ_g^* represents the liquid volume divided by the gas flow rate. As expected, η increases with increasing τ_g^*. For the reactor in this study, η approaches 1 at $\tau_g^* > 0.1$ second. These results show that a majority of NH_3 entering a reactor can be absorbed into the liquid media and converted to NH_4^+. As can be seen for the flow rate studies near 33 sccm ($\tau_g^* = 0.04$ s), η appears to have a slight dependence on the gas composition (which varied from 0.37 to 4.06%). In contrast, the accumulation rate depends strongly upon the NH_3 gas composition. For example, the accumulation rate of 0.31 mM/h at 0.37 mol% NH_3 gas

and 33 sccm increased to 3.5 mM/h (data not shown) at 4.06 mol% NH_3 gas and 30 sccm. Thus, as expected, increasing the combined concentration and flow rate by nearly 100% resulted in a similar increase of the accumulation rate (113%).

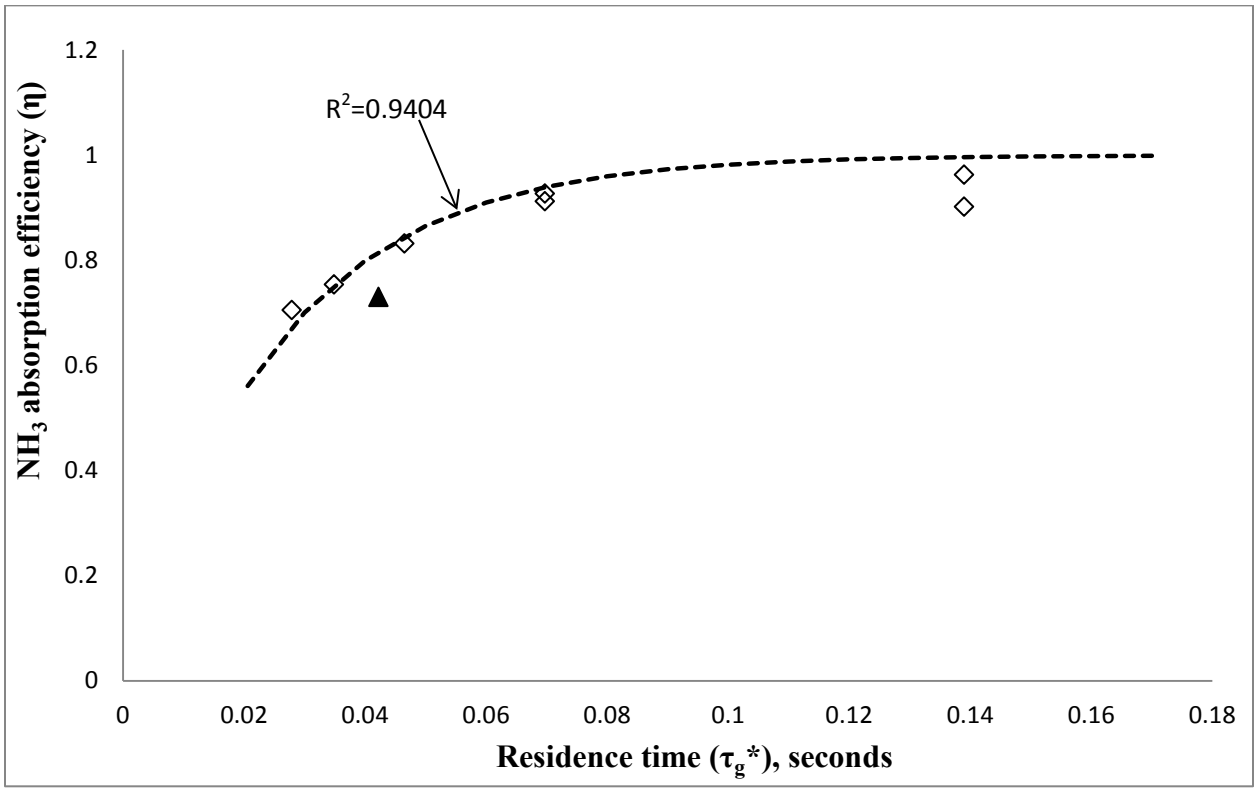

Figure 4-4. NH_3 absorption efficiency (η) versus residence time (τ_g^*) for 4.06% NH_3 (◇) and 0.37% NH_3 (▲) in the 3-L bioreactor. The dotted line represents the solution of Equation 4-3 applied to the definition of efficiency.

Since, for this study, the NH_3 delivery occurred via bubbling through the liquid while the liquid was continuously stirred, η was modeled using a material balance of one bubble rising via plug flow through a well-mixed solution according to:

$$\frac{dC_g}{d\tau_g} = -k_o a(C_g - C_l) = -k_o a(C_g) \qquad (4\text{-}1)$$

Here, τ_g is any residence time represented as the distance traveled by the rising bubble divided by the bubble velocity, C_g is the NH_3 concentration in the bulk gas bubble, C_l is the NH_3 dissolved concentration in the bulk liquid, and k_oa is the overall mass-transfer coefficient. For this model, it was assumed that the bubble velocity is constant. Since the bubble only contains at most 4.06% NH_3 (approximately a 1.5% change in the bubble radius if all NH_3 disappears), it is reasonable to assume a constant bubble size and velocity during the short residence time. It was also assumed C_l is negligible based on the following analysis. For a bubble at 298 K and 1 atm with 4.06% NH_3 gas, the NH_3 concentration in the bubble (C_g) would be1.66 mM. Furthermore, at equilibrium, the fraction (f) of total NH_3 species in the liquid (both dissolved NH_3 and NH_4^+) that is in the form of just NH_3 is represented by [83]:

$$f = \frac{1}{1+10^{(10.06-pH-0.0327*T)}} \tag{4-2}$$

where T is temperature (°C). Under the experimental conditions of pH=5.5 and 37 °C, f is 4.5 x 10^{-15}. Since the upper NH_3 absorption capacity (which includes NH_4^+ formation) is on the order of 10^4 mM as noted in this section, then the upper dissolved NH_3 concentration in the liquid is on the order of 10^{-11} mM. Thus, C_l is negligible compared to C_g. Essentially, the NH_3 entering the liquid reacts instantaneously. Since NH_3 is very soluble in water and rapidly forms NH_4^+, the liquid film mass-transfer resistance is very small in comparison with the resistance by the gas film. Therefore, the overall mass-transfer coefficient k_oa is approximately equal to k_Ga [84] such that integration of Equation 4-1 yields

$$\frac{C_{g,out}}{C_{g,in}} = e^{-(k_Ga)\tau_g^*} \tag{4-3}$$

Here, τ_g^* is the gas residence time which represents the rising distance divided by the bubble velocity (or the liquid volume divided by the gas flow rate). For the reactor used in the study, the liquid height was measured as ~3.3 cm since the bubbles entered near the bottom of the reactor. As an approximation, the bubble velocity was obtained by dividing the actual gas volumetric flow rate by the area of the bubble orifice (0.008 cm^2). For this integration, $k_G a$ was considered constant since the bubble size wouldn't change much and liquid velocities adjacent to the bubble would have little effect on the gas film resistance. Since the efficiency is $\eta = 1-(C_{g,out}/C_{g,in})$, the definition of η along with Equation 4-3 was used to fit the data for the 4.06% NH_3 studies as shown in Figure 4-4. Although more rigorous models can be developed, the simplistic model (although dependent upon the type of reactor) provides a realistic framework for understanding how η is strongly associated with τ_g^*. The fitted value of $k_G a$ is 36 s^{-1}. Since the model equation and measured values are in very good agreement as indicated by the R^2 value, the model does a reasonable job in characterizing the NH_3 conversion efficiency.

Since Equation 4-3 can fit experimental data quite well, it can be used to estimate the ammonia absorption efficiency under typical residence times for industrial bioreactors. Since syngas fermentation technology is still being assessed at pilot scales, industrial bioreactor parameters are not readily available in literature. Hence estimates for a 70 L pilot-scale bioreactor were performed with Equation 4-3 to see how much ammonia could potentially be absorbed into media for a previously reported study [85]. For this scenario, a syngas flow rate of 0.9 standard liters per minute (SLPM) was used, leading to τ_g^* = 78 minutes. According to Equation 4-3, 100% ammonia absorption efficiency can be obtained. According to the study, a lower syngas flow rate was used owing to the limitations on the syngas storage capacity. Even

with a 3-fold higher syngas flow rate, the ammonia absorption efficiency would still be close to 100%.

From the above scenario and the studies reported in this work, a majority of NH_3 entering a reactor has a high probability of being absorbed into the liquid media and converted to NH_4^+. Although the accumulation rate will depend upon the gas flow rate, the NH_3 composition in the gas, the liquid recycle ratio, the introduction of fresh media, and the reactor design, this work shows that NH_3 is very soluble in water and can be converted to significant levels of NH_4^+ over time to potentially affect the performance of an anaerobic fermentation system. The potential NH_3 absorption capacity is extremely high since the solubility of NH_3 in water is around 31% (w/w%) at 25 °C [86]; this is equivalent to 1.71×10^4 mM, which is much higher than used in this study.

Based on our established data that ammonia can reach 4000 ppm and most ammonia will be absorbed into media as shown in Table 4-1, ammonia accumulation can be estimated in a continuous gas feeding bioreactor for different τ_g^*. Figure 4-5 shows the accumulation of NH_4^+ for three different values of τ_g^* under the ideal condition that 100% of NH_3 is converted into NH_4^+ upon entering media (i.e. $\eta=1$). As mentioned for the 70 L pilot-scale bioreactor in this section, owing to its limited gas storage and much lower gas flow rate, the associated $\tau_g^* = 78$ minutes should be considered too long. Therefore, for this practical modeling, shorter τ_g^* were chosen. From literature, an economically acceptable τ_g^* for an industrial fermenter is in the range of 10 to 20 minutes [87]. As seen in Figure 4-5, it is obvious that for a typical bioreactor run cycle, NH_4^+ can easily reach more than 250 mM.

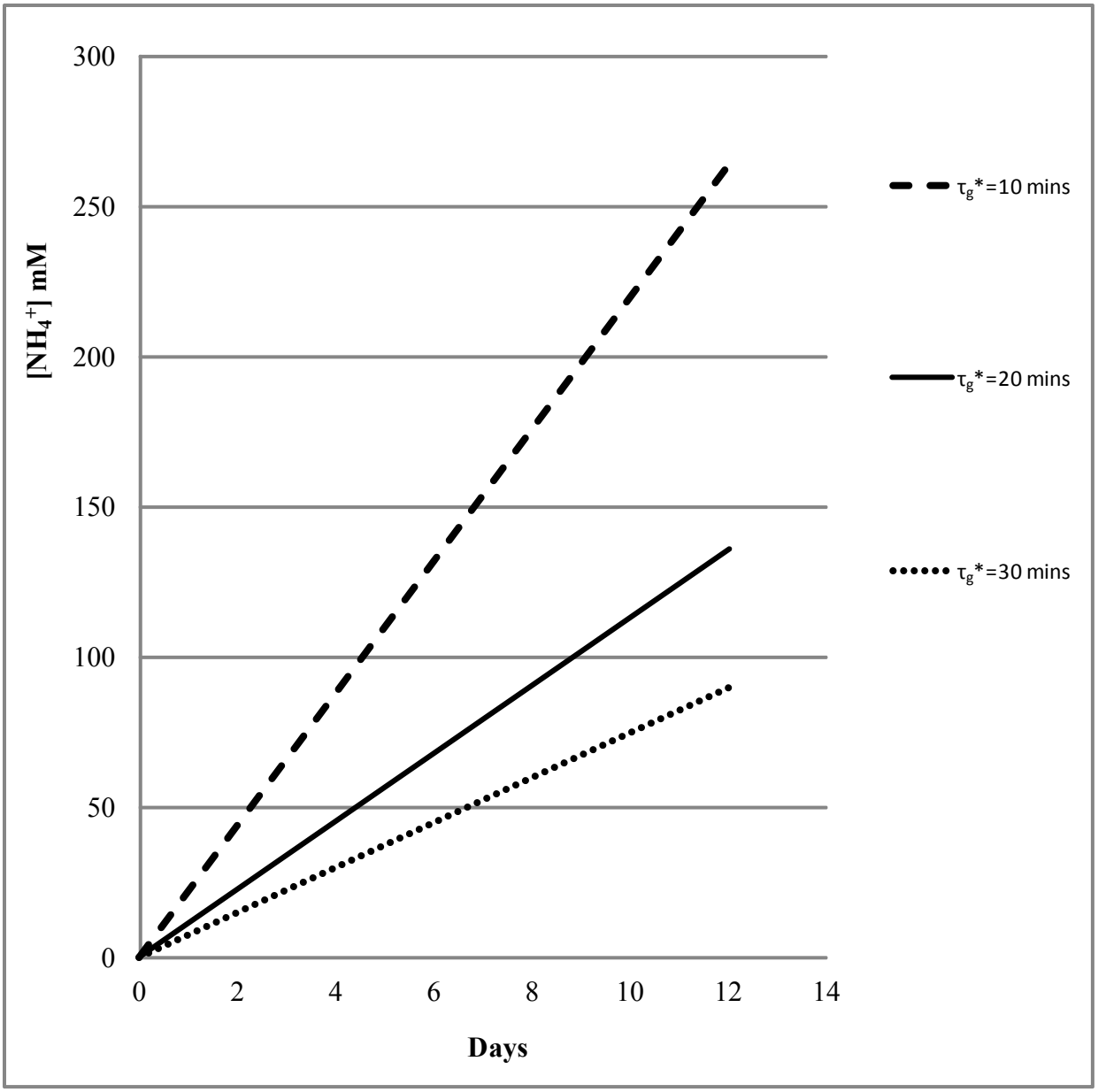

Figure 4-5. NH_4^+ accumulation under varying residence times with 4000 ppm NH_3 in the gas feed stream. Residence times (τ_g*) of 10, 20, and 30 minutes are shown.

Since cells can utilize the nitrogen element from NH_4^+ as a nutrient, the NH_4^+ consumption rate in the presence of cells was also measured in a preliminary experiment. The purpose was to assess whether the accumulation rates shown in Figure 4-5 would be suppressed

if cells were present. Preliminary results showed the NH_4^+ accumulation rate to be comparable in cell-free media and in media containing cells. Therefore, NH_4^+ has the potential to accumulate to an appreciable extent during syngas fermentation.

4.4.2 Effects of [NH_4^+] on cell growth with batch bottle runs

Eleven different concentrations of NH_4OH were added into media resulting in [NH_4^+] ranging from 0 to 500 mM. To obtain statistically reliable results, these bottle batch studies doped with [NH_4^+] were repeated four times. All four runs showed similar trends as shown in Figure 4-6. It was found that at very low [NH_4^+] (0~50 mM), cell growth was not adversely affected by NH_4^+. In two of the four runs, cell growth was even slightly stimulated by NH_4^+ at these low concentrations when compared with the control. As seen from these figures, cell growth was inhibited to different degrees when [NH_4^+] varied from 100~200 mM. When [NH_4^+] reached 250 mM, cell growth was significantly inhibited but began to increase after a long period of delay. Thus, it is possible that the cells have the ability to adapt although the study at 350 mM showed little adaptation. It should be noted that the above results were consistent with all four runs.

To see the trend clearer for the four repeated runs, Figure 4-6 was graphed as one figure (see Figure 4-7). Although it is difficult to distinguish a specific profile for a particular concentration, it was clear that there were two regions separated by the [NH_4^+] of 250 mM.

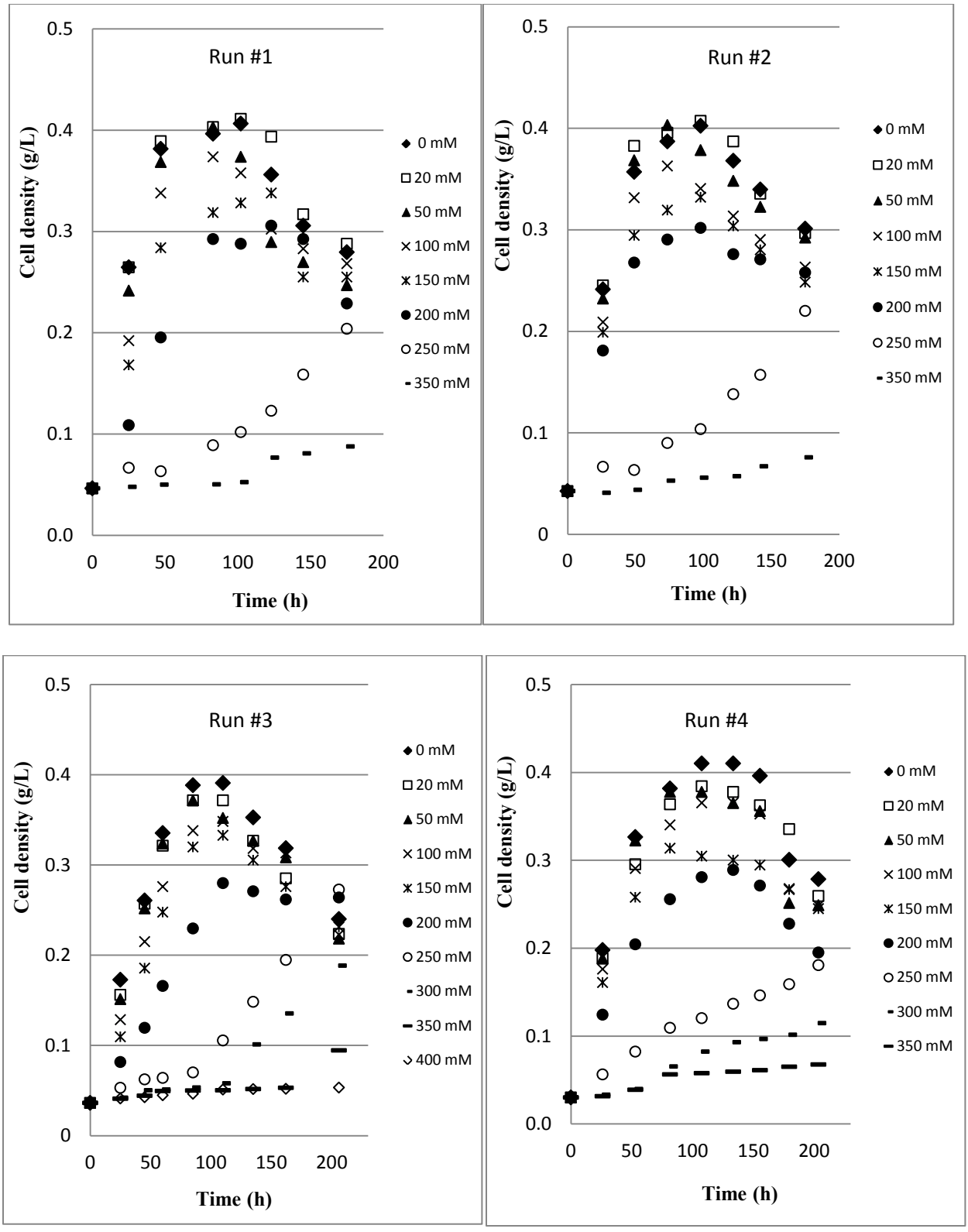

Figure 4-6. Cell growth time course under varying concentrations of NH_4OH

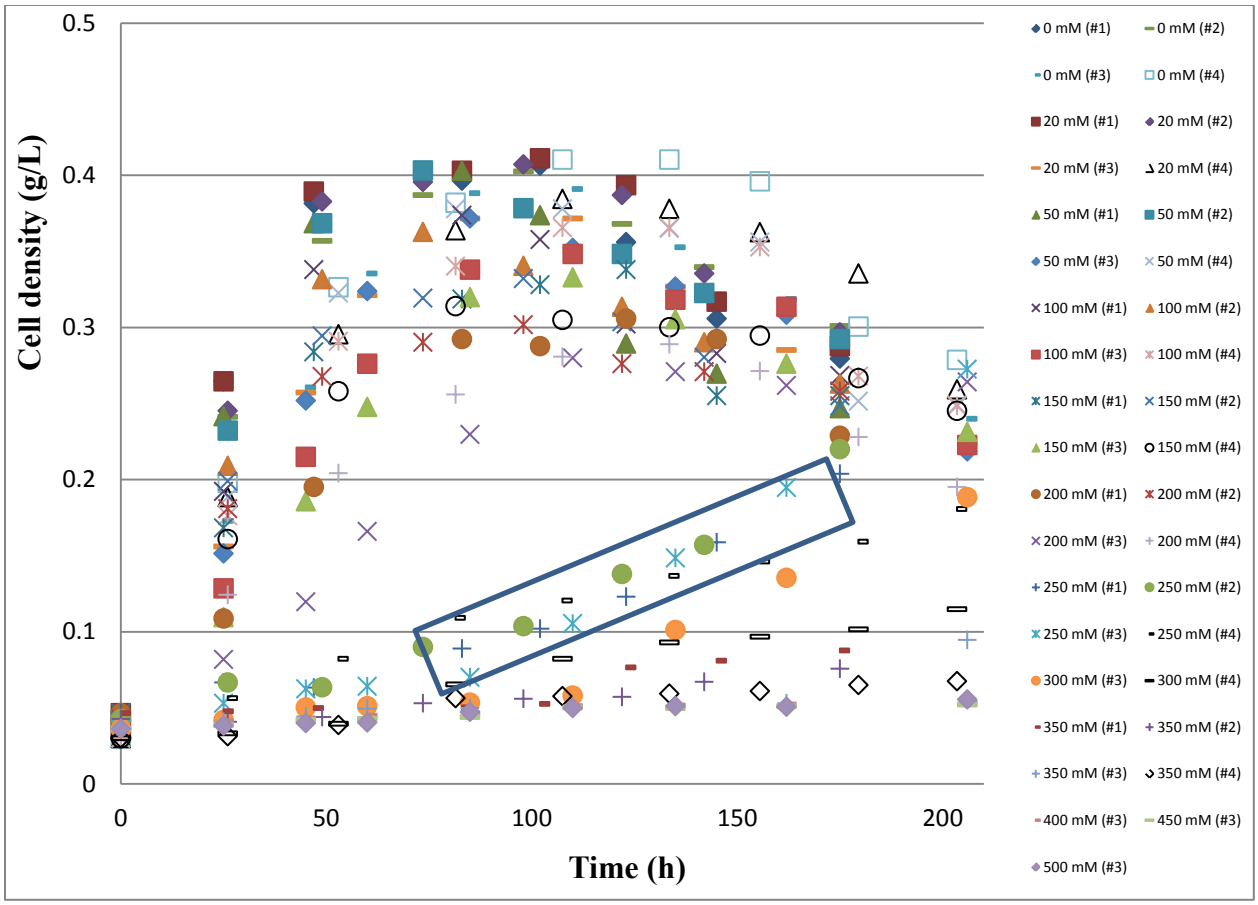

Figure 4-7. Cell growth time course under varying concentrations of NH_4OH (4 runs)

To see the inhibitory effect on cell growth under higher $[NH_4^+]$ for prolonged period, the 3rd run was extended to 422 hours with a few higher $[NH_4^+]$ doped into the media. As shown in Figure 4-8, $[NH_4^+]$ ranging from 250 to 300 mM showed that the cell concentration peaked around 200 hours with a lower cell concentration compared with those of lower $[NH_4^+]$ in media. For $[NH_4^+]$ ranging from 350 to 400 mM, cells eventually could overcome their initial dormancy and grew to an even lower cell concentration compared with that of the control. For $[NH_4^+]$ ranging from 450 to 500 mM, no appreciable cell growth was observed during the entire experimental period.

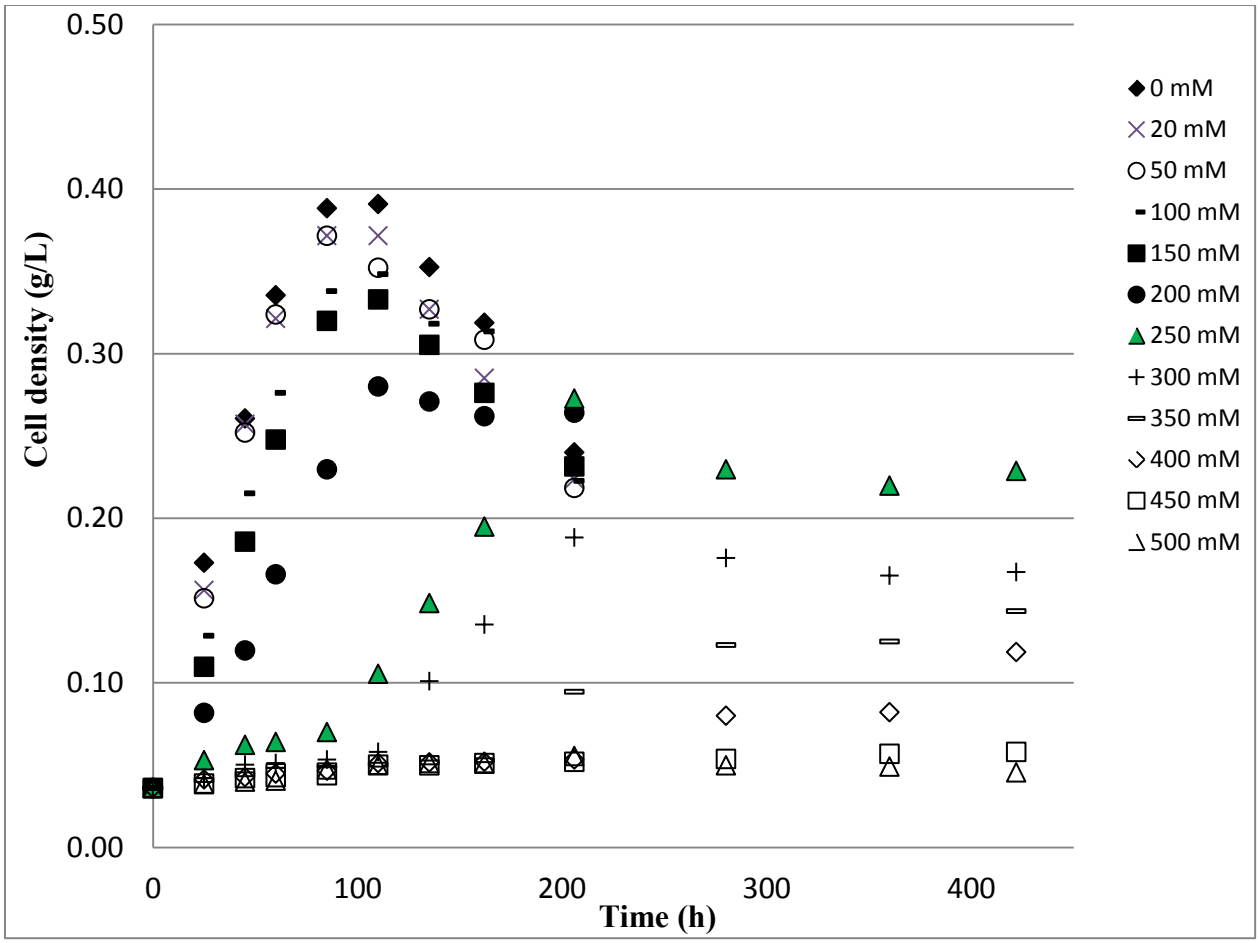

Figure 4-8. Cell growth time course under varying concentrations of NH_4OH with extended time up to 422 hours (3rd run).

4.4.3 Effects of [NH_4^+] on cell growth rate with continuous bioreactor runs

To substantiate the results obtained above, two parallel bioreactors denoted as A (doped with NH_4^+) and B (control) (see Figure 4-2) were used to run a comparative study under pH control. These bioreactor runs were operated under controlled pH of 5.5, temperature of 37 °C, and continuous gas flow. Figures 4-9 to 4-13 display the cell concentration compared with the control under varying initial concentrations of NH_4^+. The lines represent a model described later.

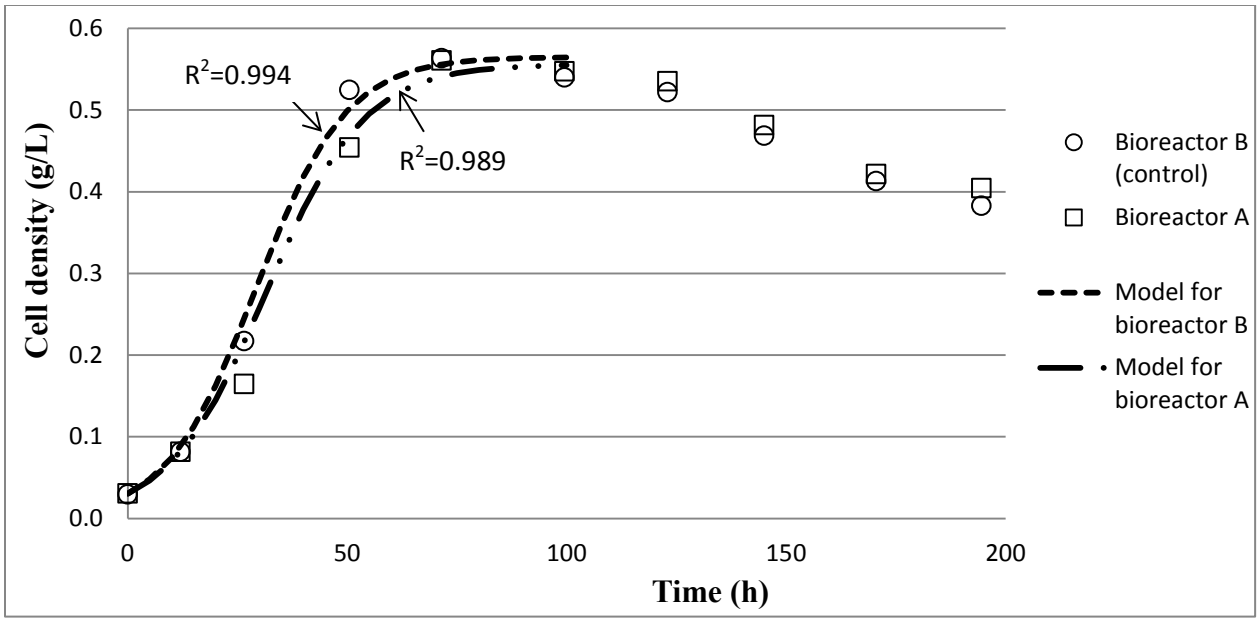

Figure 4-9. Cell concentration time course with initial 59 mM NH_4^+ doped into Bioreactor A compared with Bioreactor B (control)

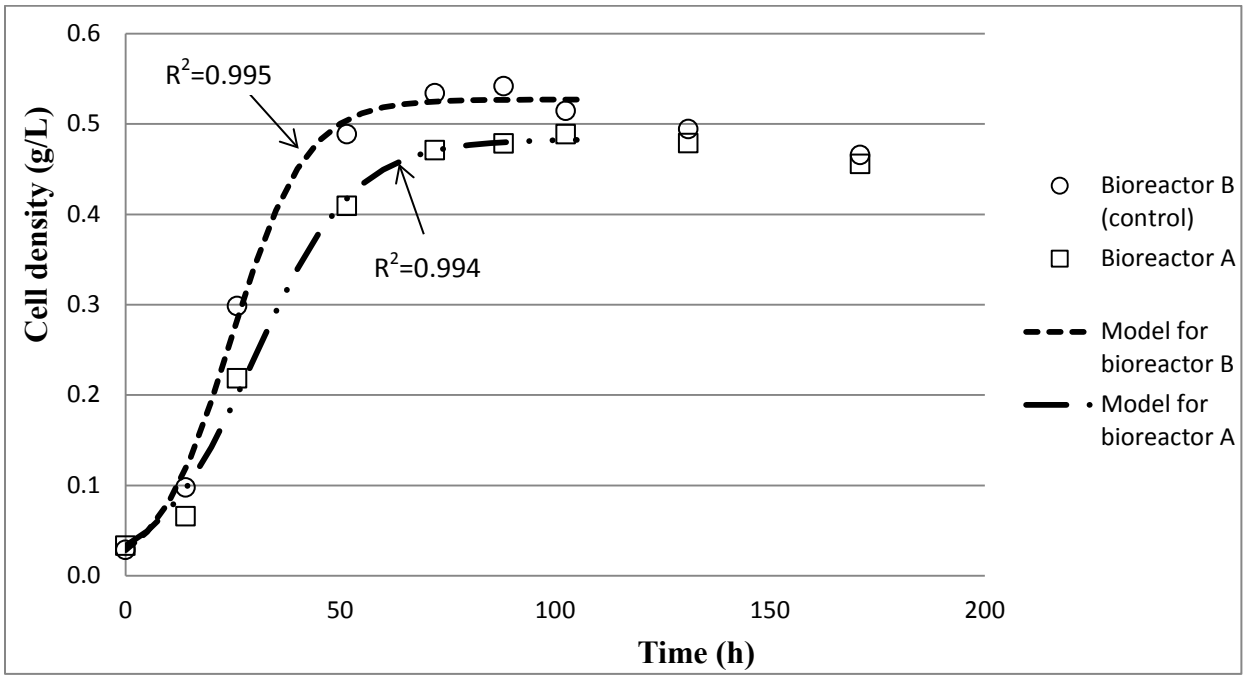

Figure 4-10. Cell concentration time course with initial 110 mM NH_4^+ doped into Bioreactor A compared with Bioreactor B (control)

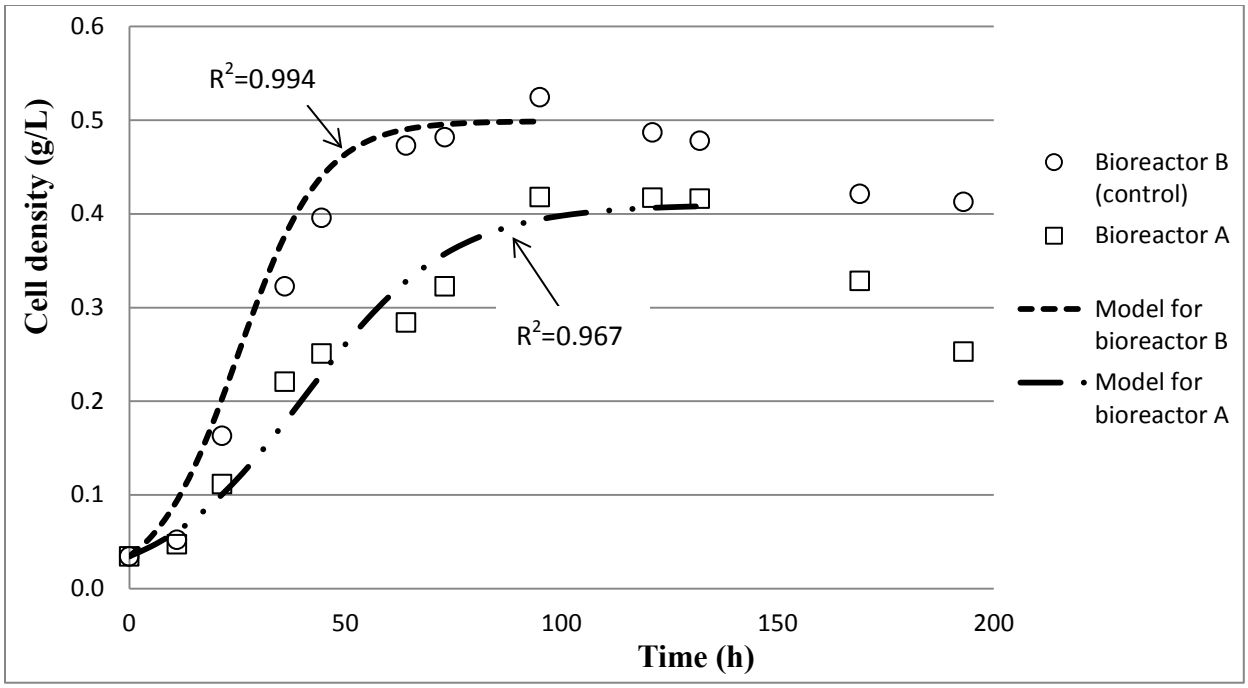

Figure 4-11. Cell concentration time course with initial 158 mM NH_4^+ doped into Bioreactor A compared with Bioreactor B (control)

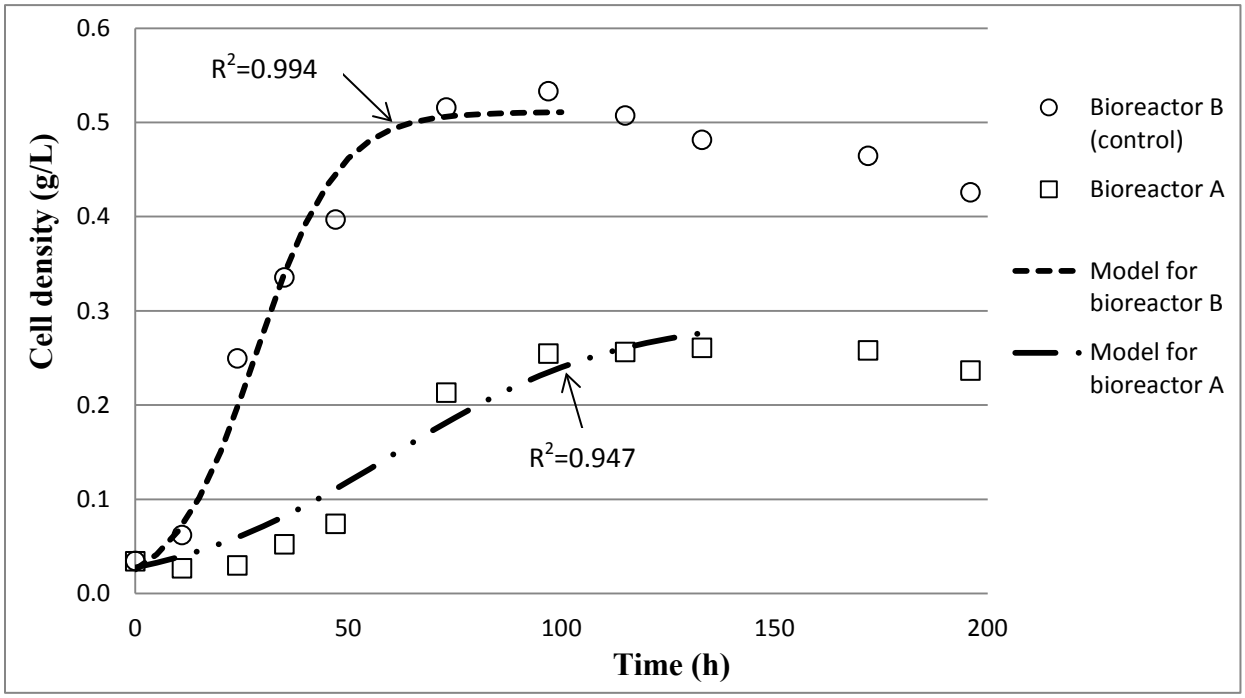

Figure 4-12. Cell concentration time course with initial 204 mM NH_4^+ doped into Bioreactor A compared with Bioreactor B (control)

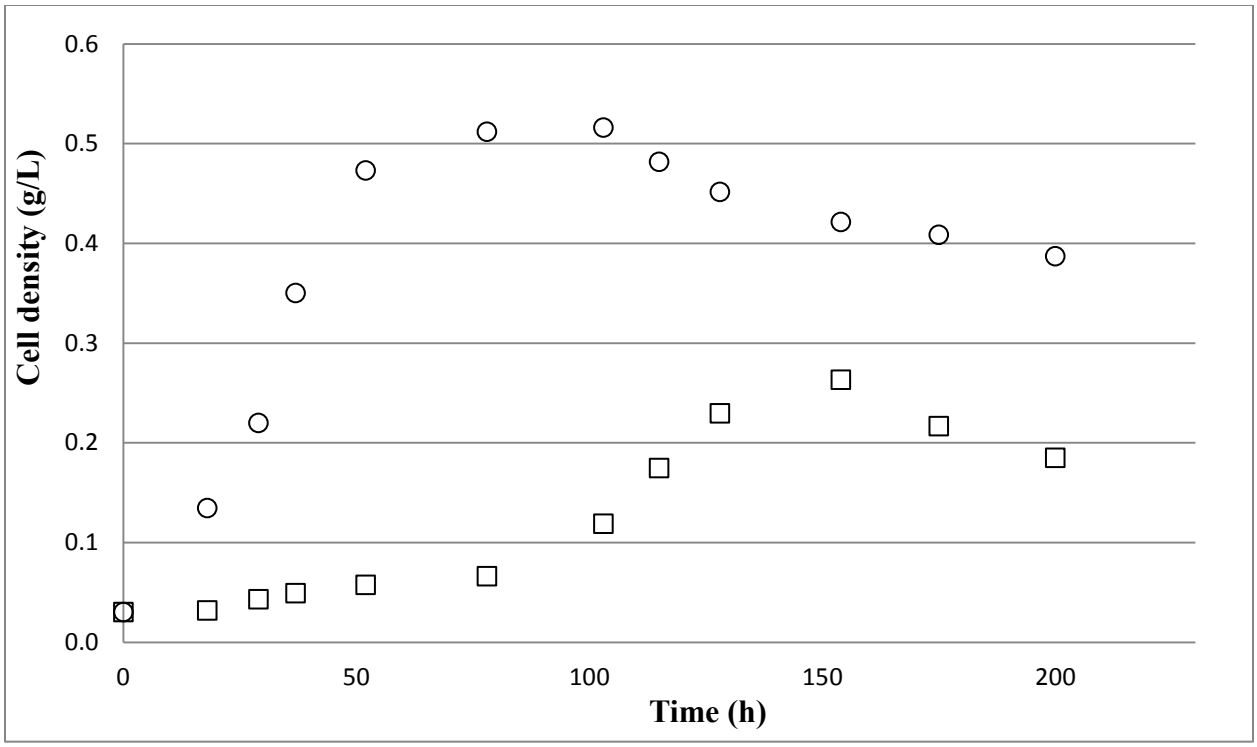

Figure 4-13. Cell concentration time course with initial 227 mM NH_4^+ doped into Bioreactor A (□) compared with Bioreactor B (control) (○)

It is not surprising that cell concentration profiles for the continuous bioreactor studies under pH control displayed similar trends to the bottle studies—higher NH_4^+ led to less growth. To quantify the cell growth rates for the continuous bioreactor runs, a logistic model was used to fit the cell concentration with time (up until the peak concentration was obtained). The concentrations after reaching the peak concentration were not fit to the model since the media was not replaced (likely resulting in some cell decrease) and the model does not account for decreases in cell concentration following the attainment of a peak concentration.

The logistic equation describes growth in terms of carry capacity. The normal approach is to use a formulation in which the specific growth rate (μ_g) is related to the amount of unused carrying capacity:

$$\mu_g = k * \left(1 - \frac{X}{X_\infty}\right) \tag{4-4}$$

Thus,
$$\frac{dX}{dt} = kX * \left(1 - \frac{X}{X_\infty}\right) \tag{4-5}$$

Equation 4-5 is valid for a well-mixed system. The integration of Equation 4-5 with the initial condition $X(0) = X_0$ yields the following equation:

$$X = \frac{X_0 * e^{kt}}{1 - \frac{X_0}{X_\infty} * \left(1 - e^{kt}\right)} \tag{4-6}$$

Here, μ_g is the cell specific growth rate, X_0 is the initial cell concentration, X is the cell mass, X_∞ is the maximum cell concentration or carrying capacity, and k is the carrying capacity coefficient (indicating how fast the cells grow).

The lines shown in Figures 4-9 to 4-12 are the fit to Equation 4-6. As is evident, the model fits the experimental data reasonably well as indicated by the R^2 value. The fitted parameters such as carrying capacity k and maximum cell mass X_∞ are shown in Table 4-2 for each of the first four bioreactor runs. In Table 4-2 and the following analysis, parameters with a subscript "1" refer to Bioreactor A that involved NH_4^+ and parameters with a subscript "2" refer to Bioreactor B that had no NH_4^+. It should be noted that the data in Figure 4-13 was not fit to Equation 4-6 since there was a much longer delayed cell growth phase for Bioreactor A.

Therefore, Equation 4-6 will not produce a good fit for this particular run since the equation does not apply well to cell growth with long delay times. This is one reason why the fit for Bioreactor A in Figure 4-12 was not as good as the fit for Bioreactor A in Figures 4-9 through 4-11.

Table 4-2. Ratios of carrying capacity coefficient and maximum cell mass for four bioreactor runs in the absence or presence of NH_4^+

	Bioreactor A (with NH_4^+)	Bioreactor B (no NH_4^+)	Ratio
59 mM doped into bioreactor A	$k_1 = 0.09$	$k_2 = 0.098$	$k_1/k_2 = 0.92$
	$X_{\infty,1} = 0.556$	$X_{\infty,2} = 0.565$	$X_{\infty,1}/X_{\infty,2} = 0.98$
110 mM doped into bioreactor A	$k_1 = 0.087$	$k_2 = 0.117$	$k_1/k_2 = 0.74$
	$X_{\infty,1} = 0.483$	$X_{\infty,2} = 0.527$	$X_{\infty,1}/X_{\infty,2}$ =0.92
158 mM doped into bioreactor A	$k_1 = 0.059$	$k_2 = 0.104$	$k_1/k_2 = 0.57$
	$X_{\infty,1} = 0.410$	$X_{\infty,2} = 0.499$	$X_{\infty,1}/X_{\infty,2} = 0.82$
204 mM doped into bioreactor A	$k_1 = 0.038$	$k_2 = 0.104$	$k_1/k_2 = 0.37$
	$X_{\infty,1} = 0.294$	$X_{\infty,2} = 0.511$	$X_{\infty,1}/X_{\infty,2} = 0.58$

To easily observe the trends, the data shown in Table 4-2 were graphed in Figure 4-14. By observing the trend, it can be concluded that the carrying capacity coefficient *k* (indicating how fast cells grow) was reduced to 37% when compared with that of the control for 204 mM NH_4^+ in media. On the other hand, the maximum cell mass X_∞ was reduced to 58% when compared with that of the control for the same amount of NH_4^+ in media.

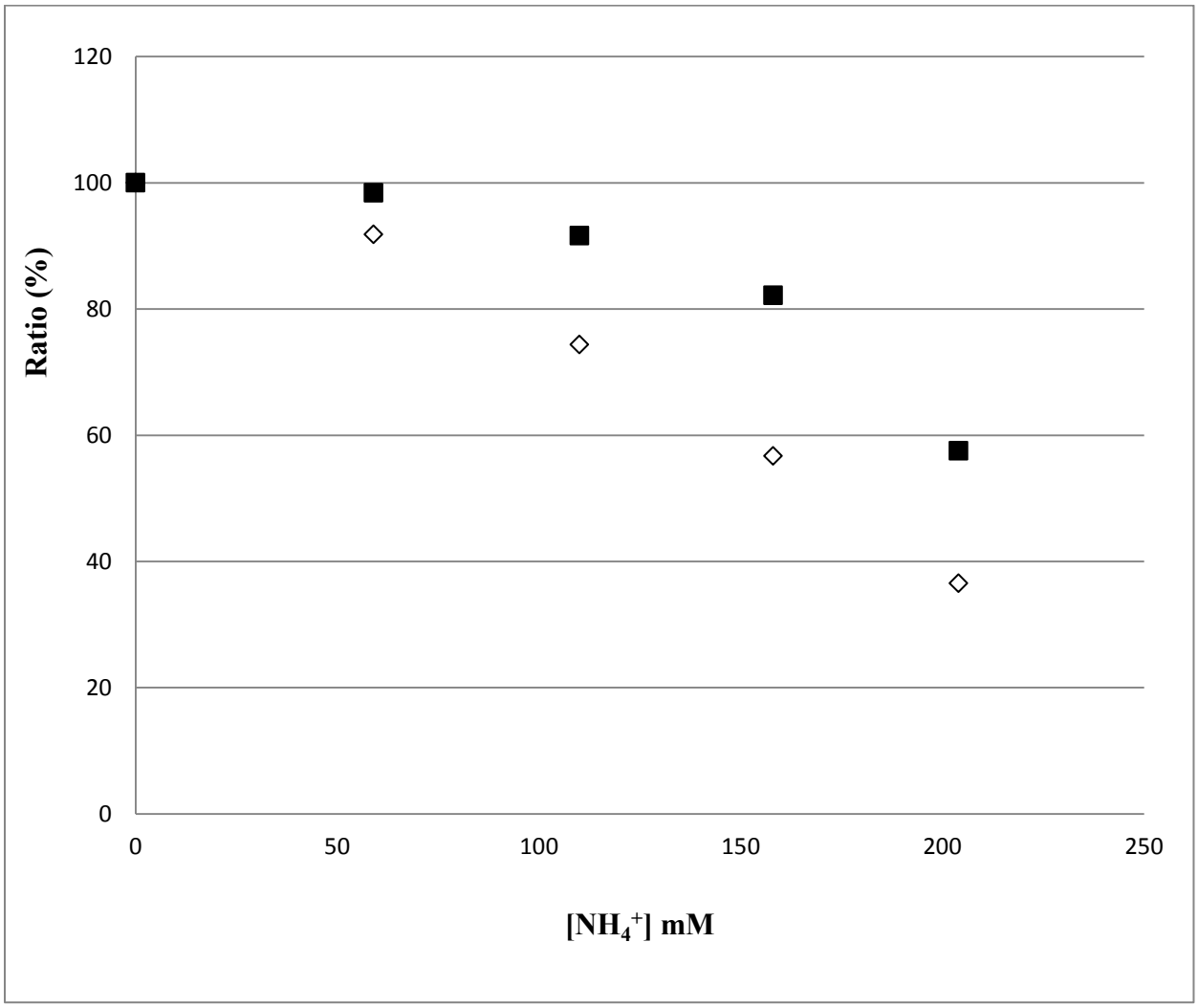

Figure 4-14. The ratio of k_1/k_2 (◇) and $X_{\infty,1}/X_{\infty,2}$ (■) for varying $[NH_4^+]$

In summary, for both bottle culture and continuous culture with pH control, it showed that at lower concentrations of NH_4^+ (up to 100 mM) there were minimal to no adverse effects on maximum cell concentration that was obtained (shown by X_∞ ratio). However, gradually increasing the concentrations of NH_4^+ in media resulted in different degrees of inhibitory effects. It can be concluded that at 250 mM NH_4^+, cell growth was substantially inhibited.

4.4.4 Modeling the effects of [NH_4^+] on cell growth for a continuous bioreactor with media recycle

To imitate an industrial application on potential cell growth, it is useful to model a continuous culture system. For this preliminary model, no cell recycle is considered. The cell specific grow rate can be expressed using Equation 4-5 according to:

$$R_x = kX * (1 - \frac{X}{X_\infty}) \tag{4-7}$$

Without cell recycle, a material balance on the cell concentration around a well-mixed fermenter (with constant volume) yields the following equation:

$$V_L \frac{dX}{dt} = F_{in}X_{in} - F_{out}X_{out} + R_x V_L \tag{4-8}$$

where F_{in} and F_{out} are the nutrient flow rates for feed and effluent streams, V_L is the culture volume, X_{in} and X_{out} are cell concentrations in feed and effluent streams, and R_x is the cell specific grow rate.

At steady state, $\frac{dX}{dt} = 0$ and if $X_{in} = 0$ (i.e. sterile feed), then Equation 4-8 becomes

$$R_x = \frac{F_{out}X_{out}}{V_L} = \frac{X_{out}}{\tau_l} \tag{4-9}$$

Here τ_l is the liquid residence time representing the liquid volume divided by the liquid flow rate. For a well-mixed bioreactor, it is valid that $X = X_{out}$. When Equations 4-7 and 4-9 are combined, the following equation is obtained.

$$kX * \left(1 - \frac{X}{X_\infty}\right) = \frac{X}{\tau_l} \tag{4-10}$$

By manipulation, Equation 4-10 can be written as Equation 4-11.

$$X = X_{\infty}\left(1 - \frac{1}{k\tau_l}\right) \tag{4-11}$$

Finally, the ratio of cell mass with doped NH_4^+ (X_1) versus cell mass for control (X_2) can be written in the form of Equation 4-12.

$$\frac{X_1}{X_2} = \frac{X_{\infty,1}\left(1 - \frac{1}{k_1\tau_l}\right)}{X_{\infty,2}\left(1 - \frac{1}{k_2\tau_l}\right)} \tag{4-12}$$

With Equation 4-12, the fitted data of Table 4-2 for varying [NH_4^+] in media was used to predict the ratio of X_1 versus X_2. In Figure 4-15, the ratio of X_1 versus X_2 was graphed as a function of τ_l. It is clear that at higher [NH_4^+] (around 204 mM) the ratio of X_1 versus X_2 is less than 0.6. As an example, a prediction was made for a 700 mL media working volume with an effluent flow rate of 0.072 mL/min used from a previous experiment [88] where τ_l is 162 hours (shown as a vertical line in Figure 4-15). It can be inferred from Figure 4-15 that at 204 mM [NH_4^+] and 162 hours (τ_l) the ratio of X_1 versus X_2 is around 0.51which is comparable to the ratio of $X_{\infty,1}/X_{\infty,2}$ (0.57).

Using this developed model, the ratio of X_1 / X_2 can be estimated for a continuous fermenter under steady-state operating conditions. It should be noted that the parameter values used in Equation 4-12 can depend upon the cell type, media composition, gas flow rate, NH_3 composition in the gas, the introduction of fresh media, and the reactor design. However, this analysis provides some insights as to how NH_4^+ in the bioreactor can potentially have a strong impact on the function of the bioreactor via its effect on the cell concentration.

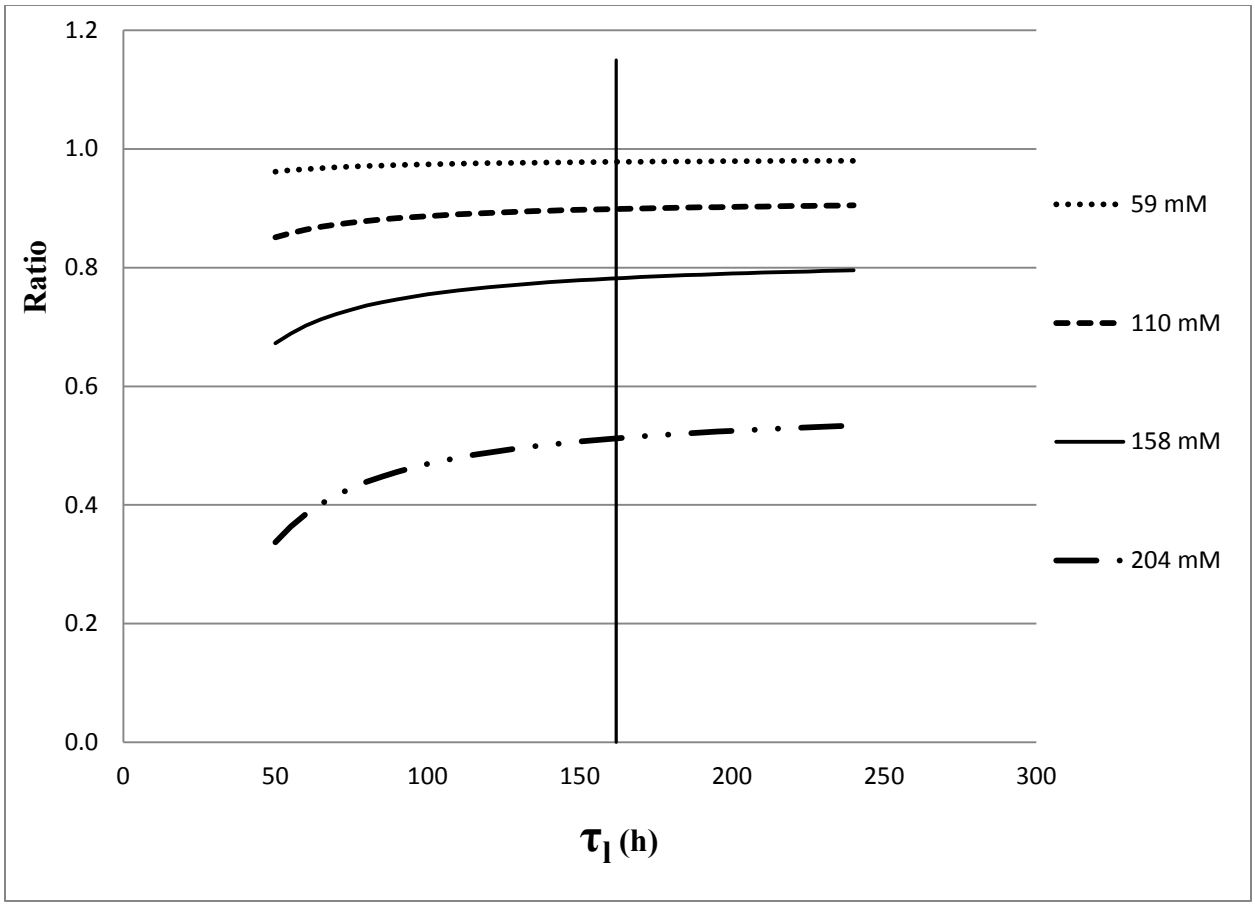

Figure 4-15. The ratio of X_1 versus X_2 is graphed with τ_l as the variable for varying $[NH_4^+]$ in media. Previous experimental τ_l value (162 hours) is shown here as a vertical line

4.4.5 Effects of other ions on cell growth

In the previous Sections 4.4.2 and 4.4.3, it was shown that NH_4^+ at higher concentrations could inhibit the cell concentration and the cell growth rate to a great extent. In previous studies [82, 89, 90], ammonia was also shown to be a strong inhibitor for different bacteria although the effects were not quantified like those shown in this study. At this injunction, it was necessary to investigate whether NH_4^+ or something else, such as ionic strength, was the contributing factor to the inhibitory effects. To this end, five different chemicals [NH_4OH, NH_4Cl, $(NH_4)_2HPO_4$, $NH_4H_2PO_4$, and $(NH_4)_2SO_4$] were used as dopants into the media of bottle studies. Since

250 mM NH_4^+ showed inhibition effects in the previous studies, 250 mM NH_4^+ was also used in this study for comparison purposes. The corresponding osmolarity was also calculated. The cell concentration time course for all these five chemicals are displayed in Figure 4-16.

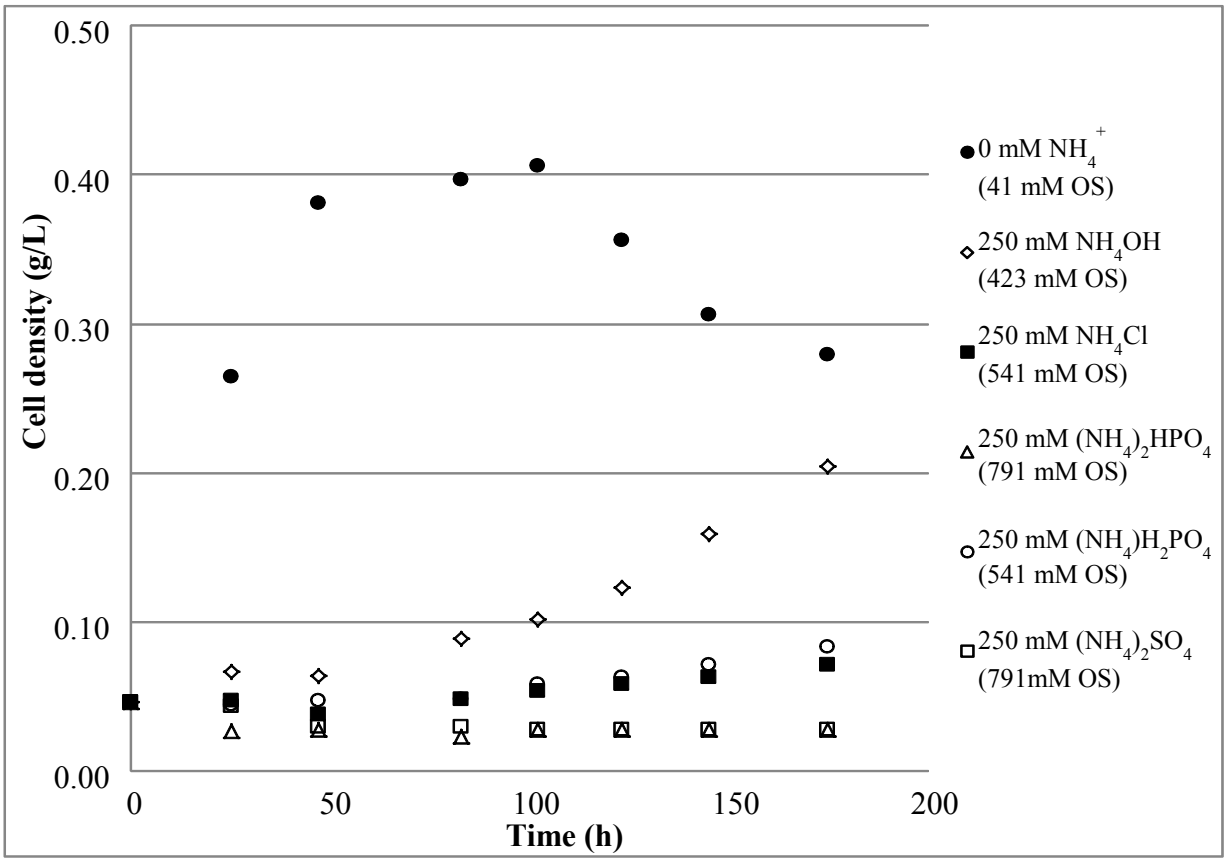

Figure 4-16. The cell density time course for five different chemicals

It is interesting to note that only 250 mM NH_4OH showed appreciable cell growth instead of all compounds as would be expected. For example, both 250 mM NH_4OH and 250 mM $NH_4H_2PO_4$ contain the same concentration of NH_4^+. Therefore, the cell growth profile was

expected to be similar. The observed discrepancy led to the hypothesis that perhaps something else besides NH_4^+ actually inhibited cell growth.

From an extensive literature review, it was found that bacteria require the presence of an outwardly directed turgor pressure to grow. By definition, turgor pressure is the pressure of the swollen cell contents against the cell wall when the external solution is more dilute than the contents of the cell. However, when the osmotic pressure of the growth media is elevated, the maintenance of a relatively constant turgor pressure can be initially achieved by an increase in the cytoplasmic potassium concentration. Gouesbet also showed that an increase in the osmolarity of the media inhibited fermentation in a dramatic fashion [91]. Cruzet also proposed that osmolarity was partially responsible for the cell growth inhibition for their bacteria, even though their cell's structure was different from that of P11[89]. Since ammonia is very soluble and exists in free NH_4^+ form at our experimental condition (37 °C and pH=6) [82], it was reasonable to propose that osmolarity or ionic strength may cause the inhibition for cell growth rather than NH_4^+ per se. To test this hypothesis, different amounts of NH_4OH and K_3PO_4 were added into batch bottles to obtain similar total osmolarity levels in media. For the accuracy of the osmolarity measurement, calculated osmolarity values were checked with actual measurements by an osmometer as displayed in Figure 4-17. It shows that there is a good agreement, especially in the middle range of osmolarity levels (100~250 mM). The value of osmolarity in the absence of NH_4^+ reflects the concentrations of ions in the media recipe.

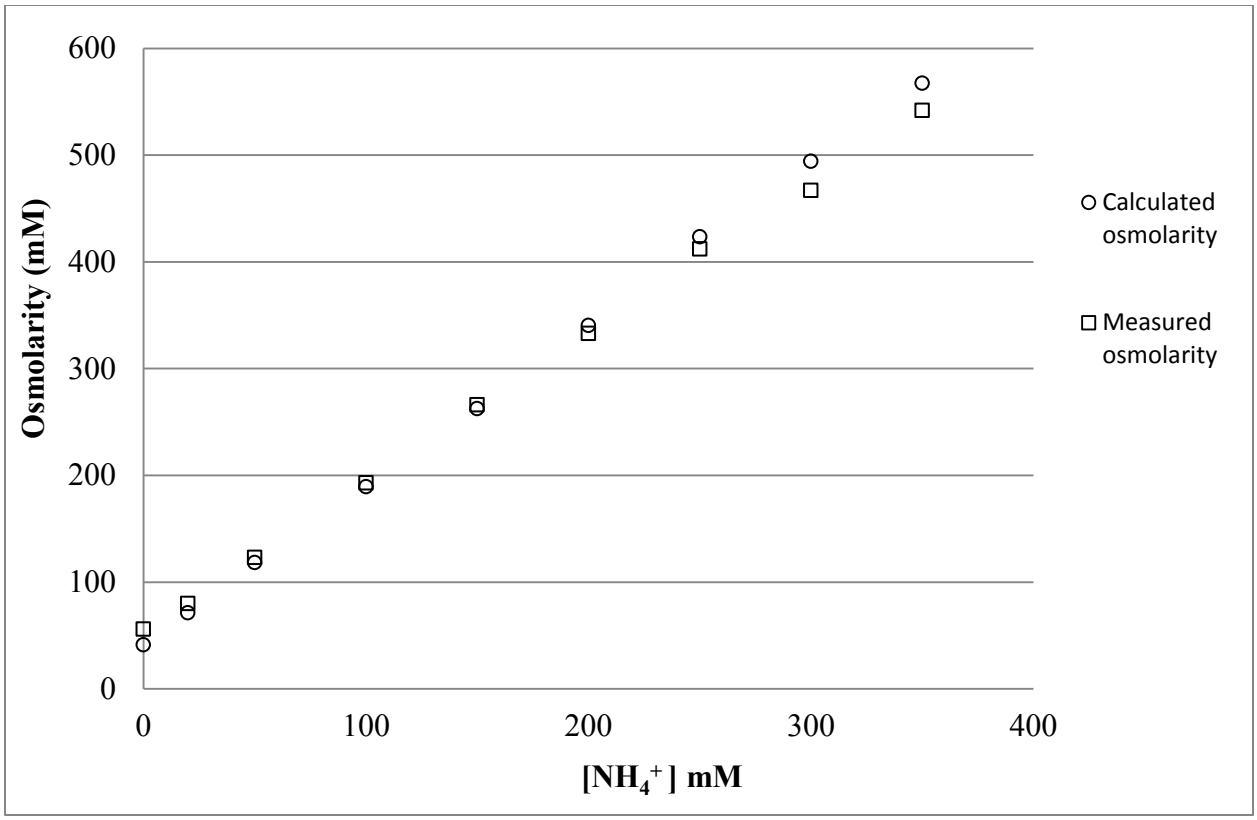

Figure 4-17. Comparison of measured and calculated total osmolarity in media with varied $[NH_4^+]$. At 0 mM $[NH_4^+]$, the osmolarity value reflects all the ions in the media recipe

Figures 4-18 and 4-19 show the cell concentrations with a few typical osmolarity levels by adding either NH_4OH or K_3PO_4 (as control). As displayed in these two figures, cell concentrations are very similar between the two studies when corresponding osmolarity levels are compared. Cell concentration was greatly reduced at osmolarity levels above 400 mM irrespective of what chemicals were present in media. By observing these two figures, a confirmation was reached that NH_4^+ affected cell growth only by accumulated osmolarity levels in the media. Actually, at lower concentrations of ammonium ion (below 50 mM), cell growth rate can potentially be stimulated since NH_4^+ is a nutrient source for cell growth.

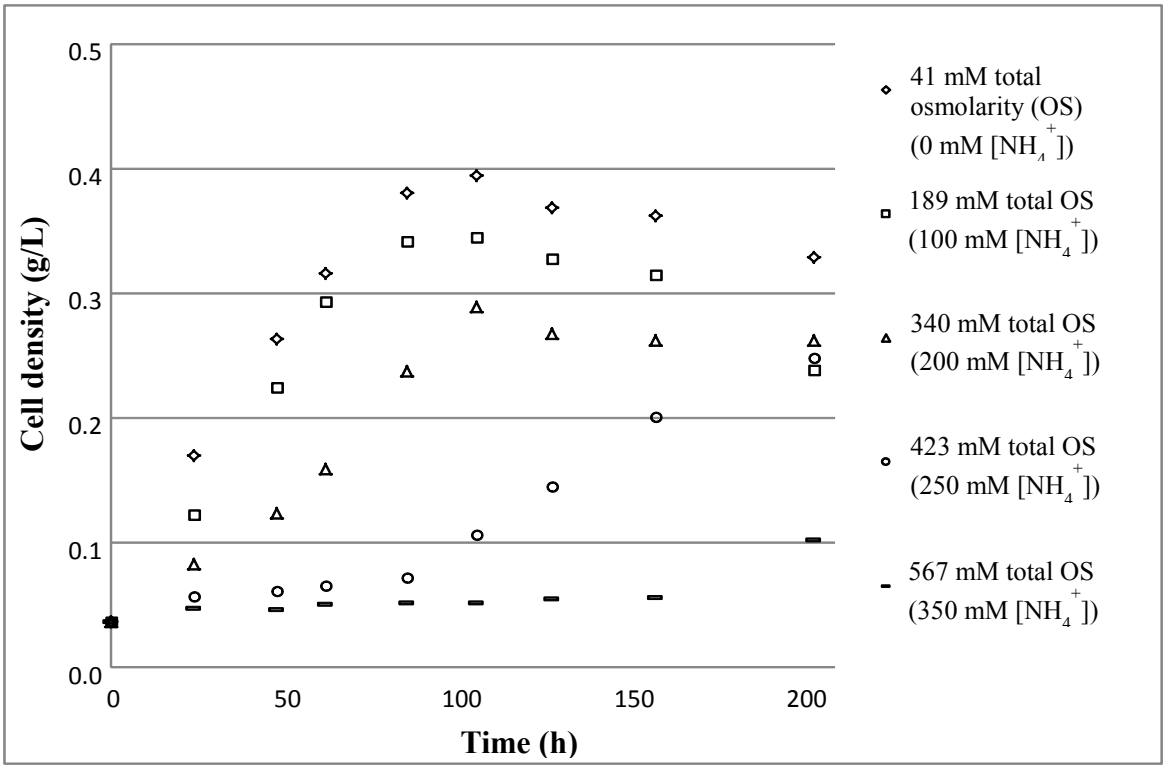

Figure 4-18. Cell concentration with varying total osmolarity levels in media by adding NH_4OH

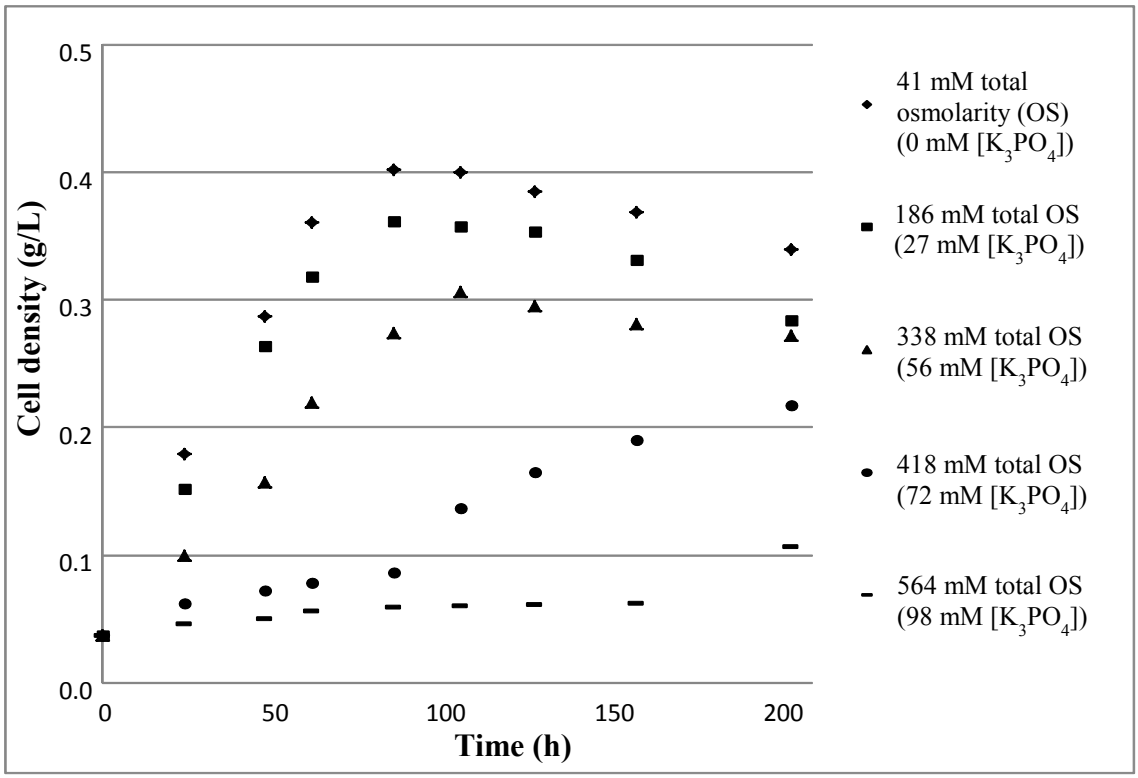

Figure 4-19. Cell concentration with varying total osmolarity levels in media by adding K_3PO_4

Since the cell concentration (and growth rate) is very sensitive to the media pH, it was useful to monitor the pH time course for the above-mentioned osmolarity studies to make sure that pH is not a factor resulting in the cell growth inhibition. Since K_3PO_4 has four ions in its formula, the concentrations of K_3PO_4 were proportionally reduced to obtain the similar osmolarity levels to those of NH_4OH. In Figures 4-20 and 4-21, the pH profiles are very similar. For the control, when acetic acid was produced with the cell growth, the pH value was reduced accordingly. For 350 mM NH_4OH or 87.5 mM K_3PO_4, there was no cell growth or acetic acid production in the initial stage, so the pH stayed constant for that period. From the pH profiles, it was concluded that media pH was not a key factor for the cell growth inhibition. In summary, NH_4^+ itself does not appear to be the culprit for cell growth inhibition. Rather, cell growth appears to be inhibited by the osmolarity, which can be increased with NH_4^+ accumulation in the media.

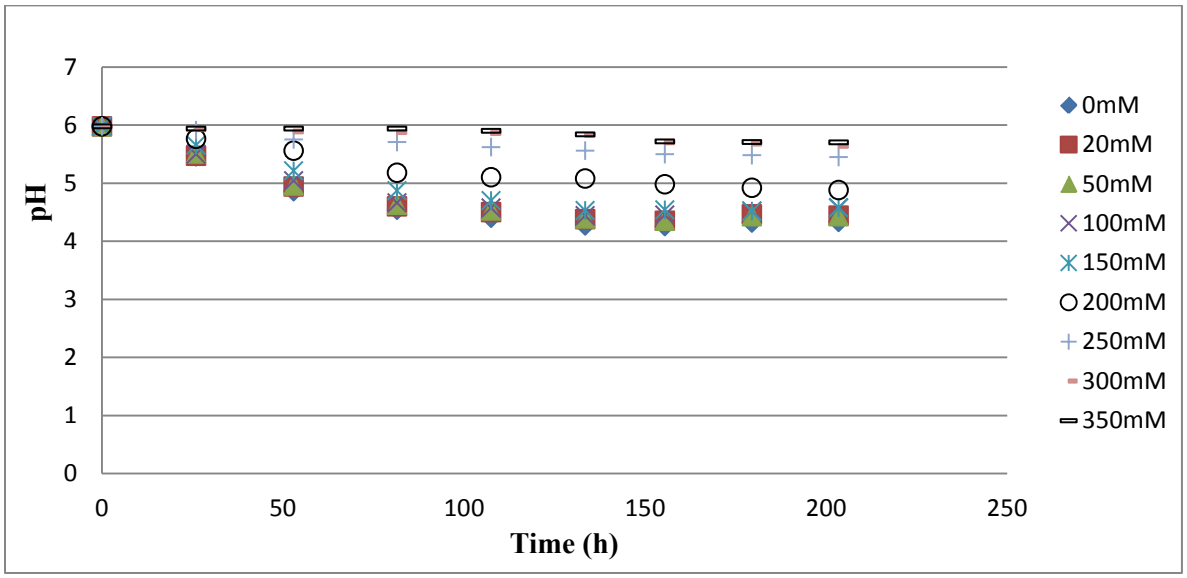

Figure 4-20. pH time courses for varying [NH_4OH]

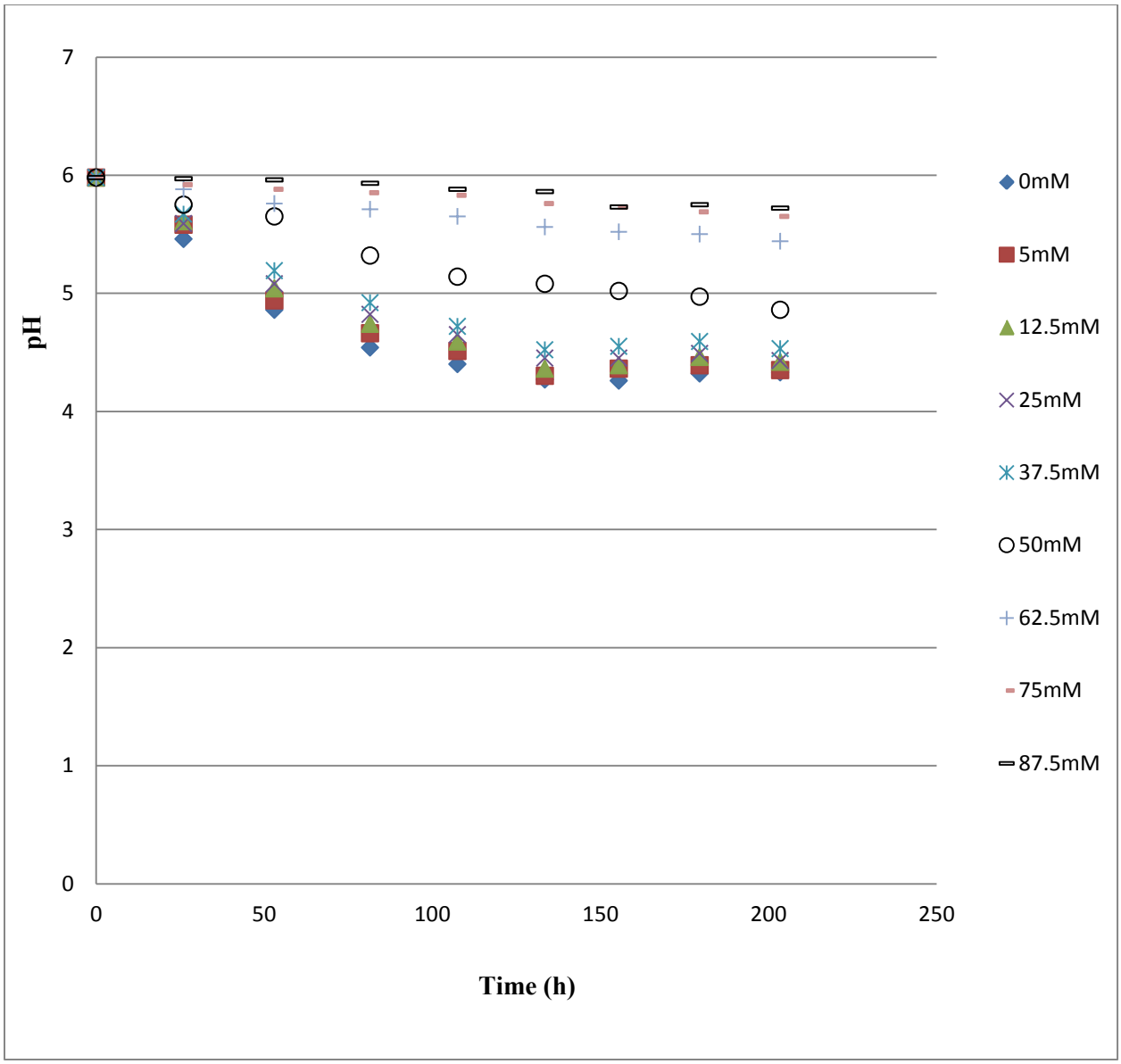

Figure 4-21. pH time courses for varying [K_3PO_4]

In all mitochondria, chloroplasts and in many bacteria, chemiosmosis involves the moving of protons out of the mitochondrion which creates a lower concentration of positively charged protons inside the membrane (approximately -200 mM). This charge and proton concentration difference create a combined electrochemical gradient across the membrane which is denoted as the proton motive force (PMF) [92]. It is possible that NH_3 can weaken the PMF by

crossing the cell membrane and then converting to NH_4^+ which can then potentially neutralize electrons. In this work, it was found that at 250 mM [NH_4^+], cell growth was significantly inhibited. The associated equilibrium concentration of NH_3 in media is around 1.125 x 10^{-12} mM at pH of 5.5 and 37 °C, since the fraction of total NH_3 species in media is around 4.5 x 10^{-15} (see Equation 4.2). Therefore, the amount of NH_3 that can cross the membrane is extremely small such that the effects of NH_3 transport on the PMF should be negligible.

Since there is abundant NH_4^+ in media at the experimental conditons and NH_4^+ may also pass through the membrane via a K^+ - NH_4^+ exchange process [92], it is necessary to investigate how much NH_4^+ and during what phase of growth NH_4^+ can be transported across the membrane. By observing Figure 4-22, it was seen that NH_4^+ only decreases during cell growth. NH_4^+ transport across the memberane likely occurs via a built-in transportation mechanism such as the wildely accepted K^+ - NH_4^+ exchange process. Since NH_4^+ did not decrease once cells approached a steady state concentration, it appears that NH_4^+ cannot freely diffuse through the cell membrane even at an elevated concentration in the extracellular media. This work further showed that for higher initial [NH_4^+] such as 158 and 207 mM, the NH_4^+ cell consumption rate was similar to the data shown in Figure 4-22 for lower initial [NH_4^+]. Since there are limited free amounts of NH_4^+ inside the cell membrane, it was reasonably proposed that NH_4^+ transported across the cell membrane during cell growth will not significantly reduce the PMF. In conclusion, it is likely that elevated osmolarity levels outside the cell membrane will disrupt the cell's ability to maintain an outwardly directed turgor pressure which is essential for the cell growth.

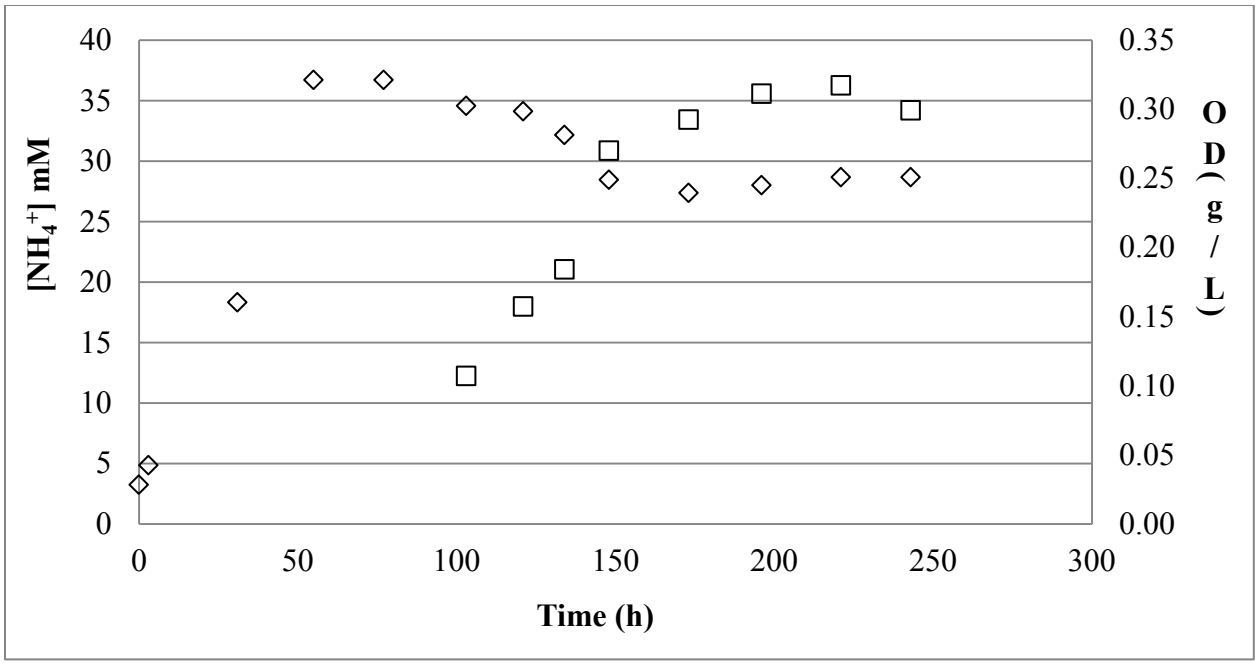

Figure 4-22. $[NH_4^+]$ and cell density (OD) time profiles. Symbol (◇) represents $[NH_4^+]$ time course and symbol (□) represents OD time course. NH_3 source was shut off at 55 hours and media was inoculated at 77 hours

4.4.6 Effects of $[NH_4^+]$ versus osmolarity on product formation

After finding that it was osmolarity instead of NH_4^+ contributing to the cell growth inhibition, the next step was to conduct a comparative study to see whether osmolarity or NH_4^+ would impact the product formation. For this end, two similar chemicals ($NH_4H_2PO_4$ and KH_2PO_4) were added into media to obtain two different elevated levels of osmolarity (276/271 and 500/484 mM). Since product formation is closely related to different cell growth phases, it was necessary to simultaneously monitor cell growth and product formation. Similar to cell grow profiles mentioned in the previous Section (4.4.5), cell growth was substantially inhibited at greater than 400 mM total osmolarity as shown in Figure 4-23 (a) & (b).

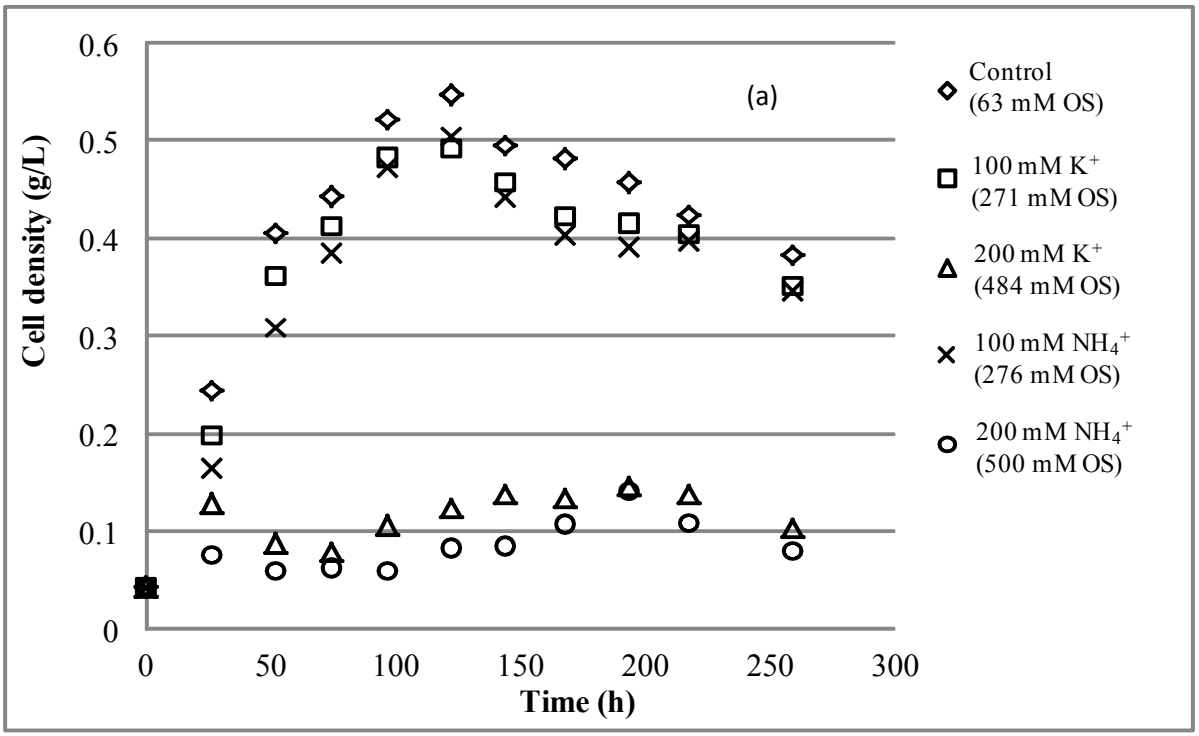

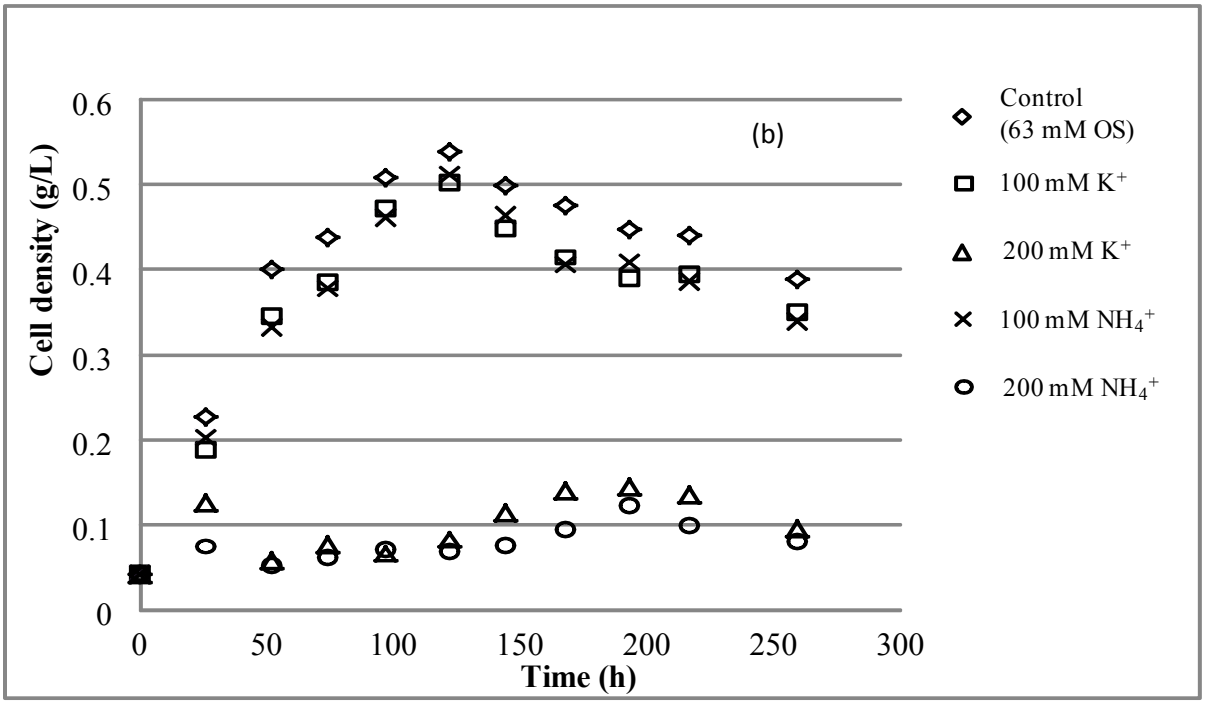

Figure 4-23. Cell growth time courses for varying [$NH_4H_2PO_4$] and [KH_2PO_4]. Here (a) & (b) are repeated experiments. OS is the total osmolarity

Figure 4-24 shows the [EtOH] profile for $NH_4H_2PO_4$ and KH_2PO_4 at two different levels of total osmolarity compared with the control. Since nearly the same level of total osmolarity for $NH_4H_2PO_4$ or KH_2PO_4 displayed similar trends, it was concluded that NH_4^+ per se did not significantly impact ethanol formation but rather the osmolarity impacted formation.

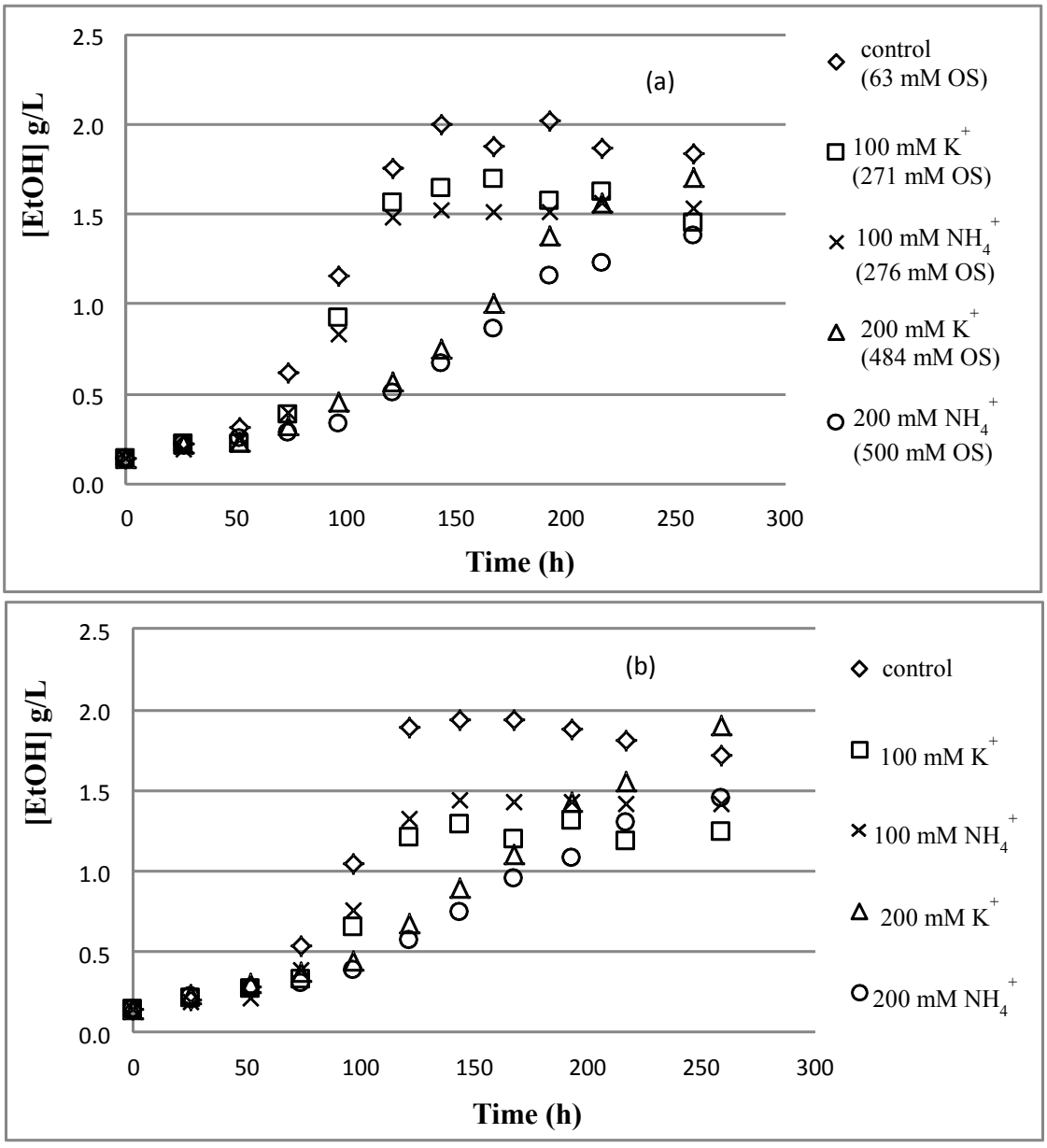

Figure 4-24. [EtOH] time courses for varying $[NH_4H_2PO_4]$ and $[KH_2PO_4]$. Here (a) & (b) are repeated experiments

Figure 4-25 shows the corresponding acetic acid production. The figure shows that at higher levels of total osmolarity, acetic acid formation was inhibited regardless of what kinds of ions were present.

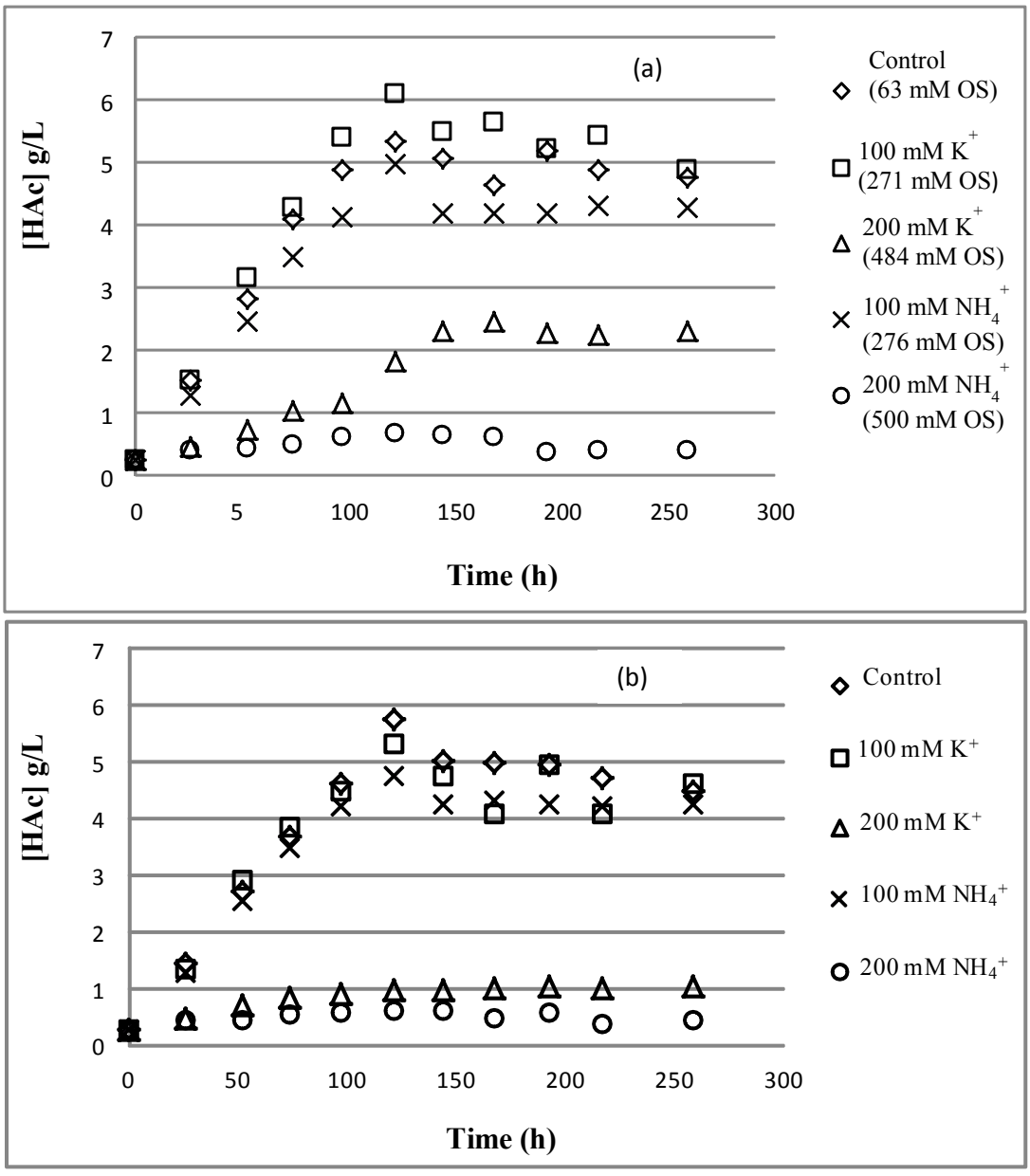

Figure 4-25. [HAc] time courses for varying $[NH_4H_2PO_4]$ and $[KH_2PO_4]$. Here (a) & (b) are repeated experiments

To see a clearer relationship, [EtOH] was normalized with cell density as shown in Figure 4-26. Figure 4-26 showed that a high level of osmolarity eventually lead to much higher [EtOH] per cell mass after prolonged time.

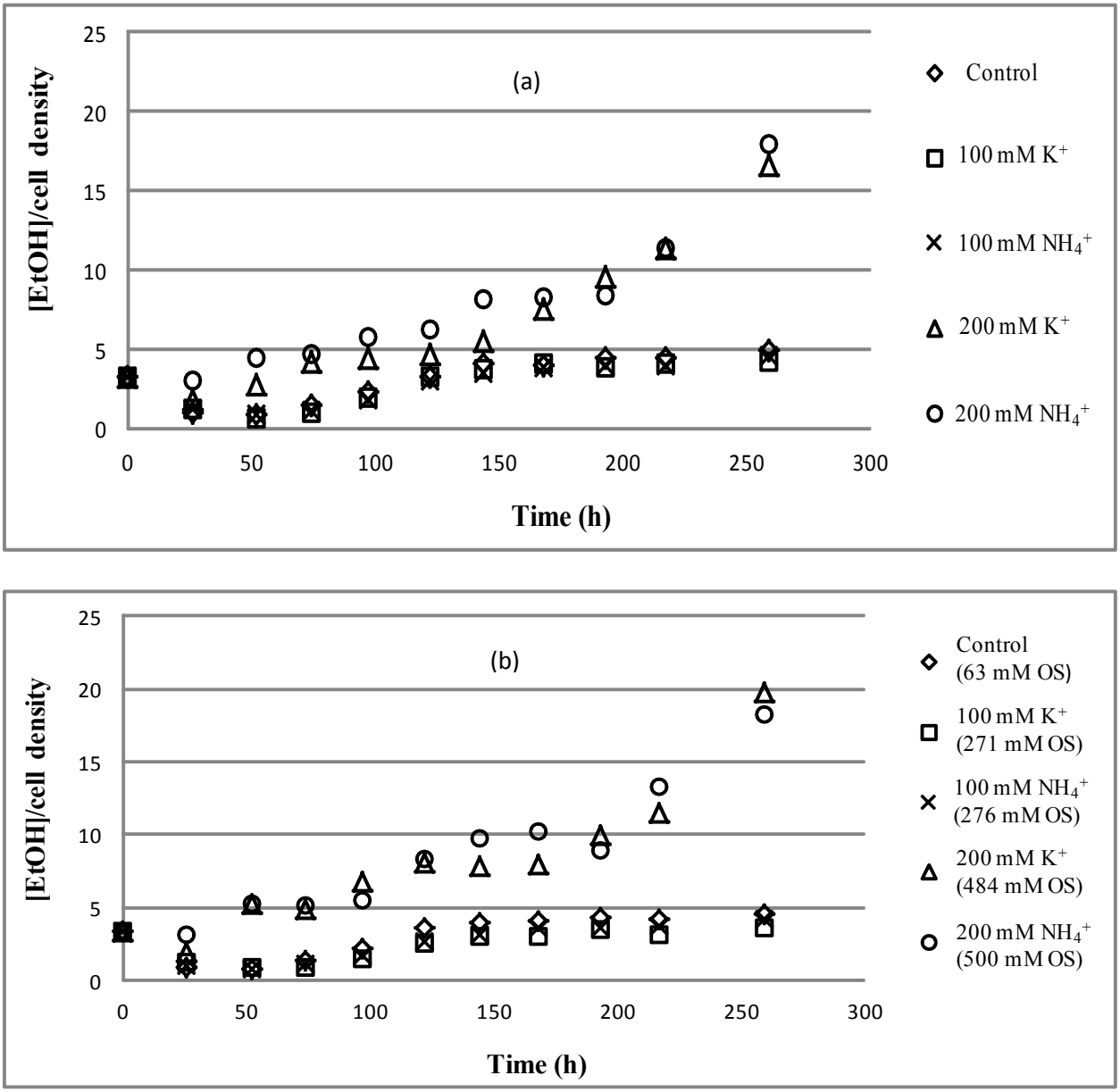

Figure 4-26. [EtOH]/cell density versus time. Here (a) & (b) are repeated runs

However, since the cell mass is low, the corresponding EtOH is still similar to the amounts with the lower osmolarity. These results show that there are competing outcomes with osmolarity. High osmolarity reduces cell concentration, which is not beneficial, but increases the ratio of EtOH produced per cell mass, which is beneficial.

Now that higher osmolarity doped into media from beginning can lead to higher ratio of [EtOH]/cell density, it was necessary to further investigate whether [EtOH] can be increased if total osmolarity is increased after cell growth reaches a stationary phase. For this run, at 141 hours, after cell growth in both media (doped with 100 mM $NH_4H_2PO_4$ or KH_2PO_4 initially) reached the stationary phase, additional 100 mM $NH_4H_2PO_4$ or KH_2PO_4 was added into the media to see whether there was an effect on ethanol production. Figure 4-27 shows the cell growth time course. Figure 4-28 showed the corresponding [EtOH] time course for varying total osmolarity and ion sources. From Figure 4-28, it is clear that there is no observable effect on ethanol production compared with control (100 mM $NH_4H_2PO_4$ or KH_2PO_4 doped initially). However, [EtOH] can shoot up higher than that of the control (0 mM) after a prolonged time (>250 hours) when 200 mM $NH_4H_2PO_4$ or KH_2PO_4 was doped from the beginning. Thus, the osmolarity effect appears to be strongest during the growth phase. Therefore, it was proposed that higher levels of osmolarity altered the metabolic pathway for ethanol production during the cell exponential growth phase, not in the stationary phase. The detailed biological mechanism is unknown at this stage. Further investigation is merited. Figure 4-29 displayed the [HAc] time course for varying total osmolarity and ion sources. It was plausible that [HAc] decreased with higher levels of osmolarity. More runs are needed to statistically prove this point.

To get an insight about [EtOH] per cell density, Figure 4-30 was developed. It showed that [EtOH]/cell density could rise to significant level when 200 mM $NH_4H_2PO_4$ or KH_2PO_4 was doped from beginning. The magnitude was much higher than [EtOH] without accounting for cell density.

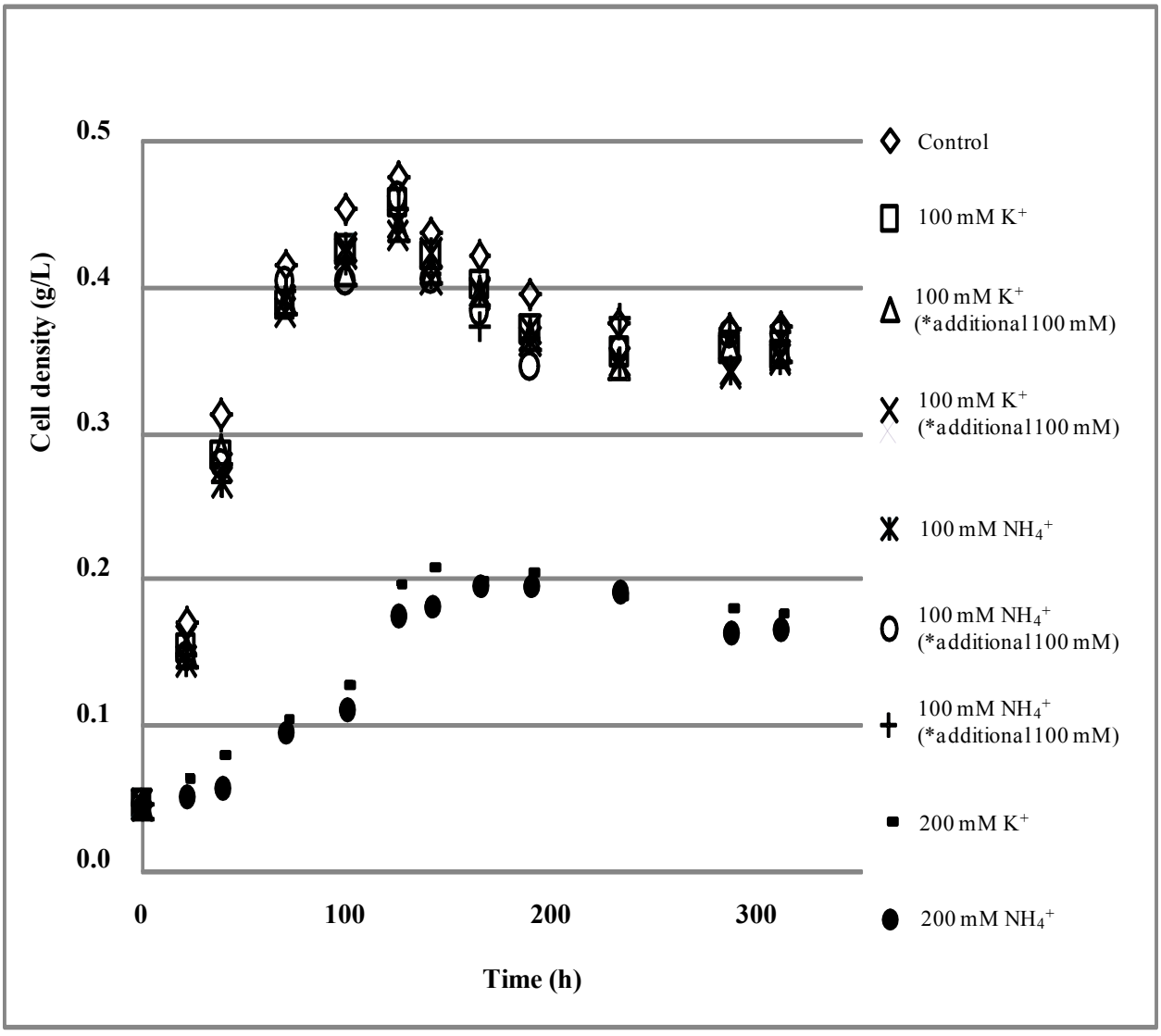

Figure 4-27. Cell growth time courses for varying [$NH_4H_2PO_4$] and [KH_2PO_4]

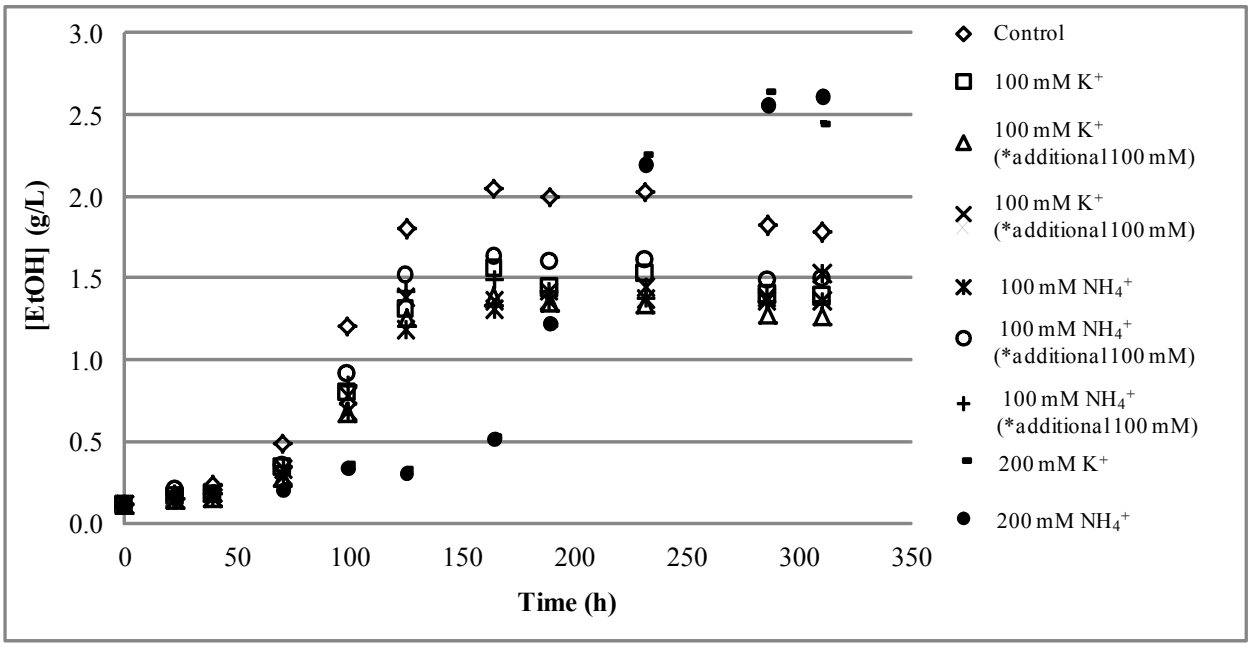

Figure 4-28. [EtOH] time courses for varying $[NH_4H_2PO_4]$ and $[KH_2PO_4]$

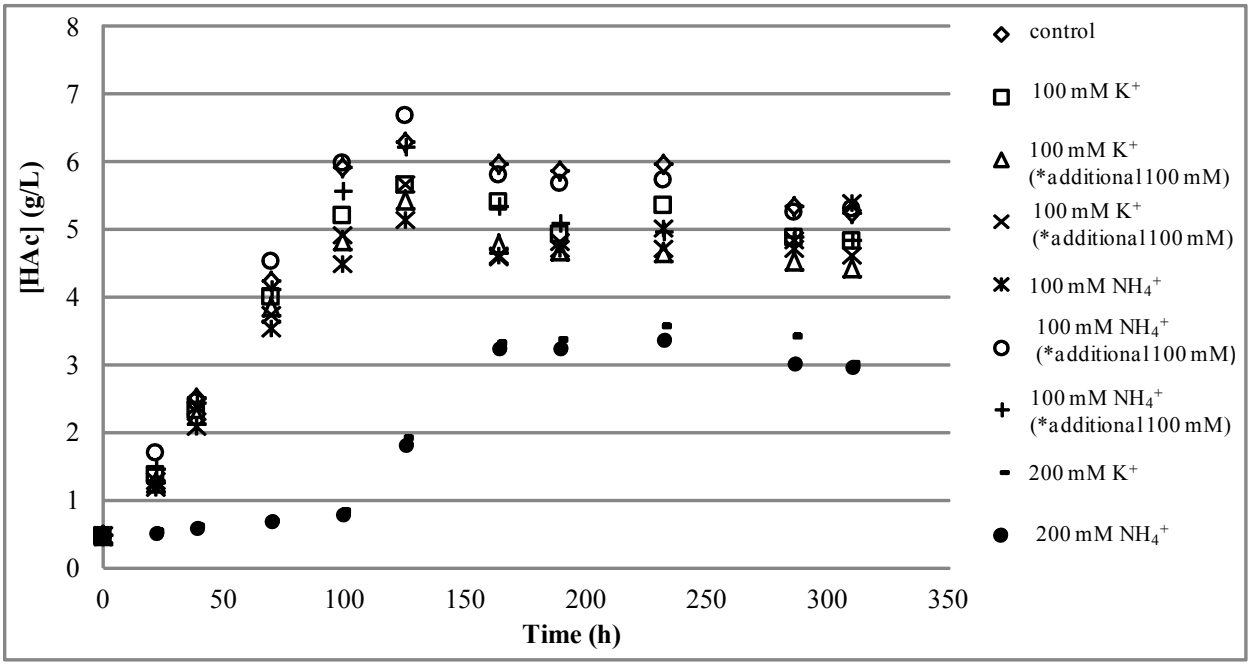

Figure 4-29. [HAc] time courses for varying $[NH_4H_2PO_4]$ and $[KH_2PO_4]$

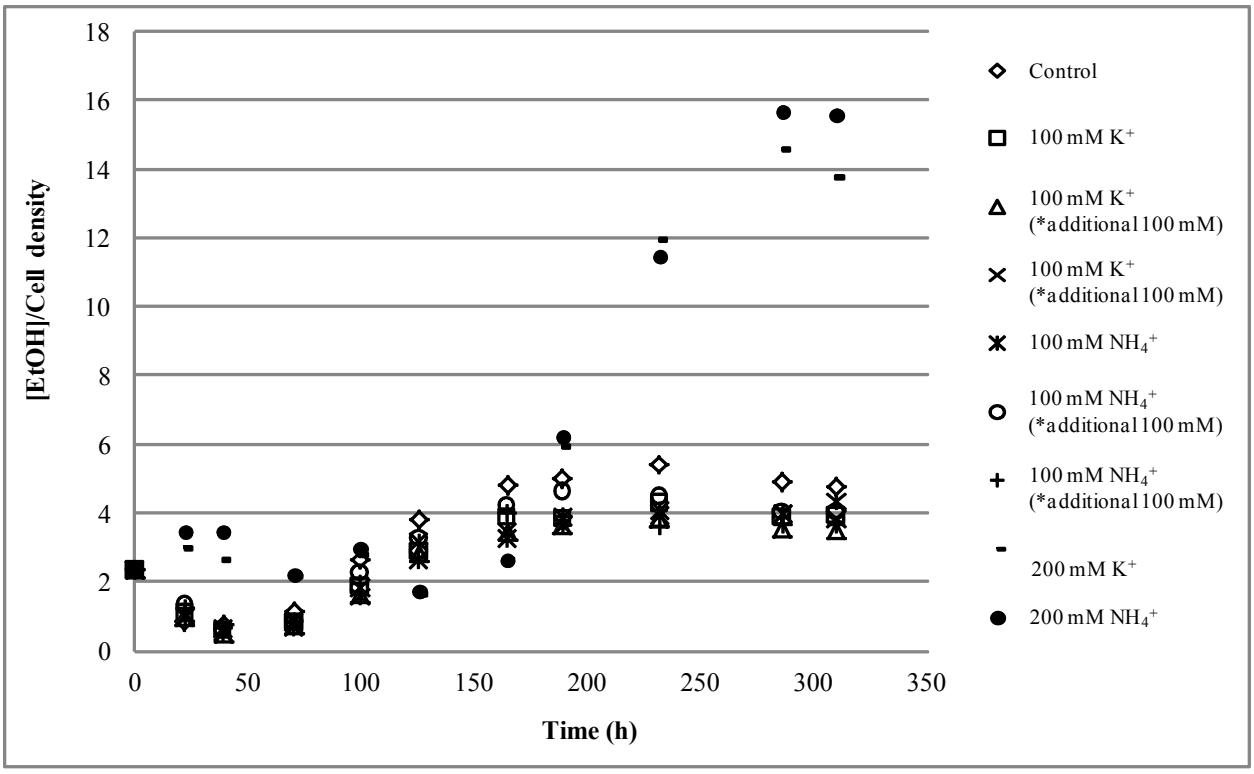

Figure 4-30. [EtOH]/cell density versus time

From the above quantitative analysis, comparatively higher osmolarity will favor higher [EtOH]/cell density. However, for industrial bioreactor runs, if NH_3 were not cleaned out of producer gas, over time NH_4^+ can be accumulated to significant levels (much higher than those tested in this work). If this happens, not only will cell growth be inhibited to dormancy but ethanol formation can also be totally inhibited if there is no cell growth at all. Therefore, even though NH_4^+ may benefit ethanol production, its adverse effect on cell growth demonstrates that NH_3 still needs to be scrubbed from any syngas stream before feeding the gas into bioreactors.

4.5 Conclusions

Key findings include: (a) NH_4^+ can build up to significant levels during a typical bioreactor run cycle. [NH_4^+] accumulated in media versus time has been calculated for given τ_g* values to quantify the effect of NH_4^+ accumulation during industrial fermentation if typical syngas is not cleaned. (b) The cell concentration and cell growth rate were substantially inhibited with increasing [NH_4^+]. It was confirmed that the effect was due to osmolarity rather than NH_4^+. (c) It was confirmed that higher osmolarity level rather than NH_4^+ per se would impact the ratio of [EtOH]/cell density. (d) The results of batch studies were confirmed in a continuous gas flow bioreactor system with pH control. Results of the continuous gas flow measurement substantiated the finding that osmolarity plays a key role in affecting cell growth. (e) Ammonia should be cleaned from syngas to mitigate negative effects on cell growth.

5. Effects of ammonia impurity in syngas on hydrogenase and alcohol dehydrogenase (ADH) activity

5.1 Introduction

One process efficiency issue is the ability of key cellular enzymes to produce reducing equivalents from syngas that are critical for product formation. As shown in Figure 1-4 in Chapter 1, the formation of reducing equivalents can occur from either H_2 via the hydrogenase enzyme and/or CO via the carbon monoxide dehydrogenase (CODH) enzyme. If the hydrogenase activity is inhibited, the decrease in reducing equivalents could potentially be offset by the utilization of CO via CODH at the expense of using CO for product formation. Therefore, to maximize carbon conversion efficiency, it is essential to keep the hydrogenase activity at its maximum level by minimizing inhibitory effects from potential hydrogenase inhibitors. Since there is an abundance of impurities in raw syngas from a gasifier, such as ammonia, significant concentrations of the impurity can potentially accumulate in the media inside a bioreactor. Therefore it is necessary to explore the positive or negative effects of impurities on hydrogenase activity. In this chapter, special effort was directed into investigation of the individual inhibitory effects of NH_4^+ on hydrogenase activity. As part of the protocol, the effects of Cl^-, their combined effects of NH_4Cl, the effects of K^+, and $H_2PO_4^+$ on hydrogenase activity were also tested.

P11, used in this study, is a strictly anaerobic acetogen which uses the metabolic pathway outlined in Chapter 1 (Figure 1-4). Typically, acetogens display a biphasic fermentation [93]. During the cell exponential growth phase, high amounts of acetate and butyrate (acidogenesis) are produced. However, during the cell stationary growth phase, more alcohols (solventogenesis) are produced. As shown in Figure 1-4 in the sloventogenic branch of the pathway, acetyl CoA is first converted to acetaldehyde via the catalyzation of aldehyde dehydrogenase. Acetaldehyde is subsequently converted to ethanol catalyzed by alcohol dehydrogenase (ADH). The following two reactions display the mechanism

$$\text{Acetyl-CoA} + \text{NADH} + \text{H}^+ \rightarrow \text{Acetaldehyde} + \text{NAD}^+ + \text{CoA-SH}$$

$$\text{Acetaldehyde} + \text{NADH} + \text{H}^+ \leftrightarrow \text{Ethanol} + \text{NAD}^+$$

ADH promoting the formation of ethanol is characterized by the forward ADH assay discussed in this text. Since the activity level of the forward ADH will affect the ethanol production, it is one of the key interests in this chapter.

5.2 Research objectives

- Investigate the individual inhibitory effects of NH_4^+ on hydrogenase activity.
- Besides NH_4^+, assess the potential inhibition of other ions in the media, such as Cl^-, $H_2PO_4^-$, and K^+ for hydrogenase activity effects since these components are found in media and are part of the experimental protocol to explore NH_4^+ effects on hydrogenase activity.
- Develop a kinetic model of hydrogenase activity valid for multiple inhibitors. Model parameters such as K_{H_2} (Michaelis-Menten constant), V_m (maximum

hydrogenase activity), K_i (inhibition constants for NH_4^+ and Cl^-, etc.) will be obtained by fitting the model to the experimental data.

- Investigate the effects of NH_4^+ on hydrogenase activity within a continuous gas feeding bioreactor under controlled pH.
- Measure the forward ADH activity under varying concentrations of NH_4^+ to find the concentration range of NH_4^+ which will directly impact forward ADH activity or ethanol production since NH_4^+ was vaguely mentioned as an inhibitor for ADH at very high concentrations [94, 95].

5.3 Materials and methods

5.3.1 Microorganism

The hydrogenase assay used *Clostridium ragsdalei* as the microbial catalyst (Clostridium strain P11; ATCC PTA-7826) that could utilize syngas to produce ethanol. P11 was passaged in 50 mL media (the same media detailed in Chapter 4) three times using strict anoxic techniques in the presence of 40% CO, 30% H_2, and 30% CO_2. The headspace was purged with the gas mixture at 20 psig and the gases were replaced on a daily basis. The third passage was used to obtain active cell samples for the hydrogenase assay. All studies were conducted at 37 ºC.

5.3.2 Hydrogenase assay

Two Hungate tubes (size: 60x125mm), one containing a cell solution and the other containing an electron acceptor solution, were prepared separately in an anaerobic chamber. The electron acceptor solution contained the following reagents: 0.3 ml of 1 M phosphate buffer

(mixture of 1 M KH_2PO_4 and 1 M K_2HPO_4 at pH=6), 2.3 ml of degassed water, and 0.4 ml of 0.04 M benzyl viologen dichloride (BV). BV is the electron acceptor for the electrons released from H_2 via hydrogenase. The cell solution contained the following reagents: 0.3 ml of 1 M phosphate buffer (pH=6), 1.8 ml of degassed water, 0.3 ml of 0.5 M dithiothreitol (DTT), 0.3 ml of active P11 cells. DTT was freshly made before each assay owing to its instability in water. All reagents were purchased from Sigma-Aldrich (St. Louis, MO).

To study the potential inhibitory effects of ions on the hydrogenase assay, 0.3 ml of various ion solutions were added to the electron acceptor solution (in place of an equivalent amount of water) prior to running the assay. In one study, NH_4Cl of 0.0 (control), 1.34 or 2.67 M was added. In another study, $NH_4H_2PO_4$ of 0.0 (control), 2.40 or 4.80 M was added. Since it was important to assess the unique effect of NH_4^+ alone, it was important to also perform studies using KH_2PO_4 of 0.0 (control), 1.34 mM and 2.67 M and KCl of 0.0 (control), 1.34 or 2.67 M. For all ion additions, H_3PO_4 was used to adjust the pH to 6 if needed.

After the two solutions were prepared in the Hungate tubes, both tubes were removed from the anaerobic chamber and purged with pure H_2 or a H_2/N_2 mixture to obtain the desired H_2 gas composition. The gases were added using two mass flow controllers, one for H_2 and one for N_2, with a total flow rate of 50 sccm. The H_2 gas flow rate was 15, 30, or 50 sccm with N_2 as the balance of the total flow rate. Thus, the H_2 gas composition assessed was 30, 60, and 100%. For the purging, two needles were inserted through the Hungate tube septum. A longer 20-gauge needle was used as the gas inlet while a shorter 22-gauge needle was used to provide a vent to maintain positive pressure inside the tube. A 4.6 ml cuvette for the spectrophotometer was also purged with the same gas mixture. All the tubes and cuvette were purged for 5 minutes.

At the end of purging, 5 psig of pressure was allowed to build up in these two Hungate tubes and the cuvette to keep air from coming in. For the cell solution tube, one minute before the end of purging, 0.3 ml triton X-100 (prepared in a 1ml syringe/needle assembly done in the anaerobic chamber) was injected to permeate the cell wall to expose hydrogenase in the cells to the solution. After these procedures, the two Hungate tubes were placed in a water bath at 37 °C for five minutes. Finally, 2 ml from the electron acceptor solution tube and 0.67 ml from the cell solution tube were transferred and injected into the cuvette. After shaking vigorously a few times, a 22-gauge needle connected to a 0.3 psig check valve was quickly inserted and then removed to relieve excess pressure and maintain a constant positive pressure in the cuvette. The ambient pressure of the study was 13.3 psi such that the cuvette pressure was always maintained at a total pressure of 0.93 atm (13.6 psi). After mixing, the final concentrations for the various ion studies were obtained: 0, 180 mM, and 360 mM $NH_4H_2PO_4$; 0, 100 mM, and 200 mM KCl; 0, 100 mM, and 200 mM NH_4Cl; 0, 100 mM, and 200 mM KH_2PO_4.

The cuvette was placed in a heat-controlled spectrophotometer at 37 °C during the course of the assay which converted oxidized BV to reduced BV. The absorbance (Abs) of reduced BV was monitored at 546 nm and converted to an associated concentration where $C_{BV}=Abs/(\varepsilon*b)$. Here, ε is the extinction coefficient (7.55 mM^{-1} cm^{-1} at 546 nm) and b is the cuvette path length of 1 cm. The production rate of reduced BV (R_{BV}) was obtained from the initial slope of the concentration vs. time curve. Initial slope data is important for the analysis since knowledge of the H_2 partial pressure is important. With initial slope data, the known initial H_2 partial pressures could be utilized. Since the rate of H_2 consumption (R_{H2}) is equal to $-½R_{BV}$ according to an electron balance, the hydrogenase activity relative to the cell mass (U/mg) was obtained by dividing $1/2R_{BV}$ by the cell density. The activity U represents one μmol H_2 consumed per

minute. It is important to account for the cell density or turbidity since higher cell density will give higher hydrogenase activity readings. Figure 5-1 shows an example of the absorbance (Abs) time course for a typical run of hydrogenase activity. The initial slope used for the above calculation is shown in the figure after an initial perturbation period that was caused by vigorous shaking of the mixture.

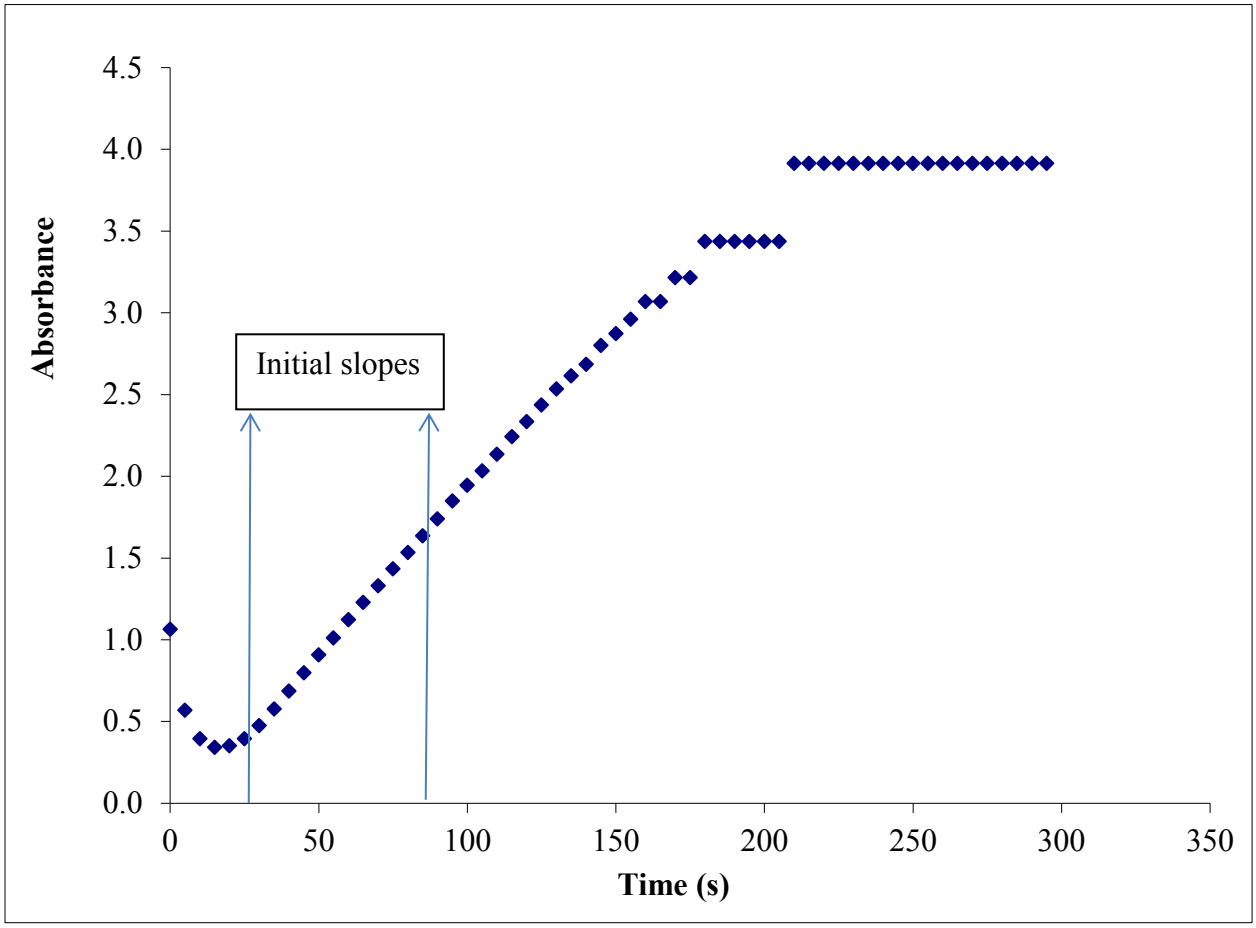

Figure 5-1. The initial slope for the study of the hydrogenase activity

The cell density of the inoculum was measured using a spectrophotometer at 660 nm to obtain the optical density (OD). The OD is proportional to the cell density (~0.43 g/L per OD

unit) based on a linear calibration chart. This calibration is only good for the OD ranging from 0~0.4. For any OD larger than 0.4, it was necessary to dilute the solution such that the OD was within the linear calibration range. The cell density in the assay cuvette was calculated based on the dilution of the cells after all solutions were mixed together.

5.3.3 Measurement of hydrogenase activity in a continuous gas-feeding bioreactor

For the continuous bioreactor runs, there were two parallel bioreactors, denoted as Bioreactor A (inlet gas was initially doped with NH_3 until a specified NH_4^+ concentration was obtained) and Bioreactor B (control). The detailed protocol was mentioned in Chapter 4 (Section 4.3.3). For this hydrogenase activity study, five different concentrations of NH_4^+ (59,110, 158, 204, 227 mM) were targeted. The protocol for the hydrogenase activity measurement was the same as detailed above in Section 5.3.2. The cell samples taken from both bioreactors were sealed in two air-tight syringes (1mL). Hydrogenase activities were measured simultaneously with OD measurement so that the cell concentration could be accounted for.

5.3.4 Forward alcohol dehydrogenase (ADH) assay

Acetaldehyde was used as the substrate for the forward ADH assay. The protocol used in this work was adapted from Ahmed's dissertation [88] as detailed below: 0.4 mL 1M Tris-HCl, 0.5 mL 0.08 M dithiothreitol (DTT), 0.1 mL 5% v/v triton X-100, 0.1 mL 0.01 M NADH, 0.4 mL 0.1 M acetaldehyde and 1.5 mL degassed DI water. This above-mentioned formula is for the control assay in the absence of NH_4^+. For the comparative assay, 0.3 mL of [$NH_4H_2PO_4$] (0.5, 1, 1.5, or 2 M) was used to replace the same volume of water to reach a desired [NH_4^+] (50, 100, 150, or 200 mM) in the cuvette. All chemicals were purchased from Sigma-Aldrich. DTT and NADH should be freshly prepared prior to each run owing to their instability in water. All the

above reagents were added into a 4.5 mL optical glass cuvette in an anaerobic chamber. After sealing and removing this cuvette from the anaerobic chamber, it was purged with pure N_2 for one minute. For the purging, two needles were inserted through the cuvette septum. A longer 20-gauge needle was used as the gas inlet while a shorter 22-gauge needle was used to provide a vent to maintain positive pressure inside the tube. After purging with 5 psig in the cuvette headspace, the cuvette was placed in a 37 °C receptacle of a UV-visible spectrophotometer set at 340 nm wavelength. A gas-tight syringe (1 mL) was used to inject 0.5 mL cell source into the cuvette. After shaking vigorously for a few times, the cuvette was placed back in the receptacle and the kinetic recording process was started. The concentration of NADH was calculated using Beer's law ($C=Abs/(\varepsilon \cdot b)$), where ε is the extinction coefficient for NADH (6.22 $mM^{-1}cm^{-1}$ @ 340 nm), b is the cuvette path length (1 cm). As show in the reaction (Acetaldehyde + NADH + $H^+ \leftrightarrow$ Ethanol + NAD^+), the change of NADH is the same as that of acetaldehyde on a molar basis. The maximum reaction rate ($R=\Delta C/\Delta t$) was calculated from the initial linear slope of the curve after a short lag phase. R was then divided by the measured cell mass and converted into specific activity (U/mg), where U represents μmols of acetaldehyde consumed per minute.

5.4 Results and discussions

As detailed in Chapter 4 (Section 4.4.1), since NH_4^+ is very soluble in water, NH_4^+ can be built up to significant levels over time to potentially affect the performance of an anaerobic fermentation system. For this hydrogenase activity study, the effects of NH_4^+ concentrations up to 360 mM on hydrogenase activity were assessed.

5.4.1 Ammonium chloride (NH_4Cl) inhibition

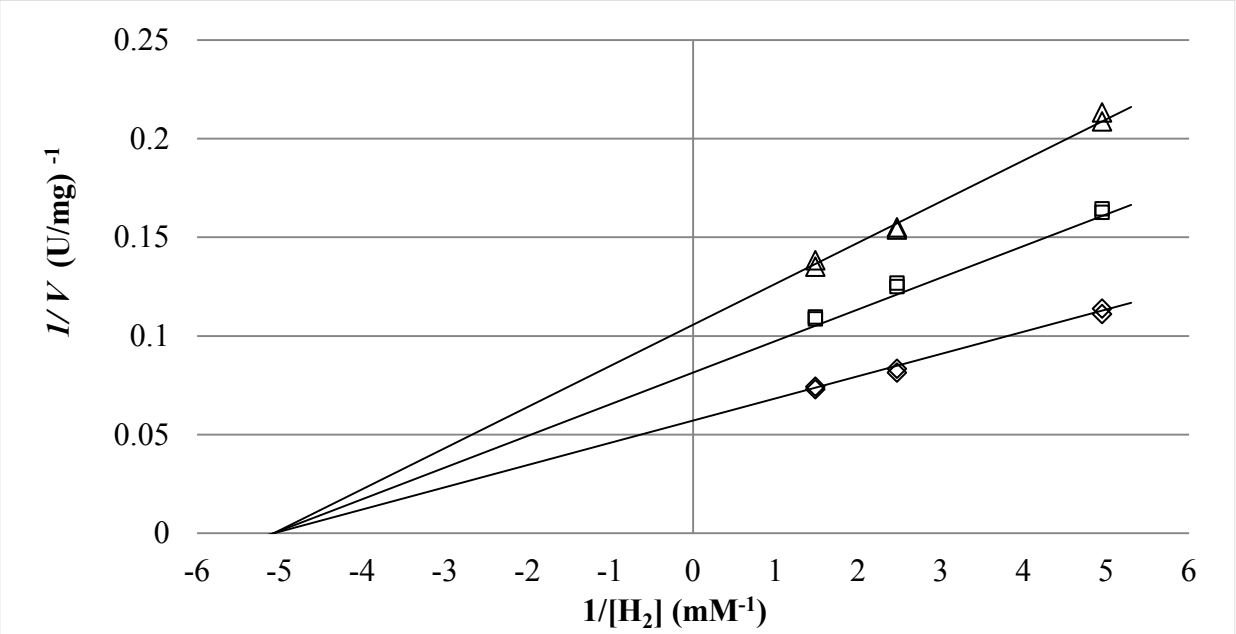

Figure 5-2. Double reciprocal plot showing the non-competitive inhibition of hydrogenase by NH_4Cl. The solid lines represent Equation 5-6. The concentrations of NH_4Cl in units of mM are (◇) 0, (□) 100, (△) 200

Figure 5-2 shows the effect of H_2 concentration ($[H_2]$) on hydrogenase activity (V) as a function of different concentrations of NH_4Cl. The x- and y- axis show inverse values of $[H_2]$ and V, respectively, to obtain model parameters. The lines represent a model described later in Section 5.5.1. $[H_2]$ was based on Henry's law for H_2 (H_{H_2}) and the H_2 gas partial pressure (P_{H_2}) according to:

$$[H_2] = H_{H_2} P_{H_2}$$

The value of H_{H_2} is 7.2 x 10^{-6} mM Pa^{-1} for H_2 corrected for 37 °C [67]. It was assumed that H_2 behaved as an ideal gas. Thus 30, 60, and 100 % H_2 at a total pressure of 9.42 x10^4 Pa equated to $[H_2]$ of 0.20 mM, 0.41 mM and 0.68 mM, respectively. As the NH_4Cl concentration increases,

the activity decreases. This trend is observed at all [H_2]. At 1/[H_2]=5 mM^{-1}, *V* was 9.0 U/mg for 0 mM NH_4Cl, 6.2 U/mg for 100 mM NH_4Cl, and 4.8 U/mg for 200 mM NH_4Cl. Thus, at 200 mM NH_4Cl, the hydrogenase activity was 53% compared to that of the control.

5.4.2 Ammonium ion (NH_4^+) inhibition

Since it was important to assess the unique contribution of NH_4^+ alone, studies were also performed using $NH_4H_2PO_4$. Figure 5-3 shows the effect of [H_2] on *V* as a function of different concentrations of $NH_4H_2PO_4$. As shown, when the $NH_4H_2PO_4$ concentration increased, the activity decreased. This trend was observed at all [H_2]. It should be noted that initial studies with KH_2PO_4 of 100 mM and 200 mM showed no hydrogenase inhibition as shown in Figure 5-4 so $H_2PO_4^-$ is not an inhibitor. Thus, NH_4^+ is the only inhibitor of hydrogenase for this study.

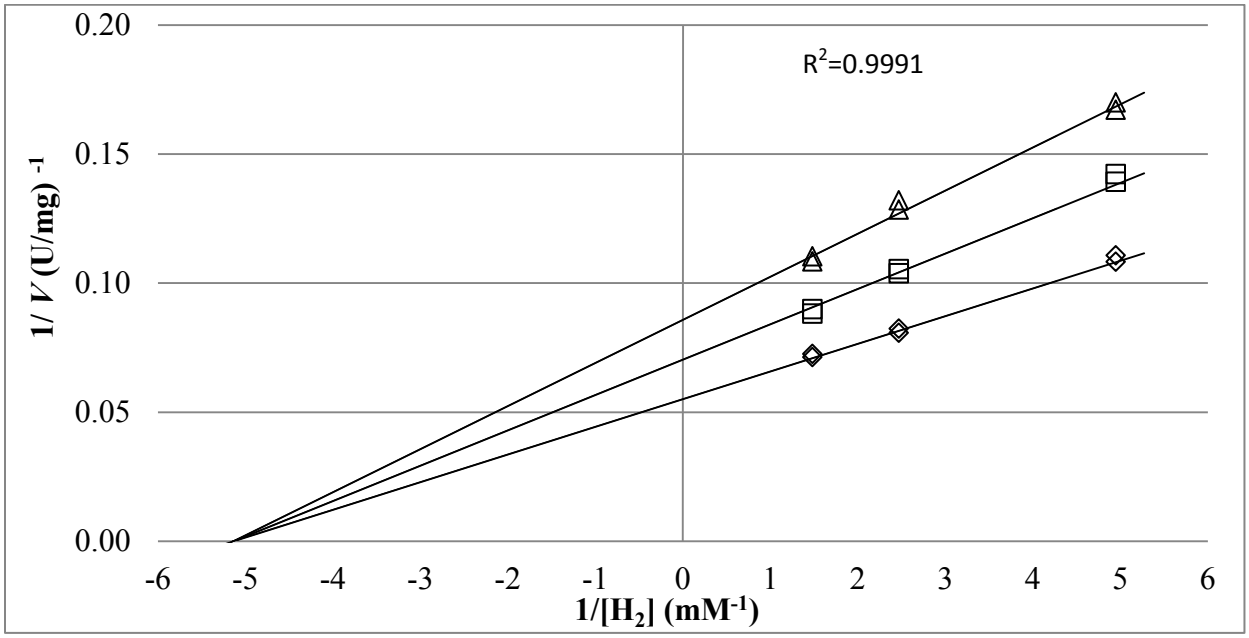

Figure 5-3. Double reciprocal plot showing the non-competitive inhibition of hydrogenase by $NH_4H_2PO_4$. The solid lines represent Equation 5-2. The concentrations of NH_4^+ in units of mM are (◇) 0, (□) 180, (△) 360

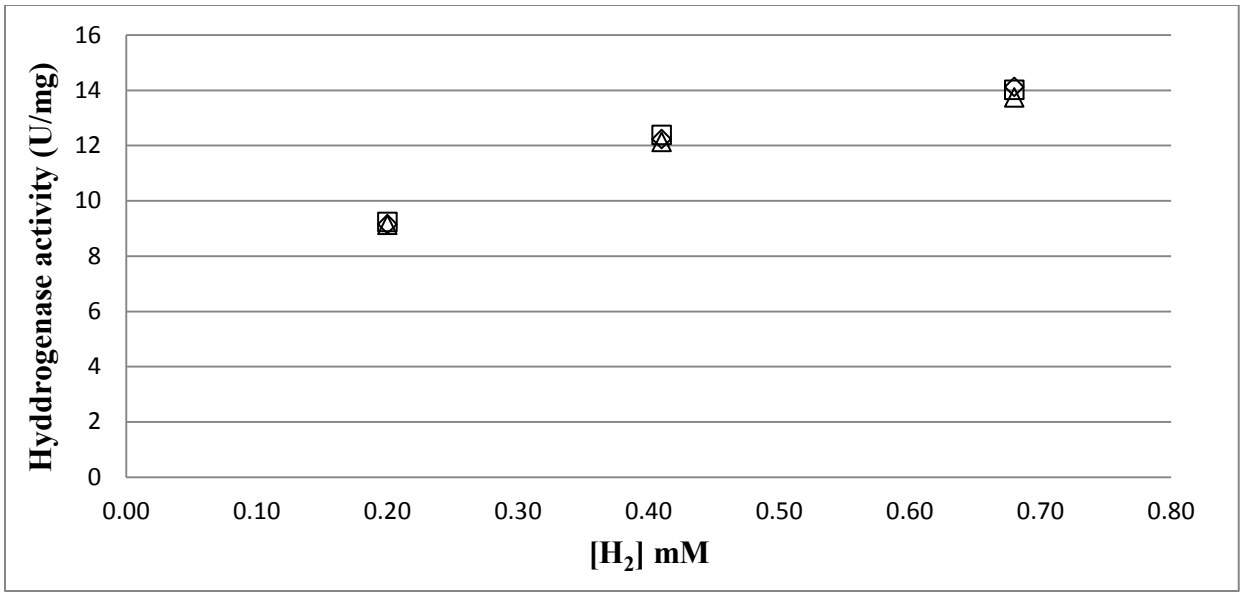

Figure 5-4. Hydrogenase activity versus H_2 concentration [H_2] for varying concentrations of KH_2PO_4. The concentrations of KH_2PO_4 are (◇) 0, (□) 100, and (△) 200 mM

5.4.3 Chloride ion (Cl^-) inhibition

Since the studies shown in Figure 5-2 also include Cl^-, Figure 5-5 shows the effect of [H_2] on *V* as a function of different concentrations of KCl. As before, the lines represent a model described in Section 5.5.1. As noted, when the KCl concentration increased, the activity decreased. This trend was observed at all [H_2]. It should be noted that initial studies with KH_2PO_4 of 100 mM and 200 mM showed no hydrogenase inhibition as shown in Figure 5-4 so K^+ is not an inhibitor. Thus, Cl^- is a key inhibitor of hydrogenase and will therefore contribute to the inhibition effects shown in Figure 5-2. As expected for similar amounts of enzyme, when comparing Figures 5-3 and 5-5, it should be noted that the controls (no ion addition) for both studies showed very similar activity as a function of [H_2]. When comparing ion effects at $1/[H_2]$=

5 mM^{-1}, *V* was 7.2 U/mg for 180 mM NH_4^+ whereas *V* was 7.8 U/mg for 100 mM Cl^-. Thus, it appears that Cl^- is a greater inhibitor of hydrogenase as compared to NH_4^+.

In Figure 5-5 for Cl^-, the hydrogenase activity at 200 mM Cl^- was 65% compared to that of the control. As previously noted in Figure 5-2 at 200 mM NH_4Cl, the hydrogenase activity was reduced to 53% compared to that of the control. Since NH_4^+ and Cl^- were the only inhibitors in Figure 5-2, it can be seen that the additional 12% reduction in activity is from NH_4^+ with Cl^- being the stronger inhibitor. With all of the above findings, a kinetic model was developed (in Section 5.5.1) to provide insights on the inhibition of NH_4^+.

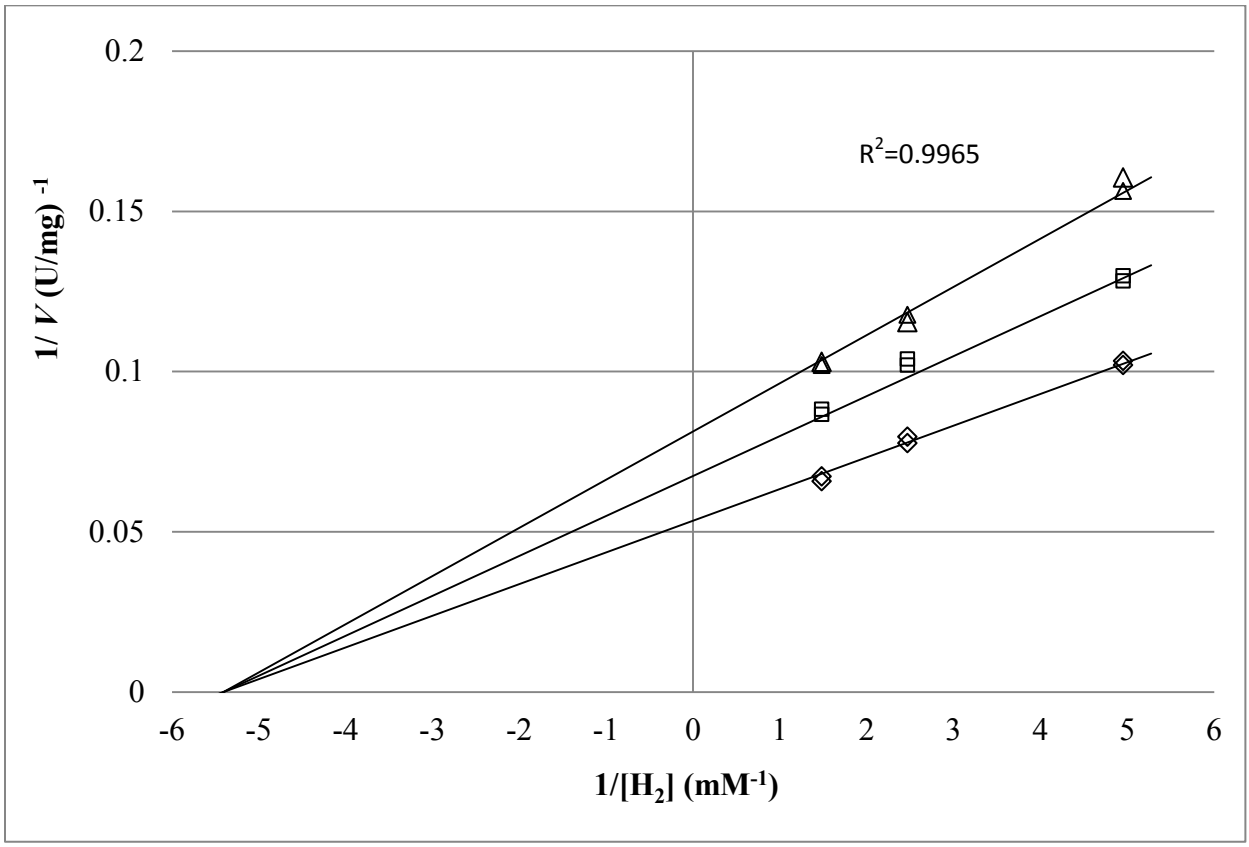

Figure 5-5. Double reciprocal plot showing the non-competitive inhibition of hydrogenase by KCl. The solid lines represent Equation 5-2. The concentrations of Cl^- in units of mM are (◇) 0, (□) 100, (△) 200

5.5 Discussion

5.5.1 Hydrogenase Kinetic Model

There are three major enzyme inhibitions namely competitive, non-competitive and uncompetitive. For non-competitive inhibition, inhibitors bind on sites other than the active sites resulting in reduced enzyme affinity to the substrates. For non-competitive inhibition with a single inhibitor [96]:

$$V = \frac{V_m}{\left(1+\frac{K_{H_2}}{[H_2]}\right)\cdot\left(1+\frac{C_i}{K_i}\right)} \tag{5-1}$$

where V is the enzyme activity, V_m represents the maximum hydrogenase activity under the specific experimental conditions, K_{H_2} is the Michaelis-Menten constant for H_2, C_i is the concentration of inhibiting species (e.g. Cl^-), and K_i is the inhibition constant for the inhibiting species. Equation 5-1 can be rearranged into a double reciprocal plot according to:

$$\frac{1}{V} = \frac{K_{H_2}}{V_m}\left(1+\frac{C_i}{K_i}\right)\cdot\left(\frac{1}{[H_2]}\right)+\frac{1}{V_m}\left(1+\frac{C_i}{K_i}\right) \tag{5-2}$$

As seen from Equation 5-2, a plot of $1/V$ versus $1/[H_2]$ will give a straight line.

The entire data set of Figure 5-3 for NH_4^+ alone was simultaneously regressed to Equation 5-2 using statistical software (SAS 9.2.3, SAS Institute, Cary, NC). The model is shown as lines in Figure 5-3. The values were V_m = (18.2 ± 0.5) U/mg, K_{H_2} = (0.19 ± 0.1) mM, and $K_{NH_4^+}$ = (649 ± 35) mM. The model fit the data very well as indicated by the R^2 value and confirms that the NH_4^+ inhibition is non-competitive. According to Equation 5-1, when $C_i = K_i$,

the activity is reduced by ½. Thus, when the NH_4^+ concentration becomes 649 mM, the enzyme activity is compromised by one-half. As a result of NH_3 impurity in the syngas, significant NH_4^+ concentrations that affect activity can occur rather rapidly as shown by the NH_4^+ accumulation data in Chapter 4 Section 4.4.1 (although the time will depend upon the reactor conditions). The K_{H_2} value obtained in this study from P11 was comparable to published data for other bacteria using pure enzyme assays although it should be noted that the type of hydrogenase can be different among species. It is reasonably proposed that P11cells harbor both type I and II hydrogenases. Adams and Mortensen reported that the K_{H_2} value for hydrogenase I of *Clostridium pasteurianum* is around 0.18 mM using methylene blue as the electron acceptor [97]. Dobrindt and Blaut reported that the K_{H_2} value for *Sporomusa sphaeroides* is 0.34 mM with benzyl viologen as the electron acceptor [98].

Similar to the NH_4^+ data, the entire data of Figure 5-5 for the Cl^- studies was also fit simultaneously to Equation 5-2 with the model shown as lines in Figure 5-5. The regressed parameters were V_m = (18.7 ± 1.0) U/mg, K_{H_2} = (0.19 ± 0.02) mM, and K_{Cl^-} = (384 ± 41) mM. The model fit the data very well as indicated by the R^2 value and confirms that the Cl^- inhibition is non-competitive. As expected, V_m was similar for both ion studies since the cell source, cell preparation, and enzyme analysis methods were the same. However, it is feasible that V_m could vary when cell samples are taken at different stages of growth since V_m includes the amount of hydrogenase. In contrast, a proper assay should always give the same K_{H_2} since K_{H_2} is independent of the amount of hydrogenase. This is confirmed by the agreement in values of K_{H_2}. Note that K_{Cl^-} is smaller than $K_{NH_4^+}$ such that Cl^- is a greater inhibitor as compared to NH_4^+.

As noted above, both NH_4^+ and Cl^- are non-competitive inhibitors. To look at the combined effects to understand the results of Figure 5-2, it can be shown for multiple inhibitors that the model is similar to Equation 5-1 according to:

$$V = \frac{V_m}{\left(1+\frac{K_{H_2}}{[H_2]}\right)\cdot\left[1+\sum_i\left(\frac{C_i}{K_i}\right)\right]} \tag{5-3}$$

Thus, in the presence of both NH_4^+ and Cl^-:

$$V = \frac{V_m}{\left(1+\frac{K_{H_2}}{[H_2]}\right)\cdot\left[1+\left(\frac{[NH_4^+]}{K_{NH_4^+}}+\frac{[Cl^-]}{K_{Cl^-}}\right)\right]} \tag{5-4}$$

Since $[NH_4^+]=[Cl^-]=[NH_4Cl]$ for the study in Figure 5-2, Equation 5-4 becomes:

$$V = \frac{V_m}{\left(1+\frac{K_{H_2}}{[H_2]}\right)\cdot\left[1+[NH_4Cl]\cdot\left(\frac{1}{K_{NH_4^+}}+\frac{1}{K_{Cl^-}}\right)\right]} = \frac{V_m}{\left(1+\frac{K_{H_2}}{[H_2]}\right)\cdot\left(1+\frac{[NH_4Cl]}{K_{NH_4Cl}}\right)} \tag{5-5}$$

As seen, $1/K_{NH_4^+}+1/K_{Cl^-}$ was replaced with $1/K_{NH_4Cl}$ since the K's are just a combination of constants. From the regressed K_i values noted above of the independent NH_4^+ and Cl^- experiments, it can be estimated that K_{NH_4Cl} is 241 mM.

For the combined NH_4^+ and Cl^- study, the associated double-reciprocal plot for Figure 5-2 is

$$\frac{1}{V} = \frac{K_{H_2}}{V_m}\cdot\left[1+\left(\frac{[NH_4Cl]}{K_{NH_4Cl}}\right)\right]\cdot\left(\frac{1}{[H_2]}\right)+\frac{1}{V_m}\cdot\left[1+\left(\frac{[NH_4Cl]}{K_{NH_4Cl}}\right)\right] \tag{5-6}$$

By regressing the data in Figure 5-2 using Equation 5-6, the regressed parameters were V_m = (17.5 ± 1.3) U/mg, K_{H_2} = (0.20 ± 0.03) mM, and K_{NH_4Cl} = (235 ± 25) mM. As expected, the regressed value of K_{NH_4Cl} from an independent experiment is very close to the calculated value of K_{NH_4Cl} = 241 mM noted above. This consistency establishes confidence that the proposed kinetic model (Equation 5-3) is valid for this study. Since the K_{H_2} regressed parameter was the same for all three independent experiments, it reaffirms that K_{H_2} is an intrinsic parameter. On the other hand, V_m depends on the total amounts of enzyme in the assay [96]. Since $K_{NH_4^+} > K_{Cl^-} > K_{NH_4Cl}$, it is reaffirmed that Cl^- has a stronger inhibitory effect on hydrogenase as compared to NH_4^+.

For media used to grow the cells in this study, the total Cl^- concentration was 4.74 mM. According to Equation 5-1 with the fitted parameters for Cl^-, this concentration would reduce the hydrogenase activity to 98.8% as compared with the activity in the absence of Cl^-. Thus, it is unlikely that Cl^- in media will have a significant effect upon the hydrogenase activity as compared to the accumulation of NH_4^+ resulting from the NH_3 impurity in syngas. Since Cl^- is basically absent in *E. coli* cells [99], it is likely that there is no specific transporter to transport Cl^- across the cell membrane. Therefore, this suggests that Cl^- in the media would likely not be a hydrogenase inhibitor during whole cell applications. However, care still should be taken regarding the amount of Cl^- in media since Cl^- is inhibitory to cell growth [100].

As shown, accumulating NH_4^+ can be a major inhibitor of hydrogenase activity during syngas fermentation. As mentioned earlier, it is important to keep the hydrogenase activity at its maximum level to enable a more efficient process for converting available carbon (both CO and CO_2) to carbon-containing products. According to Equation (5-1), the ratio of V in the presence of NH_4^+ (V_{NH4+}) relative to V in the absence of NH_4^+ (V_0) at the same H_2 concentration is:

$$\frac{V_{NH_4^+}}{V_0} = \left(\frac{V_{m,NH_4^+}}{V_{m,0}}\right)\left(1+\frac{C_{NH_4^+}}{K_{NH_4^+}}\right)^{-1} \qquad (5\text{-}7)$$

When the enzyme level is the same in the presence or absence of NH_4^+ (i.e. $V_m = V_{m,NH4+}$), then the reduction in enzyme activity in the presence of NH_4^+ is affected by the $(1+C_{NH4+}/K_{NH4+})$ term. Figure 5-6 shows Equation 5-7 (with $V_m = V_{m,NH4+}$) as a function of the NH_4^+ concentration.

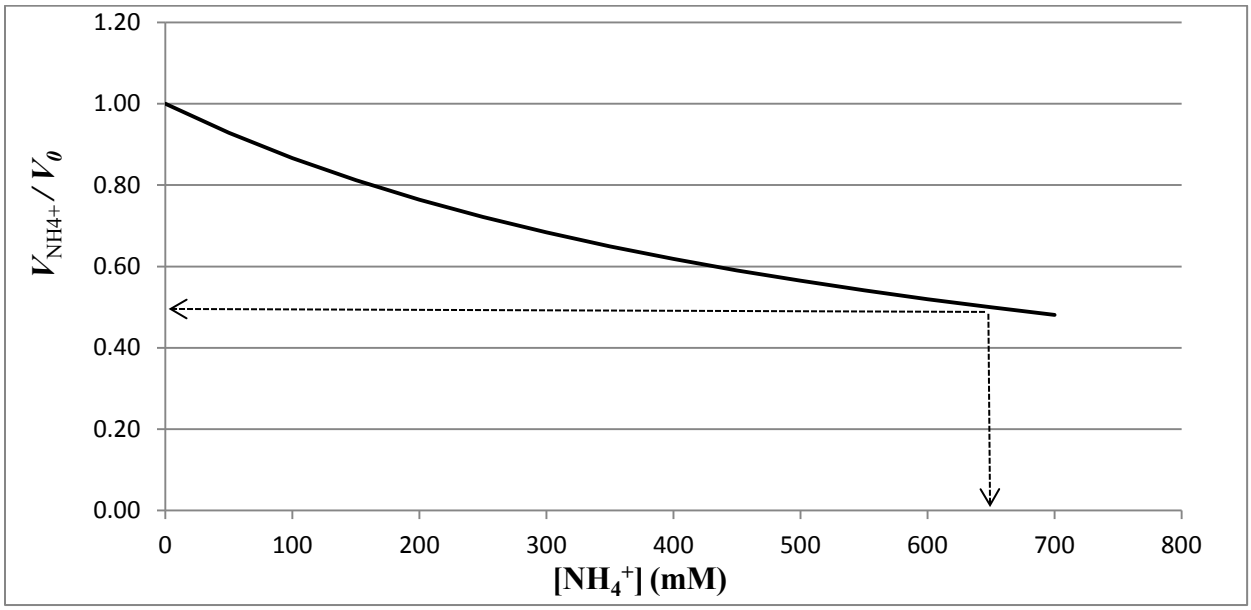

Figure 5-6. V_{NH4+}/V_0 versus $[NH_4^+]$. V_{NH4+} is the hydrogenase activity as a function of $[NH_4^+]$; V_0 is the hydrogenase activity in the absence of NH_4^+

It should be noted that the enzyme parameters are limited to pH 6 and 37 ºC as obtained in this study. Since NH_3 is very soluble in water, NH_3 in syngas can rapidly lead to very high NH_4^+ concentrations which can significantly reduce the activity of hydrogenase. For example, at 650 mM of [NH_4^+] (representing less than 5% of saturation), the hydrogenase activity is 50% of V_0. Obviously, the rate of NH_4^+ accumulation depends on the syngas flow rate, reactor design, and concentration of ammonia in the syngas. However, the important point is that NH_4^+ can have a significant impact on hydrogenase activity if NH_3 is not cleaned from the syngas.

5.5.2 Effects of NH_4^+ on hydrogenase activity within active whole cells

To further show evidence that external NH_4^+ in media can impact a cellular system, exposing P11 to NH_4^+ obtained from NH_3 flowing in a gas stream showed that hydrogenase activity was adversely affected. This study using two 3L bioreactors with 700 mL media was conducted at controlled pH of 5.5. The results are shown in Figures 5-7 to 5-11 with cell density on the primary y-axis.

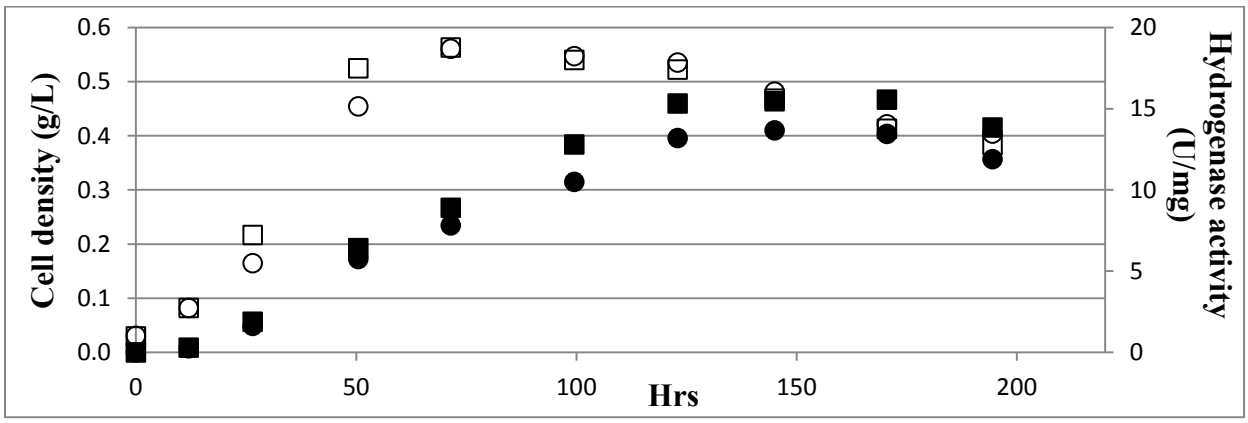

Figure 5-7. Cell density and hydrogenase activity versus time with and without NH_4^+ extracellular exposure. (□) and (○) represent cell density for control and 59 mM NH_4^+, respectively. (■) and (●) represent hydrogenase activity for control and 59 mM NH_4^+, respectively

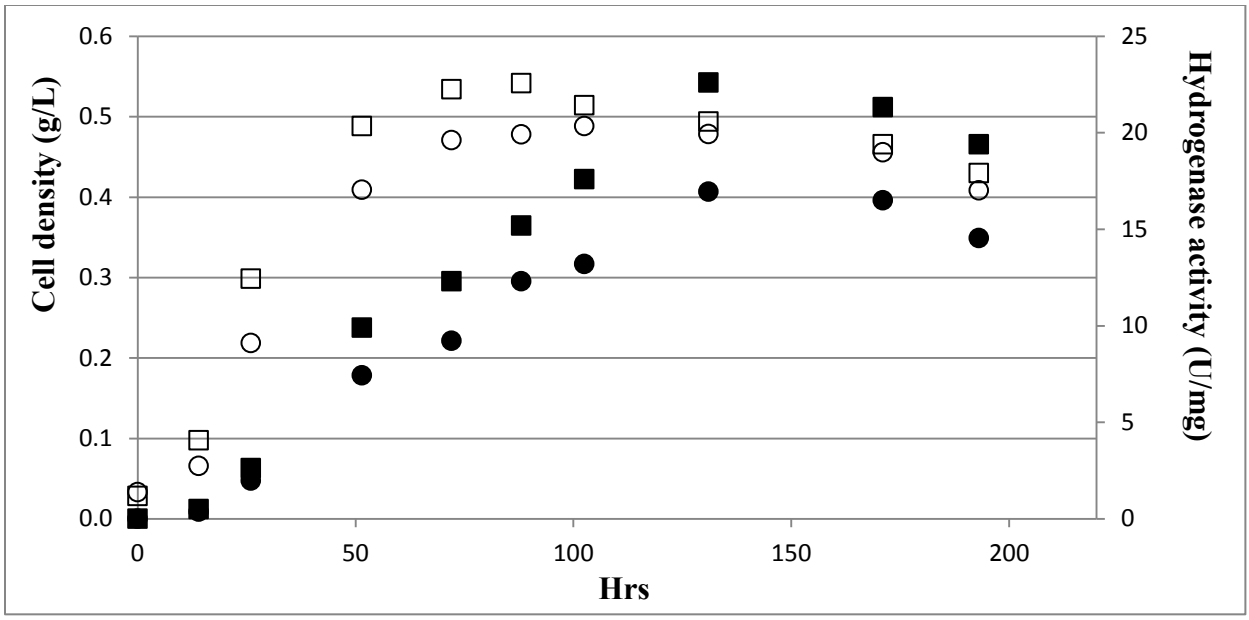

Figure 5-8. Cell density and hydrogenase activity versus time with and without NH_4^+ extracellular exposure. (□) and (○) represent cell density for control and 110 mM NH_4^+, respectively. (■) and (●) represent hydrogenase activity for control and 110 mM NH_4^+, respectively

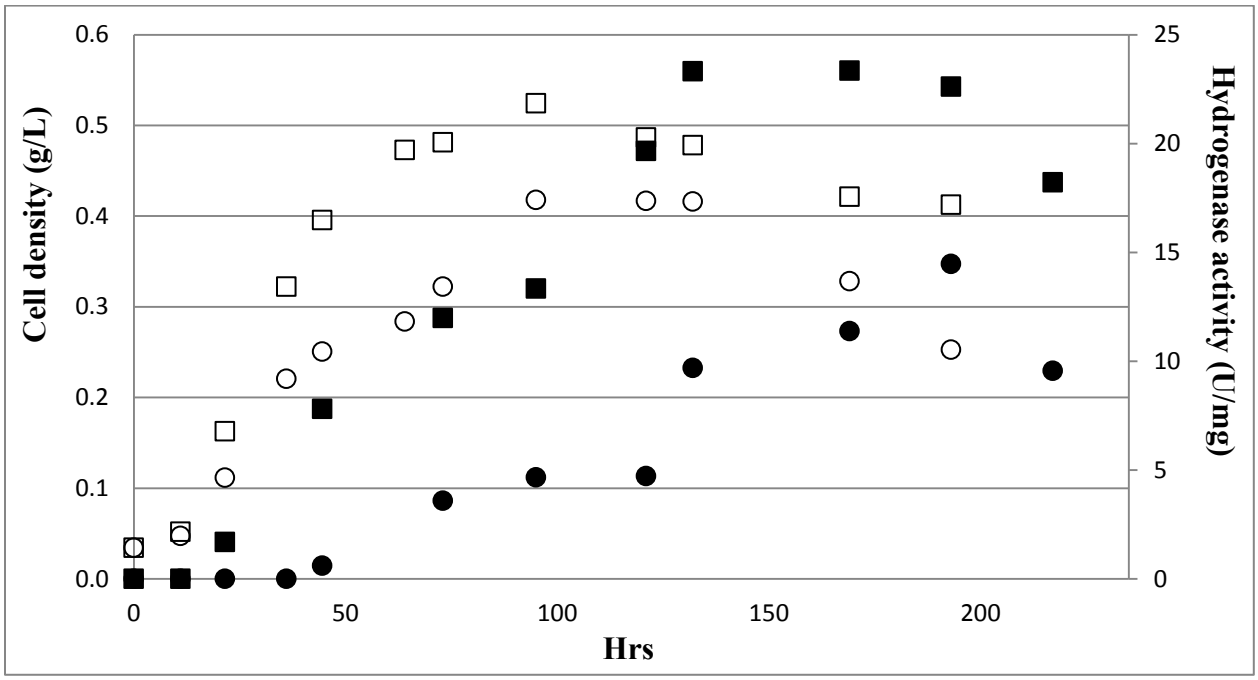

Figure 5-9. Cell density and hydrogenase activity versus time with and without NH_4^+ extracellular exposure. (□) and (○) represent cell density for control and 158 mM NH_4^+, respectively. (■) and (●) represent hydrogenase activity for control and 158 mM NH_4^+, respectively.

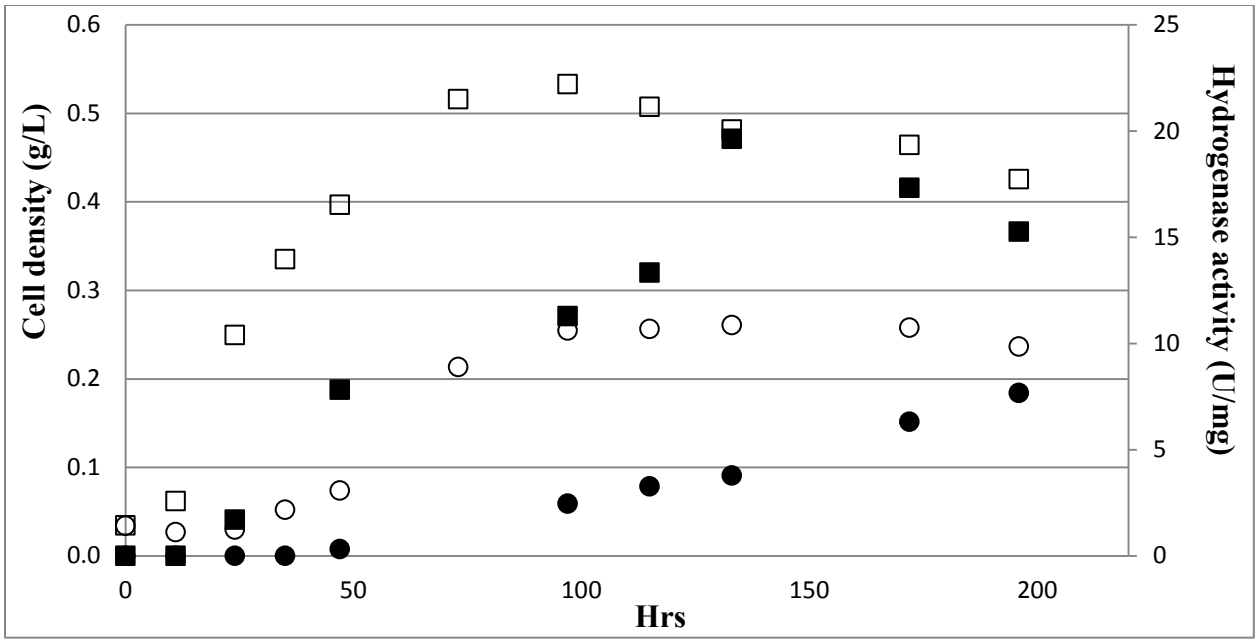

Figure 5-10. Cell density and hydrogenase activity versus time with and without NH_4^+ extracellular exposure. (□) and (○) represent cell density for control and 204 mM NH_4^+, respectively. (■) and (●) represent hydrogenase activity for control and 204 mM NH_4^+, respectively

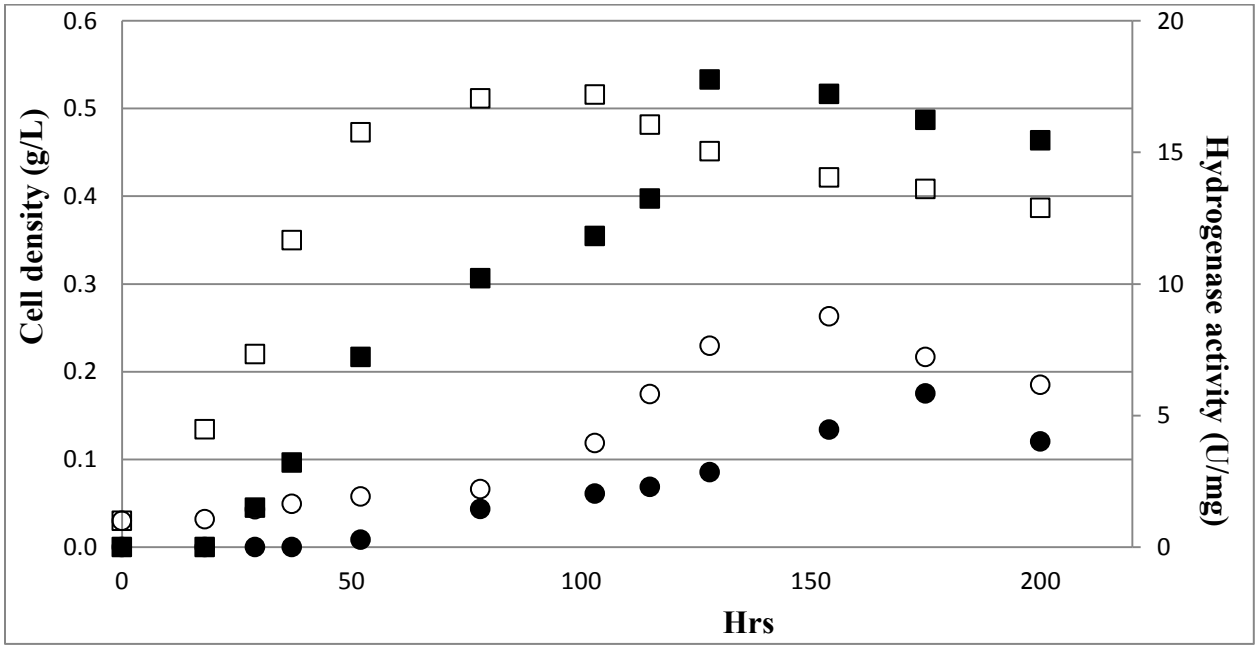

Figure 5-11. Cell density and hydrogenase activity versus time with and without NH_4^+ extracellular exposure. (□) and (○) represent cell density for control and 227 mM NH_4^+, respectively. (■) and (●) represent hydrogenase activity for control and 227 mM NH_4^+, respectively

As noticed, the cell density and hydrogenase activity were lower in the presence of NH_4^+ as compared to those of the controls. For all of the studies at 100 hours, the cell density, hydrogenase activity (in U/mg) in the bioreactors, and hydrogenase activity prediction using Equation (5-7) (with $V_m = V_{m,NH4+}$) in the NH_4^+ studies as compared to those of the controls are listed in Table 5-1

Table 5-1. For all of the studies at 100 hours, the cell density, hydrogenase activity (in U/mg) in the bioreactors and hydrogenase activity prediction using Equation (5-7) (with $V_m = V_{m,NH4+}$) in the NH_4^+ studies as compared to those of the controls

$[NH_4^+]$ (mM)	59	110	158	204	227
Cell density relative to control	1.01	0.95	0.80	0.48	0.23
V_{NH4+}/V_0 (Bioreactor runs)	0.82	0.75	0.35	0.22	0.17
V_{NH4+}/V_0 (if $V_m=V_{m,\ NH4+}$) (Prediction)	0.92	0.86	0.80	0.76	0.74

Table 5-1 was graphed into Figure 5-12 to easily identify trends. From Figure 5-12, the hydrogenase activity prediction using Equation 5-7 appears linear. This is consistent with Figure 5-6 since for $[NH_4^+]$ ranging from 59 to 227 mM, the hyperbolic curve is approximately linear. However, the measured hydrogenase activities in the bioreactors appear non-linear. At 158 mM $[NH_4^+]$, the hydrogenase activity in the bioreactors was significantly reduced to less than 40% compared with that of the control. As for the cell density, there appears a threshold $[NH_4^+]$ around 204 mM at which cell density was reduced to less than 50% compared with that of the control. It also appears that both cell density and hydrogenase activity were significantly affected at $[NH_4^+]$ around 204 mM and 158 mM, respectively.

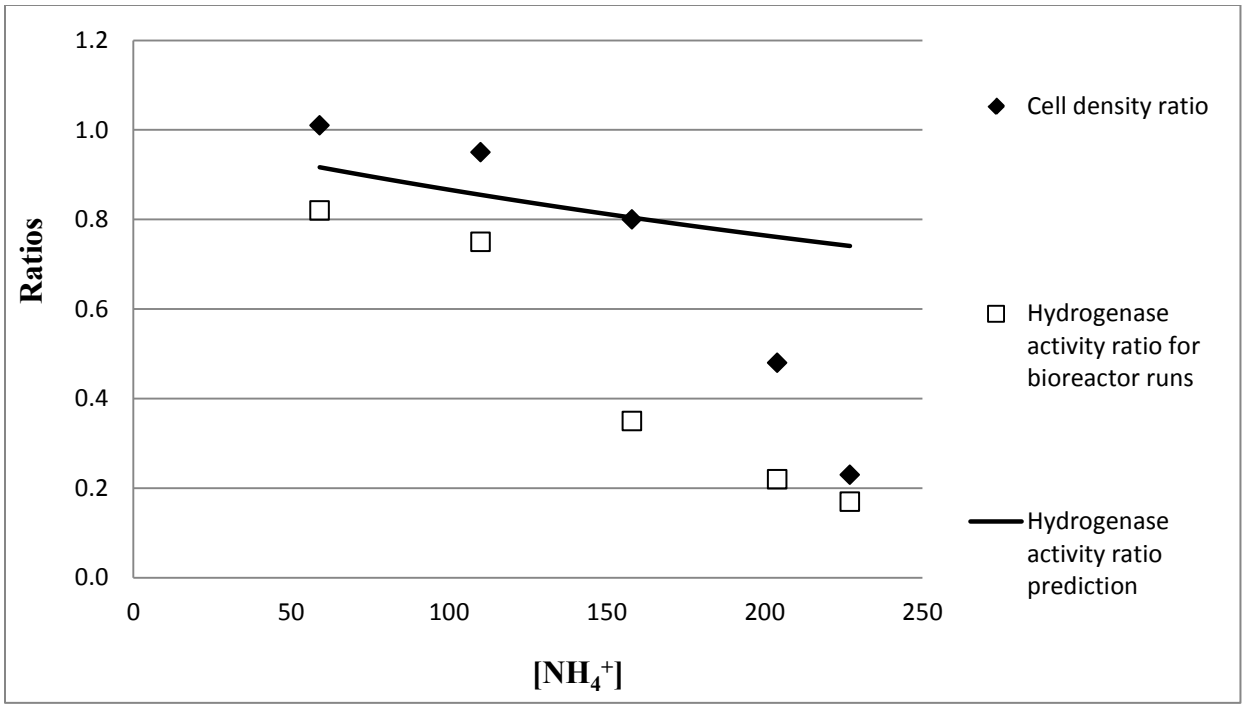

Figure 5-12. Ratios of cell density and hydrogenase activity in the bioreactors and from prediction

To address the inconsistency of Equation 5-7 predictions with the data in Figure 5-12, the effect of the C_{NH4+}/K_{NH4+} term would only be important if the NH_4^+ inhibition was irreversible since the assay was performed in the presence of pure H_2 and no NH_4^+ addition (only the cells were exposed to NH_4^+ prior to the assay). Thus, since the experimental activity ratio was even smaller than expected by just the C_{NH4+}/K_{NH4+} term, it is apparent that NH_4^+ exposure to cells significantly affects V_m (i.e. the amount of hydrogenase enzyme per unit mass of cells) in addition to the C_{NH4+}/K_{NH4+} term. Although it is not clearly evident as to what decreased the cell density (whether the reduced hydrogenase activity caused the decreased cell density or was a result of the decreased cell density), it is clear that extracellular NH_4^+ directly affects V_m in the cellular system studied. Thus, if hydrogenase is exposed to the concentrations noted in Figure 5-

6 during syngas fermentation, it is likely that the ratio of activities (Equation 5-7) shown in Figure 5-6 would be even lower due to the decrease in V_m following NH_4^+ exposure.

Since it has been established that NH_4^+ can accumulate rapidly in media following exposure to syngas containing an ammonia impurity, that NH_4^+ can inhibit hydrogenase, and that NH_4^+ likely effects the hydrogenase enzyme level, the question still arises as to the NH_4^+ concentration that would be exposed to hydrogenase during syngas fermentation. In the assay studies used to develop the model parameters, the cell wall was disrupted to expose hydrogenase directly to NH_4^+. However, there could be a gradient between the extracellular NH_4^+ and the NH_4^+ at the site of the hydrogenase during syngas fermentation such that Equation 5-7 would have to be based on the NH_4^+ concentration at the hydrogenase site as compared to the extracellular NH_4^+ concentration. Studies have shown that hydrogenases are usually associated with the plasma membrane [101] such that the exposure concentration of NH_4^+ could be similar to the extracellular concentration. Since *E. coli* has been shown to be a paradigm organism for studying many bacteria [102], a qualitative aspect of the question could be potentially answered by understanding the NH_4^+ uptake pathway in *E. coli*. It was reported that NH_4^+ may enter *E. coli* through a K^+- NH_4^+ exchange process [103]. A high level of intracellular K^+ is vital for effective NH_4^+ uptake driven by a high K^+_{in}/K^+_{out} ratio. However, the energy requirement for NH_4^+ uptake is quite complex requiring both a membrane potential and ATP [102]. Since K^+ is present in many bacterial media formulations (including the media used in this study), it is feasible that the amount of K^+ could be abundant to satisfy the required K^+_{in}/K^+_{out} ratio such that NH_4^+ accumulation in the media could effectively interact with hydrogenase. Although this analysis is only qualitative, it does suggest that hydrogenase will likely have some exposure to NH_4^+ that is in the extracellular solution, especially since it was also shown that extracellular NH_4^+ did affect

the activity with whole cells. Further studies would need to be performed to address the actual NH_4^+ concentrations that would be observed in the vicinity of hydrogenase during syngas fermentation. However, the important point is that NH_4^+ accumulation has a great potential to affect both the amount of hydrogenase enzyme and the associated enzyme activity. Thus, to maximize hydrogenase activity, it would be critical to remove NH_3 in syngas prior to syngas fermentation.

5.5.3 Effects of NH_4^+ on the activity of forward ADH

It is informative to study the effects of NH_4^+ on forward ADH activity since it directly catalyzes the ethanol formation according to the metabolic pathway. As shown in Figure 5-13, at a lower range of $[NH_4^+]$, the forward ADH activity was actually stimulated based on these two runs. However, with increasing $[NH_4^+]$, the forward ADH activity was reduced but essentially to levels near $[NH_4^+] = 0$. The ADH enzyme activity analysis showed that the forward ADH activity was not adversely affected by NH_4^+ in our experimental range of $[NH_4^+]$ up to 200 mM. In literature, NH_4^+ was regarded as an inhibitor of ADH activity only at elevated concentrations [94, 95]. Since the elevated concentrations mentioned in literature are vague, it is impossible to compare this finding with that unspecified value. Therefore, the [EtOH] or [HAc] trends observed in Chapter 4 should not be attributed significantly to ADH activities affected from NH_4^+ per se. However, it would be valuable to pursue the ADH activity effects further regarding the noticeable increase in activity shown in Figure 5-13. To sum up, NH_4^+ affects cell growth via elevated osmolarity. However, NH_4^+ non-competitively inhibits the hydrogenase activity and positively promotes forward ADH activity. There is an intertwined relationship between cell growth and hydrogenase activity. However, there is no clear relationship between cell growth and forward ADH activity. As to the detailed biological mechanisms, it is still unclear.

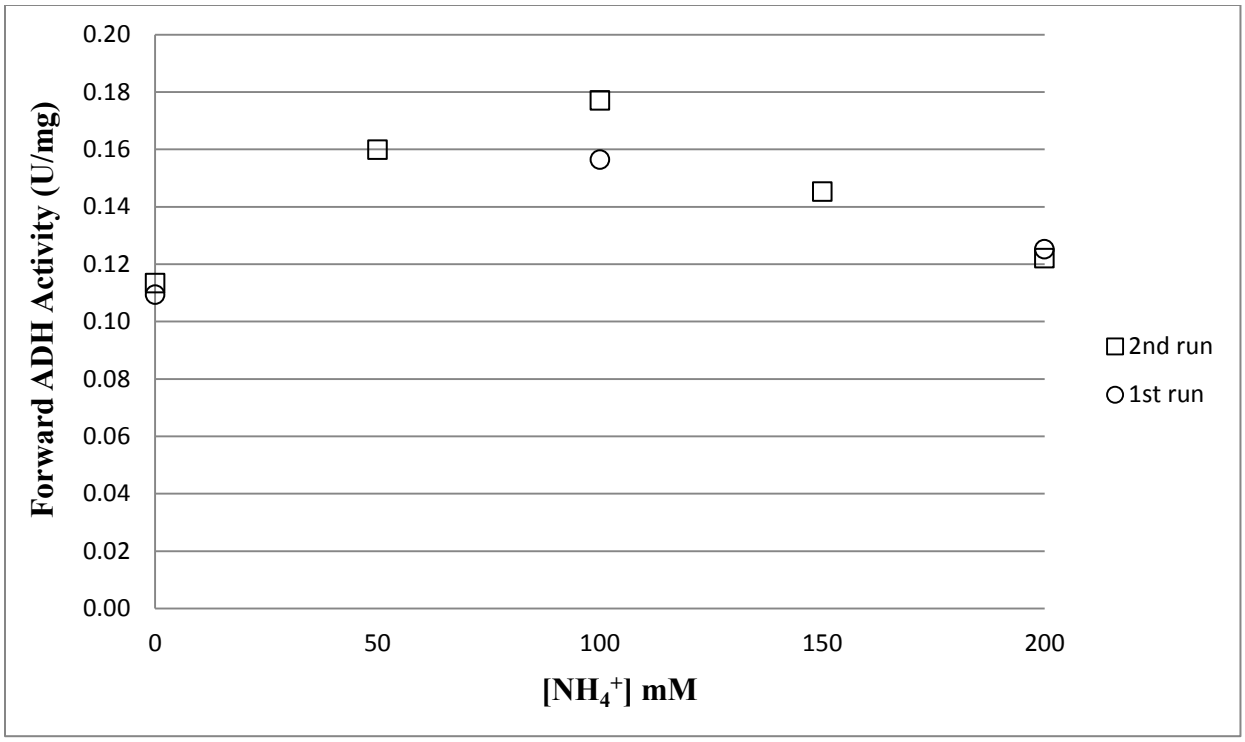

Figure 5-13. Forward ADH activity as a function of varying [NH_4^+]

5.6 Conclusions

Since NH_4^+ can easily be accumulated to high concentrations in the media and potentially transported across cell membranes, it is necessary to pre-treat raw syngas to remove ammonia before feeding it into the syngas-fermentation stage for commercial processes. For biofuel production, the variability in types of gasifiers, feed (biomass and/or coal), and operating conditions all can influence the compositions of raw syngas that can be used. Depending on the end products and bioprocesses being used, there may be limits for the amounts of syngas impurities that can be tolerated. For a profitable commercial process, the limits must be chosen based on a viable economic analysis. For syngas fermentation, the most efficient process for converting available carbon (both CO and CO_2) to carbon-containing products would involve

utilizing all of the available H_2 for reducing equivalents with the remaining reducing equivalents obtained from CO. When H_2 is utilized, it is important that the hydrogenase activity be the most efficient to minimize the loss of CO to reducing equivalents instead of valuable products. Based on the findings of this work, NH_3 can have a significant negative impact on syngas fermentation using *C. ragsdalei* via the reduction of hydrogenase activity (via both enzyme amount and non-competitive inhibition) if NH_3 is not cleaned from the syngas. Further studies regarding the effects of NH_3 on other bacteria suitable for biofuel production are highly recommended.

6. Effects of benzene in syngas on P11 cell growth and ethanol production

6.1 Introduction

Raw syngas generated from a commercial gasifier will contain light or heavy volatile tars. From the established database of syngas compositions (Chapter 3), it was shown that volatile benzene (C_6H_6) normally can reach 0.3 mol% (upper limit: 0.6 mol%) for biomass gasification [60]. Therefore, it is necessary to investigate the effects of C_6H_6 at this realistic concentration on cell growth and ethanol production. This investigation will be used for making sound judgment as to whether raw syngas needs to go through specific downstream treatment for benzene removal which will incur extra cost on the whole operating system.

6.2 Research objectives

- Calculate the volatile C_6H_6 concentration change from the exit of a gasifier at a high temperature (at least 700 °C) to a bioreactor running at 37 °C.
- Design an adjustable gas feeding system so that varying C_6H_6 gas composition can be obtained and delivered to a media from which the soluble C_6H_6 can be measured in the media.

- Use two continuous bioreactors (one is control) under controlled pH and monitored redox to study the effects of soluble C_6H_6 on cell growth by incrementally increasing [C_6H_6] in media.
- Investigate and quantify the effects of soluble C_6H_6 on ethanol or acetic acid production.

6.3 Materials and methods

6.3.1 Microorganism and cell growth media preparation

The same bacteria--*Clostridium ragsdalei*, denoted as P11, was used for this C_6H_6 study. The media recipe and cell preparation steps are the same as detailed in Chapter 4 Section 4.3.1. As customary, the third passage was used as the active cell source for the inoculation of bioreactors.

6.3.2 Accumulation and measurement of C_6H_6 in media and associated $K_L a$

For this research, varying soluble C_6H_6 in the media is a prerequisite to quantify the effects of C_6H_6 on the cell growth and product formation. To achieve this goal, an adjustable gas feeding system was devised as outlined in Figure 6-1. Two identical rotameters were used (Cole Parmer, PMR1-010370) that had been calibrated with N_2 or syngas. For all studies, a total gas flow rate of 100 sccm entering both rotameters (and the bioreactor) was used.

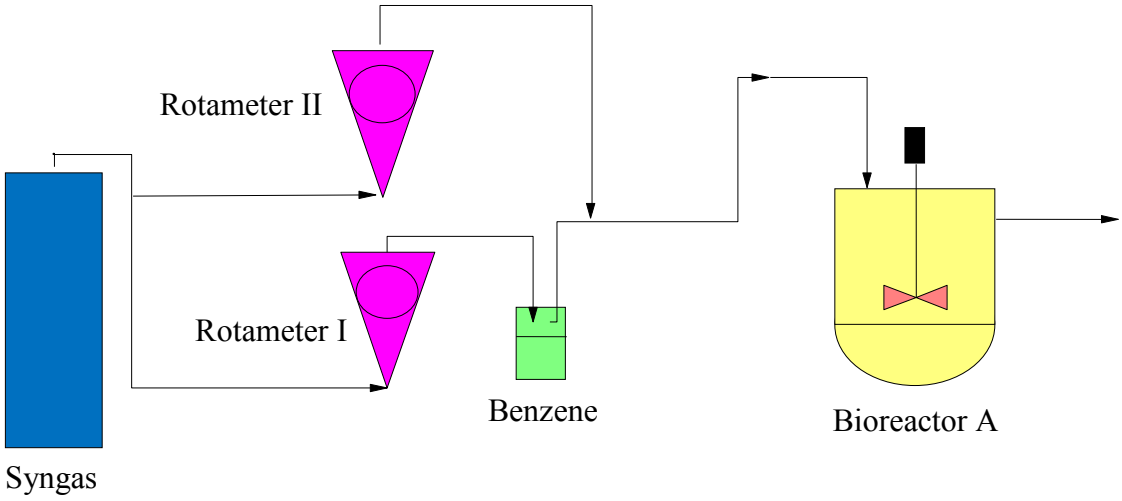

Figure 6-1. Schematic bioreactor setup for the C_6H_6 study with two rotameters to adjust the syngas flow rate passing through the C_6H_6 bottle

By finely adjusting both rotameters simultaneously, part of the total gas flow was diverted through the C_6H_6 bottle to enable the gas to contain volatile C_6H_6. These two rotameters were monitored and fine-adjusted every two hours during the day or every 4 hours during the night to make sure the targeted gas flow rate was remained constant. Flow through the C_6H_6 bottle was 5, 10, 20, 30, 40, 50, 75, or 100 % of the total flow. For determining the mass-transfer coefficient for C_6H_6 transfer to media, N_2 was used as the feeding gas which was split into the two rotameters before recombining and feeding into the bioreactor. For each flow rate passing through the C_6H_6 bottle, $[C_6H_6]$ was monitored with time in the reactor until steady state was reached (taking about 40 hours). The N_2 feeding gas doped with C_6H_6 was fed into a bioreactor with 1 L working media at controlled temperature of 37 °C. The $[C_6H_6]$ in the media was measured using a GC/MS.

6.3.3 Bioreactor study for cell growth and product formation

For the continuous bioreactor runs, there were two parallel bioreactors in place, denoted as Bioreactor A (doped with C_6H_6 in the gas inlet) and Bioreactor B (control). Both bioreactors were purchased from New Brunswick Scientific (Model: BIOFLO 110).The setup for Bioreactor A is schematically shown in Figure 6-1. In contrast, there are no splits in the gas feeding stream for Bioreactor B—only a single gas stream flowed through the bioreactor. Both Bioreactor A and B were initially filled with 1L media under controlled pH of 5.5, stirring speed of 200 rpm, and temperature of 37 °C. Bioreactor A was purged with a portion (5, 10, 20, 40, or 75% of total flow) of N_2 passing through the C_6H_6 bottle. The purging enabled the media to reach one of five different equilibrium C_6H_6 concentrations (0.64, 1.18, 1.72, 2.33, and 3.44 mM) that were studied and the concentrations corresponded to the 5, 10, 20, 40, or 75% diverted flow, respectively. As a control, Bioreactor B was purged with N_2 at the same total gas flow rate as Bioreactor A. Once the C_6H_6 equilibrium was obtained in Bioreactor A, the gas flow was switched from N_2 to syngas with flow still being diverted through the C_6H_6 bottle as before. Bioreactor B was also switched to 100 sccm syngas. After purging with pure syngas or syngas/C_6H_6 for 3 hours, 1% (v %) cysteine sulfide was injected into both bioreactors. Afterwards, 10 % (v %) cell sources were injected into both bioreactors. The OD for both bioreactors was measured immediately. Liquid samples were taken on a daily basis to get the values for the OD, [EtOH], and [HAc]. For this series of runs, only a single run was conducted for each flow rate passing through the C_6H_6 bottle.

6.3.4 Liquid analysis

The protocol for measuring the OD, [EtOH], and [HAc] was detailed in Chapter 4 Section 4.3.6. As for the measurement of [C_6H_6] in the media, an Agilent 7890A/5975C GC/MS

was used with a polyethylene glycol (PEG) column characterized by high polarity (J&W scientific, DB-WAX 121-7022). This column is 20 meters in length, 0.18 mM internal diameter, and 0.18μM film thickness. Its temperature range is 20~250 °C. To detect trace amount of [C_6H_6], this type of polarized column was chosen. The temperature profile for this method was set at a constant temperature of 35°C for 5 minutes, increased to 180 °C at the rate of 40 °C/min, then held for another 3 minutes with a total running time of 11.6 minutes. The purpose of holding the temperature at 35 °C for 5 minutes was to make sure all the injected C_6H_6 was vaporized. The method for this analysis was saved on the GC/MS with the following key parameters: split ratio: 10:1, equilibration time: 0.25 min, postrun time: 2 min, carrier flow rate (Helium): 2.0 ml/min.

6.4 Results and discussions

6.4.1 Prediction of [C_6H_6] in a bioreactor exposed to raw syngas

Obviously, there is a huge temperature difference between the syngas coming out of a gasifier and the syngas feeding into a bioreactor. From the raw syngas compositional database, it was found that the highest volatile [C_6H_6] was around 0.6 mol%. At this point, it would be interesting to calculate the dew point for this syngas mixture with a 0.6 mol% C_6H_6 gas composition. Using Raoult's law for just C_6H_6 since it is the only potential condensable species at the given temperatures,

$$Y_{C6H6} * P = X_{C6H6} * P_{C6H6}^{*} \quad (6\text{-}1)$$

At the dew point, the gas-phase composition is essentially the same as the composition from the gasifier. From Equation 6-1, the dew point temperature can be calculated assuming a pressure (P) of 1 atm and gas mole fraction of 0.006 C_6H_6. From Equation 6-1, $P^*_{C6H6} = 0.006$. Now, the Antoine equation with corresponding parameters for C_6H_6 [104] can be used to find the temperature (dew point in this case) by using Excel as shown below.

A	B	C
14.1603	2948.78	-44.5633

Antoine Equation: log(P)=A-B/(T+C)

T (K)	log (P)	P (kPa)	atm
251	-0.123884934	0.751822	0.00742
250	-0.193415767	0.640596	0.006322
249	-0.263626819	0.544971	0.005378

Thus, the dew point for this syngas mixture (doped with 0.6mol % C_6H_6) is around 250K (-23°C). From the above calculation, it is clear that at a fixed pressure, dew point temperature is closely related to the concentration of C_6H_6 in the syngas.

6.4.2 Measurement of [C_6H_6] in media and K_La calculation

To determine the [C_6H_6] in the media under different gas feeding flow rates going through the C_6H_6 bottle, it is necessary to use known [C_6H_6] to obtain a calibration chart for the GC/MS. For this end, 0.1, 0.25, 1, 2, 3, 4 mM [C_6H_6] were used as standards. This calibration was repeated five times as shown in Figure 6-2. As predicted, the [C_6H_6] is linear with area percentage measured by the GC/MS.

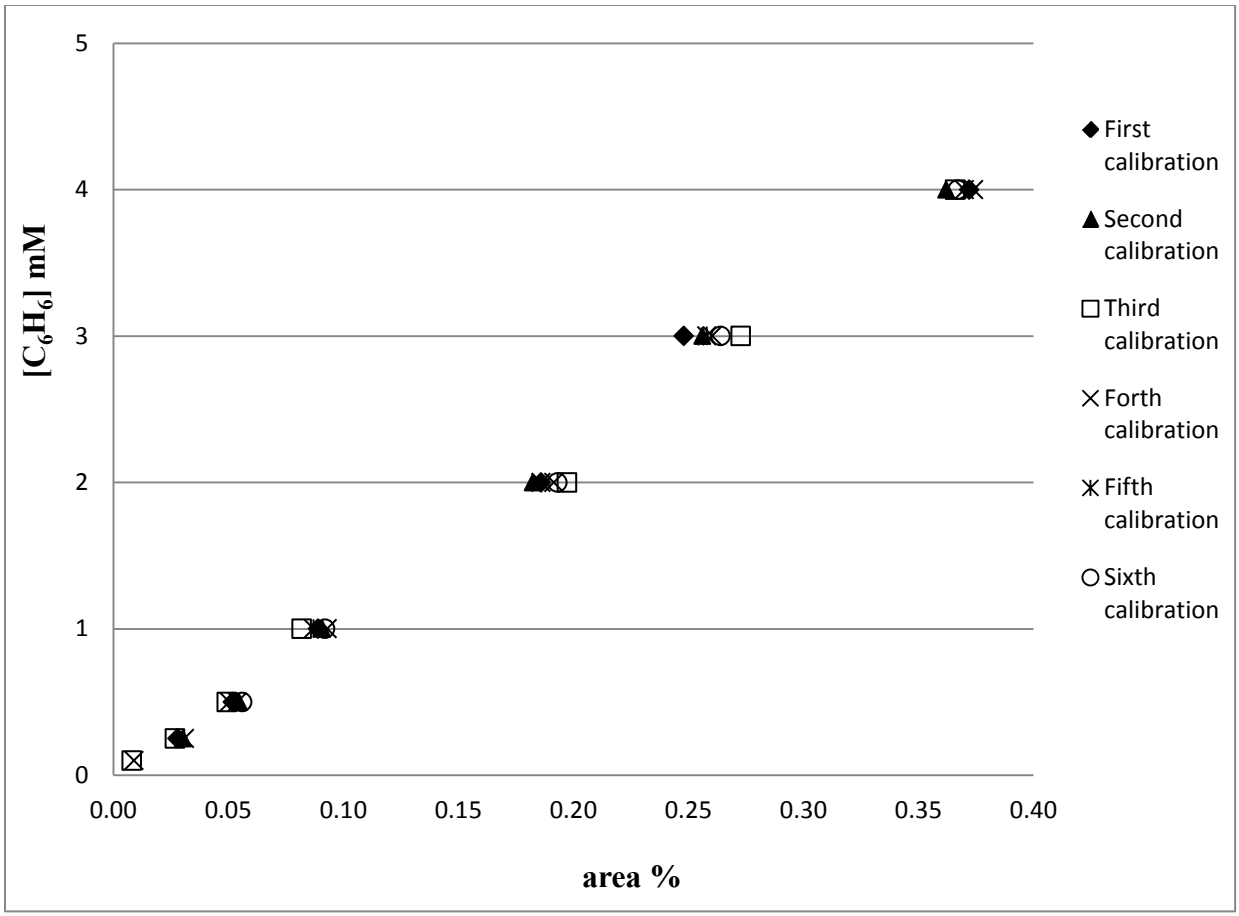

Figure 6-2. [C_6H_6] in media with respect to area % measured by the GC/MS

By using the GC/MS calibration shown in Figure 6-2, the time course of [C_6H_6] in the media was determined for the varying gas flow rates passing through a C_6H_6 bottle and is shown in Figure 6-3. Regardless of the varying gas flow rates, it would take around one day to obtain saturated [C_6H_6] in the media. The [C_6H_6] time profile provided critical information as to the [C_6H_6] in the media during the entire bioreactor run. As is evident, higher gas flow rates passing through the C_6H_6 bottle will carry more volatile C_6H_6 into the media and result in higher [C_6H_6] in the media which is in equilibrium with the partial pressure of C_6H_6 in the bioreactor headspace.

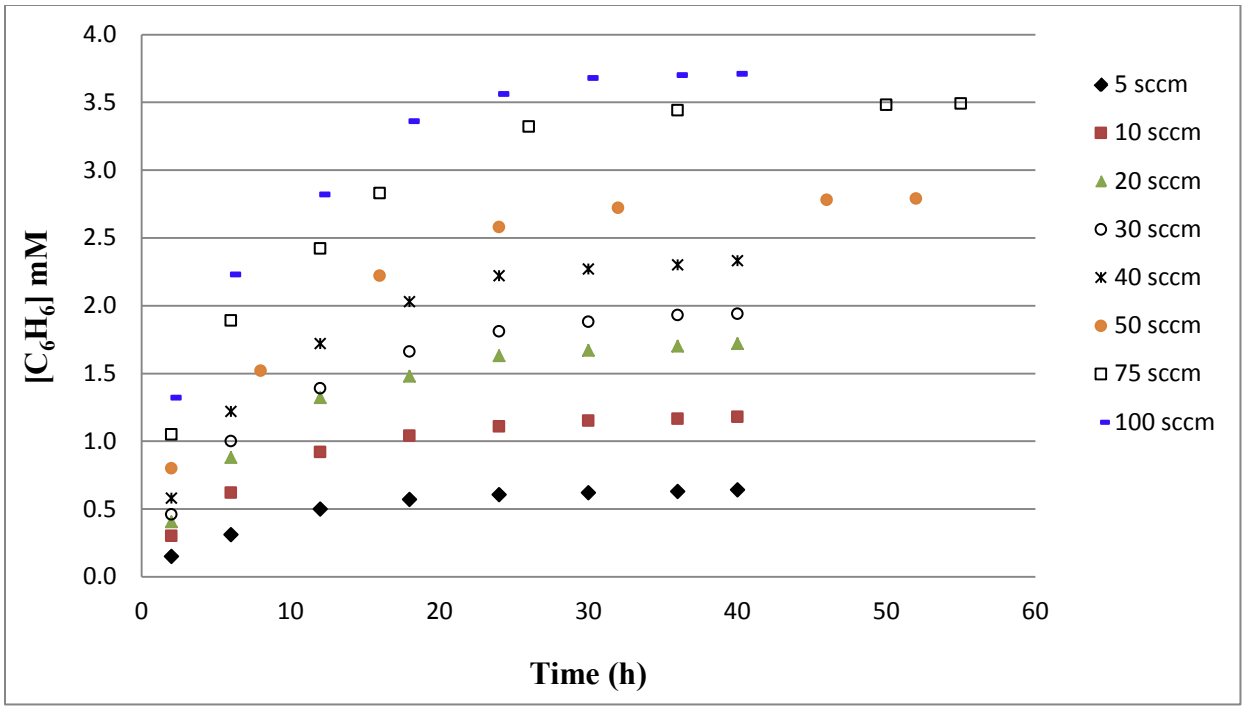

Figure 6-3. $[C_6H_6]$ time profile with 5-100 sccm N_2 passing through a C_6H_6 bottle

As shown in Figure 6-3, the $[C_6H_6]$ in the media was monitored with time until the media was nearly saturated under this gas feeding condition. In this case,

$$\frac{dC}{dt} = k_L a\,(C^* - C) \tag{6-2}$$

Where k_La is the volumetric mass-transfer coefficient and C* is the saturated C_6H_6 concentration in the media. Integration of equation 6-2 with C = 0 at t = 0 gives

$$\ln[C^*/(C^* - C)] = k_L a * t \tag{6-3}$$

As shown in Figure 6-4, a plot of $\ln[C^*/(C^* - C)]$ versus time will give an estimate of k_La for the experiment with 100 sccm N_2 passing through the C_6H_6 bottle (see Figure 6-3). Here, C* is the saturated concentration which is equal to the steady-state concentration. From the slope in Figure 6-4, k_La was 0.13 h^{-1}. By using saturated $[C_6H_6]$ **(C*)** in Figure 6-3 for varying C_6H_6 flow

rates, similar k_La values were obtained (ranging from 0.11 to 0.13 h^{-1}). Since the total gas flow rate was fixed at 100 sccm and the bioreactors were run at similar operating conditions, the slightly varying k_La values obtained from varying C_6H_6 flow rates in Figure 6-3 are consistent with expectations that the values should be similar.

As mentioned in Chapter 4 Section 4.4.1, the mass transfer coefficient for NH_3 entering water is around 0.36 s^{-1} (or 1296 h^{-1}). Since NH_3 is very soluble in water and rapidly forms NH_4^+, the liquid film mass-transfer resistance is very small in comparison with the resistance by the gas film. By comparison, the mass-transfer coefficient for C_6H_6 entering water under these experimental conditions is around 0.13 h^{-1} which is much smaller than the mass-transfer coefficient for NH_3. It is clear that the resistance for C_6H_6 entering into water from a gas phase lies in the liquid film.

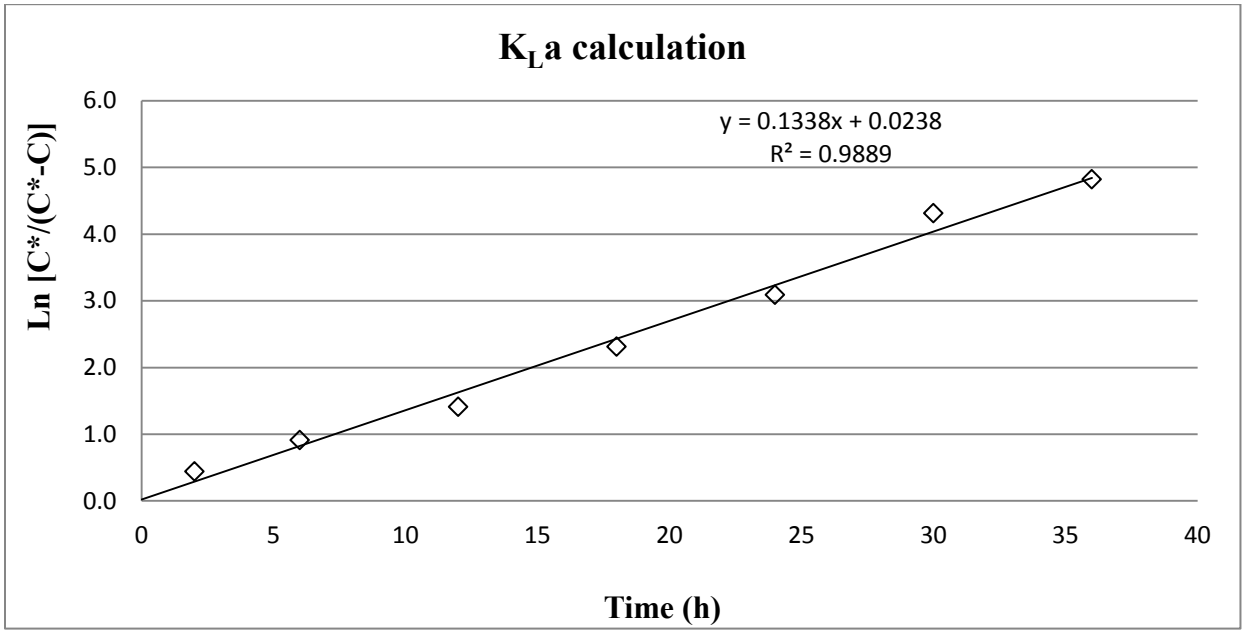

Figure 6-4. K_La calculation for 100 sccm N_2 passing through a C_6H_6 bottle

Since volatile C_6H_6 in a continuous gas stream passing through a bioreactor could result in an equilibrium amount of C_6H_6 in the media, an analysis was performed to determine how close the measured saturated C_6H_6 concentration in the media was to the predicted saturation value using Henry's law.

Henry's law is valid for low pressure. Therefore, Henry's law can be applied for this prediction and is denoted as:

$$K_H=P/X \tag{6-4}$$

Here, the unit for Henry's law constant (K_H) is atm, the unit for pressure (P) is atm, and X is mole fraction (dimensionless) in the liquid.

Since Henry's law constant literature values vary at a specific temperature, here the Henry's law constant at 37 °C ranging from 400 to 415 atm [67] was chosen for the calculation. For this experiment, the liquid volume of C_6H_6 that was removed from the C_6H_6 source bottle was measured over time to enable the calculation of a molar flow rate entering the bioreactor. The total gas molar flow rate was also known. Therefore, the fraction of C_6H_6 in the bioreactor headspace could be calculated to obtain the C_6H_6 partial pressure ($P_{C6H6}=P * y_{C6H6}$). The upper theoretical [C_6H_6] in the bioreactor liquid was calculated ($X_{C6H6} = P_{C6H6} / K_H$) using 400 atm for the Henry's law constant and excluding the water partial pressure in the headspace. Since vaporized water will dilute P_{C6H6} in the bioreactor headspace, the water partial pressure was taken into account [$y_{C6H6}= y_{C6H6} / (1+y_{H2O})$] for the lower theoretical limit. y_{H2O} was estimated from the water vapor in equilibrium with water at the bioreactor temperature. The lower theoretical [C_6H_6] was calculated with 415 atm for the Henry's law constant and including the water partial pressure from the bioreactor headspace. Figure 6-5 shows measured [C_6H_6] values

as well as the upper and lower theoretical predictions. It is clear that the measured [C_6H_6] was slightly lower than the lower theoretical [C_6H_6]. This slight discrepancy can partially be explained by the loss of vaporized C_6H_6 from taking and transporting the liquid samples to the GC/MS for the measurement.

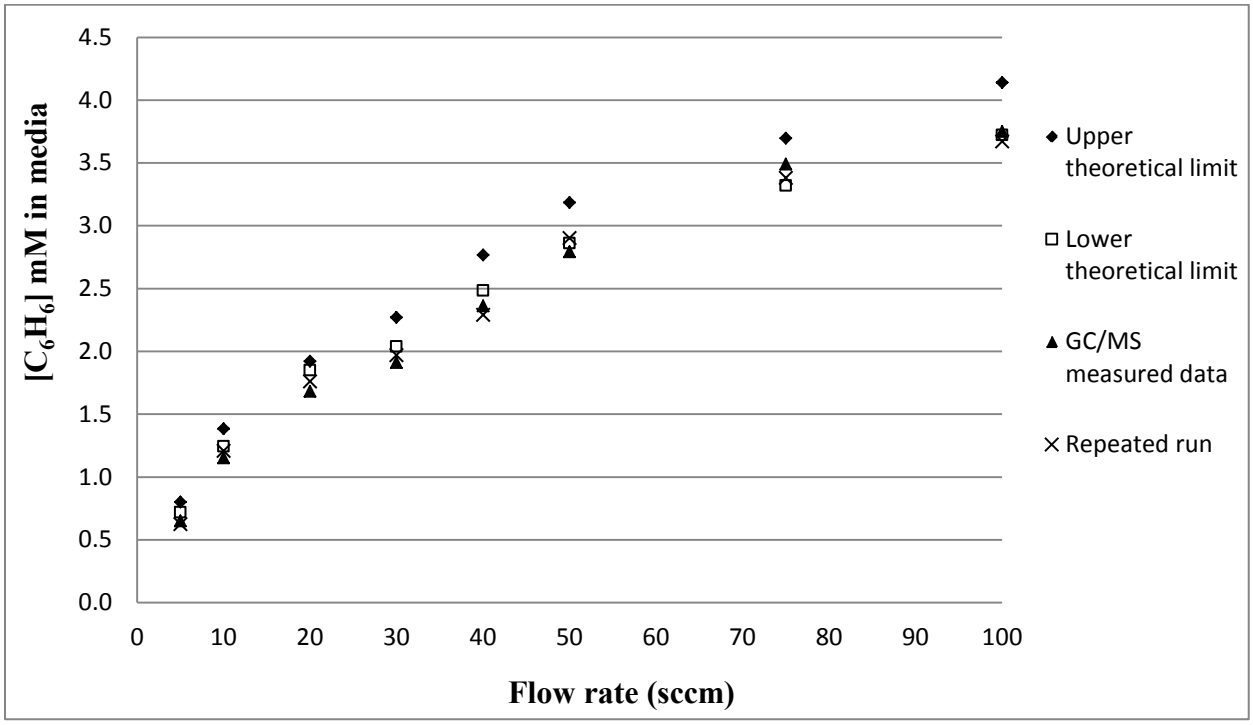

Figure 6-5. Comparison of calculated upper or lower [C_6H_6] with the GC/MS measured value

Based on the data from Figure 6-5, Figure 6-6 was graphed with respect to the % C_6H_6 in the bioreactor headspace corresponding to the individual gas flow rate. As predicted, the calculated [C_6H_6] in the media should be linear with respect to % C_6H_6 in the bioreactor headspace following Henry's Law. As shown in Figure 6-6, the measured [C_6H_6] in the media also approximate a linear relationship.

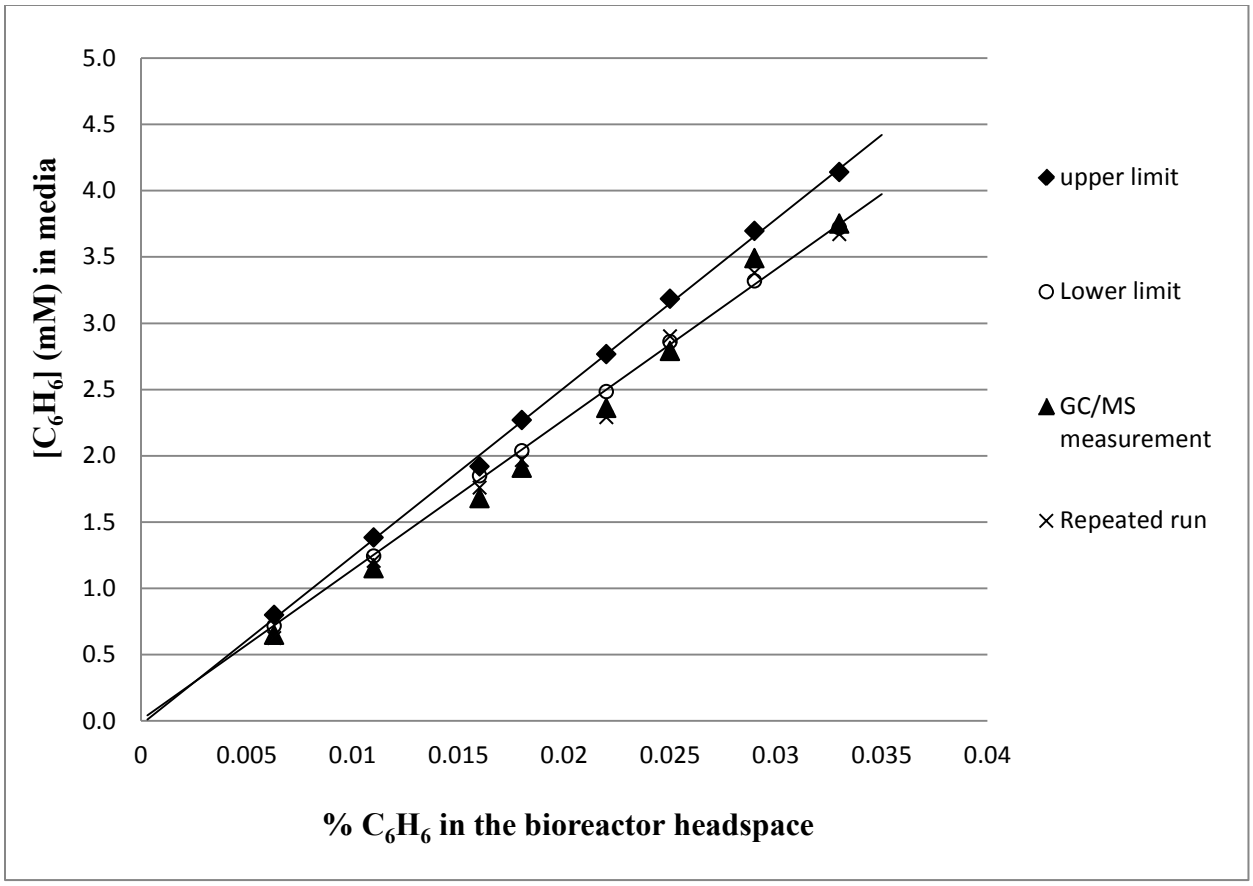

Figure 6-6. Comparison of the calculated upper or lower limit of [C_6H_6] with the GC/MS measured value

Via calibration Figure 6-5, several targeted [C_6H_6] in the media can be easily obtained by varying the gas flow rates passing through a C_6H_6 bottle. This laid the necessary preparatory work for the following cell growth inhibition studies.

6.4.3 Effects of C_6H_6 on cell growth

Initially, as shown in Figure 6-7, both Bioreactor B (control) and Bioreactor A were run with clean syngas. However, at 140 hours, Bioreactor A was switched to syngas doped with

C_6H_6 (30 sccm syngas passing through the C_6H_6 bottle). It was clear that C_6H_6 accelerated the death of the cells compared with that of the control.

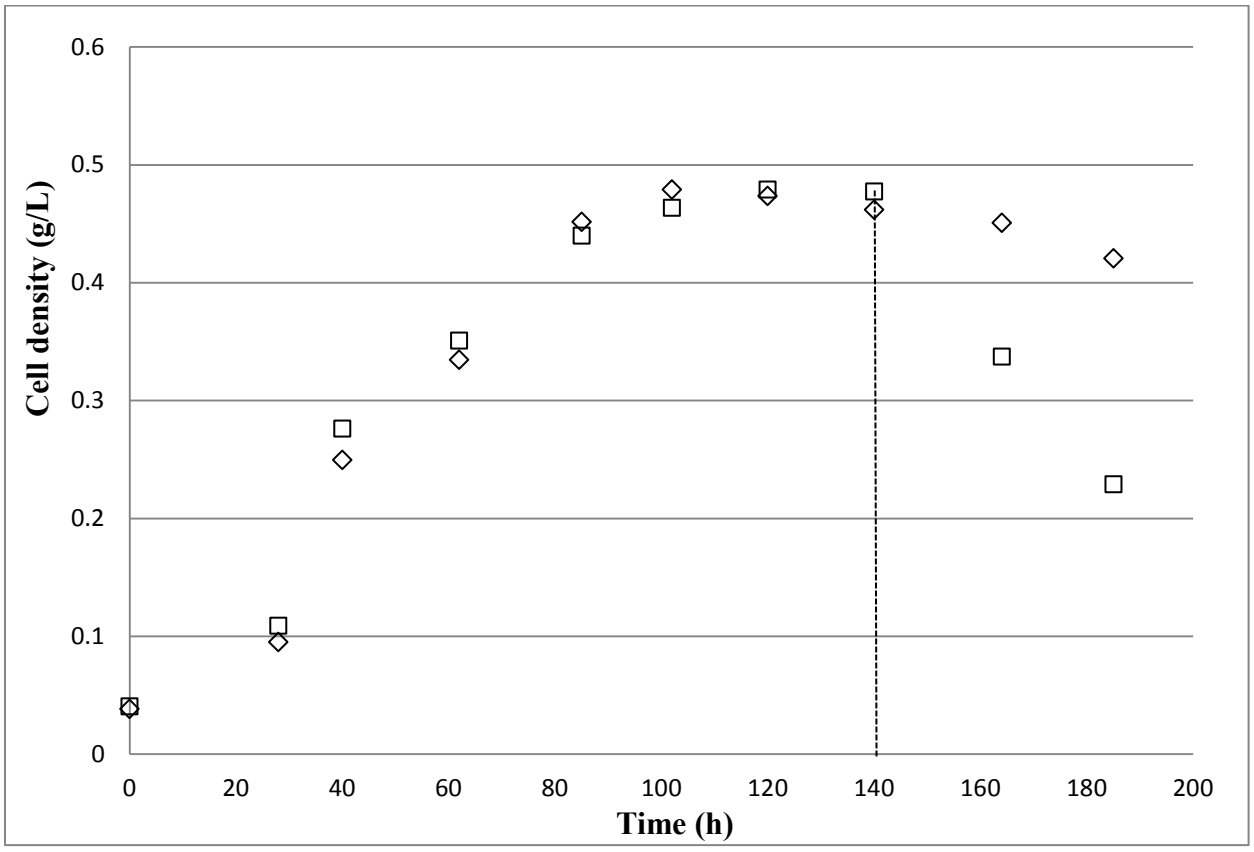

Figure 6-7. Cell growth time courses for Bioreactor B (control) (◇) and Bioreactor A (doped with 2.0 mM C_6H_6 in the media starting at 140 hours) (□)

From our established database, it was found that C_6H_6 compositions exiting from a gasifier can range from 0.07 to 0.6 mol% depending on the operating conditions and feedstocks. Furthermore, it was also noticed that C_6H_6 composition of 0.3 mol% was most common among all different types of gasifier and operating conditions and feedstocks. Therefore, here 0.3 mol% of C_6H_6 exiting from a gasifier was used to calculate the expected [C_6H_6] in the media. According to Henry's law ($K_{H,\ C6H6}$ = 400atm at 37 °C), the saturated concentration of C_6H_6 in

the media is around 0.41 mM [67]. However, if using $K_{H,\ C6H6}$ = 400atm at 37 °C for the upper limit and a C_6H_6 composition of 0.6 mol%, the saturated concentration of C_6H_6 in the media is around 0.83 mM (upper limit). Therefore, it is appropriate to study the effects of $[C_6H_6]$ on the cell growth starting with lower concentration on the similar magnitude. To obtain a quantitative analysis, a few incremental higher $[C_6H_6]$ were chosen. Figures 6-8 to 6-12 show the effects of varying $[C_6H_6]$ on cell growth compared with those of the controls. It was evident that with increasing $[C_6H_6]$ in the media, cell growth was inhibited to a greater extent. The dotted lines in all figures represent a model described later.

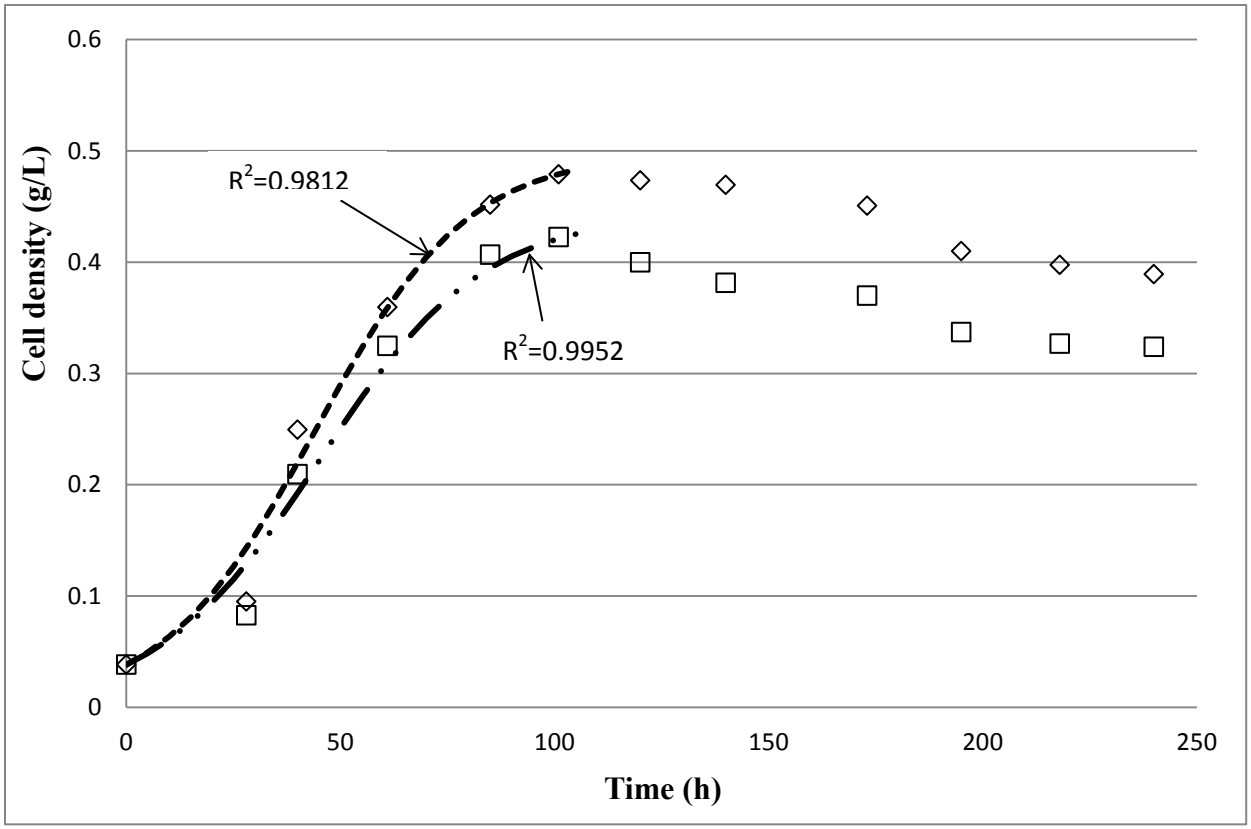

Figure 6-8. Cell growth time courses for Bioreactor B (control) (◇) and Bioreactor A (doped with 0.64 mM C_6H_6 in media) (□). The two dotted lines represent models of Equation 6-2

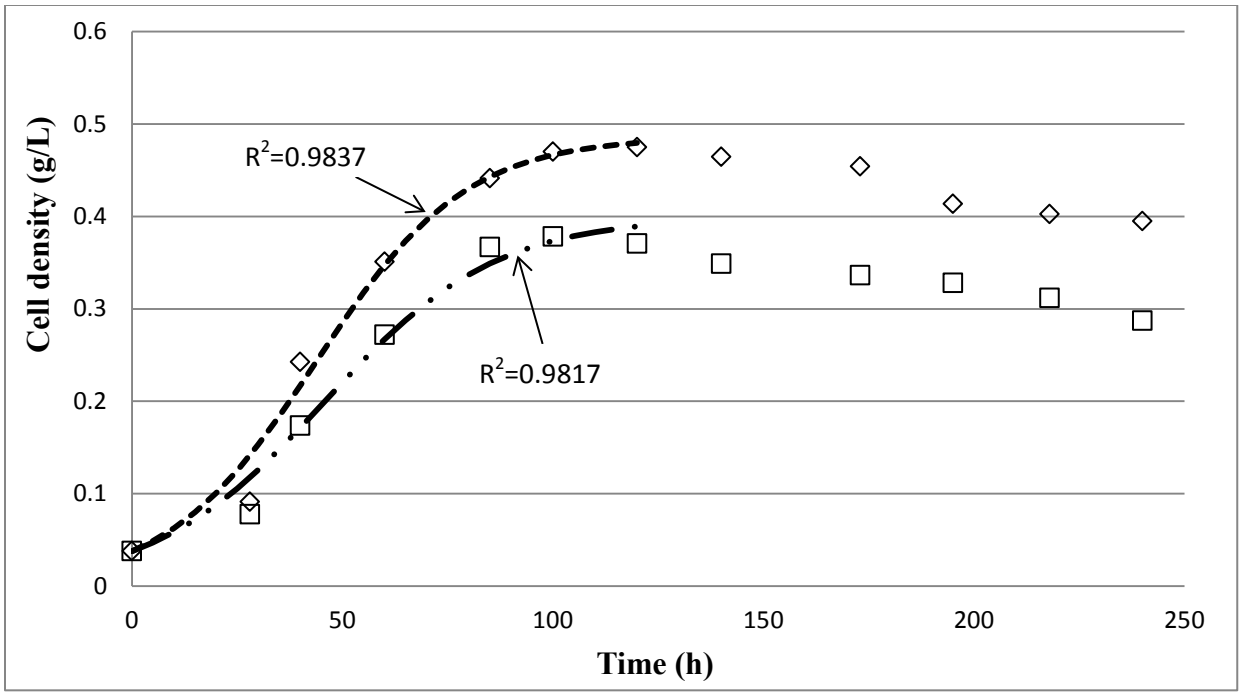

Figure 6-9. Cell growth time courses for Bioreactor B (control) (◊) and Bioreactor A (doped with 1.18 mM C_6H_6 in the media) (□). The two dotted lines represent models of Equation 6-2

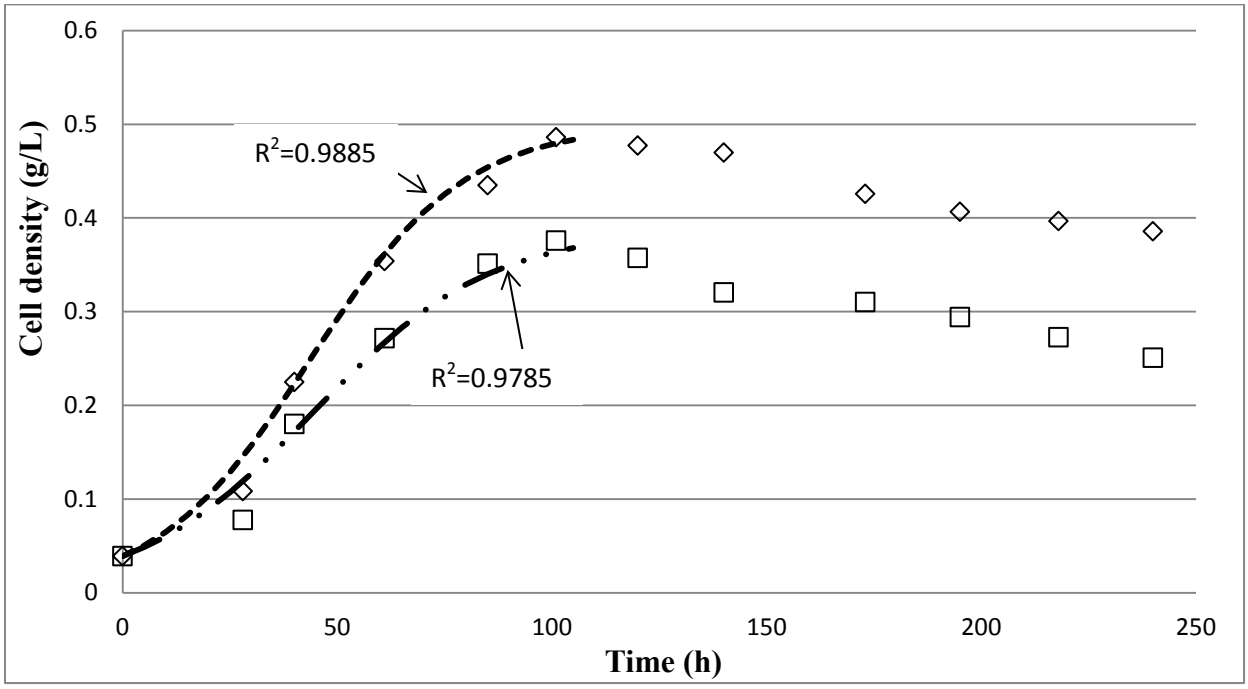

Figure 6-10. Cell growth time courses for Bioreactor B (control) (◊) and Bioreactor A (doped with 1.72 mM C_6H_6 in the media) (□). The two dotted lines represent models of Equation 6-2

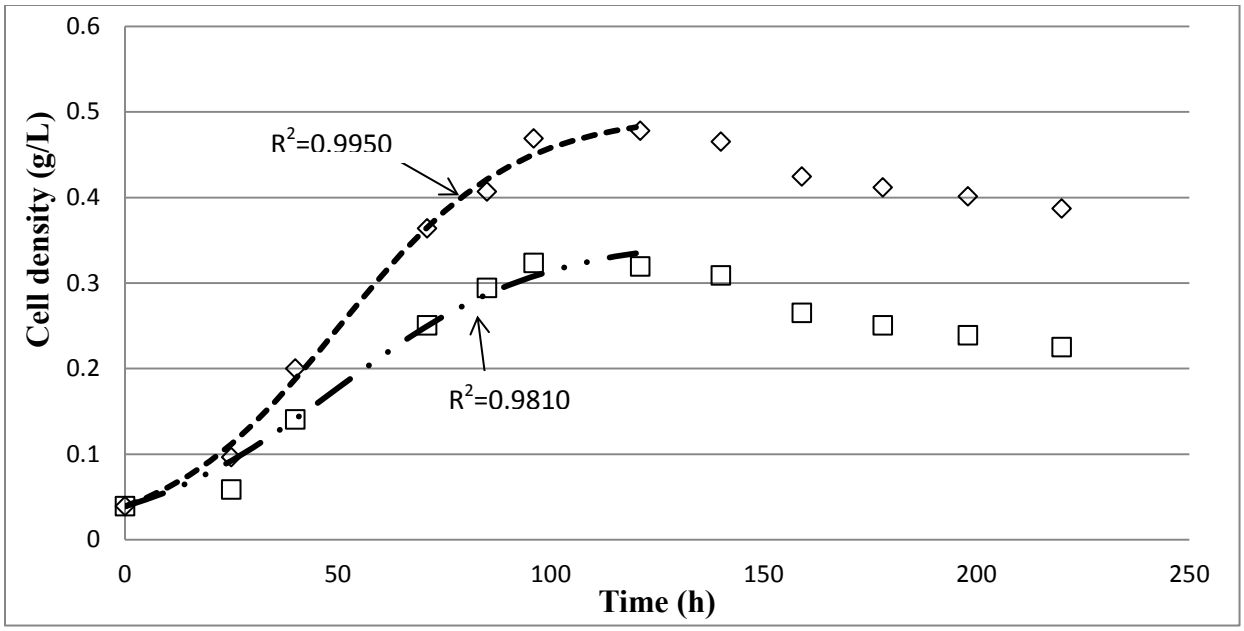

Figure 6-11. Cell growth time courses for Bioreactor B (control) (◊) and Bioreactor A (doped with 2.33 mM C_6H_6 in the media) (□). The two dotted lines represent models of Equation 6-2

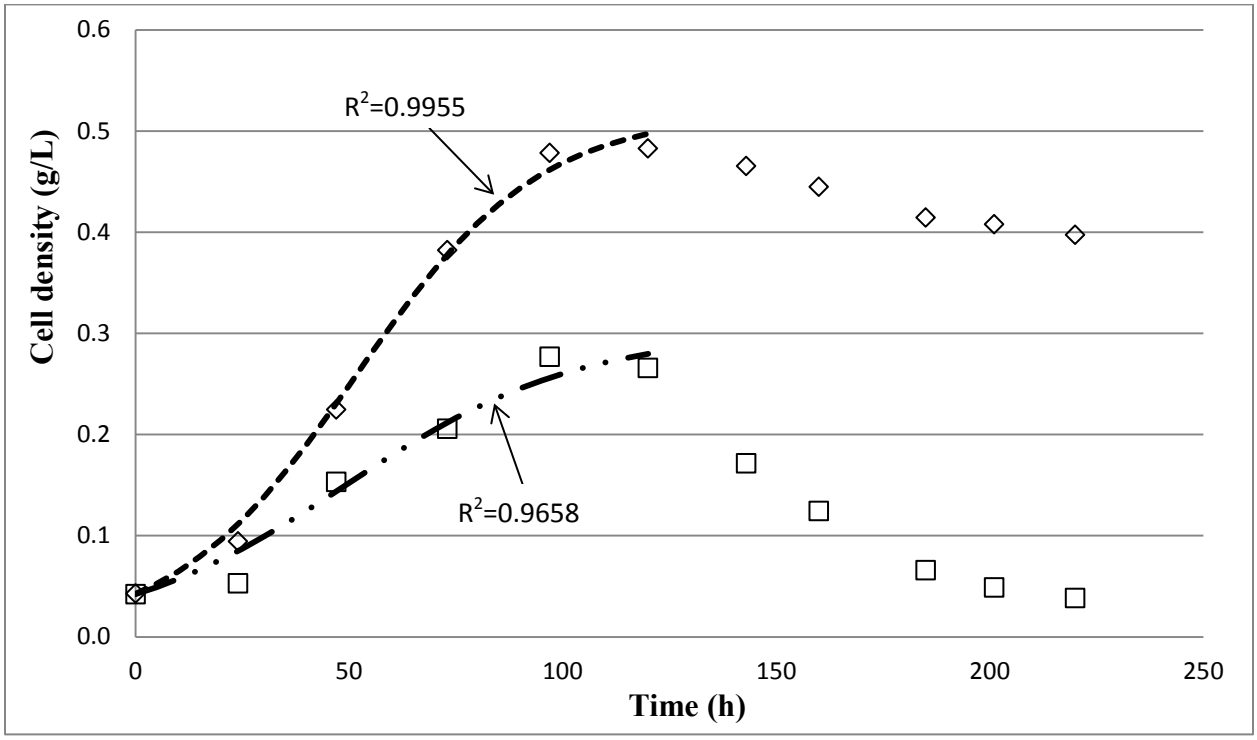

Figure 6-12. Cell growth time courses for Bioreactor B (control) (◊) and Bioreactor A (doped with 3.44 mM C_6H_6 in the media) (□). The two dotted lines represent models of Equation 6-2

It is not surprising that the cell growth rates (slopes of the lines) for continuous gas feeding bioreactors under controlled pH were affected by [C_6H_6] in the media. To quantify the cell growth rates for those bioreactor runs, a logistic equation (explained in Chapter 4 Section 4.4.3) was used to fit the experimental data.

$$\frac{dX}{dt} = kX * \left(1 - \frac{X}{X_\infty}\right) \tag{6-5}$$

Equation 6-5 is valid for a well-mixed system. The integration of Equation 6-5 with the initial condition $X(0) = X_0$ yields the following equation:

$$X = \frac{X_0 * e^{kt}}{1 - \frac{X_0}{X_\infty} * (1 - e^{kt})} \tag{6-6}$$

Here, μ_g is the cell specific growth rate, X_0 is the initial condition (cell density at the beginning), X is cell mass, X_∞ is the maximum cell mass or carrying capacity, and k is the carrying capacity coefficient (indicating how fast the cells grow).

The lines showed in Figures from 6-8 to 6-12 were fit to Equation 6-6. Since Equation 6-6 is only valid for the cell exponential growth phase and not suitable for the cell stationary phase, only the data for the cell exponential growth phase was fit to Equation 6-6. As is evident, the model fits the experimental data reasonably well as indicated by the R^2 value. The fitted parameters such as carrying capacity k and maximum cell mass X_∞ are listed in Table 6-1 for each of the five bioreactor runs. In Table 6-1 and the following analysis, parameters with a subscript "1" refer to Bioreactor A that involved C_6H_6 and parameters with a subscript "2" refer to Bioreactor B that had no C_6H_6.

Table 6-1. Ratios of cell growth rate and carrying capacity for Bioreactor A (doped with C_6H_6) and B (control)

	Bioreactor A (with C_6H_6)	Bioreactor B (no C_6H_6)	Ratio
0.64 mM C_6H_6	$k_1 = 0.052$	$k_2 = 0.056$	$k_1/k_2 = 0.93$
	$X_{\infty,1} = 0.454$	$X_{\infty,2} = 0.499$	$X_{\infty,1}/X_{\infty,2} = 0.91$
1.18 mM C_6H_6	$k_1 = 0.049$	$k_2 = 0.056$	$k_1/k_2 = 0.87$
	$X_{\infty,1} = 0.399$	$X_{\infty,2} = 0.486$	$X_{\infty,1}/X_{\infty,2} = 0.82$
1.72 mM C_6H_6	$k_1 = 0.049$	$k_2 = 0.056$	$k_1/k_2 = 0.87$
	$X_{\infty,1} = 0.387$	$X_{\infty,2} = 0.499$	$X_{\infty,1}/X_{\infty,2} = 0.78$
2.33 mM C_6H_6	$k_1 = 0.042$	$k_2 = 0.049$	$k_1/k_2 = 0.86$
	$X_{\infty,1} = 0.352$	$X_{\infty,2} = 0.498$	$X_{\infty,1}/X_{\infty,2} = 0.71$
3.44 mM C_6H_6	$k_1 = 0.037$	$k_2 = 0.047$	$k_1/k_2 = 0.79$
	$X_{\infty,1} = 0.300$	$X_{\infty,2} = 0.518$	$X_{\infty,1}/X_{\infty,2} = 0.58$

To easily observe the trends, the data shown in Table 6-1 were graphed in Figure 6-13. By observing the trend, it was concluded the ratios of carrying capacity and maximum cell mass in the presence of C_6H_6, relative to the absence, decrease with the increasing [C_6H_6] in the media.

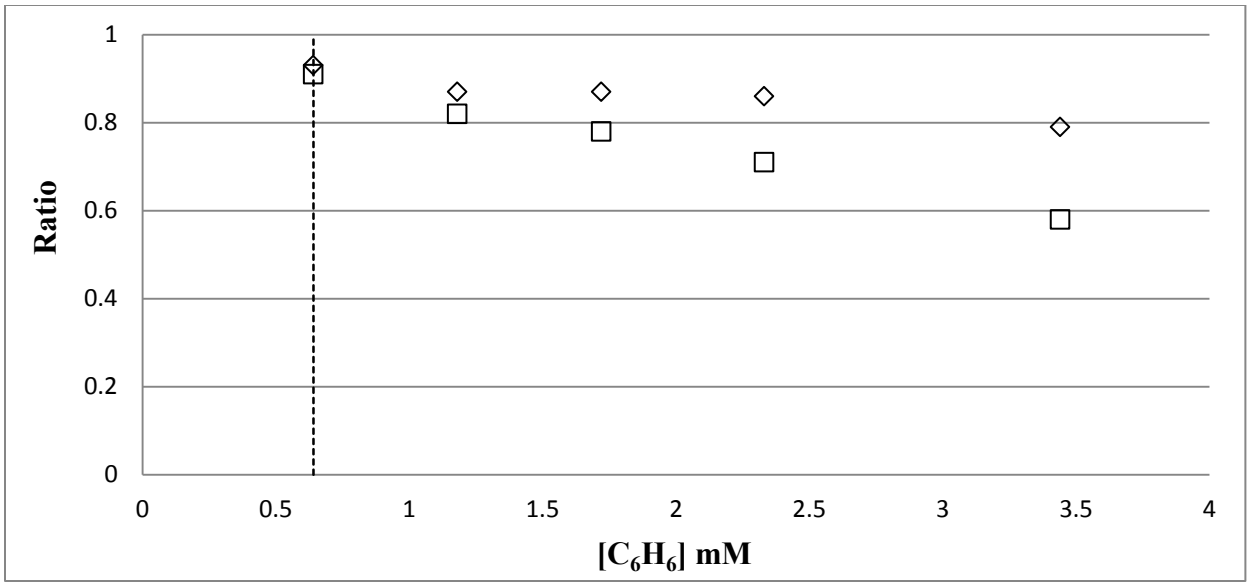

Figure 6-13. The ratio of k_1/k_2 (◇) and $X_{\infty,1}/X_{\infty,2}$ (□) for varying $[C_6H_6]$ in the media. The dotted line shows the concentration close to the realistic saturated $[C_6H_6]$ in the media

From our established syngas compositional database, the gas composition of C_6H_6 exiting a gasifier is normally around 0.3 mol% with an upper limit of 0.6 mol%. As stated before, if this syngas mixture were feed into a bioreactor, the saturated $[C_6H_6]$ in the media at 37 °C is around 0.41mM (upper limit: 0.83 mM). Therefore, in Figure 6-13, $[C_6H_6]$ below 0.83 mM will likely only be of interest for industrial applications.

As a comparison, Figure 4-14 in Chapter 4 shows that the carrying capacity coefficient *k* (indicating how fast cells grow) was reduced to 37% when compared with that of the control for 204 mM NH_4^+ in media. Additionally, the maximum cell mass X_∞ was reduced to 58% when compared with that of the control for the same amount of NH_4^+ in media. However, as shown in Figure 6-13, the carrying capacity coefficient *k* was reduced to 79% of the control value at 3.44 mM $[C_6H_6]$ in the media. Similarly, the maximum cell mass X_∞ was reduced to 58% of the

control value at 3.44 mM [C_6H_6] in the media. Thus, it is evident that C_6H_6 is a more potent cell growth inhibitor compared with NH_4 at the same concentration. However, since NH_3 is very soluble and converted into NH_4^+ instantaneously which can accumulate up to 200 mM during a normal bioreactor run, therefore, NH_3 should be targeted for removal during the raw syngas cleanup processes. On the other hand, even 3.44 mM [C_6H_6] in the media can significantly inhibit cell growth, however, the most realistic saturated [C_6H_6] in the media at 37 °C is around 0.41 mM with upper limit of 0.83 mM which showed negligible inhibitory effects on cell growth as shown in Figure 6-13. In this end, depending on the feasibility of the specific processes or end products targeted, C_6H_6 can be left untreated in a syngas stream.

6.4.4 Modeling with the media recycling

To scale up for industrial application, it is useful to model the continuous culture. To simplify, no cell recycle would be considered in this simplistic model. As detailed in Chapter 4 Section 4.4.4, the cell concentration in the presence of an impurity could be predicted relative to the cell concentration in the absence of an impurity according to:

$$\frac{X_1}{X_2} = \frac{X_{\infty,1}\ (1-\frac{1}{k_1\tau_l})}{X_{\infty,2}\ (1-\frac{1}{k_2\tau_l})} \tag{6-7}$$

Here, τ_l is the liquid residence time representing the liquid volume divided by the liquid flow rate, X is the cell mass (parameters with a subscript "1" refer to Bioreactor A that involved C_6H_6 and parameters with a subscript "2" refer to Bioreactor B that had no C_6H_6), X_∞ is the maximum cell concentration, and k is the carrying capacity coefficient.

With Equation 6-7, the fitted data of Table 6-1 for varying [C_6H_6] in the media was used to predict the ratio of X_1 versus X_2. In Figure 6-14, the ratio of X_1 versus X_2 was graphed as a

function of τ_l. It is clear that at higher [C_6H_6] (around 3.44 mM) the ratio of X_1 versus X_2 is less than 0.6. As an example, a prediction was made for a 700 mL media working volume with an effluent flow rate of 0.072 mL/min used from a previous experiment [88] where τ_l is 162 hours (shown as a vertical line in Figure 6-14). It can be inferred from Figure 6-14 that at 3.44 mM [C_6H_6] and 162 hours (τ_l) the ratio of X_1 versus X_2 is around 0.56 which is comparable to the ratio of $X_{\infty,1}/X_{\infty,2}$ (0.58).

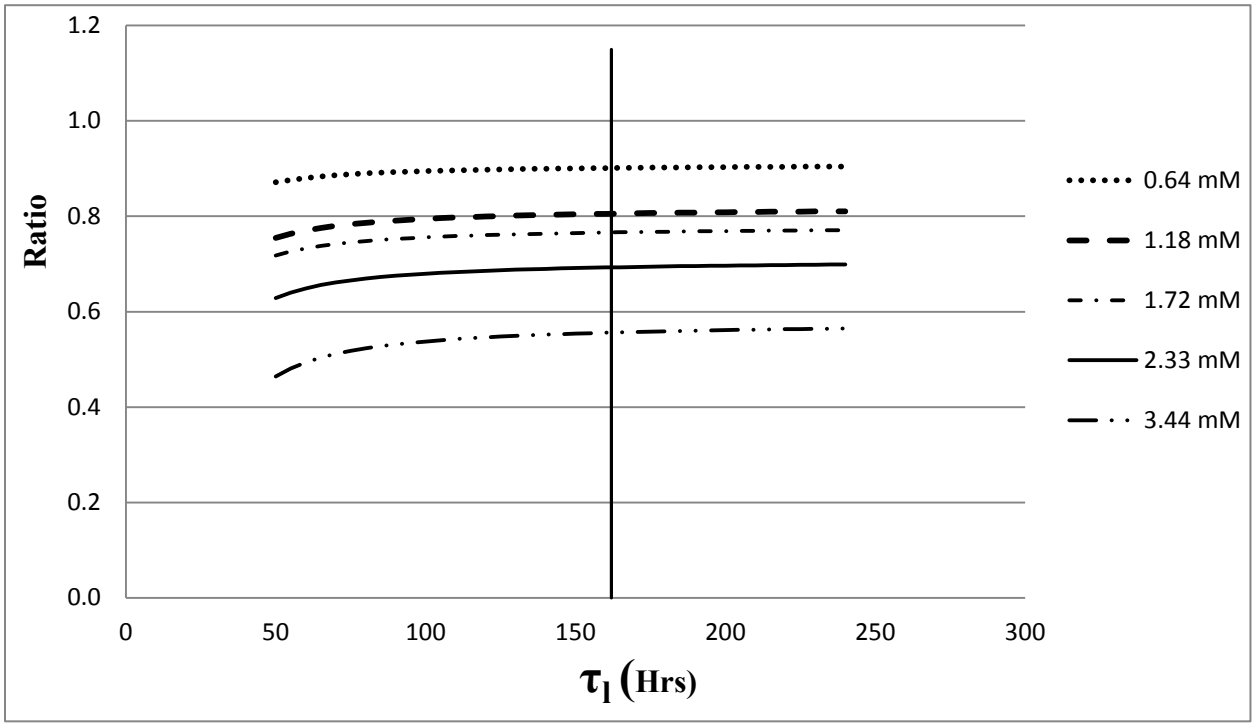

Figure 6-14. The ratio of X_1 versus X_2 is graphed with τ_l as the variable for varying [C_6H_6] in the media. Previous experimental τ_l value (162 hours) is shown here as a vertical line

Using this developed model, the ratio of X_1 / X_2 can be estimated for a continuous fermenter under steady-state operating conditions in the presence of benzene impurity. It should

be noted that the parameter values used in Equation 6-7 can depend upon many parameters such as the cell type, media composition, gas flow rate, C_6H_6 composition in the gas, the introduction of fresh media, and the reactor design. As seen, this analysis provides some insights as to how C_6H_6 in the bioreactor can potentially have a strong impact on the function of the bioreactor via its effect on the cell concentration. However, as a reminder, since the realistic saturated [C_6H_6] in media is around 0.41 mM (upper limit: 0.83 mM), cell mass will be only reduced by less than 10% compared with that of the control according to Figure 6-14. Therefore, C_6H_6 can be ignored as a targeted impurity for removal depending on the specific processes.

6.4.5 Effects of C_6H_6 on product formation

Besides the cell growth rates that were monitored, the effects of C_6H_6 on end product distribution were also studied. Figures from 6-15 to 6-19 show the ethanol and acetic acid profiles for varying [C_6H_6] in the media compared with those of the control. As [C_6H_6] in the media increased, the concentration profiles for ethanol and acetic acid gradually diverted from those of the corresponding controls. As a known fact, products formed by cells are normally related to the cell growth cycle. Primary products (HAc in this case) are growth associated and secondary products (EtOH in this case) are non-growth associated and are made in the stationary phase [105]. For the bacteria used in this study (P11), it typically displays a "biphasic fermentation" pattern. During the cell exponential growth phase, it produces higher amount of HAc and sufficient amount of ATP which provides cellular energy. When cell growth reaches stationary state and cells have enough energy, the metabolism switches to solventogenesis [88]. By observing the acetyl-CoA pathway and associated key enzymes as outlined in Chapter 1 Figure 1-4, it is clear that HAc can be converted into Acetaldehyde and then converted into EtOH via Acetaldehyde Dehydrogenase and ADH, respectively, if the conditions are favorable.

It was proposed that factors like pH, ATP levels, acid concentration, sporulation, availability of reducing energy and ion-limitation can regulate or affect the metabolic pathway leading to EtOH production [88]. At higher [C_6H_6] such as 2.33 or 3.44 mM, as compared with that of the control, the widely accepted acidogenesis to solventogenesis conversion mechanism appeared to be altered. Unexpectedly, part of the HAc was not converted into EtOH following the acetyl-CoA pathway compared with that of the control. Therefore, it was reasonable to propose that at higher [C_6H_6] such as 2.33 or 3.44 mM, C_6H_6 could potentially affect at least one of those factors listed above such as ATP levels, sporulation, and reducing agents etc. Additionally, it was proposed that the inhibition of forward ADH activity resulted from C_6H_6 as found in Chapter 7 Section 7.4.3 might lead to the explanation of the disruption of the conversion. However, the detailed mechanism merits further study.

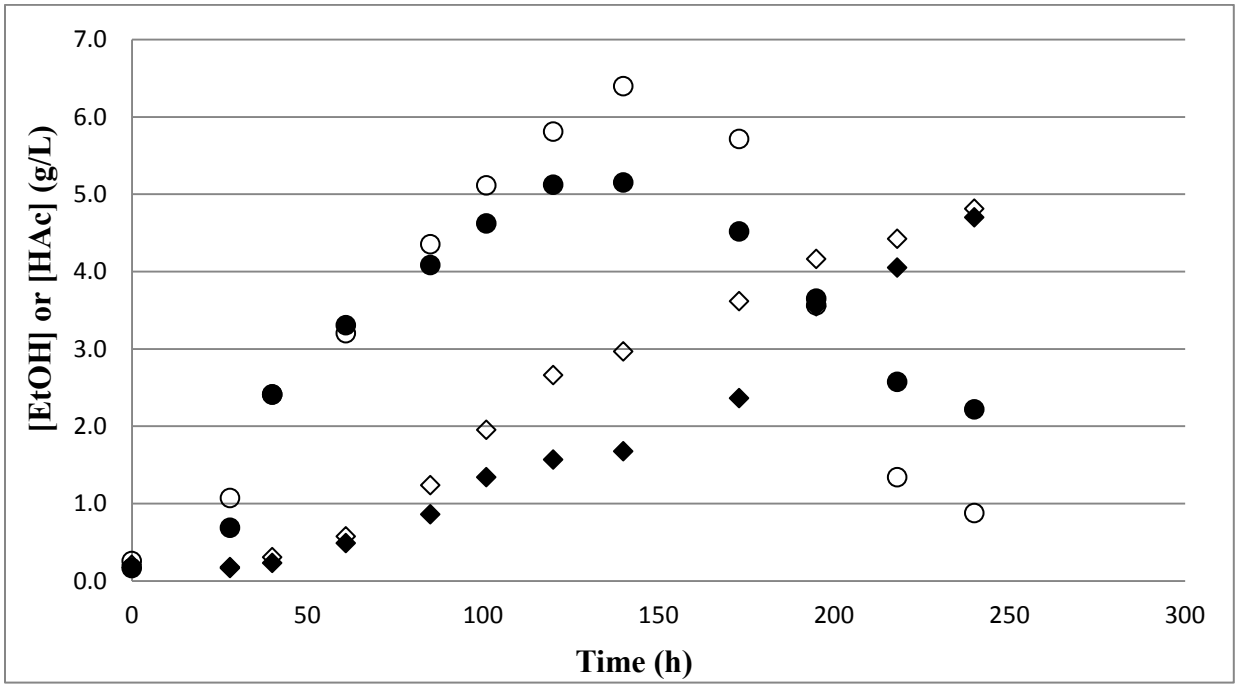

Figure 6-15. [EtOH] or [HAc] time profiles for Bioreactor B (control) and Bioreactor A (doped with 0.64 mM [C_6H_6] in media). Here the symbols are (◇) [EtOH] for control, (◆) [EtOH] for 0.64 mM C_6H_6, (○) [HAc] for control, (●) [HAc] for 0.64 mM C_6H_6

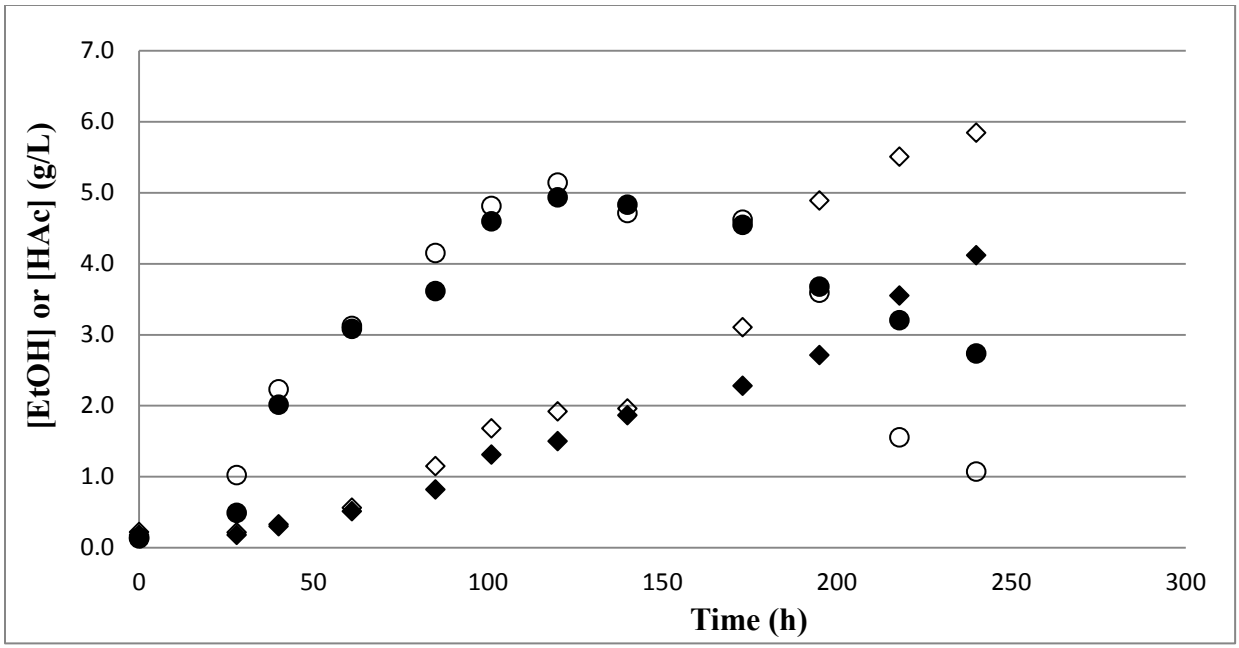

Figure 6-16. [EtOH] or [HAc] time profiles for Bioreactor B (control) and Bioreactor A (doped with 1.18 mM [C_6H_6] in media). Here the symbols are (◇) [EtOH] for control, (◆) [EtOH] for 1.18 mM C_6H_6, (○) [HAc] for control, (●) [HAc] for 1.18 mM C_6H_6

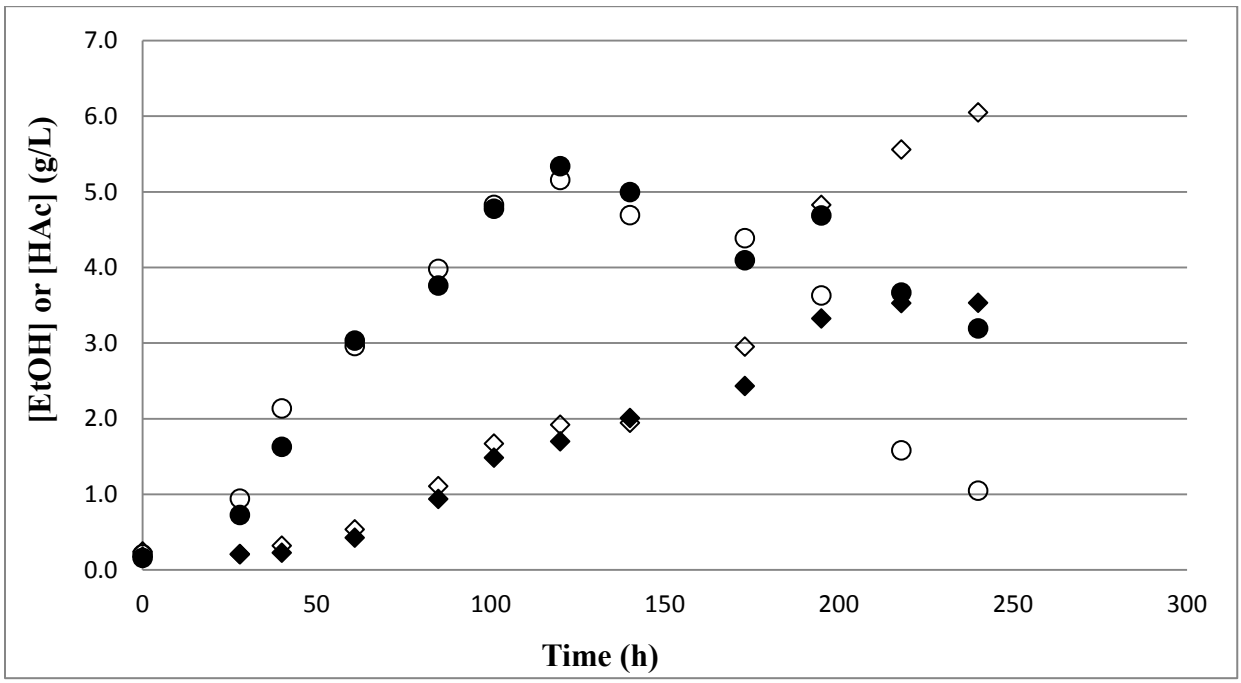

Figure 6-17. [EtOH] or [HAc] time profiles for Bioreactor B (control) and Bioreactor A (doped with 1.72 mM [C_6H_6] in media). Here the symbols are (◇) [EtOH] for control, (◆) [EtOH] for 1.72 mM C_6H_6, (○) [HAc] for control, (●) [HAc] for 1.72 mM C_6H_6

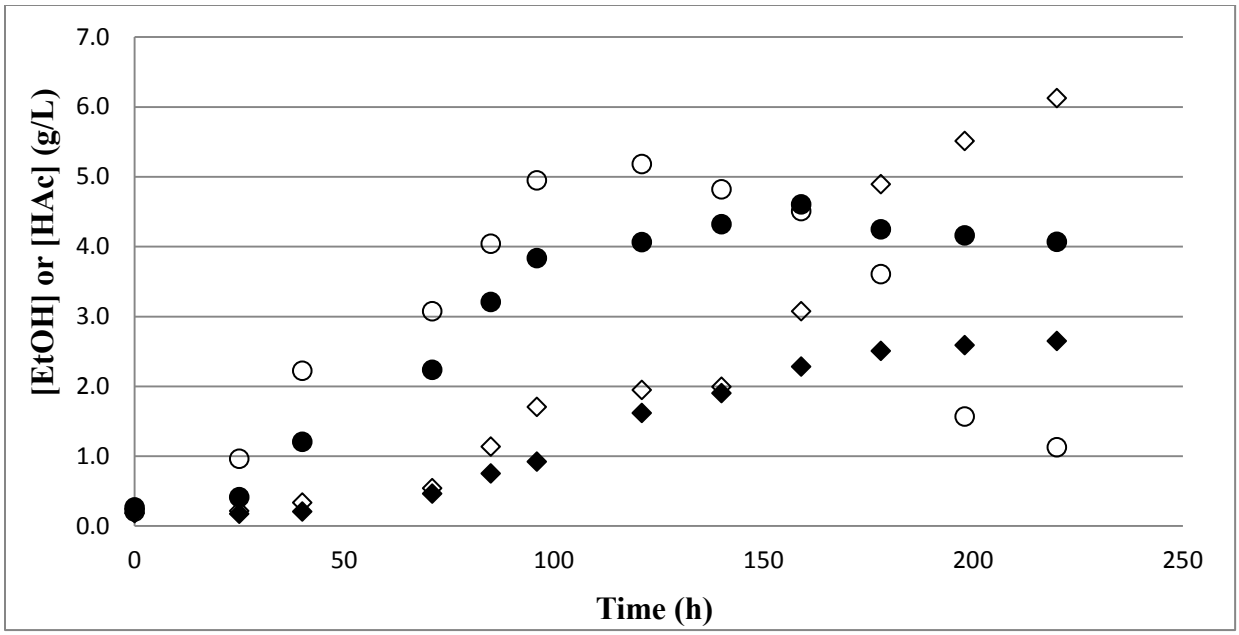

Figure 6-18. [EtOH] or [HAc] time profiles for Bioreactor B (control) and Bioreactor A (doped with 2.33 mM [C_6H_6] in media). Here the symbols are (◇) [EtOH] for control, (◆) [EtOH] for 2.33 mM C_6H_6, (○) [HAc] for control, (●) [HAc] for 2.33 mM C_6H_6

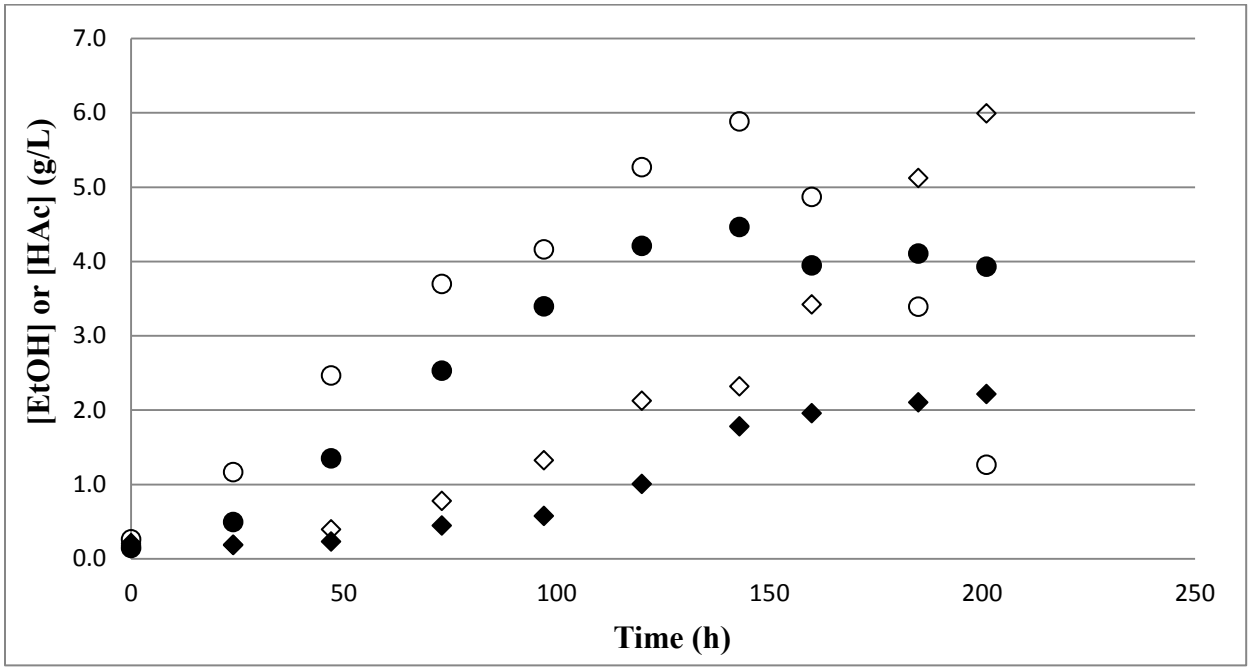

Figure 6-19. [EtOH] or [HAc] time profiles for Bioreactor B (control) and Bioreactor A (doped with 3.44 mM [C_6H_6] in media). Here the symbols are (◇) [EtOH] for control, (◆) [EtOH] for 3.44 mM C_6H_6, (○) [HAc] for control, (●) [HAc] for 3.44 mM C_6H_6

By comparing the cell growth profiles (Figures 6-8 to 6-12) to their corresponding [EtOH] or [HAc] profiles (Figures 6-15 to 6-19), it can be deduced that the level of cell density is closely related to the end product formation. At higher [C_6H_6], such as 3.44 mM in this study, lower cell density led to lower ethanol production. As shown particularly in Figure 6-19, [HAc] leveled off after reaching its peak concentration. This was different from that of the control which showed the continuous conversion of acetic acid to ethanol during the cell stationary growth phase.

Furthermore, by comparing the end product profiles involving NH_4^+ (Chapter 4 Section 4.4.6) with those involving C_6H_6, some insights can be seen. Since the osmolarity level for the media doped with C_6H_6 basically remains constant compared with that of the control, it is concluded that the pattern of the end product distribution is not contributed from the levels of osmolarity in the media. However, as for NH_4^+, higher levels of osmolarity in the media regardless of types of ions will eventually result in a higher ratio of [EtOH] to cell density. In this regard, it is C_6H_6 per se which disrupts the conversion from acetic acid to ethanol.

In addition, the redox profiles for both Bioreactor A and Bioreactor B were recorded. Since redox profiles for those runs were very similar, here only the redox profile for 2.33 mM [C_6H_6] in the media was displayed as shown in Figure 6-20. After observing the trends in Figure 6-20, redox was excluded as a contributing factor for the cell growth inhibition and the end product re-distribution.

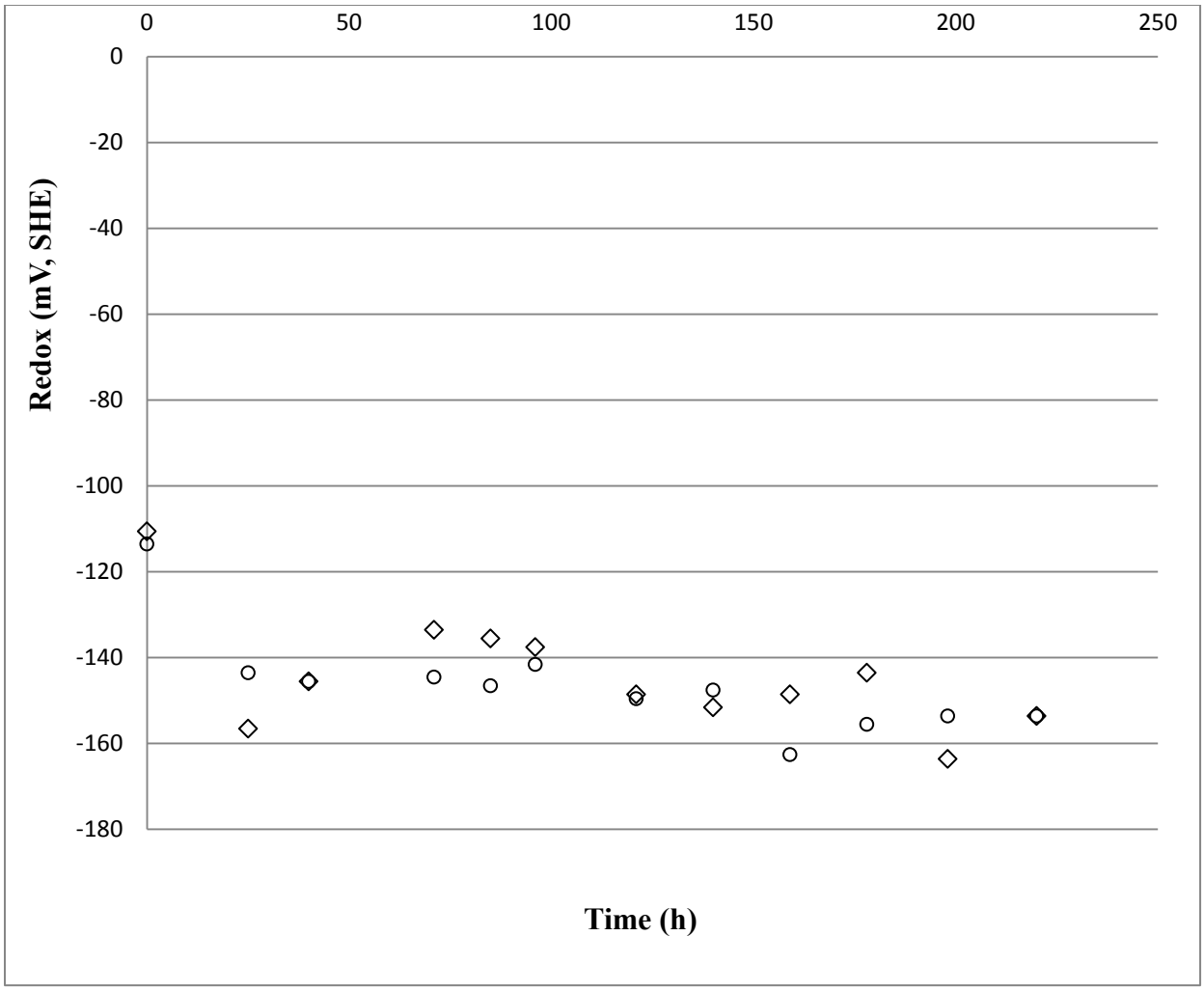

Figure 6-20. Redox time courses for both Bioreactor A (doped with 2.33 mM [C_6H_6] in the media) and Bioreactor B (control). The symbols are (○) for Bioreactor A and (◇) for Bioreactor B

Since C_6H_6 is a small molecule which can freely move across cell membranes, it can potentially impact the metabolic pathway leading to ethanol or acetic acid production as shown in this work. As for the detailed inhibitory mechanism, it is unclear at this point and beyond the scope of this work. However, it merits further investigation especially from a biological standpoint.

6.5 Conclusions

This work showed that C_6H_6 at concentrations above 1.72 mM in the media started to show appreciable cell growth inhibition and could potentially alter the metabolic pathway leading to the end production formation. However, according to the established syngas compositional database (0.3 mol % C_6H_6 with a upper limit of 0.6 mol %), the realistic saturated [C_6H_6] in media is only around 0.41 mM with upper limit of 0.83 mM (calculated via Henry's law) which did not significantly affect the cell growth and end production distribution. Therefore, it is unnecessary to cleanup C_6H_6 from any syngas streams. However, as a caveat, it is necessary to distinguish C_6H_6 from tars (heavy or light). Tars can be comprised of phenol, naphthalene, and compounds with multiple benzene rings. In conclusion, C_6H_6 can be left untreated but other tar species should be assessed, especially species with high solubility such as phenol.

7. Effects of benzene in syngas on hydrogenase and ADH activity

7.1 Introduction

Since C_6H_6 can reach 0.6 mol% (upper limit) for biomass gasification [60], it is necessary to investigate whether C_6H_6 can dramatically inhibit hydrogenase activity besides cell growth and ethanol production. As mentioned in Chapter 5 Section 5.1, hydrogenase plays a significant role in syngas fermentation by providing necessary electrons for product formation from dissociating H_2. In addition, the forward ADH activity will directly catalyze the formation of ethanol as detailed in Chapter 5 Section 5.1. The quantification of the effects of C_6H_6 on the activities of hydrogenase and forward ADH will provide insights to make a holistic judgment as to the options of the raw syngas cleanup system.

7.2 Research objectives

- Establish a model for hydrogenase inhibition with C_6H_6 as the sole inhibitor and regress experimental data to find the inhibition constant for C_6H_6. In addition, identify the inhibition type (competitive, non-competitive, and uncompetitive) for C_6H_6 based on the experimental data.

- With the fitted parameters and realistic [C_6H_6] in the media from a gasifier, calculate percentages of hydrogenase activity reduction associated with industrial applications.
- Measure the forward ADH activity with the doped [C_6H_6] in the enzymatic assay to compare with that of the control to obtain additional insights of the effects of C_6H_6 on ethanol formation.

7.3 Materials and methods

7.3.1 Microorganism and cell growth media preparation

The same bacteria--*Clostridium ragsdalei*, denoted as P11, was used for the hydrogenase and forward ADH activity studies with C_6H_6 as a targeted inhibitor. The media recipe and preparation steps are the same as detailed in Chapter 4 Section 4.3.1. As mentioned previously, the third passage was used as the active cell source for these hydrogenase / forward ADH activity comparative studies.

7.3.2 Hydrogenase assay

The protocol for this hydrogenase assay is very similar to the protocol detailed in Chapter 5 Section 5.3.2. Two Hungate tubes (size: 60x125mm), one containing a cell solution and the other containing an electron acceptor solution, were prepared separately in an anaerobic chamber. The electron acceptor solution contained the following reagents: 0.3 ml of 1 M phosphate buffer (mixture of 1 M KH_2PO_4 and 1 M K_2HPO_4 at pH=6), 2.3 ml of degassed water, and 0.4 ml of 0.04 M benzyl viologen dichloride (BV). BV is the electron acceptor for the electrons released from H_2 via hydrogenase. The cell solution contained the following reagents:

0.3 ml of 1 M phosphate buffer (pH=6), 1.8 ml of degassed water, 0.3 ml of 0.5 M dithiothreitol (DTT), 0.3 ml of active P11 cells. DTT was freshly made before each assay owing to its instability in water. This protocol is for the control assay. All reagents were purchased from Sigma-Aldrich (St. Louis, MO).

To study the potential inhibitory effects of C_6H_6 on the hydrogenase activity for the initial run, 2.3 ml of 0, 5, 10, 15, 20 mM [C_6H_6] was used to replace the same amount of DI water in the electron acceptor solution. The remaining reagents and quantities in the electron acceptor solution were unchanged. The cell solution was the same as the control. The corresponding resultant [C_6H_6] in the cuvette was 0, 2.87, 5.74, 8.61, and 11.48 mM, respectively. For this initial run, after both solutions in the Hungate tubes were prepared and removed from the anaerobic chamber, they were purged with pure H_2.

Since the initial hydrogenase studies showed inhibition, additional studies were performed to develop a model. For the hydrogenase inhibition modeling assay, 2.3 ml of 0, 5.23, 7.84 mM [C_6H_6] was used to replace the same amount of DI water in the electron acceptor solution. The cell solution was the same as the control. The corresponding resultant [C_6H_6] in cuvette was 0, 3, and 4.5mM, respectively. After the two solutions were prepared in the Hungate tubes, both tubes were removed from the anaerobic chamber and purged with pure H_2 or a H_2/N_2 mixture to obtain the desired H_2 gas composition. The gases were added using two mass flow controllers, one for H_2 and one for N_2, with a total flow rate of 50 sccm. The H_2 gas flow rate was 15, 30, or 50 sccm with N_2 as the balance of the total flow rate. Thus, the H_2 gas composition assessed was 30, 60, and 100%. For the purging, two needles were inserted through the Hungate tube septum. A longer 20-gauge needle was used as the gas inlet while a shorter 22-gauge needle was used to provide a vent to maintain positive pressure inside the tube. A 4.6 ml

cuvette for spectrophotometer was also purged with the same gas mixture. The cuvettes and cell solution Hungate tubes were purged for 5 minutes as usual. However, the purging time for the electron acceptor tubes was shortened to just 1 minute purposely to avoid excessive loss of vaporized C_6H_6 from solution since C_6H_6 is very volatile.

At the end of purging, 5 psig of pressure was allowed to build up in these two Hungate tubes and the cuvette to keep air from coming in. For the cell solution tube, 20 seconds before the end of purging, 0.3ml triton X-100 (prepared in a 1ml syringe/needle assembly done in the anaerobic chamber) was injected to permeate the cell wall to expose hydrogenase in the cells to the solution. After these procedures, the two Hungate tubes were placed in a water bath at 37 °C for five minutes. Finally, 2 ml from the electron acceptor solution tube and 0.67 ml from the cell solution tube were transferred and injected into the cuvette. After shaking vigorously a few times, a 22-gauge needle connected to a 0.3 psig check valve was quickly inserted and then removed to relieve excess pressure and maintain a constant positive pressure in the cuvette. The ambient pressure of the study was 13.3 psi such that the cuvette pressure was always maintained at a total pressure of 0.93 atm (13.6 psi).

The cuvette was placed in a heat-controlled spectrophotometer at 37 °C during the course of the assay which converted oxidized BV to reduced BV. The absorbance (Abs) of reduced BV was monitored at 546 nm and converted to an associated concentration where C_{BV}=Abs / (ε∗b). Here, ε is the extinction coefficient (7.55 mM^{-1} cm^{-1} at 546 nm) and b is the cuvette path length of 1 cm. The production rate of reduced BV (R_{BV}) was obtained from the initial slope of the concentration versus time curve. Initial slope data is important for the analysis since knowledge of the H_2 partial pressure is important. With initial slope data, the known initial H_2 partial pressures could be utilized. Since the rate of H_2 consumption (R_{H2}) is equal to -½R_{BV} according

to an electron balance, the hydrogenase activity relative to the cell mass (U/mg) was obtained by dividing $1/2R_{BV}$ by the cell density. The activity U represents one μmol H_2 consumed per minute. It is important to account for the cell density since higher cell density will give higher hydrogenase activity readings.

7.3.3 Forward Alcohol Dehydrogenase (ADH) assay

Acetaldehyde was used as the substrate for the forward ADH assay. The protocol used in this assay was modified from Ahmed's dissertation [88] as detailed below: 0.4 mL 1M Tris-HCl, 0.5 mL 0.08 M dithiothreitol (DTT), 0.1 mL 5% v/v triton X-100, 0.12 mL 0.01 M NADH, 0.4 mL 0.1 M acetaldehyde and 1.5 mL degassed DI water. The total volume was added up to 3.02 mL excluding the cell source in a 4.5 mL capacity cuvette. This above-mentioned formula is for the control assay. For the comparative assay, 1.5 mL of varying $[C_6H_6]$ (0, 1, 2, 3, 4, 5 mM) was added to substitute the same amount of water to reach the final $[C_6H_6]$ of 0, 0.5, 0.99, 1.49, 1.99, or 2.48 mM in the cuvette. All chemicals were purchased from Sigma-Aldrich. DTT and NADH were freshly made prior to each run owing to their instability in water. All the above reagents were added into a 4.5 mL optical glass cuvette in an anaerobic chamber. After sealing and removing this cuvette from the anaerobic chamber, it was purged with pure N_2 for one minute. For the purging, two needles were inserted through the cuvette septum. A longer 20-gauge needle was used as the gas inlet while a shorter 22-gauge needle was used to provide a vent to maintain positive pressure inside the tube. After purging with 5 psig in the cuvette headspace, the cuvette was placed in a 37 °C receptacle of a UV-visible spectrophotometer set at 340 nm wavelength. A gas-tight syringe (1 mL) was used to inject 0.5 mL cell source into the said cuvette. After shaking vigorously for a few times, the cuvette was placed back in the

receptacle and the kinetic recording process was started. The concentration of NADH was calculated using Beer's law (C=Abs / (ε∗b)), where ε is the extinction coefficient for NADH (6.22 $mM^{-1}cm^{-1}$ @ 340 nm) and b is the cuvette path length (1 cm). As show in the reaction (Acetaldehyde + NADH + H^+ ↔ Ethanol + NAD^+), the change in NADH is equivalent to the change in acetaldehyde on a molar basis. The maximum reaction rate ($R=\Delta C/\Delta t$) was calculated from the initial linear slope of the curve after a short lag phase. Reaction rate R was then divided by measured cell mass and converted into specific activity (U/mg), where U represents μmols of acetaldehyde consumed per minute.

7.4 Results and discussions

7.4.1 Effects of [C_6H_6] on hydrogenase activity

For the initial hydrogenase activity study, 0, 2.87, 5.74, 8.61, 11.48 mM [C_6H_6] (final concentration) was doped into a cuvette, respectively. The hydrogenase activity reduction profile is shown in Figure 7-1. Hydrogenase activities, as expected, decreased with the increasing [C_6H_6] in the assay cuvettes. At 11.48 mM [C_6H_6], the hydrogenase activity was reduced roughly to 50% of the control value. From Equation 7-1 listed below, it can be deduced that the inhibition constant for C_6H_6 should be approximately around 11.5 mM since when $C_i = K_i$, the hydrogenase activity will be reduced by half according to Equation 7-1.

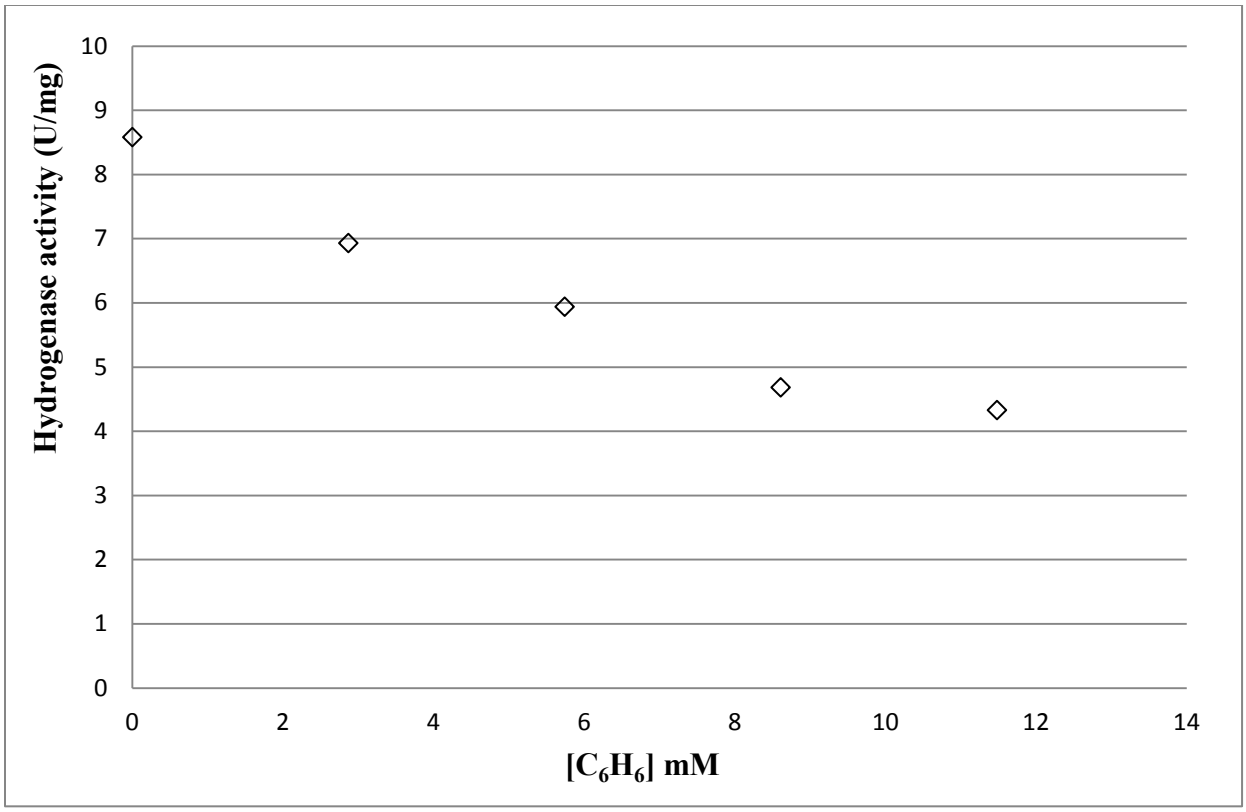

Figure 7-1. Hydrogenase activity with varying [C_6H_6]

7.4.2 Hydrogenase inhibition kinetic model

This kinetic model is the same as that used in Chapter 5 Section 5.5.1. The three major enzyme inhibitions namely competitive, non-competitive and uncompetitive, affect enzymes in different ways. For the non-competitive inhibition, inhibitors bind on sites other than the active sites resulting in reduced enzyme affinity to the substrates. For non-competitive inhibition with a single inhibitor [96]:

$$V = \frac{V_m}{\left(1+\frac{K_{H_2}}{[H_2]}\right)\left[1+\frac{C_i}{K_i}\right]} \quad (7\text{-}1)$$

Where, V is the enzyme activity, V_m represents the maximum hydrogenase activity under the specific experimental conditions, K_{H2} is the Michaelis-Menten constant for H_2, C_i is the

concentration of inhibiting species (e.g. C_6H_6), and K_i is the inhibition constant for the inhibiting species. Equation 7-1 can be rearranged into a double reciprocal plot with C_6H_6 as the sole inhibitor according to:

$$\frac{1}{V} = \frac{K_{H_2}}{V_m}\left[1 + \frac{C_{C6H6}}{K_{C6H6}}\right]\left(\frac{1}{[H_2]}\right) + \frac{1}{V_m}\left[1 + \frac{C_{C6H6}}{K_{C6H6}}\right] \quad (7\text{-}2)$$

As seen from Equation 7-2, a plot of 1/V versus 1/ $[H_2]$ will give a straight line.

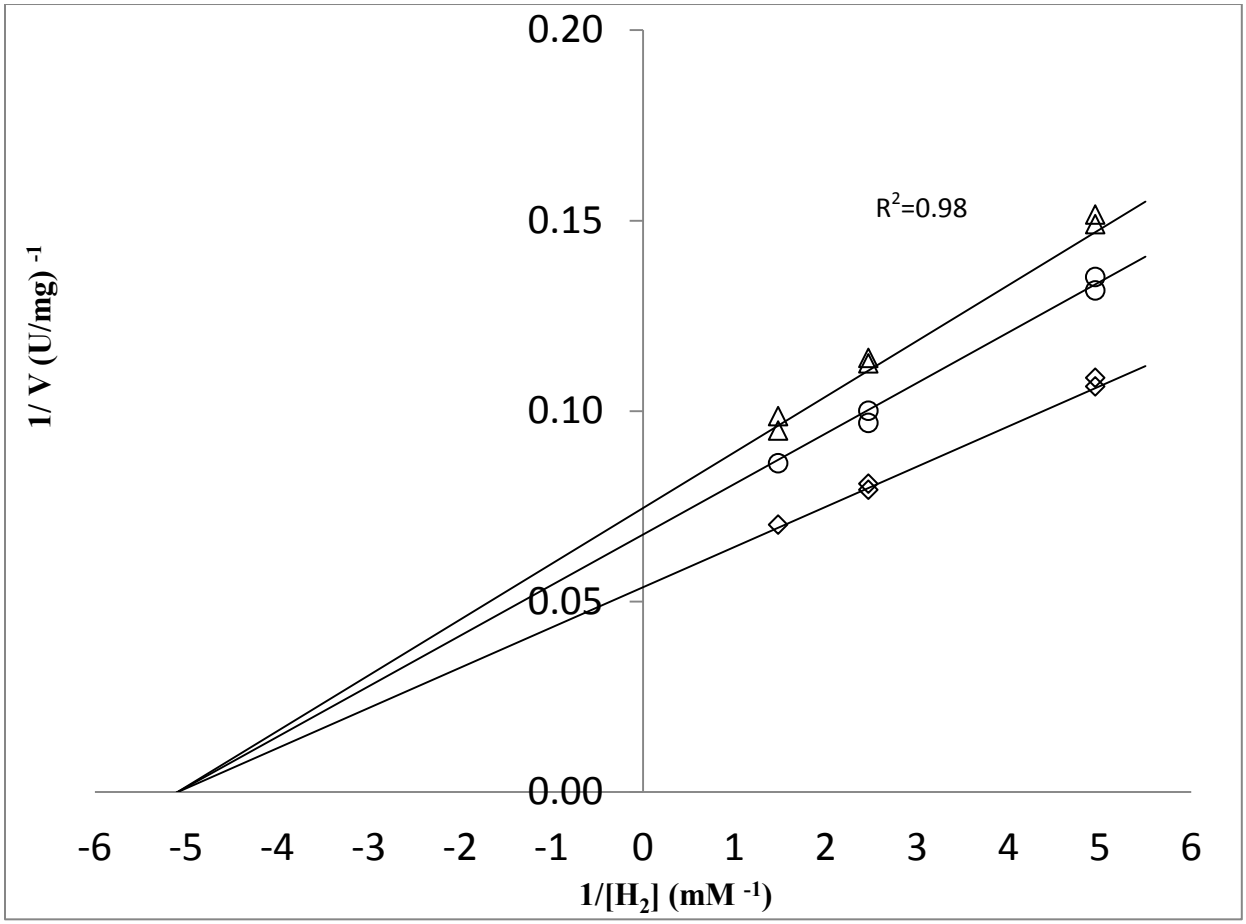

Figure 7-2. Double reciprocal plot showing the non-competitive inhibition of hydrogenase by C_6H_6 as at various H_2 concentrations. The solid lines represent Equation 7-2. The concentrations of C_6H_6 in units of mM are (◇) 0, (○) 3, (△) 4.5

The entire data set of Figure 7-2 for C_6H_6 alone was simultaneously regressed to Equation 7-2 using statistical software (SAS 9.2.3, SAS Institute, Cary, NC). The model is shown as lines in Figure 7-2. The values were V_M = (18.77 ± 0.96) U/mg, K_{H2} = (0.196 ± 0.022) mM, and K_{C6H6} = (11.40 ± 1.32) mM. The model fits the data reasonably well as indicated by the R^2 value and confirms that the C_6H_6 inhibition is non-competitive. It is interesting to compare this K_{H2} value with those reported in Chapter 5 Section 5.5.1 to see how consistent they are. In section 5.5.1, the K_{H2} is (0.19 ± 0.1) mM, (0.19 ± 0.02) mM, and (0.20 ± 0.03) mM for NH_4^+, Cl^-, and NH_4Cl hydrogenase inhibition, respectively. It is clear that there is a good agreement among them as expected them to be. According to Equation 7-1, when $C_i = K_i$, the activity is reduced by ½. Thus, when the C_6H_6 concentration becomes 11.4 mM, the enzyme activity is compromised by one-half. The K_{H2} value obtained in this study from P11 was comparable to published data for other bacteria although it should be noted that the type of hydrogenase can be different among species. Adams and Mortensen reported that the K_{H2} value for hydrogenase I of *Clostridium pasteurianum* is around 0.18 mM using methylene blue as the electron acceptor [106]. Dobrindt and Blaut reported that the K_{H2} value for *Sporomusa sphaeroides* is 0.34 mM with benzyl viologen as the electron acceptor [98]. By comparing the magnitude of the inhibition constants obtained in Chapter 5 for NH_4^+ and Cl^-, it is evident that C_6H_6 is a much potent inhibitor for hydrogenase activity even though [C_6H_6] is low in the media comparing with other ions such as NH_4^+.

According to Equation 7-1, the ratio of V in the presence of C_6H_6 (V_{C6H6}) relative to V in the absence of C_6H_6 (V_0) at the same H_2 concentration is:

$$\frac{V_{C66}}{V_o} = \left(\frac{V_{m,C6H6}}{V_{m,o}}\right)\left(1 + \frac{C_{C6H6}}{K_{C6H6}}\right)^{-1} \qquad (7\text{-}3)$$

When the enzyme level is the same in the presence or absence of C_6H_6 ($V_{m,o} = V_{m,\ C6H6}$), then the reduction in enzyme activity in the presence of C_6H_6 is affected by the $(1+C_{\ C6H6}/K_{\ C6H6})$ term. Figure 7-3 shows Equation 7-3 (with $V_{m,o} = V_{m,\ C6H6}$) as a function of the C_6H_6 concentration. It should be noted that the enzyme parameters are limited to pH of 6 and 37 ºC as obtained in this study.

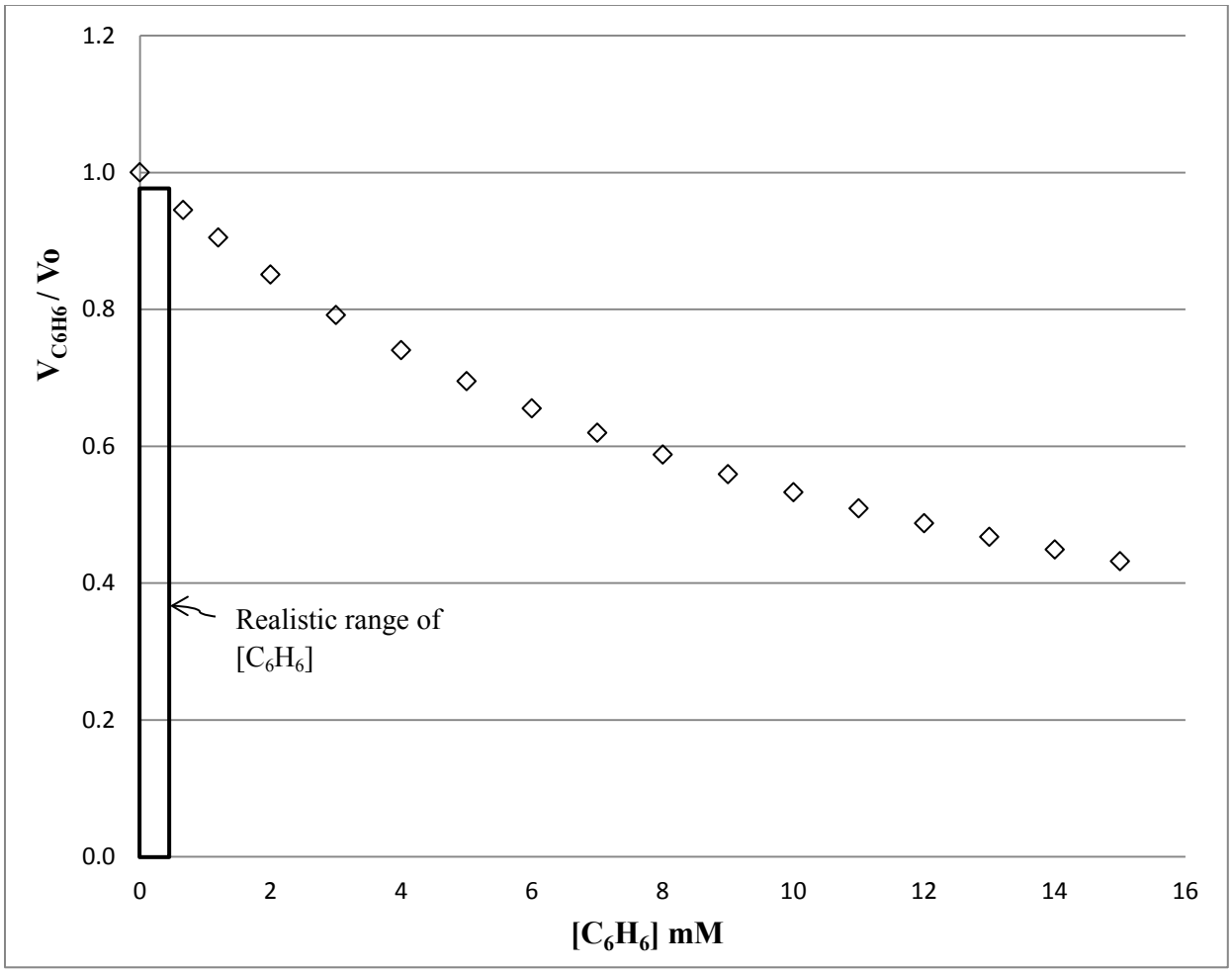

Figure 7-3. V_{C6H6} / V_0 versus C_6H_6. V_{C6H6} is the hydrogenase activity as a function of C_6H_6; V_0 is the hydrogenase activity in the absence of C_6H_6

As highlighted by the bar in Figure7-3, at realistic [C_6H_6] of 0.41 mM (upper limit 0.83 mM) in the media that is associated with typical C_6H_6 impurities in syngas (see Chapter 6), the

hydrogenase activity was only reduced by less than 5%. Therefore, for industrial syngas fermentation, C_6H_6 can be left in the syngas feeding stream without special treatment. This is consistent with the findings of the effects of C_6H_6 on cell growth and product formation shown in Chapter 6.

7.4.3 Effects of C_6H_6 on forward ADH activity

As detailed in Section 7.3.3 in this chapter, 0, 0.5, 0.99, 1.49, 1.99, 2.48 mM [C_6H_6] (final concentration) was added into an assay cuvette, respectively. The forward ADH activity reduction profile is shown in Figure 7-4. As noted, there is a steep drop in the forward ADH activity for [C_6H_6] ranging from 0 to 1 mM. At realistic [C_6H_6] of 0.41 mM, the forward ADH activity was roughly reduced by 30% compared with the control value. As discussed in Chapter 6, at [C_6H_6] of 0.64 mM, [EtOH] was barely affected compared with the control. To rationalize this inconsistency, it was hypothesized that for this forward ADH assay, ADH was exposed to C_6H_6 in the media for a short period (less than 15 minutes). However, in the bioreactor runs, ADH was possibly protected by the cell walls even though C_6H_6 can partially move across cell membranes. Another hypothesis is that ADH in the active whole cells can adapt to a lower [C_6H_6] which will dampen the explicit inhibitory effects from C_6H_6. It was also proposed that for ethanol production, there were other contributing parameters (such as pH, redox) besides the forward ADH activity alone. These above rationales can partially explain the discrepancy observed in the notable reduction of forward ADH activity and slight reduction in [EtOH] compared with that of the control. However, further studies should be conducted to assess the hypotheses.

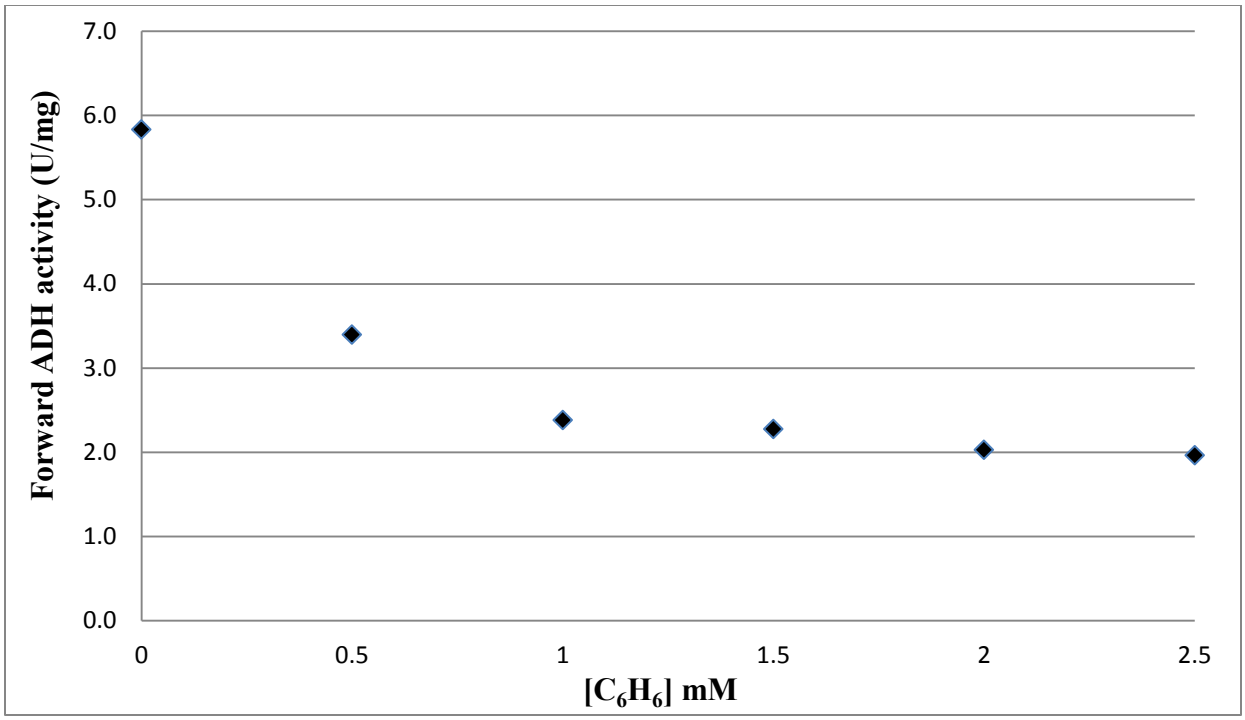

Figure 7-4. Forward ADH activity with varying [C_6H_6]

7.5 Conclusions

Combining the experimental results from this chapter with those of Chapter 6, it was concluded that for industrial fermentations, C_6H_6 can be left untreated upon exiting from a gasifier. From a theoretical standpoint, it was shown that C_6H_6 is a potent inhibitor for both hydrogenase and forward ADH activity at elevated concentrations such as above 6.5 mM for hydrogenase inhibition and over 0.5 mM for forward ADH activity. However, these concentrations are much greater than would be expected from a bioreactor exposed to syngas containing a C_6H_6 impurity.

8. Conclusions and future work

The focus of this work was to establish a syngas compositional database and identify the potential impurities which can potentially affect cell growth, enzymatic activities and ethanol production. A summary of the key findings is listed below.

8.1 Key findings

- In this work, a syngas compositional database was established. Some key impurities such as NH_3 and C_6H_6 were identified as potential cell growth inhibitors.
- It was found that NH_3 in syngas can convert into NH_4^+ instantaneously upon entering the media and NH_4^+ can accumulate to high concentrations (250 mM) and subsequently raise the osmolarity level of the media which in turn can inhibit cell growth. It was also found that P11 cells used in this study can adapt to the elevated osmolarity (up to 500 mM) to some extent.
- Since NH_4^+ can raise the level of osmolarity substantially, it was found that higher osmolarity level will eventually lead to higher [EtOH] per cell density.

- NH_4^+ can non-competitively inhibit hydrogenase activity with an inhibition constant of (649±35) mM. As part of the protocol, it was concluded that the inhibition constants for NH_4^+, Cl^-, NH_4Cl, and C_6H_6 are in the following order: $K_{NH4+} > K_{Cl-} > K_{NH4Cl} > K_{C6H6}$. Therefore, for the same concentration of the above-listed species, C_6H_6 is the most potent inhibitor for hydrogenase.
- Since benzene is sparsely soluble in the media, it was found that at a realistic $[C_6H_6]$ (around 0.41 mM), there is a negligible effect on cell growth and ethanol production.
- However, from a theoretical standpoint, when $[C_6H_6]$ reached 2.3 mM in the media, the cell growth was significantly inhibited and the widely-accepted acidogenesis-to-solventogenesis conversion mechanism was partially disrupted.
- It was shown that C_6H_6 is a non-competitive inhibitor for hydrogenase activity. Since the inhibition constant [K_{C6H6}= (11.40±1.32) mM] is very low, C_6H_6 by far is a more potent inhibitor compared with NH_4^+. Since the realistic $[C_6H_6]$ in the media is only around 0.41 mM (upper limit 0.83 mM), hydrogenase activity will only be reduced by less than 5% in an industrial setting.
- In addition, the forward ADH activity with respect to NH_4^+ and C_6H_6 was also analyzed. It was found that at lower $[NH_4^+]$ (up to 200 mM) there was no adverse effect on forward ADH activity. However, C_6H_6 can significantly inhibit forward ADH activity even starting at 0.5 mM. This forward ADH inhibition resulted from C_6H_6 and may partially explain why the widely-accepted acidogenesis-to-solventogenesis conversion mechanism was partially disrupted at $[C_6H_6]$ over 2.3 mM.

8.2 Conclusions

Since the syngas composition from various biomass and coal blends will generate different gas compositions, an understanding of the positive or adverse effects of impurities from raw syngas on biofuel production will provide critical information regarding the need for efficient gas cleaning processes for commercialization. This work shows that some potential impurities, without cleaning, may have a large impact on the fermentation processes. Therefore, a cleanup system suitable for syngas fermentation processes is evident although the degree of cleanup would likely depend upon the feedstock and the associated syngas generation process. Additionally, it is important to recognize that studies involving "clean" syngas should be carefully interpreted since the absence of syngas impurities can bias the experimental results needed for assessing the commercialization potential of the syngas fermentation process.

To design an efficient gas cleanup system, coupling the findings in the literature with the current work, NO_x, heavy tars (C_6^+), and NH_3 should be targeted for removal. However, acetylene (C_2H_2), ethylene (C_2H_4), ethane (C_2H_6), and benzene (C_6H_6) can be left alone.

8.3 Future work

Since syngas fermentation is still in its initial process of commercialization, there are a few key bottlenecks to be resolved to improve the cell growth rate, carbon utilization efficiency, and ethanol production such as bioreactor design, mass-transfer efficiency, media optimization,

effects of syngas impurities etc. As for the effects of syngas impurities on fermentation processes, the following key issues are identified for future studies.

- The effects of SO_2 and H_2S on the syngas fermentation still need to be quantified when the necessary safety procedures are in place.
- One of the tar components--phenol (C_6H_5OH), which is quite soluble in water (8.3 g/100 mL at 20 °C) compared with C_6H_6, should be targeted for studying its effects on cell growth, enzymatic activity, and product formation.
- After the potential effects from all the syngas impurities have been identified and quantified, an efficient raw syngas cleanup system should be designed, tested, and scaled up suitable for the industrial syngas fermentation process.
- Beyond the traditional syngas purification unit operations such as cyclones, adsorption columns, water or oil scrubbers and various types of filter, new technologies such as hot catalytic gas conditioning downstream of a gasifier should be explored and scaled up to a commercial level.
- On the other end of the spectrum, besides investigating the effects of syngas impurities on cell growth and end product formation, it is advisable to cultivate new microbial catalysts or genetically engineered organisms that can tolerate the inhibitory effects of the potential syngas impurities to a greater extent. If this happened, the syngas cleanup system can be greatly simplified or even phased out. In addition, metabolic engineering is also the way to go to increase the yield of targeted products and broaden the spectrum of end products.
- Initially, the syngas impurities under varying operating parameters and feedstocks were predicted using Aspen Plus II ®, although the results were not reported in

this work. There was a wide discrepancy between the predicted values and the experimental values under similar conditions for the trace amounts of impurities. As such, an advanced kinetic model should be developed to improve the consistency between experimental and predicted impurity levels.

REFERENCES

[1] Google [Internet]. Obama announces ethanol balancing act. [Cited 2012 May 18]. Available from: http://wwwmsnbcmsncom/id/30579857/ns/us_news-environment/t/obama-announces-ethanol-balancing-act/#T612llKqZng

[2] Perlack RD, Wright LL, Turhollow AF, Graham RL, Stokes BJ, Erbach DC. Biomass as feedstock for a bioenergy and bioproducts industry: The technical feasibility of a billion-ton annual supply. Oak Ridge National Laboratory 2005.

[3] Google [Internet]. Administration UEI. Annual Energy Review. [Cited 2012 May 18]. Available from: http://www.eia.gov/totalenergy/data/annual/pdf/aer.pdf

[4] Google [Internet]. Alternative Fuels. [Cited 2012 May 18]. Available from: http://wwwparagonexpocom/indexphp/DE-Green/alternative-fuelshtml

[5] Rasskazchikova TV, Kapustin VM, Karpov SA. Ethanol as high-octane additive to automotive gasoline. Production and use in Russia and abroad. Khimiya i Tekhnologiya Topliv i Masel 2004:3~7.

[6] Google [Internet]. Renewable energy trends in consumption and electricity. [Cited 2012 May 18]. Available from:http://www.eia.doe.gov/cneaf/solar.renewables/page/trends/rentrends.html.

[7] Yacobucci BD, Womach J. Fuel ethanol: Background and public policy issues. Washington, DC: Congressional Research Service; 2004 December. 21p. RL-30369

[8] Curtis B. 2007 year in review U.S. ethanol industry: The next inflection point. Washington DC, BCurtis Energies and Resource Group 2008; 52p.

[9] Searchinger T, Heimlich R, Houghton RA, Dong F, Elobeid A, Fabiosa J, et al. Use of U.S. croplands for biofuels increases greenhouse gases through emissions from land-use change. Science 2008;319:1238~1240.

[10] Kim S, Dale BE. Global potential bioethanol production from wasted crops and crop residues. Biomass Bioenergy 2004;26:361.

[11] Wyman CE. Ethanol from lignocellulosic biomass: Technology, economics, and opportunities. Bioresour Technol 1994;50:3.

[12] Ford J, Todd French W, Hernandez R, Easterling E, Zappi M, Morrison C, et al. Development and comparisons of efficient gas-cultivation systems for anaerobic carbon monoxide-utilizing microorganisms. Bioresour Technol 2008;99:638~643.

[13] Clausen EC, Gaddy, J.L. Concentrated sulfuric acid process for converting lignicellulosic materials to sugars. United States; 1988.

[14] Kaylen M, Van Dyne, D.L., Choi, Y.S., Blase, M. Economic feasibility of producing ethanol from lignocellulosic feedstocks. Bioresour Technol 2000;72:19.

[15] Ackerson MD, Clausen EC, Gaddy JL. Bioconversion of synthesis gas into fuels. 2 ed. Washington, DC, USA: Publ by ACS; 1993, p. 286.

[16] Maschio G, Lucchesi A, Stoppato G. Production of syngas from biomass. Bioresour Technol 1994;48:119~126.

[17] Henstra AM, Sipma J, Rinzema A, Stams AJM. Microbiology of synthesis gas fermentation for biofuel production. Curr Opin Biotechnol 2007;18:200~206.

[18] Kianpour K. Biofuel necessary, requires research- Cellulosic ethanol industry makes gains, becomes increasingly cost-effective, http://www.cavalierdaily.com/2012/02/23/biofuel-necessary-requires-research/. 2012.

[19] Jackson M. Biomass, natural gas, coal to liquids-processing technology business overview, Synthenol Energy Corporation. 2012.

[20] Google [internet]. Coskata homepage. [Cited 2012 May 25]. Available from: http://www.coskata.com/process/index.asp?source=D5E7FB22-6034-405B-898B-58DE4651645D.

[21] Gavrilescu M, Chisti Y. Biotechnology—a sustainable alternative for chemical industry. Biotechnol Adv 2005;23:471~499.

[22] Donovan J, Stowe N. Is the future of biofuels in algae? http://www.renewableenergyworld.com/rea/news/article/2009/06/is-the-future-of-biofuels-in-algae. Environmental and Energy Study Institute (EESI) newsletter; 2009.

[23] Sheehan J, Dunahay T, Benemann J, Roessler P. A Look Back at the U.S. Department of Energy's Aquatic Species Program—Biodiesel from Algae. National Renewable Energy Laboratory, NREL/TP-580-24190, http://www.nrel.gov/docs/legosti/fy98/24190.pdf. 1998.

[24] Kovalyova S. European body sees algae fuel industry in 10-15 years. http://large.stanford.edu/publications/power/references/kovalyova/. 2009.

[25] Phillips J, Klasson K, Clausen E, Gaddy J. Biological production of ethanol from coal synthesis gas. Appl Biochem Biotechnol 1993;39-40:559~571.

[26] Bredwell MD, Srivastava P, Worden RM. Reactor Design Issues for Synthesis-Gas Fermentations. Biotechnol Progr 1999;15:834~844.

[27] Abrini J, Naveau H, Nyns EJ. Clostridium authoethanogenum, Sp-Nov, an anaerobic bacterium that produces ethanol from carbon-monoxide. Arch Microbiol 1994;161:345~351.

[28] Ahmed A, Cateni BG, Huhnke RL, Lewis RS. Effects of biomass-generated producer gas constituents on cell growth, product distribution and hydrogenase activity of Clostridium carboxidivorans P7T. Biomass Bioenergy 2006;30:665~672.

[29] Ahmed A, Lewis RS. Fermentation of biomass-generated synthesis gas: Effects of nitric oxide. Biotechnol Bioeng 2007;97:1080~1086.

[30] Munasinghe PC, Khanal SK. Biomass-derived syngas fermentation into biofuels: Opportunities and challenges. Bioresour Technol 2010;101:5013~5022.

[31] Xu D, Tree DR, Lewis RS. The effects of syngas impurities on syngas fermentation to liquid fuels. Biomass Bioenergy 2011;35:2690~2696.

[32] Hurst KM, Lewis RS. Carbon monoxide partial pressure effects on the metabolic process of syngas fermentation. Biochem Eng J 2010;48:159~165.

[33] Klasson KT, Ackerson CMD, Clausen EC, Gaddy JL. Biological conversion of synthesis gas into fuels. Int J Hydrogen Energy 1992;17:281~288.

[34] Abubackar HN, Veiga MC, Kennes C. Biological conversion of carbon monoxide: Rich syngas or waste gases to bioethanol. Biofuels, Bioprod Biorefin 2011;5:93~14.

[35] Kwong SCW, Randers L, Rao G. On-line assessment of metabolic activities based on culture redox potential and dissolved oxygen profiles during aerobic fermentation. Biotechnol Progr 1992;8:576~579.

[36] Girbal L, Croux C, Vasconcelos I, Soucaille P. Regulation of metabolic shifts in Clostridium acetobutylicum ATCC 824. FEMS Microbiology Reviews 1995;17:287~297.

[37] Lee SK, Chou H, Ham TS, Lee TS, Keasling JD. Metabolic engineering of microorganisms for biofuels production: from bugs to synthetic biology to fuels. Curr Opin Biotechnol 2008;19:556~563.

[38] Frankman AW. Redox, pressure and volume effects on syngas fermentation. Chemical Engineering: Brigham Young University; 2009.

[39] Hu P. Thermodynamic, Sulfide, Redox Potential, and pH Effects on Syngas Fermentation. Chemical Engineering: Brigham Young University; 2011.

[40] Saxena J, Tanner RS. Effect of trace metals on ethanol production from synthesis gas by the ethanologenic acetogen, Clostridium ragsdalei. J Ind Microbiol Biotechnol 2011;38:513~52.

[41] Maddipati P, Atiyeh HK, Bellmer DD, Huhnke RL. Ethanol production from syngas by Clostridium strain P11 using corn steep liquor as a nutrient replacement to yeast extract. Bioresour Technol 2011;102:6494~6501.

[42] Datar RP, Shenkman RM, Cateni BG, Huhnke RL, Lewis RS. Fermentation of biomass-generated producer gas to ethanol. Biotechnol Bioeng 2004;86:587~594.

[43] Olson SJ, Nguyen-Phuoc B, Ibsen K. Gas cleanup technologies suitable for biomass gasification to liquid fuels. 2006 AIChE National Meeting, San Francisco, CA 2006;http://www.nt.ntnu.no/users/skoge/prost/proceedings/aiche-2006/data/papers/P61312.pdf.

[44] Younesi H, Najafpour G, Mohamed AR. Ethanol and acetate production from synthesis gas via fermentation processes using anaerobic bacterium, Clostridium ljungdahlii. Biochem Eng J 2005;27:110~119.

[45] Do YS, Smeenk J, Broer KM, Kisting CJ, Brown R, Heindel TJ, et al. Growth of Rhodospirillum rubrum on synthesis gas: Conversion of CO to H2 and poly-β-hydroxyalkanoate. Biotechnol Bioeng 2007;97:279~286.

[46] Higman C, Burgt Mvd. Gasification. 1st ed. Amsterdam, Boston: Gulf Professional Publishing; 2003.

[47] Gasifications Technology Council, Gasification: redefining clean energy, http://www.gasification.org/Docs/Final_whitepaper.pdf. 2008.

[48] Demirbas A. Sustainable cofiring of biomass with coal. Energy Conversion and Management 2003;44:1465~1479.

[49] McKendry P. Energy production from biomass (part 1): Overview of biomass. Bioresour Technol 2002;83:37~46.

[50] Kumabe K, Hanaoka T, Fujimoto S, Minowa T, Sakanishi K. Co-gasification of woody biomass and coal with air and steam. Fuel 2007;86:684~689.

[51] McIlveen-Wright DR, Pinto F, Armesto L, Caballero MA, Aznar MP, Cabanillas A, et al. A comparison of circulating fluidised bed combustion and gasification power plant technologies for processing mixtures of coal, biomass and plastic waste. Fuel Process Technol 2006;87:793~801.

[52] Nowacki P. COAL GASIFICATION PROCESSES. Park Ridge, NJ, USA: Noyes Data Corp; 1981.

[53] McKendry P. Energy production from biomass (part 3): gasification technologies. Bioresour Technol 2002;83:55~63.

[54] Dabai F, Paterson N, Millan M, Fennell P, Kandiyoti R. Tar formation and destruction in a fixed-bed reactor simulating downdraft gasification: Equipment development and characterization of tar-cracking products. Energy Fuels 2010;24:4560~4570.

[55] Dowd RA. Wabash river coal gasification repowering project: A DOE assessment. 2000.

[56] Babu SP. Biomass gasification for hydrogen production-process description and research needs. Task 33: thermal gasification of biomass (IEA bioenergy technology report) ExCo56, Dublin, Ireland, www.ieatask33.org. 2005.

[57] Pan YG, Velo E, Roca X, Manya JJ, Puigjaner L. Fluidized-bed co-gasification of residual biomass/poor coal blends for fuel gas production. Fuel 2000;79:1317~1326.

[58] Bowser TJ, Weckler PR, Patil KN, Mireles DeWitt CA. Design and testing of a low-cost, pilot-scale batch gasifier for food processing byproducts. Appl Eng Agric 2005;21:901~906.

[59] De Jong W, Unal O, Andries J, Hein KRG, Spliethoff H. Biomass and fossil fuel conversion by pressurised fluidised bed gasification using hot gas ceramic filters as gas cleaning. Biomass Bioenergy 2003;25:59~83.

[60] Rollins ML, Reardon L, Nichols D, Lee P, Moore M, Crim M, et al. Economic evaluation of CO_2 sequestration technologies task 4, biomass gasification-based processing. Report FC26-00NT40937-03, National Energy Technology Lab, Pittsburgh, PA. 2002.

[61] Spencer DF, Gluckman MJ, Alpert SB. Coal gasification for electric power generation. Science 1982;215:1571~1576.

[62] Tong ASF, Lai KCK, Ng KTW, Tsang DCW, Liu T, Liu J, et al. Renewable energy generation by full-scale biomass gasification system using agricultural and forestal residues. Practice Periodical of Hazardous, Toxic, and Radioactive Waste Management 2007;11:177~183.

[63] Devi L, Ptasinski KJ, Janssen FJJG. A review of the primary measures for tar elimination in biomass gasification processes. Biomass Bioenergy 2002;24:125~140.

[64] Torres W, Pansare SS, Goodwin Jr JG. Hot gas removal of tars, ammonia, and hydrogen sulfide from biomass gasification gas. Catal Rev Sci Eng 2007;49:407~456.

[65] Sherwood TK, Pigford RL, Wilke CR. Mass transfer. New York: McGraw-Hill; 1975.

[66] Bird RB, Steward WE, Lightfoot EN. Transport phenomena. 2nd ed. New York: John Wiley; 2008.

[67] Sander R. Compilation of Henry's law constants for inorganic and organic species of potential importance in environmental chemistry. Air chemistry department; Max-Planck Institute of Chemistry (Mainz, Germany). http://mbi.osu.edu/2010/ws6materials/henry.pdf. 1999.

[68] John HP. Chemical engineer's handbook. 4th ed. New York: McGraw-Hill, Inc; 1963.

[69] Richard GG. Transport phenomena and unit operations: a combined approach. New York: Wiley; 2002.

[70] Janssen LPBM, Warmoeskerken MMCG. Transport phenomena data companion. E. Arnold, Baltimore, MD, USA; 1987.

[71] Brenda enzyme database. http://www.brenda-enzymes.info/.

[72] Afolabi PR, Mohammed F, Amaratunga K, Majekodunmi O, Dales SL, Gill R, et al. Site-directed mutagenesis and X-ray crystallography of the PQQ-containing quinoprotein methanol dehydrogenase and its electron acceptor, cytochrome c(L). Biochemistry 2001;40:9799~9809.

[73] Gergel D, Cederbaum AI. Inhibition of the Catalytic Activity of Alcohol Dehydrogenase by Nitric Oxide Is Associated with S Nitrosylation and the Release of Zinc†. Biochemistry 1996;35:16186~16194.

[74] Kashiwagi M, Fuhshuku K-I, Sugai T. Control of the nitrile-hydrolyzing enzyme activity in Rhodococcus rhodochrous IFO 15564: preferential action of nitrile hydratase and amidase depending on the reaction condition factors and its application to the one-pot preparation of amides from aldehydes. J Mol Catal B: Enzym 2004;29:249~258.

[75] Allais JJ, Louktibi A, Baratti J. Oxidation of methanol by the yeast Pichia pastoris: purification and properties of the formate dehydrogenase. Agricultural and Biological Chemistry 1983;47:2547~54.

[76] Meakin GE, Jepson BJN, Richardson DJ, Bedmar EJ, Delgado MJ. The role of bradyhizobium japonicum nitric oxide reductase in nitric oxide detoxification in soya bean root nodules. Biochem Soc Trans 2006;34:195~6.

[77] Itoh H, Hirota A, Hirayama K, Shin T, Murao S. Properties of ascorbate oxidase produced by Acremonium sp. HI-25. Biosci Biotechnol Biochem 1995;59:1052~6.

[78] Picton R, Eggo MC, Merrill GA, Langman MJS, Singh S. Mucosal protection against sulphide: importance of the enzyme rhodanese. Gut 2002;50:201~205.

[79] Hyman MR, Ensign SA, Arp DJ, Ludden PW. Carbonyl sulfide inhibition of CO dehydrogenase from Rhodospirillum rubrum. Biochemistry 1989;28:6821~6826.

[80] Stark GR, Blaschko H, Dawson CR, Green DE, Goldberger R, Hayaishi O. Ascorbic acid oxidase. In: Boyer PD, Lardy H, Myrback K, editors. The Enzymes. 2nd ed. New York: Academic Press; 1963, p. 297~311.

[81] Liou JSC, Balkwill DL, Drake GR, Tanner RS. Clostridium carboxidivorans sp. nov., a solvent-producing clostridium isolated from an agricultural settling lagoon, and reclassification of the acetogen Clostridium scatologenes strain SL1 as Clostridium drakei sp. nov. Int J Syst Evol Microbiol 2005;55:2085~2091.

[82] Calli B, Mertoglu B, Inanc B, Yenigun O. Effects of high free ammonia concentrations on the performances of anaerobic bioreactors. Process Biochem 2005;40:1285~1292.

[83] Patoczka J, Wilson DJ. Kinetics of the desorption of ammonia from water by diffused aeration. Sep Sci Technol 1984;19:77~93.

[84] Doran PM. Bioprocess engineering principles. Chapter 9: Mass transfer. San Diego, CA 92101: Academic Press INC.; 1995, p. 190~217.

[85] Kundiyana DK, Huhnke RL, Wilkins MR. Syngas fermentation in a 100-L pilot scale fermentor: Design and process considerations. J Biosci Bioeng 2010;109:492~498.

[86] Perry DL, Phillips SL. Handbook of inorganic compounds: CRC Press; 1995.

[87] Romero LE, Gomez JM, Caro I, Cantero D. A kinetic model for growth of Acetobacter aceti in submerged culture. Chem Eng J 1994;54:B15~B24.

[88] Ahmed A. Effects of biomass-generated syngas on cell-growth, production distribution and enzyme activities of Clostridium Carboxidivorans P7. Dissertation, Chemical Engineering. Stillwater, OK: Oklahoma State University; 2006, p. 149~151.

[89] Cruz HJ, Freitas CM, Alves PM, Moreira JL, Carrondo MJT. Effects of ammonia and lactate on growth, metabolism, and productivity of BHK cells. Enzyme Microb Technol 2000;27:43~52.

[90] Salerno MB, Park W, Zuo Y, Logan BE. Inhibition of biohydrogen production by ammonia. Water Res 2006;40:1167~1172.

[91] Gouesbet G, H Abaibou, L F Wu, Mandrand-Berthelot MA, Blanco C. Osmotic repression of anaerobic metabolic systems in Escherichia coli. J Bacteriol 1993;175:214~221.

[92] Google [internet]. Chemiosmosis. [Cited 2012 May 25]. Available from: http://enwikipediaorg/wiki/Chemiosmosis.

[93] Girbal L. How neutral red modified carbon and electron flow in Clostridium acetobutylicum grown in chemostat culture at neutral pH. FEMS Microbiology Reviews 1995;16:151~162.

[94] Goodman BE. Transport of samll molecules across cell membranes: water channels and urea transporters. Adv Physiol Educ 2002;26:146~157.

[95] Hess M, Antranikian G. Archaeal alcohol dehydrogenase active at increased temperatures and in the presence of organic solvents. Appl Microbiol Biotechnol 2008;77:1003~013.

[96] Shuler ML, Kargi F. Enzymes. In: Acrivos A, editor. Bioprocess engineering (basic concepts). second ed: Prentice Hall PTR; 2002, p. 67~72.

[97] Adams MWW, Mortenson LE. The physical and catalytic properties of hydrogenase-II of Clostridium pasteurianum- A comparison with hydrogenase-I J Biol Chem 1984;259:7045~7055.

[98] Dobrindt U, Blaut M. Purification and characterization of a membrane-bound hydrogenase from Sporomusa sphaeroides involved in energy-transducing electron transport. Arch Microbiol 1996;165:141~147.

[99] Kellenberger E. Structure and function at the subcellular level. In: Neidhardt FC, editor. Escherichia coli and Salmonella. 2 ed. Washington D. C.: ASM Press; 1996, p. 17~28.

[100] Calli B, Mertoglu B, Inanc B, Yenigun O. Effects of high free ammonia concentrations on the performances of anaerobic bioreactors. Process Biochem 2005;40:1285.

[101] Bagyinka C, Kovács KL, Rak E. Localization of hydrogenase in Thiocapsa roseopersicina photosynthetic membrane. Biochem J 1982;202 255~258.

[102] Silver S. Transport of inorganic cations. In: Neidhardt FC, editor. Escherichia coli and Salmonella: Cellular and molecular biology. 2 ed. Washington D.C.: ASM Press; 1996, p. 1091~1102.

[103] Barnes JEM, Jayakumar A. NH_4^+ transport systems in *Escherichia coli.* In: Bakker EP, editor. Alkali cation transport systems in Prokaryotes. Boca Raton, FL: CRC Press, Inc.; 1993, p. 397~409.

[104] Reklaitis GV, Schneider DR. Introduction to material and energy balances: Wiley; 1983.

[105] Shuler ML, Kargi F. Bioprocess engineering (Basic concepts). 2nd ed: Prentice Hall PTR; 2002.

[106] Adams MWW, Mortenson LE. The physical and catalytic properties of hydrogenase-II of Clostridium pasteurianum- A comparison with hydrogenase-I J Biol Chem 1984;259:7045.

[107] Chmielniak T, Sciazko M. Co-gasification of biomass and coal for methanol synthesis. Appl Energy 2003;74:393~403.

[108] Smeenk J, Steinfeld G, Brown RC, Simpkins E, Dawson MR. Evaluation of an integrated biomass gasification/fuel cell power plant. http://www.iowaswitchgrass.com/__docs/pdf/Evaluation%20of%20an%20Integrated%20Biomass%20Power%20Plant.pdf.

[109] Jand N, Brandani V, Foscolo PU. Thermodynamic limits and actual product yields and compositions in biomass gasification processes. Ind Eng Chem Res 2006;45:834~843.

[110] Brown R, Meehan P. Syngas composition. Iowa State University; 2008.

[111] Phillips S, Aden A, Jechura J, Dayton D, Eggeman T. Thermochemical ethanol via indirect gasification and mixed alcohol synthesis of lignocellulosic biomass. Technical Report: NREL/TP-510-41168. 2007.

[112] Specht M, Bandi A, Baumgart F, Murray CN, Gretz J. Synthesis of methanol from biomass/CO_2 resources. In: Eliasson B, Riemer PWF, Wokaun A, editors. Greenhouse gas control technologies. Pergamon, Amsterdam; 1999.

[113] Lv P, Yuan Z, Wu C, Ma L, Chen Y, Tsubaki N. Bio-syngas production from biomass catalytic gasification. Energy Convers Manage 2007;48:1132~1139.

[114] Di Blasi C, Signorelli G, Portoricco G. Countercurrent fixed-bed gasification of biomass at laboratory scale. Ind Eng Chem Res 1999;38:2571~2581.

[115] Demirbas A. Biomass gasification for power generation in Turkey. Energy Sources, Part A: Recovery, Utilization and Environmental Effects 2006;28:433~445.

[116] Pfeifer C, Proll T, Puchner B, Hofbauer H. H_2-rich syngas from renewable sources by dual fluidized bed steam gasification of solid biomass. In: Berruti F, Bi X, Pugsley T, editors. 2007 ECI conference on the 12th international conference on fluidization-New horizons in fluidization engineering Vancouver, Canada; 2007.

[117] Fluidized-bed gasification process. Oklahoma State University.

[118] Priyadarsan S, Annamalai K, Sweeten JM, Holtzapple MT, Mukhtar S. Co-gasification of blended coal with feedlot and chicken litter biomass. 2 ed. Langford Lane, Kidlington, Oxford, OX5 1GB, United Kingdom: Elsevier Ltd; 2005, p. 2973~2980.

[119] Zhang RG, Na YJ, Lu QG. Experimental study on coal gasification in a circulating fluidized bed. Chinese Society for Electrical Engineering 2005;25.

APPENDIX (RAW SYNGAS COMPOSITIONAL DATABASE)

This raw syngas compositional database was established through extensive literature review, augmented by technical reports from twelve U.S. institutions which have gasification facilities. For the gas composition which is left blank in the tables A1-A13, it should be treated as non-measured or not targeted for measurement.

A-1: Syngas compositions, feedstocks, and operating conditions from several gasifiers

Operating Parameters	[48]	[50]	[50]
Gasifier type		Downdraft fixed bed	
Reactor size (L)		Di=22 mm; L=700 mm	
Feedstock	Biomass	Japanese cedar and Mulia coal	60 wt% of coal, 20 wt% of pine, 20 wt% PE wastes
Pressure (MPa)		Atmospheric pressure	
Temperature (º C)		900	890
Particle size (mm)		0.5-1.0 mm	
Gasification agents		Air-steam	
Feeding rate (g/h)		12 $mmol_{-carbon}$/min	
Steam/air			
Inlet airflow rate			
Special conditions		1. Consumption of air (mol/$mol_{-carbon}$ feed): 0.5 (air-fuel) 2. An increase of the biomass ratio	1. Consumption of air (mol/$mol_{-carbon}$ feed): 0.1(air-fuel ratio). 2. Consumption of steam (mol/$mol_{-carbon}$ feed):0.9 (steam ratio)
Syngas Compositions			
CO	20-30 (V %)	22.1-23.9 (V %)	17 (V %)
CO_2	15-20	26.1-33.7	20
H_2	30-40	47.9-37.5	40
CH_4	10-15	2.6-4.6	15
N_2	1		
C_2H_4		0.8-2.9 (C_2H_4 & C_2H_6)	
C_6H_6			
Tar ($C_{10}H_8$)			
NH_3			
Nitric oxide			
H_2S + COS			
H_2S			
SO_2			
H_2O	6		
Location	Turkey		

A-2: Syngas compositions, feedstocks, and operating conditions from several gasifiers

Operating Parameters	[51]	[51]	[51]	[51]
Gasifier type	Fluidized bed system	Fluidized bed system	Fluidized bed system	FERCO SilvaGas Processs
Reactor size (L)				
Feedstock	100 % coal	20 % biomass & 80% coal	100 % coal	20 % biomass & 80% coal
Pressure (MPa)				
Temperature (º C)	846	846	850	850
Particle size (mm)				
Gasification agents	Air-steam	Air-steam	Air-catalyst (dolomite)	Air-catalyst (dolomite)
Feeding rate (g/h)				
Steam/air				
Inlet airflow rate (kg/h)				1.97
Special conditions				
Syngas Compositions				
CO	19.4 (% vol/vol)	23.3 (% vol/vol)	34.7 (% vol/vol)	35.2 (% vol/vol)
CO_2	26.5	24.9	31.9	31
H_2	45	42	30.6	28.5
CH_4	7.4	7.5	1.7	4.2
N_2				
C_2H_2				
C_{2+}				
C_2H_4				
C_2H_6	1.7	2.3	1.1	1.1
C_3-Fract.				
C_6H_6				
Tar ($C_{10}H_8$)				
NH_3				
Nitric oxide				
Remarks	1. Char production ratio (g/g daf): 480. 2. Carbon loss in the ash (%): 8	1. Char production ratio (g/g daf): 350. 2. Carbon loss in the ash (%): 7.7	1. Char production ratio (g/g daf): 135. 2. Carbon loss in the ash (%): 7.2	1. Char production ratio (g/g daf): 133. 2. Carbon loss in the ash (%): 6.3
Location	Portugal	Portugal	Spain	Spain

A-3: Syngas compositions, feedstocks, and operating conditions from several gasifiers

Operating Parameters	[55]	[55]	[56]	[56]	[56]
Gasifier type	E-Gas TM gasifier (two stages)	E-Gas TM gasifier (two stages)	Bubbling fluidized bed process	Forced internal circulation fluidized bed	FERCO SilvaGas Processs
Reactor size (L)					
Feedstock	Typical coal	Petroleum coke	bagasse	Biomass	Wood chips
Pressure (MPa)	2.90	2.90	2.24		
Temperature (º C)	1400	1400	850		850-1000
Particle size (mm)					
Gasification agents	Oxygen	Oxygen	Air & steam	Air-blown	steam
Feeding rate (g/h)					
Steam/air					
Inlet airflow rate					
Special conditions					Consumption of steam (kg/kg feed): 0.45 (steam to wood chips ratio)
Syngas Compositions					
CO	46.31 (V %)	48.6 (V %)	26 (V %)	20-30 (V %)	43.17 (V %)
CO_2	16.22	15.40	37	15-25	13.46
H_2	33.44	33.20	19	30-45	21.22
CH_4	2.17	0.50	17	8-12	15.83
N_2		1.90		1-5	
C_{2+}			1		5.47
C_6H_6					
Tar ($C_{10}H_8$)				0.5-1.5 g/Nm^3	
NH_3				500-1000 ppmv	
Nitric oxide					
Ar		0.60			
H_2S + COS	130 ppmv				
H_2S	106 ppmv			20-50 ppmv	
Total S (ppm)		69 ppmv			
Remarks				Particles: 10-20 g/Nm^3	

A-4: Syngas compositions, feedstocks, and operating conditions from several gasifiers

Operating Parameters	[57]	[57]	[58]	[58]	[58]
Gasifier type	Fluidized-bed reactor	Fluidized-bed reactor	Pilot-scale batch gasifier	Pilot-scale batch gasifier	Pilot-scale batch gasifier
Reactor size (L)	4.57	4.57			
Feedstock	Pine chips	Black coal	100 % wood pellets	100 % sludge	50 % sludge
Pressure (MPa)	0.14	0.14			
Temperature (º C)	840-910	840-910	700-750	700-750	700-750
Particle size (mm)	0.75-1.20	0.75-1.20			
Gasification agents			Air-blown	Air-blown	Air-blown
Feeding rate (g/h)	0.863 (dry)	1.160 (dry)			
Steam/air (kg/Nm^3)	1.01	0.44			
Inlet airflow rate					
Special conditions	1. Consumption of air (Nm^3/kg feed): 0.7 2. Consumption of steam (kg/kg feed): 0.71	1. Consumption of air (Nm^3/kg feed): 0.86 2. Consumption of steam (kg/kg feed): 0.38			
Syngas Compositions					
CO	24.1 (dry, mol %)		11.9 (V %)	13.3 (V %)	16.8 (V %)
CO_2	6.75		7.2	11.8	
H_2	10.47		2.1	3.4	2.9
CH_4	2.61		0.7	1	4.2
N_2	54.77		50.7	59.3	54.2
C_2H_2	0.69				
C_{2+}					
C_2H_4			5.3		0.3
C_2H_6					
C_3-Fract.					
C_6H_6					
Tar ($C_{10}H_8$)					
NH_3					
Nitric oxide					
O_2	0.61		1.9	0.8	
Location					

A-5: Syngas compositions, feedstocks, and operating conditions from several gasifiers

Operating Parameters	[59]	[59]	[42]	[43]	[43]
Gasifier type	Pressurized fluidized bed test facility	Pressurized fluidized bed test facility	Fluidized bed gasifier	BCL Gasifier	GTI Gasifier
Reactor size (L)	Diameter: 0.1m (bed)	Diameter: 0.1m (bed)			
Feedstock	German brown coal	Crushed wood pellets (PW)	Switch grass	Wood	Wood
Pressure (MPa)	0.51	0.51		0.16	3.2
Temperature (º C)	802	824	770	870	870
Particle size (mm)					
Gasification agents	air	air	Air-flow		
Feeding rate (g/h)	2.5	3.0	25	83333 kg/h	83333 kg/h
Steam/air (kg/Nm^3)					
Inlet airflow rate			15 scfm		
Special conditions	N_2 flow to gasifier: 2.8 (kg/h)	N_2 flow to gasifier: 3.0 (kg/h)		Consumption of steam (kg/kg feed): Steam/bone dry feed: 0.4	Consumption of steam (kg/kg feed): Steam/bone dry feed: 0.76
Syngas Compositions					
CO	8.9 (V %, wet)	5.6 (V %, wet)	14.70 (V %)	22.84 (mol%, wet)	8.1 (mol%, wet)
CO_2	11.8	13.7	16.50	6.93	19.4
H_2	7	3.8	4.40	12.91	13.1
CH_4	1.4	2	4.20	8.32	7.8
N_2	64.8	62.7	56.80		
C_2H_2				0.22	
C_{2+}					
C_2H_4	0.1	0.3	2.40	2.35	0.1
C_2H_6			0.80	0.16	0.2
C_3-Fract.					
C_6H_6				0.07	0.3
Tar ($C_{10}H_8$)				0.13	0.1
NH_3				0.18	0.1
Nitric oxide					
Ar	0.5	0.5			
H_2S				0.04	0.04
H_2O	5.3	11.4		45.87	50.7
Remarks					
Location	Netherlands		Oklahoma State University		

A-6: Syngas compositions, feedstocks, and operating conditions from several gasifiers

Operating Parameters	[60]	[60]	[60]	[60]	[60]
Gasifier type	Pressurized Renugas	Atmospheric Renugas	FERCO	Pressurized Renugas	Atmospheric Renugas
Feedstock	Wood waste	Wood waste	Wood waste	Wood waste	Wood waste
Pressure (MPa)	3.38	0.180	0.180	3.37	0.166
Temperature (º C)	538	538	538	437	437
Gasification agents	Air-blown	Air-blown	Steam	Oxygen-blown	Oxygen-blown
Feeding rate (kg/h)	23708	28125	24833	23708	28125
Steam (kg/h)	1379	1649	11162	1379	1644
Inlet airflow rate (kg/h)	25630 (air)	43549 (air)		5217 (oxygen)	7374 (oxygen)
Syngas Compositions					
CO	11.7 (mol %)	12.74 (mol %)	32.69 (mol %)	14.1 (mol %)	20.63 (mol %)
CO_2	15.79	13.14	10.19	23.58	20.66
H_2	11.50	14.22	16.07	16.03	22.20
CH_4	7.52	2.48	11.99	12.73	8.15
N_2	34.75	39.66		1.70	1.71
C_2H_4	0.04	0.03	4.13	0.06	0.06
C_6H_6	< 0.6	0.19		0.34	0.34
Tar ($C_{10}H_8$)	0.08	0.06	0.30	0.11	0.11
NH_3	0.08	0.06	0.28	0.11	0.11
Ar	0.43	0.5		0.37	0.43
H_2S	0.01	0.01	0.06	0.02	0.01
H_2O	17.87	16.90	24.29	30.84	25.40
Remarks	Combustion Turbine Scenario	Combustion Turbine Scenario	Combustion Turbine Scenario	Methanol and ammonia production scenarios	Methanol and ammonia production scenarios

A-7: Syngas compositions, feedstocks, and operating conditions from several gasifiers

Operating Parameters	[61]	[61]	[61]	[61]
Gasifier type	Moving bed, Lurgi	Fluidized bed, Westing house	Entrained, Texaco	Entrained, Combustion Engineering
Reactor size (L)				
Feedstock	Coal	Coal	Coal	Coal
Pressure (MPa)				
Temperature (º C)	540	985	1315	985
Particle size (mm)				
Gasification agents	Oxygen-blown		Oxygen-blown	Air-blown
Feeding rate (kg/h)				
Steam/air (kg/Nm^3)				
Inlet airflow rate (kg/h)				
Special conditions				
Syngas Compositions				
CO	8 (V %)	43 (V %)	41 (V %)	16 (V %)
CO_2	15	6	10	6
H_2	21	29	29.6	9
CH_4	4.2	7.2	0.3	1
N_2	0.2	1.5	0.8	62
C_2H_2				
C_{2+}	0.5			
Tar ($C_{10}H_8$)	0.02 (weight fraction)			
NH_3	0.4	0.3	0.2	
Nitric oxide				
Ar				
H_2S + COS	0.7	1	1.1	<1
H_2S				
SO_2				
Total S (ppm)				
H_2O	50	12	17	5
Remarks				
Location				

A-8: Syngas compositions, feedstocks, and operating conditions from several gasifiers

Operating Parameters	[62]	[62]	[62]
Gasifier type	Bubbling fluidized bed gasifier	Bubbling fluidized bed gasifier	Bubbling fluidized bed gasifier
Reactor size (L)	Diameter:5 m; Height:5.5 m	Diameter:5 m; Height:5.5 m	Diameter:5 m; Height:5.5 m
Feedstock	Rice husk	Almond shell	Wood waste
Pressure (MPa)	Atmospheric pressure	Atmospheric pressure	Atmospheric pressure
Temperature (º C)	700/750/800/850	600/700/800/900	650/700/750/850
Particle size (mm)			
Gasification agents	air	air	air
Feeding rate (m^3/h)	4.72-6.49	1.58-1.68	3.79-5.53
Steam/air			
Inlet airflow rate			
Special conditions	Equivalence ratio: 9.06-15.56 %	Equivalence ratio: 5.93-7.12 %	Equivalence ratio: 7.19-15.43 %
Syngas Compositions			
CO			
CO_2	13.4/15.7/15.3/15.3 (V %)	13.7/14.3/13.5/13.6 (V %)	16.8/16.1/16.1/17.0 (V %)
H_2			
CH_4			
N_2			
C_2H_2			
C_6H_6			
Tar ($C_{10}H_8$)	64.8/13.7/3.7/4.6 (mg/L)	3.7/3.7/2.0/1.8 (mg/L)	1.8/11.9/5.4/4.9 (mg/L)
NH_3			
Nitric oxide	475/278/139/641 (ppm)	847/1066/1227/595 (ppm)	431/370/151/53 (ppm)
Ar			
H_2S + COS			
H_2S			
SO_2	555/0/0/280 (ppm)	0 (ppm)	119/80/29/5 (ppm)
Total S (ppm)			
O_2	1.5/0.8/2.1/0.7 (V %)	1.6/1.5/1.4/1.9 (V %)	1.8/1.5/1.0/0.6 (V %)
H_2O			
Remarks	(a) PM 10 (mg/m^3): 2.8/9.4/0.5/1.3 PM 2.5 (mg/m^3): 2.4/8.5/0.4/1.2 (b) CO, H_2, CH_4, & unsaturated C_nH_m are not listed. Sampling ports located right after the gasifier	(a) PM 10 (mg/m^3): 21.5/0.9/13.0/0.7 PM 2.5 (mg/m^3): 18.4/0.8/12.8/0.7 (b) CO, H_2, CH_4, & unsaturated C_nH_m are not listed. Sampling ports located right after the gasifier	(a) PM 10 (mg/m^3): 30.9/2.4/2.1/1.0 PM 2.5 (mg/m^3): 27.8/1.7/1.7/0.9 (b) CO, H_2, CH_4, & unsaturated C_nH_m are not listed. Sampling ports located right after the gasifier
Location			

A-9: Syngas compositions, feedstocks, and operating conditions from several gasifiers

Operating Parameters	[28]	[107]	[107]	[108]
Gasifier type	Fluidized-bed reactor	Integrated gas-steam cycles	Integrated gas-steam cycles	Fluidized-bed reactor
Reactor size (L)				
Feedstock	Switch grass	Typical coal	Petroleum coke	Shelled corn
Pressure (MPa)				
Temperature (º C)				
Particle size (mm)				
Gasification agents				
Feeding rate (kg/h)				
Steam/air (kg/Nm^3)				
Inlet airflow rate (kg/h)				
Syngas Compositions				
CO	16.50 (mol %)	45.3 (V %)	48.6 (V %)	21.7 (V %)
CO_2	15.50	15.8	15.4	12.5
H_2	5	34.4	33.2	4.1
CH_4	4.5	1.9	0.5	3.3
N_2	56	1.9	1.9	48.4
C_2H_2	0.10			
C_2H_4	1.40			
C_2H_6	0.35			
C_6H_6				
Tar ($C_{10}H_8$)				
NH_3				
Nitric oxide	150 ppm			
Ar		0.6	0.6	
Total S (ppm)		68	69	
H_2O				10
Location	Oklahoma State University			

A-10: Syngas compositions, feedstocks, and operating conditions from several gasifiers

Operating Parameters	[109]	[109]	[109]	[109]
Gasifier type	Continuous, bench-scale fluidized-bed	Continuous, bench-scale fluidized-bed	Continuous, bench-scale fluidized-bed	Continuous, bench-scale fluidized-bed
Reactor size (L)				
Feedstock	Almond shells	Almond shells	Sawdust	Sawdust
Pressure (MPa)				
Temperature (º C)	820	700	811	829
Particle size (mm)				
Gasification agents	Steam	Steam	Air	Air
Feeding rate (kg/h)				
Steam/air (kg/Nm^3)				
Inlet airflow rate				
Special conditions	(a) Consumption of steam (kg/kg feed): steam/biomass (dry)=1 (b) Catalyst: Ni-Olivine	(a) Consumption of steam (kg/kg feed): steam/biomass (dry)=0.5 (b) Catalyst: Ni-Olivine	(a) Equivalence ratio: 9.90% (b) Catalyst: Olivine bed inventory	(a) Equivalence ratio: 20.00% (b) Catalyst: Olivine bed inventory
Syngas Compositions				
CO	24.1 (V %, dry gas)	26.5 (V %, dry gas)	29.9 (V %, dry gas)	19.9 (V %, dry gas)
CO_2	19.2	24	14.2	18.3
H_2	52.4	38.8	20.1	13.2
CH_4	4.3	10.8	8.5	5.5
N_2			27.3	43.2
C_2H_2				
C_{2+}				
C_2H_4				
C_2H_6				
C_3-Fract.				
C_6H_6				
Tar ($C_{10}H_8$)	0.4 (g/Nm^3 dry)	17.7 (g/Nm^3 dry)	28.6 (g/Nm^3 dry)	24.7 (g/Nm^3 dry)
NH_3				
Nitric oxide				
Ar				
H_2S + COS				
H_2S				
SO_2				
Remarks	Gas yield: 1.88 (Nm^3 dry/kg daf)	Gas yield: 0.99 (Nm^3 dry/kg daf)	Gas yield: 1.27 (Nm^3 dry/kg daf)	Gas yield: 1.63 (Nm^3 dry/kg daf)
Location	Italy			

A-11: Syngas compositions, feedstocks, and operating conditions from several gasifiers

Operating Parameters	[110]	[111]	[111]	[112]
Gasifier type	Fluidized bed	Circulating fluidized bed	Circulating fluidized bed	
Reactor size (L)				
Feedstock	Switch grass	Dried wood	Dried wood	Biomass
Pressure (MPa)		0.16	0.16	
Temperature (º C)		890	890	
Particle size (mm)				
Gasification agents	Air-blown	Steam	Steam	Steam & O_2
Feeding rate (kg/h)	5			
Steam/air (kg/Nm^3)				
Inlet airflow rate				
Special conditions		0.4 lb of steam/lb of bone dry biomass	0.4 lb of steam/lb of bone dry biomass	
Syngas Compositions				
CO	21.05 (mol %)	25.1 (mol%, wet)	41.9 (mol%, dry)	15.8 (V %)
CO_2	16.23	7.4	12.4	34.70
H_2	8.61	15	25.1	37.30
CH_4	6.76	9	15.1	11.40
N_2	41.73			0.3
C_2H_2	0.13	0.3	0.4	
C_2H_4	2.34	2.5	4.1	
C_2H_6	0.35	0.1	0.2	
C_3-Fract.				
C_6H_6		0.1	0.1	
Tar ($C_{10}H_8$)		0.1	0.2	
NH_3		0.2	0.3	
Nitric oxide				
H_2S		0.04	0.07	
H_2O				0.50%
Location	Iowa State University	National Renewable Energy Lab	National Renewable Energy Lab	

A-12: Syngas compositions, feedstocks, and operating conditions from several gasifiers

Operating Parameters	[113]	[114]	[115]	[116]
Gasifier type	Fluidized bed reactor	Countercurrent fix-bed gasifier	Downdraft gasifier	Dual fluidized bed steam gasifier
Reactor size (L)				
Feedstock	Pine sawdust	Wood and agricultural residues	Hazelnut shells	
Pressure (MPa)				
Temperature (º C)	800			
Particle size (mm)				
Gasification agents	Air & steam	Air		
Feeding rate (kg/h)	0.47		1.7	
Steam/air (kg/Nm^3)				
Inlet airflow rate				
Special conditions	(a) Consumption of Air: 0.65 Nm^3/h (b) Consumption of steam (kg/h): 0.4 (c) Calcined dolomite feeding rate (g/h)= 14 (d) Temperature in the catalytic reactor (º C)=850	Optimal gasification conditions	Consumption of air (Nm^3/kg feed): 1.6 (dry air/dry and ash free fuel)	
Syngas Compositions				
CO	14.82 (V %)	28-30 (V %)	8.6 (V %)	24-26 (V %, dry)
CO_2	29.65	5-7	16.3	20-22
H_2	52.47	6-8	14.8	38-40
CH_4	2.9	1-2	1.4	10-11
N_2		Balance	58.7	
C_2H_2			0.1	
C_{2+}	0.16	Small amount		
C_2H_4				2-2.5
C_2H_6			0.1	
C_3-Fract.				0.5-0.7
C_6H_6				
Tar ($C_{10}H_8$)				2-5 g/Nm^3 (dry)
NH_3				1100-1700 ppmv
H_2S				130-170 ppmv
H_2O				30-45

A-13: Syngas compositions, feedstocks, and operating conditions from several gasifiers

Operating Parameters	[117]	[118]	[118]	[119]
Gasifier type	Pilot-scale fluidized bed gasifier	Fixed-bed gasifier	Fixed-bed gasifier	Pilot scale circulating fluidized bed
Reactor size (L)	25 cm in diameter			D_i=1m; H=30 m
Feedstock	Switch grass	Coal	Coal/advanced feedlot biomass=1:1	Shenhua Coal
Pressure (MPa)				Atmospheric
Temperature (º C)	770			849
Particle size (mm)				Air-steam
Gasification agents	Air			
Feeding rate (kg/h)	24.75 (Maximum)			5.4
Steam/air (kg/Nm^3)				
Inlet airflow rate	15 cfm	1.97 (kg/h)	1.97 (kg/h)	
Special conditions		(a) Particle size=(9.4±3.1) mm (b) Batch mode operation	(a) Particle size=(9.4±3.1) mm (b) Batch mode operation	(a) Consumption of air=3.23 (kg/kg feed) (b) Consumption of steam=0.51 (kg/kg feed)
Syngas Compositions				
CO	18.39 (mol %)	28.8 (mol %)	29 (mol %)	13.46 (mol %)
CO_2	15.64	3.3	4.8	12.54
H_2	4.98	8.9	8.8	10.85
CH_4	4.52	2.2	1.6	0.7
N_2	54.4	Balance	Balance	
C_2H_2	0.17			
C_{2+}				
C_2H_4	1.77			
C_2H_6	0.26			
C_3-Fract.				
C_6H_6				
Tar ($C_{10}H_8$)				
NH_3				
Nitric oxide				
Ar				
H_2S + COS				
H_2S				
SO_2				
Remarks	Location: Oklahoma State University (OSU)		Only these four gases were analyzed!	